An experimental view on shape coexistence in nuclei

Paul E. Garrett, Magda Zielińska, Emmanuel Clément

▶ **To cite this version:**

Paul E. Garrett, Magda Zielińska, Emmanuel Clément. An experimental view on shape coexistence in nuclei. Prog.Part.Nucl.Phys., 2022, 124, pp.103931. 10.1016/j.ppnp.2021.103931 . hal-03584676

HAL Id: hal-03584676
https://hal.science/hal-03584676

Submitted on 10 Mar 2022

HAL is a multi-disciplinary open access archive for the deposit and dissemination of scientific research documents, whether they are published or not. The documents may come from teaching and research institutions in France or abroad, or from public or private research centers.

L'archive ouverte pluridisciplinaire **HAL**, est destinée au dépôt et à la diffusion de documents scientifiques de niveau recherche, publiés ou non, émanant des établissements d'enseignement et de recherche français ou étrangers, des laboratoires publics ou privés.

An Experimental View on Shape Coexistence in Nuclei

Paul E. Garrett

Department of Physics, University of Guelph, Guelph, ON N1G2W1 Canada

Magda Zielińska

IRFU/DPhN, CEA Saclay, Université Paris-Saclay, 91191 Gif-sur-Yvette, France

Emmanuel Clément

Grand Accélérateur National d'Ions Lourds (GANIL), CEA/DRF-CNRS/IN2P3, 14076 Caen Cedex 05, France

Abstract

Nuclear shape coexistence is the phenomenon in which distinct shapes occur within the same nucleus and at a similar energy. In this work, we provide an overview of the experimental investigations of shape coexistence, focusing on those regions of the nuclear chart that have been the most actively investigated within the past decade. In particular, we focus on coexistence phenomena at low angular momentum and on the new experimental information, placed within the context of previous results. We first give a summary of the experimental signatures that can be used for assessing shape coexistence, and then discuss the evidence for shape coexistence from experimental results, with particular attention paid to regions where its presence has been suggested along isotopic or isotonic chains, and in regions where "islands" of such structures have been proposed. We conclude with an overview, with an emphasis on the emerging regions where indications for multiple shape coexistence exist.

Keywords: nuclear shapes, shape coexistence, collective excitations, nuclear spectroscopy

Contents

Email addresses: pgarrett@physics.uoguelph.ca (Paul E. Garrett), magda.zielinska@cea.fr (Magda Zielińska), clement@ganil.fr (Emmanuel Clément)

1. Introduction

The atomic nucleus, composed of an ensemble of protons and neutrons, can be viewed as a macroscopic object in a way that is analogous to a liquid drop. Using a set of coordinates that defines the nuclear surface, rather than describing the motions of the individual particles, provides a natural way of defining a nuclear shape. In atomic systems, their spherical shape arises

from the $1/r$ potential that the electrons experience due to the electromagnetic force originating from the point-like nucleus. In contrast, the nucleus can take a variety of shapes that include spherical, prolate, oblate, etc., that emerge as a consequence of the more complicated nucleon-nucleon interaction. The shape of a nuclear state depends on the particularities of the microscopic wave function, and thus it may change not only as a function of the number of nucleons, but it may also vary from one state to another within the same nucleus. This latter possibility, referred to as shape coexistence, was first suggested by Morinaga [1] nearly 60 years ago for the 6.05-MeV 0^+ state in ^{16}O that was deformed while the ground state possessed a spherical shape. What began as a rare and exotic phenomenon is now suggested to be widespread and perhaps lurking in nearly every nucleus [2]. Establishing shape coexistence is challenging and requires highly-refined experimental techniques, but provides one of the most demanding and stringent tests of modern theories and models of the nuclear structure. It is for this reason that studies of shape coexistence are at the forefront of nuclear structure research.

There is no strict, universal, definition of shape coexistence. The earliest examples of shape coexistence, starting with ^{16}O and expanded upon in the light-mass region, were interpreted within a view of well-developed minima in the potential energy surface of the nucleus. The early calculations often explicitly incorporated deformed $2p-2h$ and $4p-4h$ configurations that arose from promotion of particles across a closed major shell, as these kinds of solutions resulted from Hartree-Fock calculations [3]. The simple picture of states residing in a particular potential well that is separated by a significant barrier from other minima has guided much of our thinking. Figure 1 shows the results of beyond-mean-field calculations for ^{186}Pb [4]. In this work, the Skyrme interaction SLy6 was used for the Hartree-Fock-Bogoliubov mean-field calculation, and a variational calculation was performed following particle-number and angular momentum projections of the mean-field wave functions in order to mix configurations with different deformation β_2 (defined in Sect. 2). The states depicted in Fig. 1 reveal four unique sets that can be classified as a spherical ground state and 2^+ state, a prolate band with a band head with $\beta_2 \approx 0.32$, an oblate band with a band head with $\beta_2 \approx -0.2$, and another prolate band with a band head with $\beta_2 \approx 0.45$. An eigenstate does not necessarily "reside" in a particular potential well, but rather at an average deformation given by the weights associated with the mean-field states.

Poves [5] states "Shape coexistence is a very peculiar nuclear phenomenon consisting in the presence in the same nuclei, at low excitation energy, and within a very narrow energy range, of two or more states (or bands of states) which: (a) have well defined and distinct properties, and, (b) which can be interpreted in terms of different intrinsic shapes." In the context of the present work, we use a definition of shape coexistence that is closely aligned to this and also the intent stated by Wood and co-workers [6] "The meaning that we assign to coexistence here is to imply in general, coexisting collective structures and, in particular, coexisting shapes." The first part of this statement eliminates the trivial cases of assigning, for example, shape coexistence to single-particle states near closed shells possessing different quadrupole moments that arise from harmonic oscillator wave functions. The difficulty arises in the definition of "distinct" or "different intrinsic" shapes. While it may be somewhat straightforward to cite coexistence when it involves spherical states, like those at or near closed shells, and deformed configurations that are obvious due to the observation of rotational bands, large quadrupole moments, etc., it becomes very subtle when it involves different deformed configurations. For example, we would claim coexistence

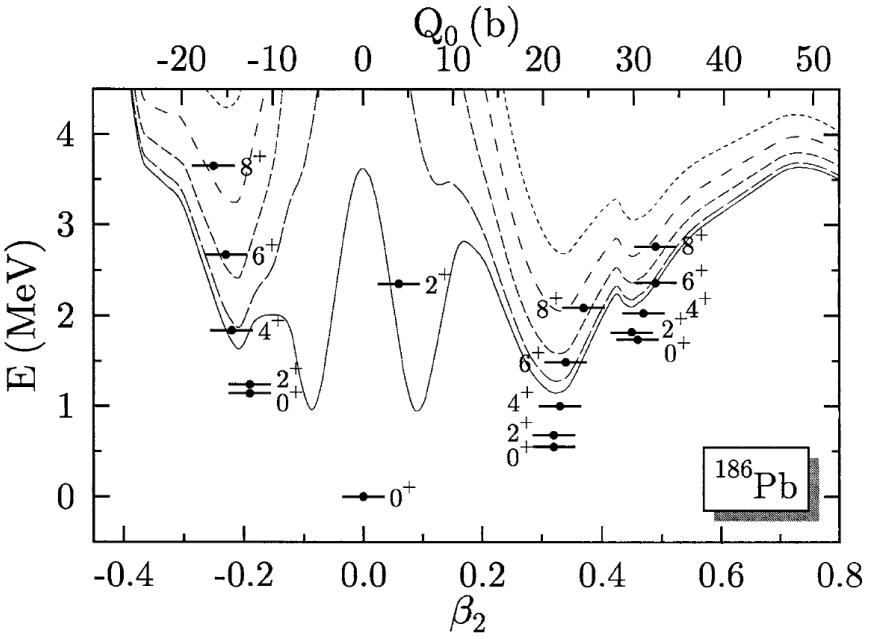

Figure 1: States predicted in beyond-mean-field calculations for ^{186}Pb for the parity and angular momentum, I^π, indicated and with projection $K = 0$ as a function of the quadrupole deformation parameter β_2. The states are plotted with their excitation energy relative to the lowest 0^+ state predicted, and are located on the horizontal axis at the effective mean deformation. The curves are the calculated particle-number- and angular-momentum-projected potential energies, with the lowest for $I^\pi = 0^+$, and increasing with spin. The large energy gain for the states compared to the potential curves arises from the mixing of the configurations. Figure taken from Ref. [4].

when it involves states (or set of states) that might possess the same magnitude of deformation $|\beta_2|$, but would have different and distinct values of the shape parameter γ, as in the above example in ^{186}Pb of oblate and prolate states. A less clear demarcation line occurs, however, when dealing with states of the same type of shape, e.g. prolate, but different values of β_2, or similar values of β_2 and different values of γ that do not lie at the extremes of prolate ($\gamma = 0°$) or oblate ($\gamma = 60°$). A similar ambiguity arises in the use of excitation energies as a guide; a state at an excitation energy of 6.05 MeV, as it is the case for the first excited state in ^{16}O, might be considered as a high-energy state in heavy nuclei. We thus avoid a hard definition of shape coexistence, and leave it fluid so that it can be adapted to the structures observed in each region of the nuclear chart.

A common feature behind all examples of shape coexistence, and indeed the reason behind the existence of competing shapes within a narrow energy window, is the tremendous gain in energy that arises from the correlations amongst the particles. One of the common mechanisms for generating shape coexistence is due to the promotion of multiple particles (for example protons) across shell gaps, thereby increasing the number of valence particles and holes that can interact with valence particles of the other type (neutrons in this example). The correlation energies that arise from both pairing *and* quadrupole-quadrupole interactions largely offset, and sometimes overcome, the energy cost of promoting particles from one orbital to another. The fact that the nucleus re-organizes into configurations that possess a different deformation from the original "normal-

ordered" state (i.e., without the multi-particle multi-hole excitation) may impact many nuclear properties, perhaps even the location of the so-called driplines [7]. The study of the properties of shape-coexisting states enables us to investigate the correlations of particles under different conditions, i.e., deformation, within the same nucleus.

There have been a number of reviews of shape coexistence, and here we mention a few only. Some of the earlier reviews by Heyde *et al.* [3] on odd-mass nuclei, and Wood and co-workers [6] on even-even nuclei, remain as definitive studies that provide a broad view of the background material. Approximately a decade ago, a further detailed review by Heyde and Wood [2] gave a comprehensive update of the tremendous progress of the field in the intervening decades since the earlier reviews. This was complemented by a special issue (see the introduction by Wood and Heyde [8]) of J. Phys. G that contained submissions from a number of authors reviewing particular aspects of shape coexistence. In the present contribution, we describe the recent progress on the *experimental* evidence for shape coexistence for regions where it has been recently suggested to emerge, as well as new results for those regions where it has been well established. For the latter, we attempt to place the new measurements in the context of previous results in order to provide a more complete picture. We do not intend to present an over-arching review on all aspects of shape coexistence – for example, we generally do not discuss superdeformed structures at high spin, nor clustering phenomena, nuclear halos, molecular states, etc. – but our focus is on shape coexistence at low spin, and ideally those that manifest at spin 0. We also do not treat the theoretical progress that has been achieved, or possible future developments, as we could not do these subjects proper justice, but instead direct the reader to the other sources (e.g., articles contained within Ref. [8] and also Refs. [2, 9–11], for example). Further, we do not discuss those regions where shape coexistence has been established, but for which there have been no, or very few, recent experimental studies. The reflections herein are biased to our own interests, and we hope our colleagues will forgive us if we do not explicitly mention their work.

2. Basic concepts and experimental fingerprints of shape coexistence

Shape coexistence can be studied via a variety of experimental probes. The first indication of nuclear deformation can be obtained from the level energies, or alternatively from the electromagnetic transition strengths. In particular, observation of low-lying 0^+ states in even-even nuclei is usually interpreted as a hint of shape coexistence. The observation of rotational bands evidences an enhanced deformation, which can be estimated from their moments of inertia.

For odd-mass and odd-odd nuclei, the spectroscopic quadrupole moment of the ground state can be measured using laser spectroscopy, bringing direct information on the charge distribution in the nucleus. If, however, a different microscopic configuration appears low in excitation energy, those simple observables may be influenced by mixing of the wave functions corresponding to different configurations. These methods are also obviously not suited to investigate properties of short-lived non-yrast states built on different microscopic configurations. Therefore a more sophisticated approach is mandatory, involving determination of complete sets of electromagnetic transition rates between low-lying excited states, and static quadrupole moments. Those can be further analysed in terms of quadrupole invariants resulting from the Kumar-Cline sum rules [12, 13] yielding model-independent information on shape parameters of individual states. Measurements

of $E0$ transition strengths bring invaluable complementary data on configuration mixing, and microscopic components of the wave functions can be deduced from nucleon-transfer cross sections. Consideration of all of the observables is important when assigning configurations and making conclusions about the structure of states.

In the following sections, we present a brief introduction to observables related to experimental shape-coexistence studies including basic formulas relating them to nuclear deformation.

2.1. Nuclear deformation and level energies

If we begin with the usual assumption that nucleus can be modelled as a liquid drop, which is an underlying concept of the Bohr model [14, 15], the nuclear surface can be described as a series of spherical harmonics. The most important contribution to departure from a spherical shape comes from quadrupole deformation, and thus a general expression can be reduced to

$$R(\theta,\phi) = R_0\left(1 + \sum_{\mu} \alpha^*_{2\mu} Y_{2\mu}(\theta,\phi)\right), \tag{1}$$

where R_0 is the radius of the nuclear surface in the spherical configuration, $Y_{2\mu}$ are the spherical harmonics of degree 2, order μ, and $\alpha_{2\mu}$ are the expansion parameters describing the deformation of the nuclear surface. This equation describes the nuclear shape with an arbitrary orientation in space. A more natural description can be achieved by applying a transformation into the principal-axis frame, using the Wigner rotation matrices, $D^J_{\nu\mu}(\alpha,\beta,\gamma)$, via

$$a_{2\mu} = \sum_{\nu} D^2_{\nu\mu}(\alpha,\beta,\gamma)\alpha_{2\nu} \tag{2}$$

with the Euler angles (α,β,γ) chosen such that $a_{2\pm1} = 0$[1]. The commonly used deformation parameters are defined as

$$a_{20} = \beta_2 \cos\gamma, \quad a_{22} = \frac{1}{\sqrt{2}}\beta_2 \sin\gamma \tag{3}$$

and the radii along the principal-axis directions are

$$R_k = R_0 + \delta R_k \tag{4}$$

with

$$\delta R_k = \sqrt{\frac{5}{4\pi}} R_0 \beta_2 \cos\left(\gamma - \frac{2\pi k}{3}\right). \tag{5}$$

Figure 2 displays the nuclear shapes calculated for $\beta_2 = 0.35$ and $\gamma = 0°$ (prolate) and $\gamma = 60°$ (oblate).

With the breaking of rotational symmetry, deformed systems can possess rotational excitations built on each intrinsic state of the nucleus, which are the familiar rotational bands observed in the

[1]The principal-axis frame here is analogous to that described for the inertia tensor in mechanics such that the products of inertia vanish, leaving only the moments about the principal axis directions.

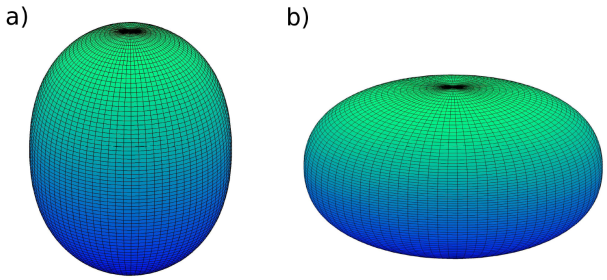

Figure 2: Shapes calculated with $\beta_2 = 0.35$ for $\gamma = 0°$, or prolate (a), and for $\gamma = 60°$, or oblate (b).

majority of nuclei. The rotational states can be described via moments of inertia, and provided that the underlying intrinsic state does not change, they evolve smoothly as a function of the angular momentum. With the assumption of axial symmetry, only rotations about an axis perpendicular to the symmetry axis are permitted, and it is possible to define a moment of inertia, $\mathcal{J}$, via the relationship

$$E = \frac{\hbar^2}{2\mathcal{J}} I(I+1). \tag{6}$$

Using the definition of the magnitude of the angular momentum as $J = \sqrt{I(I+1)}$, we can extract a *kinematic* moment of inertia via

$$\frac{\mathcal{J}^{(1)}}{\hbar^2} = \frac{1}{2}\left(\frac{dE}{dJ^2}\right)^{-1}. \tag{7}$$

Taking into account the discrete nature of the level energies, such that $\Delta E = E(I) - E(I-2) = E_\gamma$, results in

$$\frac{\mathcal{J}^{(1)}}{\hbar^2} \approx \frac{2I-1}{E_\gamma}. \tag{8}$$

While this is valid for large angular momenta, we adopt this definition for all values of spin I.

The identification of shape coexistence often begins through the observation of states at excitation energies where they are not expected, or from trends observed in energy systematics. The former implies that we have a high degree of confidence in our knowledge of the structure of the ground state so as to predict the excitation spectrum. An example of this are the "additional" 0^+ and 2^+ states that appeared in the vicinity of the presumed two-phonon vibrational triplet in ^{112,114}Cd that were identified as problematic in the early 1960s [16, 17]. The use of excitation energy systematics is typically far more reliable than focusing on individual states in nuclei, although the conjectures must be followed with detailed investigation to provide proof, for example by measurements of quadrupole moments or other quantities that are sensitive to the nuclear shape.

In the vicinity of closed shells or sub-shells, the excitation energies of shape-coexisting states are often observed to present a parabolic-like behaviour as a function of neutron number when traversing an isotopic chain (in principle, it is possible to have a similar parabolic behaviour for an isotonic chain, although identifying such structures has proven to be difficult, see, e.g., Urban *et al.* [18] for suggested neutron intruder excitations in the Sr – Sn region). This behaviour is stemming

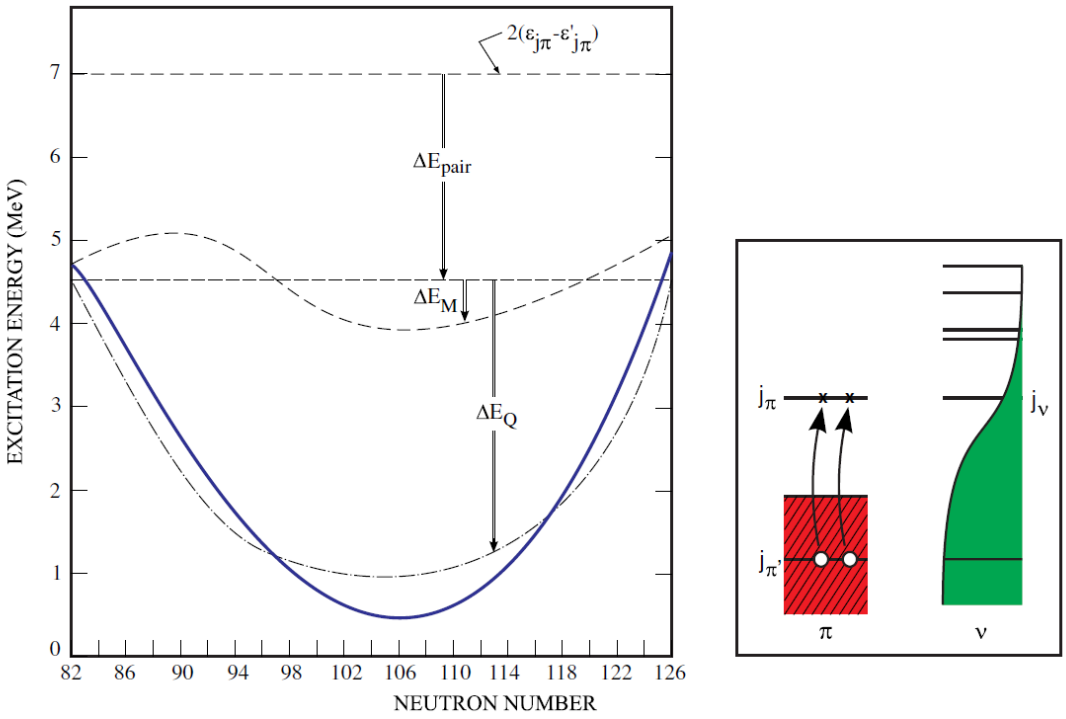

Figure 3: Schematic of the contributions to the energy of a $2p-2h$ excitation, specifically for those in the $Z = 82$ region. Figure taken from Ref. [2].

from the mechanism believed to underlie shape coexistence in these nuclei, which is illustrated, in the case for medium to heavy nuclei, in Fig. 3. An estimation of the energy of the lowest 0^+ state formed from a proton (π) $2p-2h$ configuration is [2]

$$E_i = 2(\epsilon_{j_\pi} - \epsilon_{j_{\pi'}}) - \Delta E_{pair} + \Delta E_M + \Delta E_Q \tag{9}$$

where the term $(\epsilon_j - \epsilon_{j'})$ is the energy needed to promote a particle from an orbital with energy $\epsilon_{j'}$ to an orbital with energy ϵ_j. The term ΔE_{pair} is the contribution to the pairing energy, defined as the difference in the pairing energy of the ground state and the $2p-2h$ state. The ΔE_M term is the change in the proton-neutron monopole interaction energy, and ΔE_Q is the change in the proton-neutron quadrupole interaction energy. As shown in Ref. [19], an expression for the quadrupole interaction energy is given by

$$\Delta E_Q \simeq 4\kappa N_\nu \sqrt{\Omega_\pi - N_\pi}\sqrt{\Omega_\nu - N_\nu} \tag{10}$$

where N_π (N_ν) is the number of valence proton (neutron) pairs outside the closed shells, Ω_π (Ω_ν) are the degeneracies of the proton (neutron) orbitals involved, and κ is the strength parameter for the residual quadrupole-quadrupole force $\kappa\hat{Q}_\pi \cdot \hat{Q}_\nu$. Is it this term that is mainly responsible for the parabolic-like behaviour of the energies of the so-called "intruder" states.

In many cases, identification of shape-coexisting states is based on the observation of deformed structures appearing at low excitation energy in nuclei that have spherical or weakly deformed

ground states, which is related to a simple fact: it is far easier to identify rotational-like structures in nearly spherical nuclei that have a low level density than *vice versa*.

2.2. Quadrupole moments

The spectroscopic electric quadrupole moment Q_s of a state of spin I is defined as the diagonal matrix element of the $\mu = 0$ component of the $\mathcal{M}(E2,\mu)$ quadrupole operator, with states of maximum M value:

$$\begin{aligned} eQ_s &= \sqrt{\frac{16\pi}{5}}\langle I, M = I|\mathcal{M}(E2,\mu = 0)|I, M = I\rangle, \\ &= \sqrt{\frac{16\pi}{5}}\frac{1}{\sqrt{2I+1}}(I, I, 2, 0|I, I)\langle I||\mathcal{M}(E2)||I\rangle, \end{aligned} \tag{11}$$

where $\langle I||\mathcal{M}(E2)||I\rangle$ is the reduced diagonal matrix element of the $\mathcal{M}(E2,\mu)$ operator. In order to relate the intrinsic quadrupole moment Q_0, defined in the principal-axis frame, and the spectroscopic quadrupole moment Q_s, the transformation as used in Eq. 2 must be applied. For example, for an axially symmetric rotor the reduced matrix elements of the $\mathcal{M}(E2,\mu)$ operator can be related to Q_0 as follows:

$$\langle KI_f||\mathcal{M}(E2)||KI_i\rangle = \sqrt{(2I_i+1)}(I_i, K, 2, 0|I_f, K)\sqrt{\frac{5}{16\pi}}eQ_0, \tag{12}$$

where K denotes the projection of the nuclear spin I on the symmetry axis of the nucleus. Combining Eqs. 11 and 12 yields the following relation between Q_s and Q_0:

$$Q_s = (I, K, 2, 0|I, K)(I, I, 2, 0|I, I)Q_0 = \frac{3K^2 - I(I+1)}{(I+1)(2I+3)}Q_0 \tag{13}$$

The spectroscopic quadrupole moment vanishes for spins of 0 and 1/2, even if Q_0 is nonzero, i.e., for a state that is deformed, since they have $I = K$. Thus, the ground states for all even-even nuclei, and odd-A nuclei with $I = 1/2$, have $Q_s = 0$.

The electric quadrupole operator can be expressed as

$$\mathcal{M}(E2,\mu = 0) = \int \hat{\rho}(\vec{r})r^2 Y_{20}(\theta,\phi)\, d^3r \tag{14}$$

and in order to proceed, a model of the charge density must be adopted. For simplicity, usually a constant density is assumed (we only consider the use of collective variables, as defined above, rather than using single-particle coordinates), and thus

$$\mathcal{M}(E2) = \frac{3Z}{4\pi R_0^3}\int\int_0^R r^4\, dr\, Y_{20}(\theta,\phi)\, \sin\theta\, d\theta\, d\phi = \frac{3Z}{4\pi R_0^3}\int \frac{1}{5}R^5 Y_{20}(\theta,\phi)\, \sin\theta\, d\theta\, d\phi. \tag{15}$$

Using the expression for the radius as

$$R(\theta,\phi) \approx R_0\Big(1 + \beta_2 Y_{20}(\theta,\phi)\Big) \tag{16}$$

which does *not* define the shape of an ellipsoid, leads to the relation

$$Q_0 = \frac{3}{\sqrt{5\pi}} Z R_0^2 \beta_2 \left(1 + \frac{2}{7}\sqrt{\frac{5}{\pi}}\beta_2 + \ldots\right)$$
$$\approx \frac{3}{\sqrt{5\pi}} Z R_0^2 \beta_2 \Big(1 + 0.36\beta_2\Big). \tag{17}$$

An alternative expression found in the literature is

$$Q_0 = \frac{3}{\sqrt{5\pi}} Z R_0^2 \beta_{eff} \left(1 + \frac{1}{8}\sqrt{\frac{5}{\pi}}\beta_{eff}\right)$$
$$\approx \frac{3}{\sqrt{5\pi}} Z R_0^2 \beta_{eff} \Big(1 + 0.16\beta_{eff}\Big) \tag{18}$$

that arises from the definition of the quadrupole moment of a symmetric ellipsoid, and with β_{eff} defined as the difference between the semi-major and semi-minor axis lengths

$$\beta_{eff} = \frac{4}{3}\sqrt{\frac{\pi}{5}}\frac{\Delta R}{R}. \tag{19}$$

Herein, we will use the definition of β_2 from Eq. 17.

The intrinsic quadrupole moment Q_0 can be calculated, under model assumptions, from the measured spectroscopic quadrupole moment Q_s or, alternatively, from the measured $B(E2)$ values. Equations 13 and 12 provide the necessary relations for the most common approximation of an axially symmetric rotor. An intrinsic quadrupole moment derived from a $B(E2)$ value via Eq. 12 is commonly referred to as transitional quadrupole moment Q_t.

2.3. Magnetic moments

A comprehensive discussion of various aspects of nuclear magnetic moments and their experimental studies can be found, for example, in Refs. [20, 21]. Here we briefly present the basic definitions and aspects important for shape-coexistence studies.

The magnetic dipole moment of a nuclear state with spin I, $\mu(I)$, is defined as the diagonal matrix element of the z component of the $\hat{\mu}$ magnetic dipole operator, with states of maximum M value, and can be further related to the nuclear gyromagnetic factor g:

$$\mu(I) = \langle I, M = I|\mu_z|I, M = I\rangle = gI\mu_N \tag{20}$$

where μ_N is the nuclear magneton.

Since $\hat{\mu}$ is a one-body operator, it can be written as a sum of single-particle operators, each of them acting on a specific valence particle. Moreover, one can consider orbital and spin gyromagnetic factors separately, which results in the following expression for the magnetic dipole moment μ:

$$\mu = \sum_i \mu_i = \sum_i g_l^i l_i + g_s^i s_i \tag{21}$$

The orbital gyromagnetic factors are $g_l^\pi = 1$ for protons and $g_l^\nu = 0$ for neutrons. The spin gyromagnetic factors, obtained experimentally for free protons and neutrons, are $g_s^\pi = 5.5845$ and $g_s^\nu = -3.8263$, respectively.

The single-particle magnetic moment for a valence nucleon coupled to an inert core is expressed as follows:

$$\mu = \begin{cases} \left(j - \frac{1}{2}\right) g_l + \frac{1}{2} g_s & \text{for} \quad j = l + 1/2 \\ \dfrac{j}{j+1}\left(\left(j + \frac{3}{2}\right) g_l - \frac{1}{2} g_s\right) & \text{for} \quad j = l - 1/2, \end{cases} \tag{22}$$

which assuming the experimental values for gyromagnetic factors leads to the following expressions for the so-called Schmidt values:

$$\mu = \begin{cases} j + 2.293 & \text{for} \quad j = l + 1/2 \\ \dfrac{j}{j+1}\left(j - 1.293\right) & \text{for} \quad j = l - 1/2 \end{cases} \tag{23}$$

for protons and

$$\mu = \begin{cases} -1.913 & \text{for} \quad j = l + 1/2 \\ -1.913 \dfrac{j}{j+1} & \text{for} \quad j = l - 1/2 \end{cases} \tag{24}$$

for neutrons. These expressions, while providing limiting values, reflect the important differences between the values obtained for wave functions that are dominated by valence protons or neutrons. The deviations from Schmidt values, commonly observed, are due to the influence of other nucleons via meson-exchange currents as well as core polarisation [21], and therefore the single-particle moments are usually calculated using effective proton and neutron g factors. Nonetheless, nuclear magnetic moments remain very sensitive to the specific orbitals which are occupied by the valence nucleons, especially in the case of unpaired nucleons. The sensitivity to the number of nucleon pairs occupying a given orbital is much lower, and the influence of nucleon-pair excitations on the magnetic moments is referred to as second-order core polarisation.

2.4. Kumar-Cline sum rules

The electric quadrupole operator is a rank-2 spherical tensor, and thus transforms in a similar manner as the shape coordinates shown in Eq. 2. In the principal-axis frame, this tensor, $\mathcal{M}'(E2)$, can be expressed using two parameters:

$$\begin{aligned} \mathcal{M}'(E2, \mu = 0) &= \quad Q \cos\delta \\ \mathcal{M}'(E2, \mu = \pm 2) &= \quad \frac{1}{\sqrt{2}} Q \sin\delta. \end{aligned} \tag{25}$$

By definition, in this frame of reference the $\mathcal{M}'(E2, \mu = \pm 1)$ components vanish. The parameters Q and δ are analogous to the deformation parameters β_2 and γ, but instead of the mass distribution they represent the quadrupole charge distribution. The electromagnetic matrix elements measured in the laboratory frame and the deformation parameters defined by Eq. 25 can be linked via Kumar-Cline sum rules [12, 13]. The products of the $E2$ operators coupled to zero angular momentum

are rotationally invariant and thus their expectation values can be expressed by the Q and δ on one hand, and by products of $\langle I_j||\mathcal{M}(E2)||I_i\rangle$ $E2$ matrix elements on the other hand, as shown below for the lowest-order invariant:

$$\frac{(-1)^{2I_i}}{\sqrt{2I_i+1}}\sum_j \langle I_i||\mathcal{M}(E2)||I_j\rangle\langle I_j||\mathcal{M}(E2)||I_i\rangle \begin{Bmatrix} 2 & 2 & 0 \\ I_i & I_i & I_j \end{Bmatrix} = \frac{1}{\sqrt{5}\,(2I_i+1)}\sum_j \langle I_j||\mathcal{M}(E2)||I_i\rangle^2 = \frac{1}{\sqrt{5}}\langle Q^2\rangle \tag{26}$$

where {} is a $6j$ symbol. The sum formally extends over all states I_j that can be reached from the state in question I_i via a single $E2$ transition, however, typically only a few key states contribute to it. In particular, for the ground state of even-even nuclei, the sum is generally dominated by the coupling to the 2_1^+ state, which contributes well over 90% of the total. Thus

$$\langle Q^2_{0_1^+}\rangle \approx \left|\langle 2_1^+||\mathcal{M}(E2)||0_1^+\rangle\right|^2 \tag{27}$$

leading to the well-known expression linking β_2 and $B(E2; 0_1^+ \rightarrow 2_1^+)$:

$$\sqrt{\langle\beta_2^2\rangle} \approx \frac{4\pi}{3ZR_0^2}\sqrt{B(E2; 0_1^+ \rightarrow 2_1^+)/e^2}. \tag{28}$$

Products of three quadrupole tensors coupled to angular momentum zero yield

$$\frac{(-1)^{2I_i}}{2I_i+1}\sum_{jk}\langle I_i||\mathcal{M}(E2)||I_j\rangle\langle I_j||\mathcal{M}(E2)||I_k\rangle\langle I_k||\mathcal{M}(E2)||I_i\rangle \begin{Bmatrix} 2 & 2 & 2 \\ I_k & I_i & I_j \end{Bmatrix} = \sqrt{\frac{2}{35}}\langle Q^3\cos 3\delta\rangle. \tag{29}$$

For states with an axial prolate shape $\langle\cos 3\delta\rangle = 1$; for axial oblate states $\langle\cos 3\delta\rangle = -1$; for maximally triaxial or spherical states $\langle\cos 3\delta\rangle \approx 0$. Often, in evaluating experimental data, the approximation is made

$$\langle Q^3\cos 3\delta\rangle \approx \langle Q^2\rangle^{3/2}\langle\cos 3\delta\rangle. \tag{30}$$

The evaluation of the parameter $\cos 3\delta$ requires knowledge of a more extensive set of matrix elements, including their relative signs. If we consider a 0_1^+ ground state, the expression in Eq. 29 reduces to

$$\langle Q^3\cos 3\delta\rangle = -\sqrt{\frac{7}{10}}\sum_{jk}\langle 0_1^+||\mathcal{M}(E2)||2_j^+\rangle\langle 2_j^+||\mathcal{M}(E2)||2_k^+\rangle\langle 2_k^+||\mathcal{M}(E2)||0_1^+\rangle. \tag{31}$$

To a very good approximation, the terms $\langle 0_1^+||\mathcal{M}(E2)||2_1^+\rangle\langle 2_1^+||\mathcal{M}(E2)||2_1^+\rangle\langle 2_1^+||\mathcal{M}(E2)||0_1^+\rangle$ and $\langle 0_1^+||\mathcal{M}(E2)||2_1^+\rangle\langle 2_1^+||\mathcal{M}(E2)||2_2^+\rangle\langle 2_2^+||\mathcal{M}(E2)||0_1^+\rangle$ dominate the sum for even-even nuclei [22], thus

$$\langle\cos 3\delta\rangle \approx -\sqrt{\tfrac{7}{10}}\langle Q^2_{0_1^+}\rangle^{-3/2}\Big(\left|\langle 0_1^+||\mathcal{M}(E2)||2_1^+\rangle\right|^2\langle 2_1^+||\mathcal{M}(E2)||2_1^+\rangle + 2\langle 0_1^+||\mathcal{M}(E2)||2_1^+\rangle\langle 2_1^+||\mathcal{M}(E2)||2_2^+\rangle\langle 2_2^+||\mathcal{M}(E2)||0_1^+\rangle\Big). \tag{32}$$

Assuming identical charge and mass distributions, one can relate the Q^2 and δ quantities to the deformation parameters β_2 and γ by [23]

$$\langle Q^2 \rangle = q_0^2 \langle \beta_2^2 \rangle \tag{33}$$

and

$$\langle Q^3 \cos 3\delta \rangle = q_0^3 \langle \beta_2^3 \cos 3\gamma \rangle \tag{34}$$

with $q_0 = \frac{3}{4\pi} Z e R_0^2$ and $R_0 = 1.2A^{1/3}$ fm. The expressions depend upon the convention chosen for the collective variables; for example, using the lengths of the semi-axes leads to the formulas given in the appendix of Ref. [24].

A finite value of $\langle Q^2 \rangle$ may result from both a static deformation, β_{stat}, which would be the case for well-deformed rotational nuclei, as well as a dynamic deformation, β_{dyn}, that would arise for vibrational or non-collective systems. These can be distinguished based on the fluctuations in $\langle Q^2 \rangle$ that can be determined via

$$\sigma\langle Q^2 \rangle = \sqrt{\langle Q^4 \rangle - \langle Q^2 \rangle^2}\ ; \tag{35}$$

however, in order to obtain the $\langle Q^4 \rangle$ invariant, products of four matrix elements need to be considered, which requires a level of detail that is difficult to achieve experimentally. Similarly, fluctuations in $\langle Q^3 \cos 3\delta \rangle$ can be evaluated, requiring even more extensive experimental data. Another measure that can be used to infer if the deformation is static or dynamic is the magnitude of the spectroscopic quadrupole moment; values close to 0 imply a spherical, maximally triaxial or completely γ-soft shape, whereas for more axially symmetric nuclei large values imply static deformation.

2.5. Two-state mixing model

The phenomenological two-state mixing model is based on the assumption that the observed physical states with the same spin-parity $\mathrm{I}^{\pi}_{1,2}$ can be expressed as linear combinations of two unperturbed states $\mathrm{I}^{\pi}_{A,B}$:

$$\begin{aligned} \mid I_1^\pi \rangle &= +\cos\theta_I \mid I_A^\pi \rangle + \sin\theta_I \mid I_B^\pi \rangle \\ \mid I_2^\pi \rangle &= -\sin\theta_I \mid I_A^\pi \rangle + \cos\theta_I \mid I_B^\pi \rangle \end{aligned} \tag{36}$$

where $\cos\theta_I$, $\sin\theta_I$ are the mixing amplitudes, and θ_I is referred to as the mixing angle. The transitions between states belonging to different unperturbed structures are usually assumed to be forbidden. If the structures 1 and 2 form rotational bands, it is possible to deduce the mixing angles θ_I from the perturbation of level energies with respect to a rigid-rotor behaviour. They can also be obtained from e.g. $E0$ (Sec. 2.6) or $E2$ transition strengths. In the latter case, Eq. 36 applied to an example of $0^+_{1,2}$ and $2^+_{1,2}$ states yields the following relations between physical and unperturbed matrix elements:

$$\begin{aligned} \langle 2_1^+ || E2 || 0_1^+ \rangle \equiv M_{11} &= \sin\theta_0 \sin\theta_2 \langle 2_B^+ || E2 || 0_B^+ \rangle + \cos\theta_0 \cos\theta_2 \langle 2_A^+ || E2 || 0_A^+ \rangle \\ \langle 2_1^+ || E2 || 0_2^+ \rangle \equiv M_{12} &= \cos\theta_0 \sin\theta_2 \langle 2_B^+ || E2 || 0_B^+ \rangle - \sin\theta_0 \cos\theta_2 \langle 2_A^+ || E2 || 0_A^+ \rangle \\ \langle 2_2^+ || E2 || 0_1^+ \rangle \equiv M_{21} &= \sin\theta_0 \cos\theta_2 \langle 2_B^+ || E2 || 0_B^+ \rangle - \cos\theta_0 \sin\theta_2 \langle 2_A^+ || E2 || 0_A^+ \rangle \\ \langle 2_2^+ || E2 || 0_2^+ \rangle \equiv M_{22} &= \cos\theta_0 \cos\theta_2 \langle 2_B^+ || E2 || 0_B^+ \rangle + \sin\theta_0 \sin\theta_2 \langle 2_A^+ || E2 || 0_A^+ \rangle . \end{aligned} \tag{37}$$

Solving for θ_0, θ_2 yields

$$\begin{aligned} \tan\theta_0 &= R \pm \sqrt{R^2+1} \\ \tan\theta_2 &= \frac{M_{11}\tan\theta_0 + M_{12}}{M_{21}\tan\theta_0 + M_{22}} \end{aligned} \tag{38}$$

where

$$R = \frac{M_{11}^2 + M_{21}^2 - M_{12}^2 - M_{22}^2}{2(M_{11}M_{12} + M_{21}M_{22})}.$$

Assuming a weak mixing between the $2^+_{A,B}$ states (i.e., $\theta_2 = 0$), which is a reasonable approximation for e.g. $N \approx 60$ nuclei described in Sec. 3.4.1, Eq. 38 can be simplified to

$$\tan\theta_0 = \frac{\langle 0^+_2 || E2 || 2^+_1 \rangle}{\langle 0^+_1 || E2 || 2^+_1 \rangle}. \tag{39}$$

The two-level mixing model can be also applied to two-nucleon transfer cross sections, see Sec. 2.7, or α-decay hindrance factors (Sec. 3.7); in such cases it is assumed that the unperturbed configurations are the same in projectile and ejectile, or mother and daughter nuclei. Despite its simplicity, the two-state mixing model can describe remarkably well the experimental data for numerous nuclei, as demonstrated in the following sections. In some cases a satisfactory reproduction of all observables required its extension to three-level mixing, and such examples are presented in Sec. 3.1.2 and Sec. 3.1.3.

2.6. $E0$ transition strengths

$E0$ transitions, that are allowed only for $\Delta J = 0$ decays, are sensitive to the changes in the nuclear charge-squared radii since the $E0$ operator has the form

$$\mathcal{M}(E0) = \sum_i e_i r_i^2 \tag{40}$$

where the sum extends over the A bodies in the nucleus with their charges e_i and radial positions r_i. It can also can be expressed in terms of the collective variables from the Bohr model [26]:

$$\mathcal{M}(E0) = \frac{3Z}{4\pi}\left(\frac{4\pi}{5} + \beta_2^2 + \frac{5\sqrt{5}}{21\sqrt{\pi}}\beta_2^3\cos\gamma\right). \tag{41}$$

The usual quantity quoted when referring to $E0$ transitions are the $\rho^2(E0)$ values, defined via

$$\Gamma(E0) = \frac{1}{\tau(E0)} = \rho^2(E0)\sum_j \Omega_j(Z,\Delta E) \tag{42}$$

where $\Gamma(E0)$ is the partial width for the decay, $\tau(E0)$ the partial lifetime, and $\Omega(Z,\Delta E)$ the electronic factor that depends on the atomic number Z and the energy of the transition ΔE. The nuclear-structure information is contained in the $\rho(E0)$ quantity, defined by

$$\rho(E0) = \frac{1}{eR^2}\left\langle I_f \left| \mathcal{M}(E0) \right| I_i \right\rangle. \tag{43}$$

The $E0$ transition strengths depend on the mixing of configurations that have different mean-square charge radii [25]. In a two-level mixing solution,

$$\rho^2(E0) = \frac{Z^2}{R^4}\cos^2\theta\,\sin^2\theta\left(\langle r^2\rangle_A - \langle r^2\rangle_B\right)^2 \tag{44}$$

where $\langle r^2\rangle_A = \langle\Psi_A|r^2|\Psi_A\rangle$ is the mean charge-squared radius for the wave function $|\Psi_A\rangle$, and similarly for $\langle r^2\rangle_B$. Using the operator expressed in the collective variables, and with the deformation parameters for the two states defined as (β_A, γ_A) and (β_B, γ_B), the $E0$ strength is characterized by [25, 26]

$$\rho^2(E0) = \left(\frac{3Z}{4\pi}\right)^2\cos^2\theta\,\sin^2\theta\cdot\left[\left(\beta_A^2-\beta_B^2\right)+\frac{5\sqrt{5}}{21\sqrt{\pi}}\left(\beta_A^3\cos\gamma_A-\beta_B^3\cos\gamma_B\right)\right]^2. \tag{45}$$

As the determination of a $\rho^2(E0)$ value requires not only the observation of an $E0$ transition and a determination of its relative intensity but also the level lifetime, the experimental information of this kind is still rather limited. Additionally, the $\rho^2(E0; I \to I)$ values for $I \neq 0$ are often affected by large uncertainties since precise intensities for the contribution of the $M1$ and $E2$ multipolarity conversion electrons to the transition must be known.

Using shell-model harmonic-oscillator wave functions, the r^2 operator only depends on the principal quantum number N and within a major shell, the $E0$ transitions should vanish. Thus, $E0$ transitions must involve configurations from different harmonic oscillator shells. In Ref. [27], important contributions to the $E0$ strength were shown to arise from the core polarization.

2.7. Single-particle content via single-nucleon transfer reactions

Single-nucleon transfer reactions, by definition, probe the single-particle composition of the nuclear wave functions. The initial ground-state wave function $|\Psi_{I_i}\rangle$ may correspond to a quasiparticle vacuum (even-even nuclei), one-quasiparticle state (odd-mass nuclei), or two-quasiparticle state (odd-odd nuclei), or a multi-particle (mp) or multi-hole state (mh)[2]. Single-nucleon transfer reactions give information on the overlap of the wave functions of the initial and the final state, where the final state is of the form

$$\Phi_{I_fM_f} = \sum_{M_i,m} a^\dagger_{jm}\left|\Psi_{I_iM_i}\right\rangle\left(I_iM_ijm\middle|I_fM_f\right). \tag{46}$$

The spectroscopic factor S_{jl} (or alternatively written as C^2S, where C refers to an isospin Clebsch-Gordan coefficient) is defined as

$$S_{jl} = \left|\langle\Psi_{I_fM_f}\middle|\Phi_{I_fM_f}(j,I_i)\rangle\right|^2 = \frac{\left|\left\langle\Psi_{I_f}\middle\|\,a^\dagger_j\,\middle\|\Psi_{I_i}\right\rangle\right|^2}{2I_f+1} \tag{47}$$

[2]The language of quasiparticles is appropriate for nuclei in the so-called superfluid or superconducting regime, where the pairing matrix elements exceed the spacing of the single-particle energy levels, as is typical for deformed nuclei. In contrast, the mh or mp terminology is better suited for nuclei in the "normal" phase, where the single particle spacing greatly exceeds the pairing matrix elements, which is the case near closed shells or in light nuclei. The pairing phase may be different for neutrons and protons, depending on the density of states near the Fermi level.

where l is the orbital angular momentum of the single-particle orbital into which the particle is transferred. This orbital angular momentum can be determined from the angular distribution of the ejectiles in the reaction for the population of a specific final state, whereas j is often inferred from knowledge of the available orbitals near the Fermi surface.

In the following, we focus our attention on the initial and final states of the nuclei under investigation, and we assume that the collision partners in the process have simple structures that are well understood, as is the case for light nuclei up to α particles. The spectroscopic strength can be extracted through a comparison of the experimental angular distributions of the ejectiles of the reaction with those predicted with a distorted-wave Born approximation (DWBA) calculation. The spectroscopic factors are excellent tools to locate the single-particle strength in odd-A nuclei, and can also be used to determine the orbital occupancies in even-even nuclei. Shape-coexisting states can be populated if a component of their wave function has a significant overlap with the initial ground-state wave function. If we consider a reaction in which the nucleon is removed, for example, from an initial state with a mp configuration, it can populate final states with the configuration of $(m-1)p$ or mp-1h. An analogous situation can arise in reaction in which a nucleon is added to an initial state with a mh configuration – it can populate final states with $(m-1)h$ or mh-1p configurations.

Sum rules for transfer reactions provide a powerful tool to determine nucleon occupancies. For a specific j transfer, the number of holes h and particles p can be found from (assuming a spin 0 for the initial state)

$$h = \sum_i (2j+1) S^i_{adding}, \quad p = \sum_i S^i_{removing} \tag{48}$$

with the summation extending over all states for the same values of the transferred angular momentum j and l. The spectroscopic factors are defined as above for the addition of nucleons, such as a (d,p) stripping reaction, and the removal of nucleons, as in a (d,t) pickup reaction. When these reactions are performed using the same initial nucleus, e.g., the same target used for the (d,p) and (d,t) reactions, the numbers of particles and holes sum to $(2j+1)$.

2.8. Probing pairing content via two-nucleon transfer reactions

Since shape coexistence manifests itself via strong correlations in the wave functions, experiments that probe these correlations are of utmost importance. Among the most important are the pairing correlations, which can be described as the binding of two nucleons in $J^\pi = 0^+$ states, and the correlation effect can be expressed in terms of a pair field that is responsible for creating and annihilating two particles in time-reversed orbits. Reactions that involve the transfer of two alike particles, such as the (p,t) two-neutron transfer or $(^3\mathrm{He},n)$ two-proton transfer reactions, specifically probe such pairing correlations.

For the two-nucleon transfer process, the spectroscopic amplitudes are defined by

$$B(I_f;[j_1 j_2]J,I_i) = \frac{1}{\sqrt{1+\delta_{j_1 j_2}}} \left\langle \Psi_{I_f M_f} \middle| \left[\left[a^\dagger_{j_1} \otimes a^\dagger_{j_2} \right]_J \otimes \Psi_{I_i} \right]_{I_f M_f} \right\rangle \tag{49}$$

where the two nucleons, with single-particle angular momenta j_1 and j_2 that couple to angular momentum J, couple to the initial angular momentum I_i resulting in the final angular momentum

I_f. To a very high degree of accuracy, when the two transferred nucleons are both of the same type, they couple to total spin $S = 0$, so $J = L$. Unlike single-nucleon transfer reactions, the spectroscopic amplitudes must be added with the final sum squared, so that there may be interference effects. In general, multiple pairs of particles that can couple to J can contribute to the sum, depending on the availability of the orbitals near the Fermi surface. The cross-section angular distributions are sensitive to the L value, and while the magnitude of the cross section is sensitive to the j components, the shapes of the angular distributions generally are not. Thus spectroscopic strengths for the transfer of a particular pair cannot be extracted from the experimental data, and often the ratios of cross sections are used to infer the nature of the final state. When available, two-nucleon amplitudes from shell-model calculations can be used to construct the spectroscopic amplitudes and combined with a reaction code to predict the cross sections.

The two-nucleon transfer cross section for the $0^+_{gs} \rightarrow 0^+_{gs}$ transition typically dominates over all other transitions, and in situations where excited 0^+ states are two-particle or two-quasiparticle states, their population cross sections are a few percent of the ground-state cross section. Exceptions to this may arise when the excited states also possess significant pairing correlations similar to those of the ground state, for example when they are mixed with the ground state, or when they have the form of pairing vibrations. Enhancements in the cross sections to excited 0^+ states may also occur when the normal pairing regime has broken down, for example as the structure evolves from that near closed shells (described as the "normal" pairing phase) to open-shell well-deformed nuclei (described as a "superfluid" pairing phase). The large two-nucleon transfer cross sections that amount to tens of percent or more relative to the cross section for population of the ground state thus signify a highly collective transition and consequently indicate that the final 0^+ state has a very special character.

3. Recent progress in experimental shape-coexistence studies

3.1. Shape coexistence in light nuclei

3.1.1. Light $N \simeq Z$ nuclei

Shape coexistence in the light $N \simeq Z$ nuclei is often closely connected to the discussion of clustering aspects in nuclei, especially those of α-particle clusters. The high binding energy of the α particle naturally led to it being considered as a sub-unit on which to build nuclear states that are pictured as geometric arrangements of the clusters in much the same way that molecules are geometrical arrangements of atoms. The experimental evidence for cluster states has been outlined in a number of excellent reviews (see, e.g., Refs. [28–30]). Since the field of clusters in nuclei has been recently reviewed by Freer *et al.* [30], and we could not do it proper justice, we refer the reader instead to the reviews listed above for the recent results in this very active area. As an example, even in the well-studied nucleus ^{12}C, recent measurements (see, e.g., Refs. [31–35]) resulted in the assignment of additional rotational states built on the 0^+_2 (the so-called Hoyle) state and identification of the $K^\pi = 3^-$ rotational band [36] that has a significantly different moment of inertia than the band built on 0^+_2.

The superdeformed band in ^{24}Mg was suggested [2] to include the states at 6.433 MeV (0^+_2), 7.349 MeV (2^+_3), and 8.439 MeV (4^+_3). In much earlier work, Warburton *et al.* [38] had proposed instead the 4^+_4 state at 9.301 MeV to be the third member of this band. The $2^+_3 \rightarrow 0^+_2$ transition

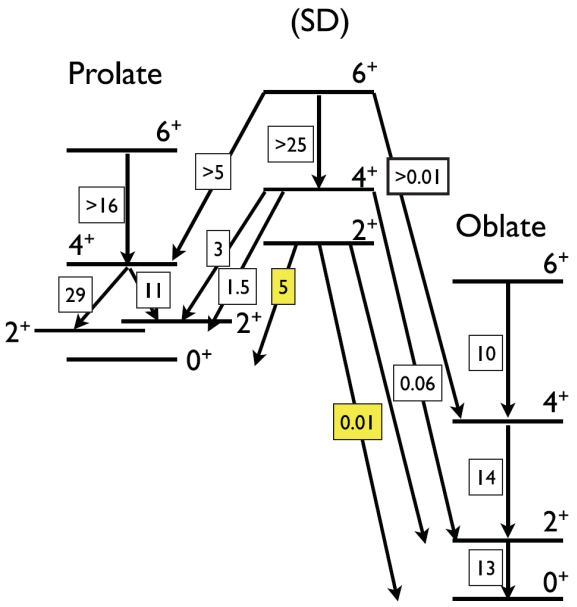

Figure 4: Partial level scheme for ^{28}Si showing the oblate ground-state band, the $K = 0$ prolate band built on the 6.691-MeV 0^+_2 state, and the candidate superdeformed band with the 2^+ member at 9.796 MeV. The transitions are labelled with $B(E2)$ values in W.u. The values highlighted in the yellow boxes for decay from the 2^+ member of the proposed superdeformed band are derived assuming 0.01 W.u for the transition to the ground state. Figure taken from Ref. [41].

is unobserved, and both 4^+ candidates decay to the 2^+_3 level with enhanced $B(E2)$ values. There are several conflicting results for the 4^+ states in question. In the evaluated data [39], the 4^+ state at 8.439 MeV has a lifetime $\tau = 5.5(16)$ fs, whereas Warburton *et al.* [38] report 26(10) fs. The potential 4^+ state at 9.301 MeV proposed by Warburton *et al.* [38] is not adopted in the evaluated data, and the situation is rather confused by the potential presence of a triplet of levels at 9.3 MeV. Using the values from Ref. [38] for consistency, the $B(E2; 4^+_{3,4} \rightarrow 2^+_3)$ values are 11(5) W.u. and 15(6) W.u., respectively. Since the 8.439-MeV state is populated in the decay of the $K = 4$ ^{24}Al ground state with a log ft value of 3.9, this state is favoured as a $K = 4$ band head [38]. Regardless of the assignment of the band members, the 0^+_2 state has been determined to be highly deformed. Its $E0$ decay was recently observed [40] to proceed with one of the largest $E0$ strengths observed across the entire nuclear chart, namely $10^3 \times \rho^2(E0; 0^+_2 \rightarrow 0^+_1) = 380(70)$. A two-level mixing calculation, assuming a maximum mixing scenario, leads to $\Delta(\beta^2_2) \gtrsim 0.43$. The ground-state band $\beta_2 = 0.497(2)$, extracted from the $B(E2; 2^+_1 \rightarrow 0^+_1)$ value via Eq. 28, implies that the superdeformed band in ^{24}Mg has $\beta_2(0^+_2) \simeq 1$ [40]. In view of the conflicting results regarding the 4^+ states discussed above, the spectroscopy of the potential members of the 0^+_2 band should be re-investigated, in particular the decay branches of the $4^+_{3,4}$ states and their lifetimes, and the unobserved $2^+_3 \rightarrow 0^+_2$ transition. The understanding of the shape of the 0^+_2 state, in particular, is of prime importance.

A candidate superdeformed band was also recently proposed in ^{28}Si [41]. An oblate shape

is assigned to the ground-state band based on a Coulomb-excitation measurement [42], which yielded a spectroscopic quadrupole moment of the 2_1^+ state of $Q = 0.17(5)$ eb. A band built on the 0_2^+ state, with transitional quadrupole moments of $|Q_t| = 0.876^{+0.110}_{-0.085}$ eb, was identified by Glatz *et al.* [43] and suggested to have a prolate shape. The recent work [41] proposed a superdeformed band as shown in Fig. 4, and noted that its 4^+ and 6^+ members were strongly populated in α-particle transfer reactions, and, most remarkably, that the 6^+ member was populated with a significant $g_{9/2}$ component in the ^{12}C(^{20}Ne,α)^{28}Si reaction [44]. Thus, ^{28}Si potentially possesses three distinct deformed shapes, but further work is required to characterize them. A key question is the location of the potential 0^+ band head of the superdeformed band that in principle could be determined through particle transfer reactions such as ^{30}Si(p,t) or ^{26}Mg(^{3}He,n). Lifetime measurements of the suggested rotational band members for the prolate and superdeformed structures would also be of great interest.

3.1.2. Shape coexistence and the "island of inversion" at N=20

Already in 1970s, mass measurements demonstrated that the binding energies of ^{31,32}Na [45] and ^{31,32}Mg [46] are unexpectedly large and do not present a decrease that usually follows a shell closure. Combined with a large increase in mean-square charge radii observed in ^{29,30,31}Na [47], this suggested a sudden onset of deformation, further supported by the observation of a low-lying 2_1^+ state [48] and an enhanced $B(E2; 2_1^+ \rightarrow 0_1^+)$ transition strength in ^{32}Mg [49–55]. This region, commonly referred to as an "island of inversion", is now understood to include nuclei whose collective ground-state properties result from an inversion of the spherical ground-state configurations with deformed intruder states related to excitations across the $N = 20$ shell gap. Strong experimental evidence exists for coexistence of these structures and their different deformations. In particular, direct reactions and laser spectroscopy have been extensively used to pin down the underlying microscopic configurations. A recent review [56] summarizes the existing experimental data on $N = 19$ and $N = 21$ isotones, with a particular focus on conclusions that can be drawn from the properties of ground and isomeric states. To complement this evaluation, we focus in the following on short-lived excited states and their decay properties.

The deformed character of the ground state in ^{32}Mg, suggested by the lowering of the 2_1^+ energy (886 keV, with respect to 1483 keV in ^{30}Mg) was supported by identification of the 4^+ and 6^+ members of the rotational ground-state band [57, 58]. The observed evolution of the moment of inertia was tentatively attributed to the admixture of a $4p-4h$ configuration increasing with spin [58]. The $B(E2; 2_1^+ \rightarrow 0_1^+)$ values resulting from several intermediate-energy Coulomb-excitation studies [49–54] as well as a fast-timing measurement following β decay of ^{32}Na [55] display a rather large spread, but all of them point to a significant deformation of at least $\beta_2 = 0.38$.

The excited 0_2^+ state in ^{32}Mg was identified at 1058 keV in a ^{30}Mg$(t,p)^{32}$Mg two-neutron transfer study [59] performed in inverse kinematics. A strong reduction of the number of observed γ-ray decays of this state with respect to the number of corresponding protons detected was attributed to the decay of the recoiling ^{32}Mg occurring far away from the reaction target, leading to the conclusion that the 0_2^+ lifetime is longer than 10 ns. On the other hand, an upper limit for this lifetime, 38 ns, was deduced by combining the upper limit for the cross section to populate the 0_2^+ state via two-proton removal [60] with the number of its observed decays in flight following the same reaction [61]. These lifetime constraints correspond to the $B(E2; 2_1^+ \rightarrow 0_2^+)$ value in the

range between 28 and 122 e^2fm^4, a precision that is insufficient to draw meaningful conclusions regarding the structure of the 0^+_2 state.

The $B(E2; 2^+_1 \rightarrow 0^+_1)$ value in ^{30}Mg was measured in low- [62] and intermediate-energy Coulomb excitation [50, 52], with the result of Ref. [52] being considerably larger than the other two. All three values correspond to $\beta_2 \geq 0.35$, and a comparison of evaluated $B(E2; 2^+_1 \rightarrow 0^+_1)$ values in ^{30}Mg and ^{32}Mg [63, 64] suggests an increase of collectivity in the latter, in line with the decreasing 2^+_1 excitation energy. The ground-state band was extended to spin 4^+ in a ^{14}C(^{18}O,2p)^{30}Mg reaction study [65], and the $E(4^+_1)/E(2^+_1)$ energy ratio of 2.3 is far from the value expected for an axial rotor. A long lifetime of 3.9(4) ns was measured for the 1789-keV state in ^{30}Mg [55], leading to a tentative 0^+ spin-parity assignment, which was later confirmed by a direct observation of its $E0$ decay to the ground state [66] and γ-ray angular correlations [67]. The measured $10^3 \times \rho^2(E0; 0^+_2 \rightarrow 0^+_1)$ transition strength of 26.2(75) [66] is consistent with weak mixing between the wave functions of the $0^+_{1,2}$ states. The (2^+) state at 2.467 MeV was proposed to be a member of the band built on 0^+_2 [55], while the sequence of (2^+) and 3^+ states at 3.543 MeV and 4.695 MeV, respectively, was interpreted as the γ band and linked to significant triaxiality of ^{30}Mg [67].

It was shown [68, 69] that the measured ^{30}Mg(t, p)^{32}Mg reaction cross sections [59] as well as evaluated $B(E2; 2^+_1 \rightarrow 0^+_1)$ values in ^{30,32}Mg [63, 64] and $\rho^2(E0; 0^+_2 \rightarrow 0^+_1)$ in ^{30}Mg [66] can be reproduced assuming three-level mixing of normal-order, $2p-2h$ and $4p-4h$ configurations. The conclusion of this analysis is that the ground state in ^{30}Mg is dominated by the normal-order configuration, while the ground state in ^{32}Mg has a predominantly intruder configuration, involving both $2p-2h$ and $4p-4h$ excitations. This is also consistent with the measured cross sections of one-neutron removal in this mass region. For example, some admixture of the intruder configuration to the ground state in ^{30}Mg is necessary to explain the population of negative-parity states in ^{29}Mg [70]. Moreover, a study of one-neutron removal from ^{31}Mg yielded a spectroscopic factor of 0.20 ± 0.04 for the 0^+_2 state in ^{30}Mg [71], which is lower than what would be expected for a pure $2p-2h$ configuration, and hence was interpreted as resulting from an important admixture of the $4p-4h$ configuration to this state. A consequence of the three-level mixing is the prediction that a 0^+_3, at approximately 2.2 MeV, is predominately the $0p-0h$ state [68, 69], however the two-proton knockout reaction failed to locate the required strength, indicating that either the reaction is strongly quenched, or that the $0p-0h$ configuration is highly fragmented or even above the neutron separation energy [61].

There exists strong experimental evidence that the ground state in ^{31}Mg is dominated largely by the $2p-2h$ intruder configuration, which includes its g factor [72] and an observation of a deformed rotational band built on the ground state, discussed below. Configurations of several states in ^{31}Mg can also be inferred from their selective population in direct reactions. The measured cross sections of one-nucleon removal reactions leading to ^{31}Mg are presented in Fig. 5. One-neutron knockout from ^{32}Mg is expected to favour the deformed intruder states, and this reaction [70] populated strongly the ground state, as well as the levels at 220 keV and 461 keV (with tentative spin assignments of $(3/2^-)$ and $(7/2^-)$, respectively). Additionally, population of the states at 945 keV and 2.244 MeV was observed. In contrast, one-proton knockout from ^{32}Al [73], having a normal-order configuration of the ground state, preferentially populated the states at 673 keV and 2015 keV (assigned as $3/2^+$ and $5/2^+$, respectively, in Ref. [74]), which consequently were

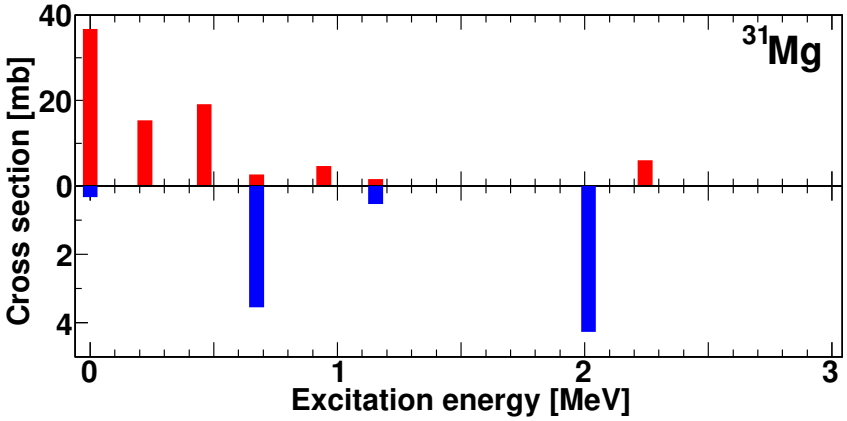

Figure 5: Cross sections for the population of states in ^{31}Mg in one-nucleon removal reactions. The bars in the top panel represent the cross sections measured in one-neutron knockout from ^{32}Mg [70], and those in the bottom panel are from one-proton knockout from ^{32}Al [73]. The former favours deformed intruder states, i.e. the ground state and the $(3/2^-)$ and $(7/2^-)$ states at 220 keV and 461 keV, respectively, and the latter the normal-ordered $3/2^+$ and $5/2^+$ states at 673 keV and 2015 keV, respectively. Note different cross-section scales used in the two panels.

suggested to have normal-order configurations. A negligible population of the ^{31}Mg ground state in this reaction is consistent with its nearly pure intruder configuration.

The decay scheme of ^{31}Mg has been extended and spins and parities of several states firmly assigned in β-γ spectroscopy following β decay of spin-polarised ^{31}Na [74, 75]. As the ground state of the parent has a predominantly intruder character, this decay preferentially feeds intruder states in the daughter nucleus. Two rotational bands dominated by the intruder configuration were proposed: a $K = 1/2^+$ deformed band based on the ground state and including, among others, the $5/2^+$ state at 945 keV, and a $K = 1/2^-$ deformed band, for which the lowest members are the states at 220 keV and 461 keV. Additionally, the 2.244-MeV level (with a firm spin-parity assignment of $1/2^+$) was strongly populated, in line with its proposed intruder configuration, which is further supported by its decay pattern favouring states in the $K = 1/2^+$ band. For each of the two proposed deformed bands, one in-band $B(E2)$ value is known. Both the $B(E2; 5/2^+ \rightarrow 1/2^+)$ value of 61(7) e^2fm^4, or 10.5(12) W.u. ($K = 1/2^+$ band) measured in low-energy Coulomb excitation [76] and $B(E2; (7/2^-) \rightarrow (3/2^-)) = 67(6)\ e^2\text{fm}^4$, or 11.6(10) W.u. ($K = 1/2^-$ band) obtained from fast timing [55] are comparable with the $B(E2; 2_1^+ \rightarrow 0_1^+)$ values in ^{30,32}Mg and indicate collective enhancements. In contrast, a considerably lower $B(E2; 3/2^+ \rightarrow 1/2^+) = 10(4)\ e^2\text{fm}^4$ was obtained for the decay of the level at 673 keV to the ground state [76], in line with different configurations of the initial and final states.

A large g factor of the ground state in ^{34}Al was interpreted as resulting from an important $2p-2h$ intruder admixture to the normal-order configuration [77]. A very different g factor obtained for the low-lying 1^+ isomer in ^{34}Al led to its association with a $1p-1h$ intruder configuration [78]. The absolute value of the quadrupole moment of this state is about 50% larger than that of the normal-order ground state in ^{32}Al [78], evidencing an enhanced deformation due to the particle-

hole excitation across the $N = 20$ shell gap. Based on β-γ and β-γ-γ coincidences observed in the β decay of ^{34}Mg, the 1^+ isomer was shown to be located only 47 keV above the normal-order ground state in ^{34}Al, which identifies ^{34}Al as a crossing point of the normal-order and intruder configurations [79].

Detailed experimental data also reveal coexistence of normal-order and intruder structures in ^{34}Si. An intermediate-energy Coulomb-excitation study [80] identified the 2^+_1 state in ^{34}Si at 3.3 MeV. The observed hindrance of the $B(E2; 2^+_1 \rightarrow 0^+_1)$ value, equal to 17(7) e^{2}fm^4, was interpreted as resulting from a small overlap between the $2p-2h$ wave function of the 2^+_1 state and the normal-order configuration of the ground state [80]. A candidate for a 2^+ state based on the normal-order configuration was observed at 5.33 MeV in the ^{36}S(^{11}B,^{13}N)^{34}Si two-proton pickup [81] and in the ^{34}P(^{7}Li, ^{7}Be)^{34}Si charge-exchange reaction [82]. This supports its proton character, which is expected for a normal-order configuration. This state is probably identical to that observed at 5.348 MeV in a recent β-decay study [83], which was found to be fed weakly by the decay of the 1^+ intruder isomer in ^{34}Al, consistent with its normal-order character.

The excited 0^+_2 state at 2.719(3) MeV was populated in β decay of ^{34}Al [84] and from the measured $10^3 \times \rho^2(E0; 0^+_2 \rightarrow 0^+_1) = 13(1)$ a rather weak mixing of the 0^+ states of $\cos^2\theta_0 = 0.78(9)$ was estimated [84]. The measured branching ratio for the 0^+_2 decay resulted in a $B(E2; 2^+_1 \rightarrow 0^+_2)$ value of 61(40) e^{2}fm^4 [84], while its later remeasurement [83] led to the reduction of the $B(E2; 2^+_1 \rightarrow 0^+_2)$ value to 47(19) e^{2}fm^4, with the uncertainty of this value dominated by the precision of the $B(E2; 2^+_1 \rightarrow 0^+_1)$ measurement [80]. The corresponding β_2 deformation of the deformed configuration, 0.27(5), is lower than those of the ground-state structures in ^{30,32}Mg. Finally, a 2^+_2 state at 4.519 MeV was proposed in a β-decay study [85] and based on its decay properties and excitation energy with respect to that of the 2^+_1 state, the importance of triaxiality in the structure of ^{34}Si was discussed. While this state has been confirmed by a subsequent β-decay study [83], contrary to the findings of Ref. [85] its decay branch to the 0^+_2 state has not been observed, and the corresponding upper limit points to it being much weaker than what is expected for a triaxial state.

The information on shape coexistence in lighter $N \approx 20$ nuclei is scarce due to their proximity to the neutron dripline, but one should note that multiple multiparticle-multihole configurations in ^{30}Na were identified via a combination of one-proton, one-neutron and one-proton–one-neutron removal reactions [86].

3.1.3. Highly deformed structures around ^{40}Ca

Highly deformed structures were identified in ^{40}Ca [87], ^{42}Ca [88], ^{44}Ti [89] and ^{38}Ar [90] using particle spectroscopy following single- and multi-nucleon transfer reactions. A compilation of these results can be found in Ref. [6]. In particular, two bands interpreted as based on $4p-4h$ and $8p-8h$ configurations were populated in ^{40}Ca via a ^{32}S(^{12}C,α)^{40}Ca cluster-transfer reaction [87]. Figure 6 shows the lowest-lying levels assigned to the 0^+_2 ($4p-4h$) and 0^+_3 ($8p-8h$) structures in ^{40}Ca, together with the observed γ band. Somewhat later, advancements in high-resolution γ-ray spectroscopy enabled extending these bands to high spin, and their strongly deformed rotational character was confirmed by the measured moments of inertia and in-band $B(E2)$ values [91–95]. Table 1 lists β_2 deformation parameters obtained from the transitional quadrupole moments measured for the known deformed structures in ^{40}Ca [91], ^{36}Ar [92], ^{38}Ar [93], ^{40}Ar [94] and ^{35}Cl [96], assuming axial symmetry, via Eq. 17. The existing experimental information for the analo-

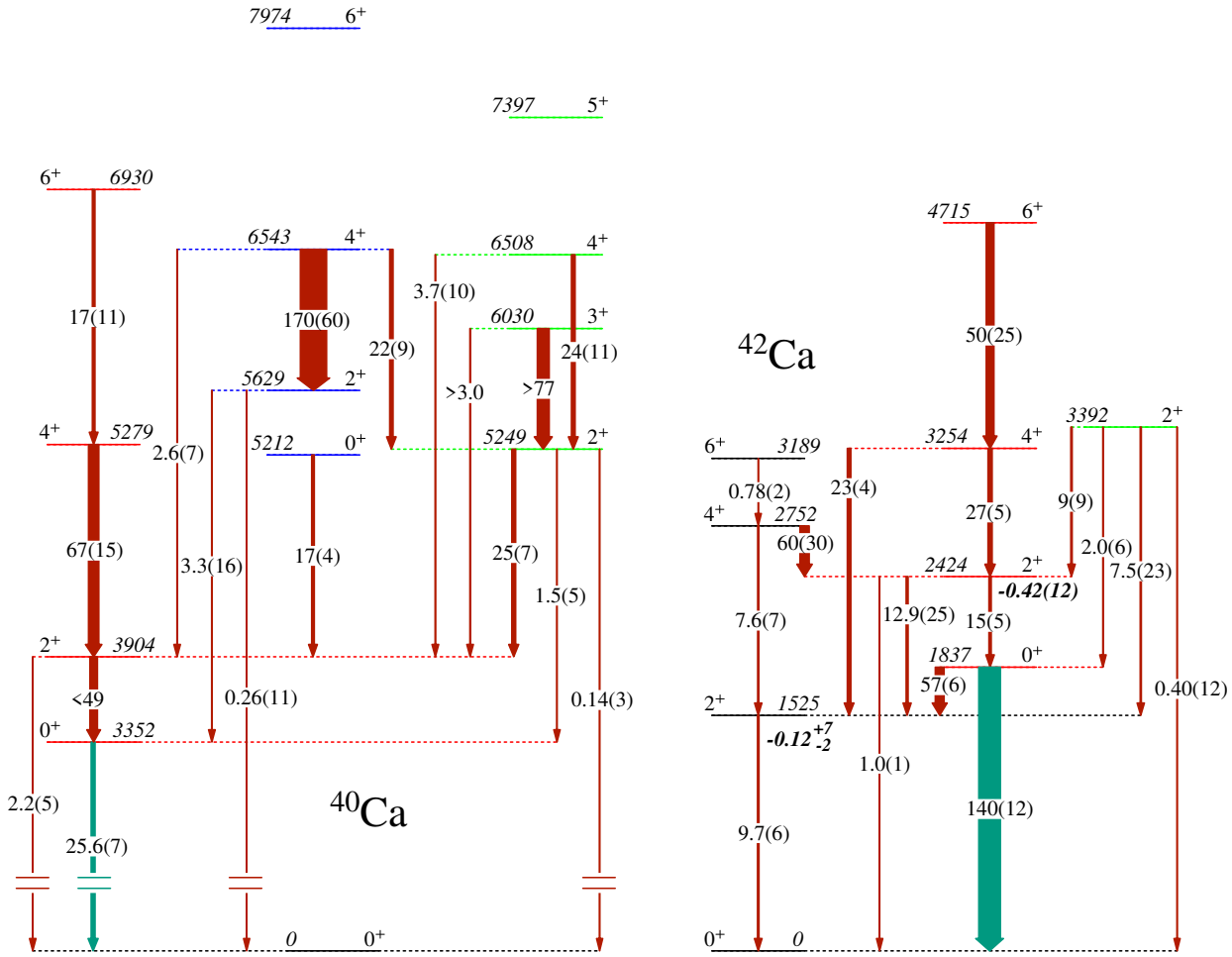

Figure 6: Selected levels in ^{40}Ca and ^{42}Ca, labelled with their I^{π} values and excitation energies in keV. Rust coloured arrows indicate transitions with $E2$ multipolarity and are labelled with $B(E2)$ values in W.u., and $E0$ transitions are represented as green coloured and labelled with their $10^3 \times \rho^2(E0)$ values, with uncertainties in parentheses (note that in cases of asymmetric uncertainties, they have been averaged for simplicity of display). For ^{40}Ca, rotational bands built on the 0_2^+ and 0_3^+ states as well as the K=2 band are presented, with all excited states drawn lowered by 2 MeV. For ^{42}Ca, the states built on the ground-state configuration are shown in addition to the 0_2^+ rotational band and the presumed K=2 bandhead. The measured quadrupole moments of the 2_1^+ and 2_2^+ states, expressed in eb, are given in italics below the levels. Data are taken from Refs. [39, 97, 102].

gous structure in ^{44}Ti [95] is also presented, as well as the β_2 deformation parameters for the 0_2^+ and 2_2^+ states in ^{42}Ca obtained from the $\langle Q^2 \rangle$ quadrupole invariants [97]. The Q_t values for specific nuclei were obtained under different assumptions. In the lifetime studies of ^{40}Ca [91] and ^{40}Ar [94] it was necessary to fit all measured lineshapes for transitions in the deformed band with a single Q_t value. For ^{36}Ar [92], ^{38}Ar [93], and ^{35}Cl [96] individual lifetimes were determined, and the β_2 deformation parameters were deduced from the weighted averages of Q_t values obtained for several decays in the middle part of the band, as those were assumed to be free of mixing with

less deformed states in the bottom of the band, and also not affected by a reduction of collectivity at higher spin observed when approaching band termination. It is worth noting that in the study of ^{38}Ar [93] various fit methods and feeding hypotheses have been tested and the obtained lifetimes were found to depend very strongly on the assumptions made. In a later measurement on ^{40}Ca [98], instead of a common fit of all lineshapes in the entire band built on the 0^+_3 state, two separate fits limited to its top and bottom sections were performed, yielding transitional quadrupole moments of $1.81^{+0.41}_{-0.26}\pm0.21$ eb and $1.18^{+0.06}_{-0.05}\pm0.13$ eb, respectively, where the first uncertainty listed is statistical and the second is systematic. The important reduction of collectivity at low spin was attributed to an admixture of configurations involving fewer nucleon pairs promoted through the N, Z=20 shell gaps.

For comparison, for each of the nuclei in question, Tab. 1 provides the β_2 deformation parameters for the ground states, calculated via Eq. 17 from the transitional quadrupole moments for the $2^+_1 \rightarrow 0^+_1$ transitions in even-even nuclei [99] and for the $11/2^- \rightarrow 7/2^-$ transition in ^{35}Cl [96]. One can see that while the β_2 parameters deduced for the highly deformed structures are distinctly larger than those of the ground states, they span a rather broad range, starting from around 0.3 and reaching values observed elsewhere only for superdeformed bands in the $A \sim 150$, $A \sim 190$ and $A \sim 230$ regions. However, contrary to those, the highly deformed structures in the $A \sim 40$ region are linked to less deformed states by intense γ-ray transitions, suggesting an important configuration mixing.

The mixing of the ground-state band members with more deformed states is also supported by the important population of the latter in single-nucleon transfer (e.g., ^{41}Ca(d, p)^{42}Ca [88]), the observed enhancement of quadrupole moments of the 2^+_1 states in Ca isotopes, see Tab. 2, as well as by the small positive values of g factors measured for these states in ^{42,44}Ca [100]. Since for the normal-order configuration of the ground states, with valence neutrons occupying the $f_{7/2}$ orbital, large negative values would be expected, this result suggests a substantial admixture of a multiparticle-multihole configuration in the 2^+_1 states, at a level close to 50% [100]. The mixing of the ground and 0^+_2 states can be estimated from the measured $E0$ transition strengths, which are known for ^{40,42,44,48}Ca and ^{38}Ar as listed in Tab. 2. One should note here a significant difference between the $\rho^2(E0)$ values obtained for ^{42,44}Ca from measurements of e^+–e^- pair production and those resulting from electron scattering studies, with the latter being lower by about one third [101, 102]. Assuming, whenever available, β_2 values from Tab. 1 for the deformed 0^+ state and a spherical shape for the normal-order configuration of the ground state, one can deduce the mixing angles $\cos^2\theta_0$ using Eq. 45, which are listed in Tab. 2. The differences between the values obtained for individual nuclei are rather large, but they all seem to point to rather limited mixing of the 0^+ states, in contrast to the findings of Ref. [100] for the 2^+ states in ^{42,44}Ca. It is interesting to note that a particularly low mixing observed for the 0^+ states in ^{38}Ar coincides with a measurement for the neighbouring ^{40}Ar of a spectroscopic quadrupole moment of the 2^+_1 state consistent with its $(d_{3/2})^{-2}$ character, which suggests a very limited mixing of the 2^+ states. The g factors measured for the 2^+_1 states in ^{36,38}Ar [103], ^{40}Ar [104] and ^{44}Ti [105] can also be explained without taking into account multiparticle-multihole excitations across the $N, Z = 20$ shell gap. On the other hand, the recently remeasured lifetime of the 2^+_1 state in ^{44}Ti [106] cannot be reproduced without accounting for those. It is clear that the existing information on the mixing of spherical and deformed configurations in the $A \sim 40$ region is incomplete and it is difficult to make firm conclusions about its

Table 1: Deformation parameters, β_2, of ground-state and excited bands in nuclei around ^{40}Ca exhibiting shape coexistence, obtained from experimental $B(E2)$ values, or, in the case of ^{42}Ca, from $\langle Q^2 \rangle$ invariant quantities. Dominant configurations ascribed to the deformed structures are also given, as well as bandhead energies. When two uncertainties are listed, the first one is statistical and the second one systematic.

	ground-state band	deformed structure		
isotope	β_2	β_2	dominant configuration	bandhead energy [MeV]
^{40}Ca	0.12(1)[99]	$0.59^{+0.14}_{-0.11}$ [91]	$8p-8h$	5.2
		$0.59^{+0.11}_{-0.07}\pm0.06$ [a][98]		
		$0.40\pm0.02\pm0.05$ [b][98]		
		0.27 ± 0.05 [91]	$4p-4h$	3.4
^{42}Ca	0.23(1)[99]	0.43(4) (0^+_2) [97]	$6p-4h$	1.8
		0.45(4) (2^+_2) [97]		
^{36}Ar	0.20(1)[99]	0.46 ± 0.03 [92]	$4p-8h$	4.3
^{38}Ar	0.135(5)[99]	$0.42^{+0.11}_{-0.08}$ [c] [93]	$4p-6h$	3.4
		>0.68 [93]	$4p-6h$	4.7
^{40}Ar	0.21(1)[99]	$0.53^{+0.20}_{-0.13} \pm 0.06$ [94]	$4p-4h$	2.1
^{44}Ti	0.28(3)[99]	-	$8p-4h$	1.9 [95]
^{35}Cl	0.12(2)[96]	0.34(2)[96]	$3p-3h$	6.6

[a] Q_t deduced from the decay of the12^+, 14^+ and 16^+ states
[b] Q_t deduced from the decay of the 6^+, 8^+ and 10^+ states
[c] Different assumptions in the analysis lead to higher Q_t values

evolution with N and Z without systematic measurements of g factors, spectroscopic quadrupole moments and $E0$ and $E2$ transition strengths.

The most detailed evidence for shape coexistence in the $A \sim 40$ mass region comes from a recent Coulomb-excitation experiment of ^{42}Ca [97, 107] that provided magnitudes and relative signs of numerous $E2$ matrix elements coupling the low-lying states in this nucleus, which were further interpreted in terms of quadrupole invariants for the $0^+_{1,2}$ and $2^+_{1,2}$ states. In particular, the spectroscopic quadrupole moment of the 2^+_2 state was measured for the first time, and its value of $-0.42(12)$ eb corresponds to $\beta_2 = 0.48(16)$. The low-lying levels in ^{42}Ca, relevant for this study, are shown in Fig. 6, together with the measured $B(E2)$ and $\rho^2(E0)$ transition rates. The $\langle Q^2 \rangle$ quadrupole invariants for the $0^+_{1,2}$ and $2^+_{1,2}$ states in ^{42}Ca [97, 107] are large and constant within the deformed band, while those for the ground-state band are considerably lower, with an important increase observed between the 0^+_1 and the 2^+_1 states. This effect can be attributed to the mixing of the 2^+ states. From the analysis of $\langle Q^2 \rangle$ fluctuations (defined by Eq. 35) one can conclude that the ground state exhibits a considerable softness, while the 0^+_2 state is more rigid [107]. This is consistent with the value of the $\langle Q^3 \cos 3\delta \rangle$ invariant for the 0^+_1 state being close to zero, which is interpreted as resulting from a γ-soft character of this state (averaging over all possible quadrupole shapes ranging from prolate to oblate yields a γ parameter of 30°).

Table 2: $\rho^2(E0; 0^+_2 \rightarrow 0^+_1)$ transition strengths (taken from Ref. [102]) and spectroscopic quadrupole moments of the 2^+_1 states in nuclei around ^{40}Ca (from Ref. [97] for ^{42}Ca and evaluated values from Ref. [39] elsewhere). The latter are also normalised to the $Q_s(2^+_1)$ values calculated from the experimental $B(E2; 2^+_1 \rightarrow 0^+_1)$ values assuming axial rotor model, i.e., using Eq. 12 ($Q_s(2^+_1)^{rot}$). Mixing angles of the 0^+ states are also given, which are deduced from the $\rho^2(E0; 0^+_2 \rightarrow 0^+_1)$ values assuming the β_2 deformation parameters for the deformed structure listed in Tab. 1.

isotope	$Q_s(2^+_1)$ [eb]	$Q_s(2^+_1)/Q_s(2^+_1)^{rot}$	$10^3 \times \rho^2(E0; 0^+_2 \rightarrow 0^+_1)$	$\cos^2\theta_0$
^{40}Ca	-	-	25.6(7)	0.70(18)
^{42}Ca	$-0.12^{+0.07}_{-0.02}$	$0.66^{+0.38}_{-0.11}$	140(12)	0.77(6) 0.83(6)[1]
^{44}Ca	-0.14(7)	0.70(35)	140(50)	-
^{36}Ar	+0.11(6)	0.7(4)	-	-
^{38}Ar	-	-	18(3)	$0.97^{+0.02}_{-0.04}$
^{40}Ar	+0.01(4)	0.06(24)	-	-

[1] Value obtained taking into account the γ deformation of the 0^+_2 state deduced from the quadrupole invariant [97].

In Ref. [107], an attempt was made to apply the two-state mixing model to the measured $E2$ matrix elements coupling the $0^+_{1,2}$ and $2^+_{1,2}$ states in ^{42}Ca. The resulting mixing angle for the 0^+ states, $\cos^2\theta_0$=0.88(4), is consistent with the value of 0.83(6) determined using the measured $\rho^2(E0; 0^+_2 \rightarrow 0^+_1)$ transition strength and deformation parameters for the 0^+_2 state obtained with the quadrupole sum rules approach, see Tab. 2. However, the $\cos^2\theta_2$=0.39(8) value obtained from the $E2$ matrix elements shows that the two-level mixing model cannot be applied to the $2^+_{1,2}$ states in ^{42}Ca, as it suggests that the 2^+_1 state has a 61% admixture of the deformed configuration, while the 2^+_2 state is dominated by the spherical one, at odds with their measured quadrupole moments. One can note here that the cross sections to populate the $2^+_{1,2}$ states in ^{42}Ca in one-neutron transfer [88] were almost identical, which suggests the same admixture of the $(f_{7/2})^2$ configuration to both states. On the other hand, their quadrupole moments are different, which means that other configurations must contribute to these states in different proportions, and this in turn implies that the two-level mixing model is overly simplified in this case.

The importance of triaxiality in this mass region is an open question. The $\langle Q^3 \cos 3\delta \rangle$ invariant determined for the 0^+_2 state in ^{42}Ca suggests a small deviation from an axially symmetric shape (γ=13(5)°). The few lowest members of $K = 2$ bands were identified in ^{44}Ti and ^{40}Ca [89, 91], and these structures were interpreted as γ bands associated with the deformed configurations ($8p - 4h$ and $4p - 4h$, respectively). A 2^+_3 state, linked by intense transitions to both the ground-state and deformed bands, is also known in ^{42}Ca (see Fig. 6 for decay properties of the proposed $K = 2$ structures in ^{40,42}Ca). Extension of this band to higher spin, as well as the identification of its counterparts in other $A \sim 40$ nuclei exhibiting shape coexistence, remains a challenge for γ-ray spectroscopy.

Shape coexistence has also been suggested for a number of odd-mass nuclei in this mass region, as shown in Fig. 7. The experimental data in support of this scenario are mostly limited to level energies and $B(E2)$ values, as discussed in Refs. [2, 3]. Early measurements, summarized

in Ref. [3], revealed evidence for the presence of intruder states, in particular through the use of transfer reactions, but often were unaccompanied by complementary data that would support shape coexistence. Remarkably, there have been few recent studies that have advanced this view. Specifically, the quadrupole moment of the excited $3/2^+$ state in ^{45}Sc, of the intruder proton $d_{3/2}^{(-1)} f_{7/2}^2$ configuration, was measured to be $Q_s = +0.28(5)$ eb [108], in comparison with $Q_s = -0.22(1)$ eb for the ground state [39]. Given the recent work on the neighbouring even-even nuclei, the odd-mass nuclei would appear to be ripe for re-investigation with modern spectrometers.

3.1.4. Shape coexistence around the "island of inversion" at $N = 28$

The development of an "island of inversion" south of ^{48}Ca is linked to the coexistence of spherical and deformed configurations in $N \approx 28$ nuclei. The most important body of evidence has been obtained for ^{44}S, using γ-ray and electron spectroscopy following fragmentation or particle knockout from intermediate-energy stable and radioactive beams [109–113]. An isomeric 0_2^+ state at 1365(1) keV in ^{44}S was observed only 36 keV above the 2_1^+ state [109], and its $E0$ decay branch corresponds to $10^3 \times \rho^2(E0; 0_2^+ \rightarrow 0_1^+) = 8.7(7)$ [110]. The mixing of the two 0^+ states can be estimated from the $\mathrm{B}(E2; 0_2^+ \rightarrow 2_1^+)/B(E2; 2_1^+ \rightarrow 0_1^+)$ ratio via Eq. 39, yielding $\cos^2\theta_0$ equal to 0.88. This, combined with the measured $E0$ transition strength, points to the deformations of the two unperturbed 0^+ states differing by $\Delta\beta_2 \approx 0.27$. Compared with β_2=0.25 estimated from the $B(E2; 2_1^+ \rightarrow 0_1^+)$ value [114], it suggests that the deformation of the 0_2^+ state is close to zero. A 2_2^+ level at 2156(49) keV was subsequently identified and assigned to the spherical configuration on the basis of a comparison with shell-model calculations [111]. A different candidate for the second member of the band built on the 0_2^+ state was proposed in Ref. [112], again with a support from theory calculations. This work also proposed a (2^+) level at 3248 keV, and the observed 1891-keV γ ray, not seen in coincidence with the $2_1^+ \rightarrow 0_1^+$ decay, was attributed to the decay of the level at 3248 keV to the 0_2^+ state. Finally, a recent lifetime measurement yielded a $B(E2; 4_1^+ \rightarrow 2_1^+)$ value of 0.61(19) W.u. [113], indicating a drastically reduced collectivity with respect to the $B(E2; 2_1^+ \rightarrow 0_1^+)$ of 7(2) W.u. This suggests that the 4^+ member of the ground-state rotational band is non-yrast and has not been identified yet, and that its mixing with the observed 4_1^+ state is limited. It is possible, as proposed by Ref. [113], that the 4_1^+ state represents a third different configuration appearing at low excitation energy, but the existing experimental information is insufficient to firmly state that a triple shape coexistence is present in ^{44}S.

A g-factor measurement of the 321-keV $7/2^-$ isomer in ^{43}S [115] suggested that this state has a normal-order $1f_{7/2}$ neutron-hole configuration. Its measured lifetime [115, 116] implies a quadrupole character of its decay to the ground state, which leads to the attribution of the $3/2^-$ spin to the latter, consistent with a neutron $2p_{3/2}$ intruder character. This configuration of the ground state was also supported by spectroscopic factors measured in one-neutron knockout reaction from ^{44}S [117]. The spectroscopic quadrupole moment of the $7/2^-$ isomer was found to be larger than expected for a single-particle state, suggesting an admixture of the intruder configuration [118]. A level at 971(6) keV was proposed as a member of the rotational band based on the deformed ground state, on the basis of an enhanced $B(E2)$ value for its population from the ground state, $B(E2; 3/2^-_{gs} \rightarrow (7/2^-_2))$=19(8) W.u., deduced from an intermediate-energy Coulomb-excitation study [119] and a reduced cross section for its population in intermediate-energy single-neutron knockout [120]. Recently measured lifetimes and γ-γ coincidence information obtained via single-

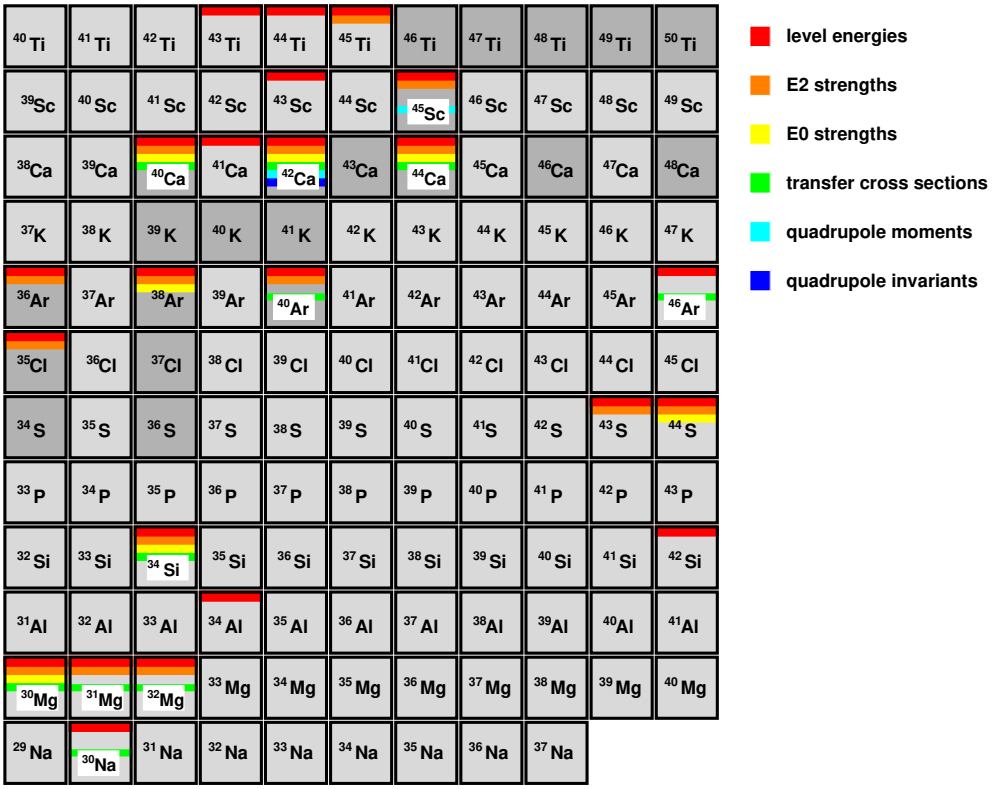

Figure 7: Summary of experimental data for nuclei exhibiting shape coexistence in the Mg-Ca region. Red bars indicate that shape-coexisting structures were proposed based on their level energies (e.g., observation of a low-lying 0^+ state, or rotational structures with very different moments of inertia), orange bars mean that additional information was obtained from $E2$ transition probabilities, yellow bars mean that information on $E0$ transition strengths is known, green bars mean measured cross sections to populate the coexisting configurations in direct reactions, light blue bars indicate that quadrupole moments of both configurations were measured, and dark blue bars correspond to quadrupole invariants. Stable nuclei are indicated with a darker shade.

proton knockout from ^{44}Cl [121] suggest that the ~970-keV γ ray observed in Refs. [119, 120] feeds not the ground state, but a 184-keV state with a tentative spin assignment of $(1/2^-)$. The measured lifetime of the state decaying via the ~970-keV γ-ray transition is consistent with its collective character (16(5) W.u.). The ordering of the two transitions proposed by Ref. [121] was, however, not confirmed by the results of one-neutron knockout from ^{44}S [117], which also casts some doubt on the lifetime obtained in Ref. [121]. A cascade of two coincident γ rays of 628 keV and 1159 keV, assigned by Ref. [121] as the $(5/2^-_3) \rightarrow (3/2^-_2) \rightarrow 3/2^-_{gs}$ transitions based on a comparison with shell-model calculations, was confirmed and extended by Ref. [117]. While it has been suggested that the band-like structure built on the $(3/2^-_2)$ state corresponds to a different intrinsic shape [121], further experimental evidence would be necessary to verify this interpretation (currently only the $B(E2; 3/2^-_{gs} \rightarrow (3/2^-_2))$ of 1.0(7) W.u. is known [122]). Finally, a candidate for a state built on the top the $7/2^-_1$ isomer was recently proposed [117] and the energy of its decay to the isomer (1532 keV) supports weak deformation of the latter. Interestingly, a recent intermediate-energy Coulomb-excitation study [122] yielded a $B(E2; 3/2^-_{gs} \rightarrow (7/2^-_2))$ value of

10(2) W.u., much lower than that of Ref. [119], and a comparable $B(E2; 7/2^-_1 \rightarrow (9/2^-))$ value of 11(4) W.u. for the population of the state built on the $7/2^-_1$ isomer, suggesting a similar collectivity of the two structures.

The contradictions between the existing data demonstrate the challenges of experimental studies in this mass region. Shape coexistence is expected to persist inside the "island of inversion", but there is very little experimental evidence for it. One can mention here the direct population of the 2150(13)-keV state in ^{42}Si observed in one-proton knockout from ^{43}P [123], which excluded the previous 4^+ assignment of this state [124] and suggested instead that it may be a low-lying 0^+_2 state predicted by various theoretical calculations. Outside the border of the "island of inversion" the experimental information on shape coexistence is also very limited; while these nuclei are less exotic and thus more accessible experimentally, the presumed intruder configurations appear at much higher excitation energies than the normal-order states in S and Si nuclei. Notably, a 0^+_2 state was identified at 3695 keV in ^{46}Ar following the ^{44}Ar(t,p)^{46}Ar two-neutron transfer reaction, and its spin-parity was unambiguously assigned based on the shape of the differential cross section [125].

Figure 7 displays a portion of the chart of the nuclides highlighting the Na – Ti nuclei, with a colour coding indicating the available data which provide evidence for shape coexistence. The lack of colour coding for other nuclei does not imply that these quantities are unknown, but are insufficient to substantiate a claim for shape coexistence. For some nuclei, like ^{42}Ca, the evidence is so strong that they provide anchors for systematics in the region – the energy patterns, $B(E2)$ values, $E0$ strengths, transfer cross sections, quadrupole moments and quadrupole invariants all point to coexisting shapes. For other nuclei, the suggestion or assignment of shape coexistence is based on the energy patterns or systematics only, and further studies are definitely required. Many of the odd-mass nuclei fall into this category. Figure 7 reveals a clustering effect of studies; in the Ar – Sc region a wealth of data exists for stable nuclei, while experimental information on shape coexistence in neutron-deficient isotopes is very limited, even though it is suggested by theoretical calculations. The Mg and Si isotopes, on the other hand, are hard to access experimentally due to their neutron-rich character and it has only been the advent of radioactive beam facilities that has enabled the wide variety of studies to elucidate their structure, with detailed transfer studies worth mentioning in particular.

3.2. Shape coexistence around Z=28

3.2.1. Vicinity of ^{56}Ni

Very similar to the observations in the immediate vicinity of $Z = N = 20$, highly deformed structures are also present near $Z = N = 28$ ^{56}Ni. For example, studies using fusion-evaporation reactions populated states in ^{56}Ni at moderate-to-high spin, and identified two well-deformed rotational bands [126]. One of these bands, built on the 0^+_3 state at 5.003 MeV, is explained as a $4p-4h$ excitation, with proton $2p-2h$ contributions revealed by its population in the (^{3}He,n) reaction (under the assumption that the ground state wave function of ^{54}Fe has a $2h$ character) [127]. The second band, observed to be built on the spin (5) state at 8.890 MeV, was also interpreted as a $4p-4h$ excitation with one particle in the $g_{9/2}$ orbital [126], and lifetimes extracted from DSAM measurements were consistent with an average transitional quadrupole moment $\bar{Q}_t$

similar to that for the highly deformed band in ^{58}Cu that had $\bar{Q}_t = 2.0(3)$ eb [128]. Highly deformed structures were also observed in the neighbouring isotope ^{58}Ni, with a negative-parity band having $\bar{Q}_t = 2.4(3)$ eb identified in Ref. [130]. The suggested configuration involved two neutrons and one proton occupying the 1/2[440] Nilsson orbital, and a proton hole in either the 1/2[321] or the 5/2[312] orbital. The spectroscopy of ^{58}Ni was studied in detail in Ref. [131], where nine rotational band structures were observed built on states at moderate spins. In addition to the above neutron two-particle and proton particle-hole configuration, other configurations that emerged from the cranked-Nilsson-Strutinsky calculations [131] were similar to the configurations assigned in ^{56}Ni and included two neutrons in the $g_{9/2}$ orbital coupled to a $4p-4h$ configuration in the pf shell. A deformed rotational band with $Q_t = 2.2^{+1.1}_{-0.8}$ eb was also identified in ^{62}Ni [129], and structures with similar moments of inertia are also known in odd-mass Ni isotopes, ^{57}Ni [132, 133], ^{59}Ni [134] and ^{63}Ni [135]. While the uncertainties are often large, the extracted β_2 values for these structures are in the range of 0.3–0.45 [135].

The states at 3531 keV (0^+_3) in ^{58}Ni, 3319 keV (0^+_3) in ^{60}Ni, and 3519 keV (0^+_4) in ^{62}Ni were observed to be populated strongly in the two-proton-transfer (^{3}He,n) reactions [136–138] or the (^{6}Li,d) or (^{16}O,^{12}C) α-particle transfer reactions, and were identified as the $T = 1$, $T = 2$, and $T = 3$ proton pairing vibration states [136, 139]. What is remarkable is that the 0^+_3 states in ^{58,60}Ni have very strong $E0$ transitions to the ground state, with $10^3 \times \rho^2(E0)$ values of 80(30) and 77^{+66}_{-42} [102], respectively, whereas it is the 0^+_2 level in ^{62}Ni, that was not observed in the proton-pair transfer reactions, which decays with a similarly enhanced $E0$ strength with $10^3 \times \rho^2(E0) = 130^{+60}_{-70}$ [140]. These $\rho^2(E0)$ values are some of the largest known between 0^+ states outside of the shape-transition regions at $N = 60$ and $N = 90$ [25, 102]. Strongly enhanced $\rho^2(E0)$ values have also been observed for the $2^+_2 \rightarrow 2^+_1$ transitions in ^{58,60,62}Ni [140, 141]. In ^{58,60}Ni, the excitation energies of the 2^+_2 states are lower than those of the 0^+_2 states, and thus cannot be easily described as members of a shape-coexisting 0^+ band. Figure 8 summarizes some of the spectroscopic data for the lowest 0^+ and 2^+ excitations in the even-even Ni isotopes. The quadrupole moments of the 2^+_1 states are consistent with a spherical shape, and the large $\rho^2(E0)$ values could naively be interpreted as indicating deformed states. The lack of known rotational structures built on these levels, however, is curious, and perhaps indicates that the origin of the $E0$ strength is related to dynamic, rather than static, deformation. In Ref. [27], calculations were performed for several nuclei including ^{58}Ni, exploring the origin of the enhancement of $E0$ transitions, and found that important contributions to the $E0$ strength arise from the core polarization. More work is required to characterize the nature of these states in the mid-shell Ni isotopes.

3.2.2. *Vicinity of ^{68}Ni*

A new region of deformed nuclei with $Z < 28$ and $N \approx 40$ has been identified and extensively investigated in the recent years. The yrast bands of the even-even Ni isotopes beyond $N = 40$ are expected to show a seniority character with neutrons occupying the $\nu g_{9/2}$ shell, similar to the $N = 50$ isotones with protons dominantly confined to the $\pi g_{9/2}$ shell. Isomeric 8^+ states arising from the alignment of a broken neutron pair with seniority $\nu = 2$ were observed in ^{68,70}Ni [146]. The $\nu = 2$ seniority multiplet should consist of pure neutron states, i.e., decaying with low $E2$ transition probabilities, as shown in Fig. 10 for ^{68}Ni. In ^{70}Ni, the 8^+_1 and 6^+_1 states present such character, while the enhanced $B(E2; 2^+_1 \rightarrow 0^+_1)$ value of 10.0(17) W.u., together with a trend

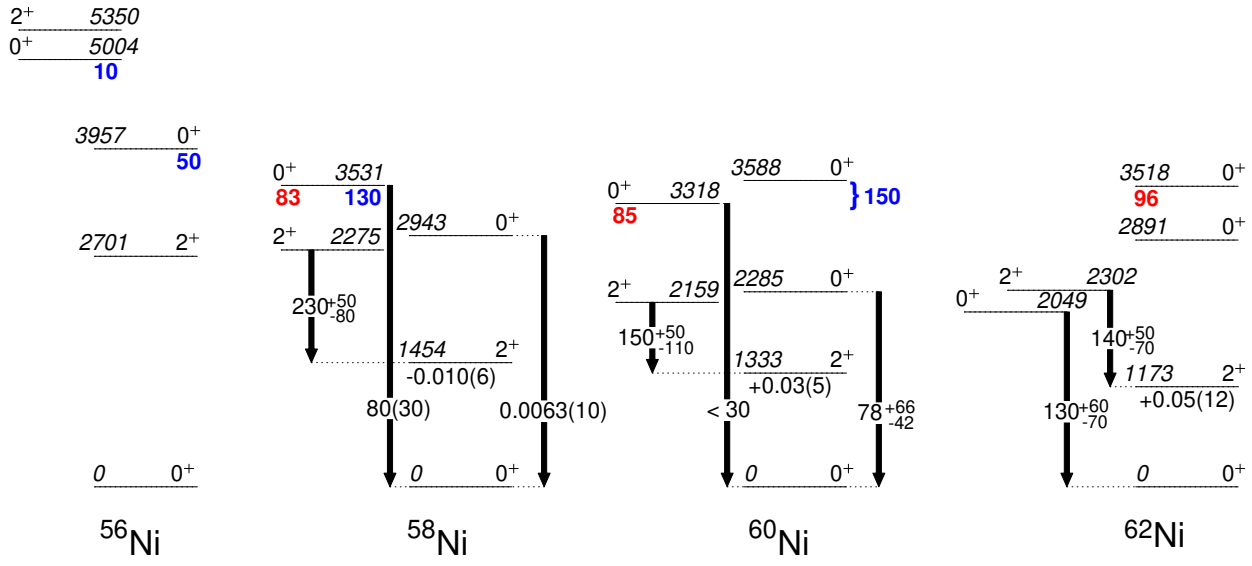

Figure 8: Spectroscopic data for low-lying 0^+ and 2^+ states in $^{56-62}$Ni. The arrows represent $E0$ transitions and are labelled with their $10^3 \times \rho^2(E0)$ values. The values under the 2_1^+ levels are the spectroscopic quadrupole moments Q_s in eb. The values, in bold, under the 0^+ states are the population strengths, expressed in percent, relative to the ground state for the (^{6}Li,d) reactions (red, left) and the (^{3}He,n) reactions (blue, right). For ^{60}Ni, the two-proton-transfer strength of 150% is attributed to the 3588-keV 0_4^+ state in Refs. [136, 137], and to the 3318-keV 0_3^+ state in Ref. [138]. As the α-transfer strength is definitely listed for the 0_3^+ state in Ref. [139], it is likely that the (^{3}He,n) strength should also be associated with the 0_3^+ state. The 5004- and 5350-keV levels in ^{56}Ni have been assigned as the lowest-spin members of the superdeformed band. Data are taken from the National Nuclear Data Center database [39] and Refs. [102, 140, 141] ($E0$), [139] (^{6}Li,d), and [127, 136–138] (^{3}He,n).

observed in the Zn isotopes, was interpreted as reflecting a strong polarization of the $Z = 28$ core [147]. It was speculated that the underlying cause was a reduction of the $Z = 28$ proton shell gap in the immediate vicinity of ^{68}Ni leading to deformation [147, 148].

The first suggestions of shape coexistence at $N = 40$ followed the identification of a low-lying 0_2^+ state in ^{68}Ni [149, 150]. This level, being the first excited state in ^{68}Ni, was initially measured to have an excitation energy of 1.77 MeV [149, 150] with later studies placing it at 1604 keV [151]. Its interpretation is that of primarily a neutron excitation, with two particles promoted from the pf orbitals to the $g_{9/2}$ orbital [2, 151, 152]. Pauwels *et al.* [152] emphasize the similarity of ^{68}Ni and ^{90}Zr, and suggest that the lowering of the ground-state energy, resulting in an artificially high 2_1^+ excitation energy, is due to the role of pairing and the mixing of 0^+ states from the $\nu(p_{1/2})^2$ and $\nu(g_{9/2})^2$ configurations [2]. Two-neutron transfer cross sections measured in the ^{66}Ni(t, p)^{68}Ni reaction showed a strong population of the 0_1^+ state and a weak population of the 0_2^+ state, consistent with the $\nu(g_{9/2})^2$ interpretation of the latter [153, 154]. The 2_1^+ and 0_2^+ states were suggested to form a band based on the the measured $B(E2; 2_1^+ \rightarrow 0_2^+) = 8.9(28)$ W.u. [155] (compared to 3.2(7) W.u. [156] for the 2_1^+ decay to the ground state) and their oblate character has been proposed [155, 157]. However, the strong population of the 2_1^+ state in the two-neutron transfer reaction was shown to be inconsistent with shell-model calculations having a

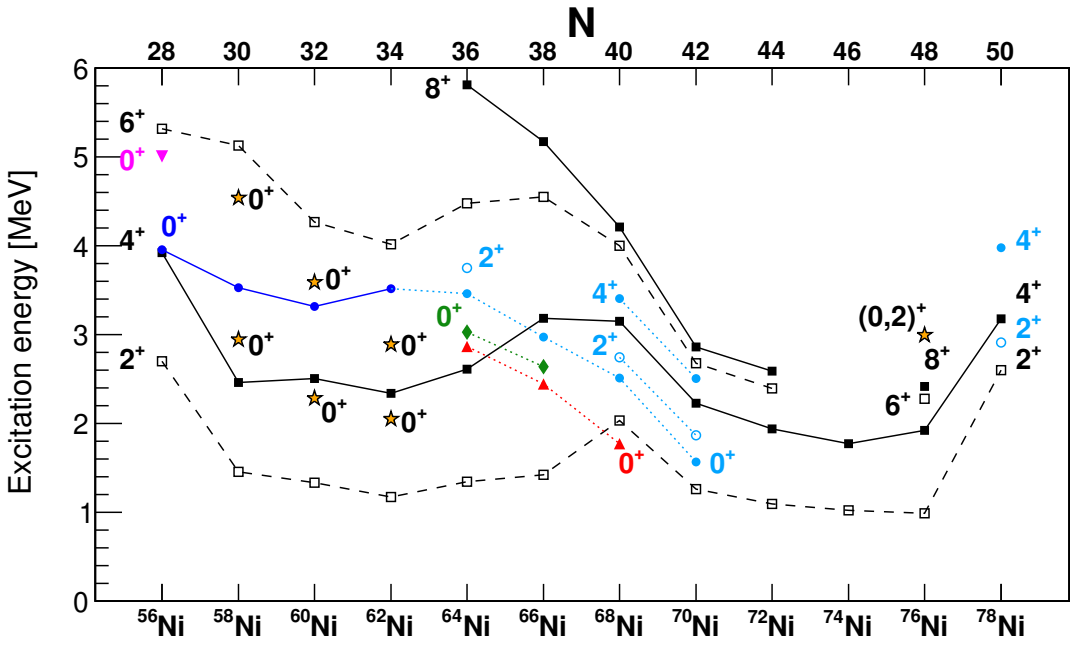

Figure 9: Energy systematics of selected positive-parity excited states in even-even $^{56-78}$Ni isotopes, showing yrast bands, three lowest 0^+ excited states and bands postulated to be built on them. The normal-order states are marked with black squares. The $\pi(2p-2h)$ states are shown with blue circles; for those observed to be populated strongly in proton-transfer reactions dark blue is used, whereas those assigned based on calculations (which predict prolate shapes) are plotted with light-coloured circles and dotted lines. The superdeformed $4p-4h$ state in ^{56}Ni is denoted with a magenta triangle. The 0^+ states presumed to be oblate and related to neutron excitations are shown with red triangles, and the presumed spherical 0^+ states with green diamonds. The states, for which the existing information is insufficient to characterize them as a specific configuration are marked with yellow stars. Data are taken from the National Nuclear Data Center database [39] and Refs. [142–145].

dominant $\nu(g_{9/2})^2$ configuration, indicating a more complex wave function that must involve two-particle components of low-j orbitals [154]. These two interpretations are illustrated in Fig. 10, highlighting that there remains uncertainty regarding the interpretation of the low-lying excited states as belonging to a deformed configuration, or as seniority or broken-pair structures.

A state at 2511 keV, tentatively assigned as (0_3^+), was observed in the β decay of a low-spin isomer in ^{68}Co [158] and its spin has recently been confirmed by an angular correlation measurement [159]. Limits on its $E0$ decay strengths were also extracted, with $10^3 \times \rho^2(E0; 0_3^+ \rightarrow 0_1^+) \leq 5$ and $10^3 \times \rho^2(E0; 0_3^+ \rightarrow 0_2^+) \leq 26$ [155, 157]. Placed in the context of the large $\rho^2(E0)$ values observed in the lighter Ni isotopes, these $\rho^2(E0)$ values are remarkably small, revealing either a similar deformation of these states or small mixing of the respective wave functions (or both). A 2_2^+ state at 2743 keV excitation energy has been proposed as a member of the 0_3^+ band [142, 157]; the energy spacing would imply $\beta_2 \sim 0.45$, i.e., twice that of the purported 0_2^+ band. The excitation energy of the 2511-keV 0_3^+ state is compatible with the shell-model predictions for an intruder state corresponding to a $2p-2h$ proton excitation across the $Z = 28$ shell [155], and also with estimates using the locations of the $\pi(1p-2h)$ and $\pi(2p-1h)$ states in ^{67}Co and ^{69}Cu, respectively [152]. If the assignments of Ref. [155] are correct, however, it would imply that the spherical 2^+

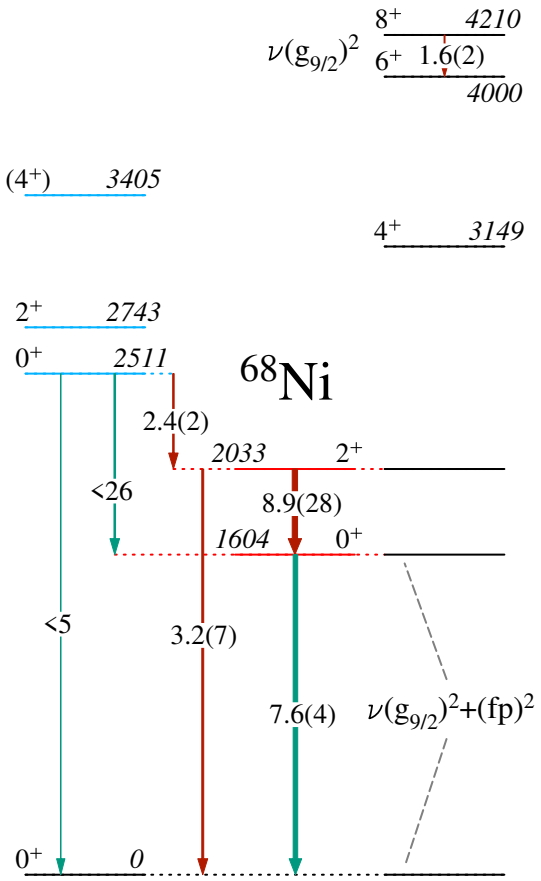

Figure 10: Partial level scheme of ^{68}Ni. The transitions are labelled with their $B(E2)$ values in W.u. (rust-coloured arrows) or $10^3 \times \rho^2(E0)$ values (green-coloured arrows). The levels are organized into deformed bands as assigned in Ref. [142, 155] (coloured levels on the left-hand side), and Refs. [142, 146, 152, 154] (black-coloured levels on the right-hand side) where they were suggested to have significant components of the labelled configurations. The two-neutron transfer cross sections measured [154] for the 0^+_2 and 2^+_1 states were shown to be consistent with $\nu(g_{9/2})^2$ and low-j neutron-pair structures, respectively.

state has yet to be observed, and also would (likely) have a very high excitation energy.

Similar deformed configurations of a proton character were postulated in ^{64}Ni [144], ^{66}Ni [145, 160, 161] and ^{70}Ni [162–164]. The systematics of low-lying excited states in $^{56-78}$Ni, including yrast bands and the three lowest 0^+ states, are presented in Fig. 9. The prolate-deformed proton intruder states are postulated to be the 0^+_4 states in ^{64,66}Ni, the 0^+_3 state in ^{68}Ni, and possibly the 0^+_2 level in ^{70}Ni, with the other low-lying 0^+ states suggested to be of a neutron nature and likely weakly-to-moderately deformed [144, 145, 160–164]. This leads to a triple shape-coexistence scenario proposed for these nuclei, and an open question of the natures of the excited 0^+ states in the lighter Ni isotopes, and the existence of low-lying deformed 0^+ states in ^{72,74}Ni close to the neutron mid-shell.

A delayed 168(1)-keV γ-ray transition in ^{68}Ni was observed in a two-proton transfer reaction ^{238}U(^{70}Zn,^{68}Ni)^{240}Pu [165], and was interpreted as the decay of another 0^+ state at 2202(1) keV

to the 2^+_1 state. This new isomer was not confirmed by Ref. [159]. The comparison with the ^{70}Zn(^{14}C,^{16}O)^{68}Ni data remains, however, puzzling. In the experiments of Refs. [149, 150], the 0^+_2 and 2^+_1 states were proposed to be located at 1770 and 2200 keV, respectively. Further measurements changed these excitation energies to 1604 and 2033 keV, respectively. This represents differences of 166 and 167 keV, very close in energy to the delayed 168(1)-keV transition observed uniquely in Ref. [165]. This systematic shift is intriguing and gives room for a possible explanation of the origin of the 168(1)-keV transition. One could speculate that the study of Ref. [165] populated a third excited 0^+ state similar to those in ^{64,66}Ni.

The systematics of the 2^+_1 excitation energy in the Fe isotopes ($Z = 26$) shows a continuous decrease from $N = 36$ to $N = 46$, which is accompanied by an increase of the corresponding reduced transition probabilities [166] clearly indicating collectivity, and suggesting that the ground states are deformed. The reproduction of the lifetimes of the 2^+_1 and 4^+_1 states in ^{64,66}Fe required a significant occupancy of the $\nu g_{9/2}$ and $\nu d_{5/2}$ orbitals coupled to the proton holes [167, 168]. One can speculate that there may be a similarity of configurations between the deformed ground states in the Fe nuclei and the deformed excited states in the Ni isotopes, as well as between the expected weakly deformed excited states in the former and the ground states in the latter. Shell-model calculations [169] predict indeed that that the 0^+_2 state in ^{66}Fe would be almost spherical, with nearly identical proton occupancies in the pf shell, and less important role of neutron ($mp - mh$) excitations across $N = 40$, compared to the 0^+_1 state.

A 0^+_2 state at 1414 keV has been identified in ^{66}Fe following β decay of ^{66}Mn [161, 169, 170] and its excitation energy agrees very well with the theoretical prediction of Ref. [169]. Additional work is required to characterize the nature of the states in the Fe isotopes, however, and the presence of shape coexistence is not yet based on firm experimental evidence.

In ^{61}Fe, a ($9/2^+$) isomeric state at 861 keV was reported. Its quadrupole moment has been measured and corresponds to a moderately deformed shape, which indicates its possible $g_{9/2}$ intruder character. This state coexists with a weakly deformed ground-state band consisting of $1/2^-$, $3/2^-$ and $5/2^-$ states, compatible with the coupling of a single neutron to the 0^+_1 and 2^+_1 states in the even-even ^{60}Fe core [171]. In ^{63}Fe, a ($9/2^+$) state is also proposed, but unplaced in the level scheme [172]. The $1/2^-_{gs}$, $3/2^-_1$, and $5/2^-_1$ states in ^{65}Fe, populated in the β decay of ^{65}Mn, are compatible with the coupling of the 0^+ ground state and the 2^+_1 state in ^{64}Fe with a single neutron in the pf shell. Low-lying $9/2^+$ and $5/2^+$ states have also been identified and associated to the intruder gd orbitals, supporting their importance just below $N = 40$, as evidenced also by the collective properties of ^{64,66}Fe [173]. No experimental evidence for shape coexistence, however, has yet been reported, and the spectroscopy of ^{67}Fe is very incomplete.

3.2.3. Co isotopes

The Co isotopes ($Z = 27$) may also be expected to exhibit shape coexistence. Unfortunately, due to its chemical properties, cobalt is almost impossible to extract rapidly from a thick ISOL target, and therefore laser spectroscopy of the ground state was achieved only for stable or very long-lived Co isotopes, whereas the key nuclei, near $N = 40$, have millisecond lifetimes that make their spectroscopy difficult to perform. In the last decade, several experimental programs have tried to address the expected shape coexistence in Co isotopes via in-beam γ-ray spectroscopy, β-decay studies, and measurements of lifetimes of states to enable the determination of transition

Table 3: Measured $B(\lambda\mu; I_i \rightarrow g.s.)$ values in odd-mass Co isotopes. The corresponding $B(E2; 2_1^+ \rightarrow 0_1^+)$ values in the even-even Ni cores are also given.

Nucleus	I_i	I_f	Excitation energy [keV]	$B(E2; I_i \rightarrow I_f)$ [W.u.] (assuming pure $E2$)	$B(M1; I_i \rightarrow I_f)$ [W.u.] (assuming pure $M1$)
^{63}Co	$(3/2^-)$	$7/2^-$	995	3.7(4) [177]	-
	$(9/2^-)$	$7/2^-$	1383	12(5) [177]	0.013(4) [177]
	$(11/2^-)$	$7/2^-$	1674	4(1) [168, 179]	-
^{64}Ni	2^+	0^+	1345	9.04(28)	-
^{65}Co	$(3/2^-)$	$7/2^-$	882	17(16) [178]	-
	$(9/2^-, 11/2^-)$	$7/2^-$	1642	-	-
	$(9/2^-, 11/2^-)$	$7/2^-$	1479	6(2) [179]	-
^{66}Ni	2^+	0^+	1424.8	7.6(13)	-

probabilities. The natures of the ground states in the Co isotopes were inferred through systematic verifications of the "core-coupling" model (for details, see, e.g., [174]). Spherical or weakly deformed excited states in Co nuclei should exhibit the characteristics of core-coupled states (weak coupling scheme), i.e., the barycentre of the lowest-lying core-coupled multiplet should be located at the 2_1^+ energy of the even-even Ni core, and the $B(E2)$ values for the decay of core-coupled states to the ground state should equal the $B(E2; 2_1^+ \rightarrow 0_1^+)$ value for the core. In contrast, the deformed states should possess rotational bands with moments of inertia and $B(E2)$ values similar to those of the deformed states in the even-even Fe cores.

The lowest-lying weak-coupled states result from the $f_{7/2}^{-1} \otimes 2_{Ni}^+$ coupling that yields the set $3/2^-$, $5/2^-$, $7/2^-$, $9/2^-$, and $11/2^-$. Candidate levels for members of this multiplet have been suggested [175, 176] in ^{63,65,67}Co with excitation energies similar to those of the 2_1^+ states in the corresponding Ni cores, although their identification in many cases is tentative due to uncertain spin-parity assignments. The hypothesis that the first $(3/2^-), (9/2^-), (11/2^-)$ states in ^{63,65}Co have a core-coupled character, which would support a weakly deformed character of the ground state, was tested by lifetime measurements [177, 178], and Tab. 3 presents the resulting $B(E2)$ values for their decay to the ground state, compared to the $B(E2; 2_1^+ \rightarrow 0_1^+)$ value in the even-even core. The $B(E2; (3/2_1^-) \rightarrow 7/2_1^-)$ and $B(E2; (11/2_1^-) \rightarrow 7/2_1^-)$ values in ^{63}Co are similar, as expected from the coupling scheme, but they are both significantly lower than the $B(E2; 2_1^+ \rightarrow 0_1^+)$ value in ^{64}Ni. The remaining values displayed in Tab. 3 agree within uncertainties with the values for the Ni cores. The systematics of $(9/2^-)$ states was extended beyond $N = 40$ in ^{69,71,73}Co, and the energies of the tentative $(9/2^-) \rightarrow (7/2^-)$ transitions are similar to those of the $2_1^+ \rightarrow 0_1^+$ transitions in the corresponding ^{70,72,74}Ni cores [180]. It should be emphasized that the uncertainties of the $B(E2)$ values are large and the $\delta(E2/M1)$ mixing ratios are, mostly, not measured. Thus, more precise measurements are needed to determine possible deviations from the weak-coupling model to probe the influence of the deformed configurations.

A $(1/2^-)$ state was reported at 1095 keV in ^{65}Co and interpreted, in a comparison with shell-model calculations, as a deformed proton state involving excitation across the $Z = 28$ shell gap [178]. While there is no unambiguous evidence to affirm this interpretation, a $1/2^-$ state cannot belong to the $\pi f_{7/2}^{-1} \otimes 2_{1Ni}^+$ multiplet, and a single-particle $p_{1/2}$ state at such a low excitation energy

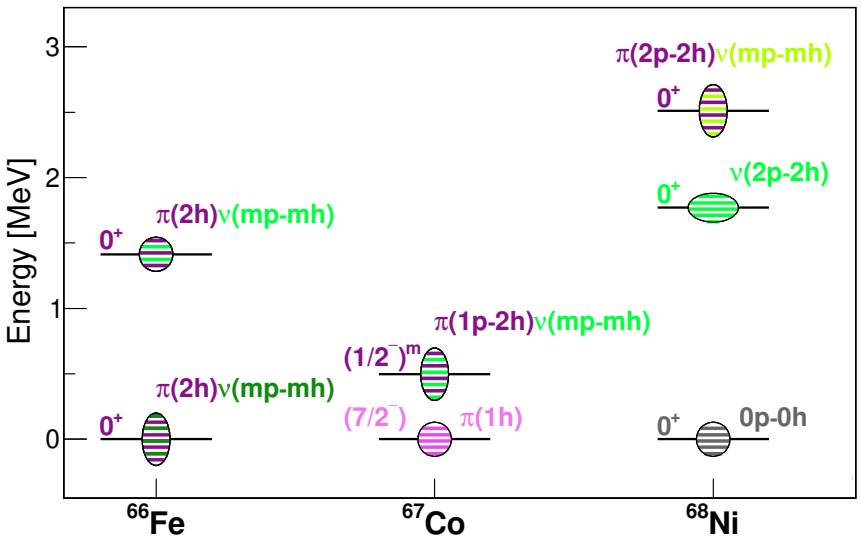

Figure 11: Dominant configurations and presumed shapes of low-lying states in $N = 40$ isotones ^{66}Fe, ^{67}Co and ^{68}Ni, resulting from calculations of Refs. [161, 169]. The vertically stretched ellipses denote prolate deformation, horizontally stretched ones oblate, and circles nearly spherical shapes. Purple shades denote proton components in the wave function, green ones neutron components, and the intensity of the color is related to the number of nucleons promoted across a shell gap according to the calculations of Refs. [161, 169].

would be surprising. A higher-lying $(3/2^-)$ state at 1223 keV has a significant branch to the $(1/2^-)$ state. While lifetimes for these states have been measured [178], the lack of knowledge of mixing ratios prevents the determination of the $B(E2)$ values. These states have been suggested to arise from the $\pi(f_{7/2}^{-2}p_{3/2}^{1})$ deformed configuration, i.e., the $1/2^-[321]$ orbital [152, 176, 178]. A $(1/2^-)$ isomeric state at 491 keV excitation energy is reported in ^{67}Co and interpreted as a deformed intruder state also. Based on this energy and that of the $7/2^-$ isomer in ^{69}Cu (1711 keV), interpreted as the $\pi(2p-1h)$ configuration, one can expect that the $\pi(2p-2h)$ 0^+ deformed state in ^{68}Ni should appear at 491+1711 = 2202 keV, i.e., close to the energy of the 2511-keV 0_3^+ state, supporting its present interpretation [152]. One could speculate that with additional neutrons added to the $\nu g_{9/2}$ orbital, the $(1/2^-)$ intruder state could become the ground state in the Co isotopes beyond $N = 40$, however, their ground-state spins and parities remain unknown. In ^{69}Co [181], an isomeric state with an unknown excitation energy, tentatively assigned as having $I^\pi = (1/2^-)$, is proposed as a candidate for a proton intruder state. A possible spin-parity inversion of the Co ground states from $7/2^-$ to $1/2^-$ should be investigated, and possible members of a rotational band built on the $(1/2^-)$ state should be sought.

Combining the observed states in the $N = 40$ isotones with the expected $p-h$ excitations, a picture as presented in Fig. 11 emerges. In this picture, the 0_3^+ state in ^{68}Ni corresponds to the $\pi(2p-2h)$ configuration, the 491 keV state in ^{67}Co the $\pi(1p-2h)$ configuration, and the ground state in ^{66}Fe has a $\pi(2h)$ configuration. The "normal" configuration, corresponding to the ground state in ^{68}Ni, the $\pi(1h)$ ground state in ^{67}Co, and the $\pi(2h)$ state in ^{66}Fe, may then appear as a low-lying 0^+ state in the latter. Further away from $Z = 28$, low-lying 0^+ states of a similar configuration were also predicted in ^{62,64}Cr ($Z = 24$), and a candidate in ^{62}Cr was observed experimentally [182].

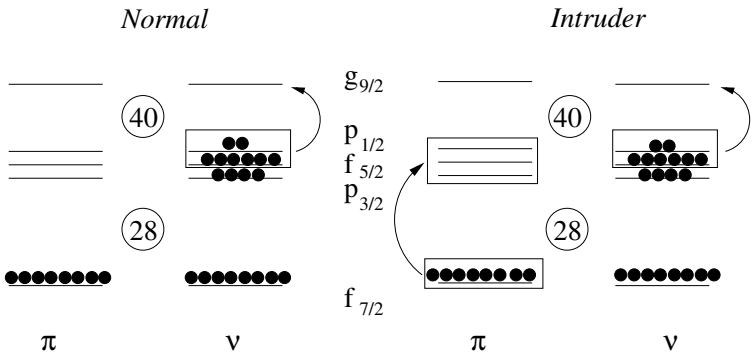

Figure 12: Schematic presentation of normal-order (e.g., 0^+_2 in ^{68}Ni, 0^+_2 in ^{66}Fe) and intruder configurations (i.e., 0^+_3 in ^{68}Ni, 0^+_1 in ^{66}Fe) of shape-coexisting states around $N = 40$.

It is stressed that while these states are labelled by their proton $p-h$ content, all of them will involve neutron $mp-mh$ contributions. In particular, both the ground and the 0^+_2 state in ^{66}Fe are predicted to have important $\nu(mp-mh)$ contributions [169], which are larger for the former, leading to its deformed nature. This particular region suffers from lack of experimental data as well as some inconsistencies between the results, but the overall reproduction of the available data by shell-model calculations provides confidence in the predicted shapes for these excitations. Experiments aimed at testing these predictions will be crucial, although challenging.

A low-spin isomer, with unknown excitation energy, is also reported in ^{68}Co [158]. Several spin-parity assignments were proposed for this isomer based on the states in ^{68}Ni that are populated by its β decay [157, 158, 183]. The spin assignments proposed in Refs. [157, 183] support its interpretation as a deformed proton state. A direct measurement of its excitation energy and, more importantly, of its spin and parity will provide an important experimental constraint on the microscopic configuration of the 0^+_3 state in ^{68}Ni.

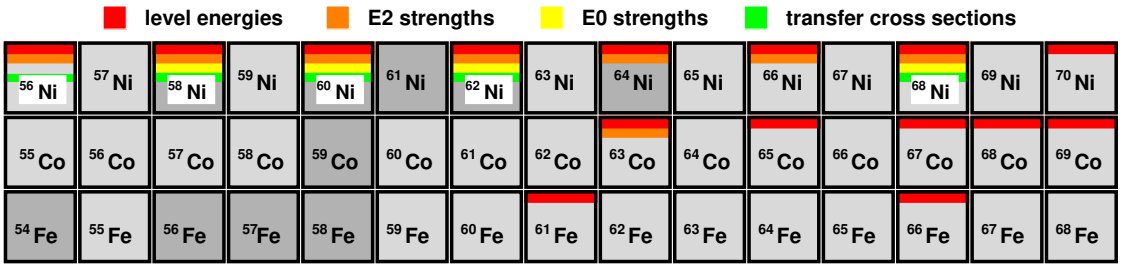

Figure 13: Summary of experimental data for nuclei exhibiting shape coexistence in the Fe-Co-Ni region. Red bars indicate that shape-coexisting structures were proposed based on their level energies (e.g., observation at low excitation energy of presumed 0^+ states in even-even nuclei, or isomers in odd-mass ones, or rotational structures with very different moments of inertia), orange bars mean that additional information was obtained from $E2$ transition strengths, yellow bars mean that information on $E0$ transition strengths is known, and green bars mean measured cross sections to populate the coexisting configurations in direct reactions. Stable nuclei are indicated with a darker shade.

Figure 13 summarizes the quantities that have been measured in the Fe – Ni isotopes that are used to support shape-coexistence assignments. We stress here that large $\rho^2(E0)$ strengths were

measured for the decay of low-lying 0^+ and 2^+ states in ^{58,60,62}Ni, and although these nuclei satisfy many of the criteria for shape coexistence, no rotational-like bands built on these states have been identified. While rich and diverse data are now available for ^{68}Ni, considerable uncertainty remains regarding the assignments of its first two excited states, which, together with the recent suggestions of shape coexistence in the ^{64,66}Ni isotopes, provides strong motivation for further studies.

3.2.4. Vicinity of ^{78}Ni

The first and most direct evidence for shape coexistence in the immediate vicinity of ^{78}Ni was obtained through the measurement of a large isomer shift for the $1/2^+$ isomer in ^{79}Zn [184]. The excitation energy of this isomer was determined in a ^{78}Zn$(d, p)^{79}$Zn study to be 1.10(15) MeV [185]. The ground-state β_2 deformation of ^{79}Zn, estimated from its measured spectroscopic quadrupole moment [184], is equal to 0.15(2), which is consistent with the values of 0.15(2) and 0.14(2) obtained from the measured $B(E2; 2_1^+ \rightarrow 0_1^+)$ values in ^{78}Zn and ^{80}Zn, respectively [186]. If the measured isomer shift is entirely attributed to an increase of deformation, it leads to an estimate of $\beta_2 \approx 0.22$ for the isomer [184]. Based on the measured g factor of the isomer [184] one can assign to it a $2h - 1p$ intruder configuration related to neutron excitation across the $N = 50$ shell gap. Similar conclusions can be drawn from a recent ^{80}Ge$(d, p)^{81}$Ge study [187], which deduced strong $3s_{1/2}$ and $2d_{5/2}$ components in 679-keV $1/2^+$ and 711-keV $5/2^+$ states, respectively, thus linking them to neutron promotion across the $N = 50$ shell gap. Low-lying states of a $2h - 1p$ intruder configuration were also identified in $N = 49$ isotones ^{83}Se [188], ^{85}Kr [189], and ^{87}Sr [190] via (d, p) transfer reactions.

Two recent measurements used β decay of ^{80}Ga to perform electron-conversion spectroscopy of ^{80}Ge [191, 192]. A conversion-electron peak at 628 keV was reported in Ref. [191], which was attributed to the decay of a 0_2^+ state at 639 keV, located just below the first excited 2_1^+ state at 659 keV and interpreted as a neutron $2p-2h$ intruder excitation across $N = 50$. However, a later study [192] did not confirm the state at 639 keV and the question of possible shape coexistence in ^{80}Ge remains open.

Two excited 0^+ states were identified in ^{82}Ge at 2.3 MeV and 3.1 MeV, respectively, and their decay patterns were observed to be different [193]. The $0_2^+ \rightarrow 2_1^+$ γ-ray transition seems to be hindered with respect to the decay of the 2_2^+ state feeding the 0_2^+ state, while no such effect is observed for the $0_3^+ \rightarrow 2_1^+$ decay. This difference was interpreted as due to an enhanced $E0$ $0_2^+ \rightarrow 0_1^+$ branch, which would suggest different deformations of the 0_1^+ and 0_2^+ states and their significant mixing. In contrast, a weak $E0$ $0_3^+ \rightarrow 0_1^+$ decay implies that either the deformations of the 0_1^+ and 0_3^+ states are more similar, or the mixing between these two states weaker.

In more exotic nuclei at and beyond $N = 50$, the hints of shape coexistence come from the observation of non-yrast states. Their spin assignments and interpretation usually result from comparisons with theoretical calculations. Notably, a sequence of 1067-keV and 2910-keV transitions feeding the ground state in ^{78}Ni was observed following the ^{80}Zn$(p, 3p)^{78}$Ni reaction and attributed to the decay of a 4_2^+ state at 3.98 MeV and a 2_2^+ state at 2.91 MeV, respectively (for comparison, the energy of the first excited state in ^{78}Ni is 2.6 MeV) [143]. These non-yrast states were interpreted as belonging to a deformed intruder configuration [143]. In a study of ^{82}Zn via a ^{83}Ga$(p, 2p)^{82}$Zn reaction, in addition to the strong $4_1^+ \rightarrow 2_1^+ \rightarrow 0_1^+$ cascade, a weaker transition was observed and tentatively assigned to the decay of a possible 0_2^+ state at 987 keV [194]. A

candidate for a 0^+_2 or 2^+_2 state was found at 2.99 MeV in ^{76}Ni in a β-decay study [195].

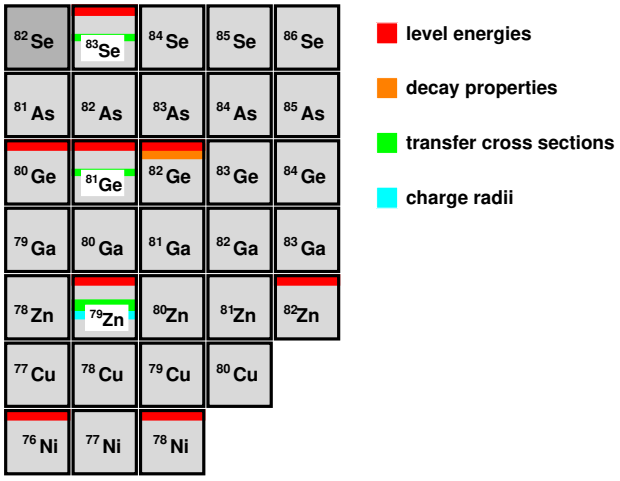

Figure 14: Summary of experimental data for nuclei exhibiting shape coexistence in the vicinity of ^{78}Ni. Red bars indicate that shape-coexisting structures were proposed based on their level energies (e.g. observation at low excitation energy of presumed 0^+ states in even-even nuclei, or isomers in odd-mass ones, or rotational structures with very different moments of inertia), orange bars mean that additional information was obtained from electromagnetic decay, green bars mean measured cross sections to populate the coexisting configurations in direct reactions, light blue bars indicate that charge radii of both configurations were measured. Stable nuclei are indicated with a darker shade.

3.3. Neutron-deficient nuclei with $N \approx Z$

The neutron-deficient nuclei close to the $N = Z$ line, between the Ge and Zr isotopic chains, have been known for a long time to exhibit shape coexistence. The support for this scenario has been obtained via a variety of probes, as illustrated in Fig. 15, and a thorough review of experimental data available before 2011 has been published in Ref. [2].

The low excitation energies of the 0^+_2 states in $^{70-76}$Ge, descending even below the 2^+_1 state in ^{72}Ge, motivated a multitude of single-nucleon and multinucleon transfer studies aimed at extracting the microscopic configurations of ground and excited states in these nuclei. These results are reviewed in Ref. [2] and point to important mixing of both proton and neutron components of the wave functions of the $0^+_{1,2}$ states, with a maximum observed for ^{72}Ge. This is consistent with the mixing angles deduced from the measured $E2$ matrix elements assuming a two-level mixing model. By applying Eq. 38 to the most recent set of $\langle 2^+_i||E2||0^+_j\rangle$ matrix elements for ^{72}Ge [196], $\cos^2(\theta_0) = 0.52(4)$ was obtained, while the same procedure applied to ^{70,74,76}Ge [198] yielded admixtures of 5%, 4% and 3%, respectively. While the unperturbed $\langle 2^+_{A,B}||E2||0^+_{A,B}\rangle$ matrix elements resulting from this analysis are very similar for ^{72,74,76}Ge and indicate that in these nuclei deformed ground-state configurations coexist with spherical excited ones, their values obtained for ^{70}Ge would rather correspond to two deformed configurations, a prolate and an oblate one. Interestingly, the $10^3 \times \rho^2(E0; 0^+_2 \rightarrow 0^+_1)$ values measured for ^{70,72}Ge are rather similar (5.2(4) and 9.18(2), respectively [102]), which suggests that if the mixing in ^{70}Ge is indeed much lower than

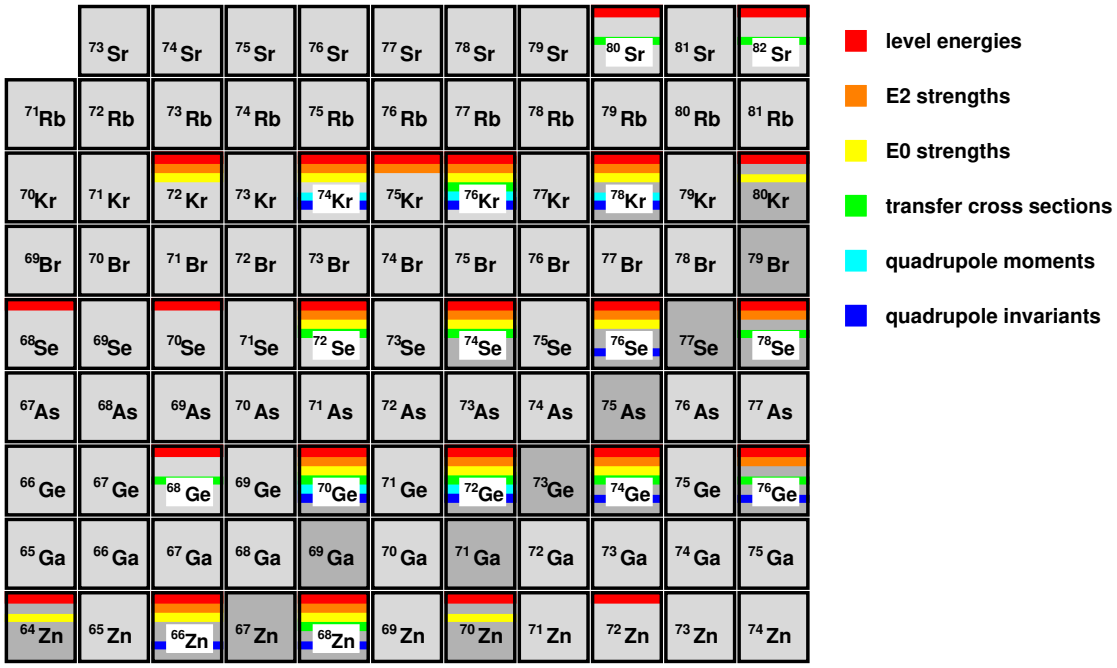

Figure 15: Summary of experimental data for nuclei exhibiting shape coexistence in the light Sr-Zn region. Red bars indicate that shape-coexisting structures were proposed based on their level energies (e.g., observation of a low-lying 0^+ state, or rotational structures with very different moments of inertia), orange bars mean that additional information was obtained from $E2$ transition probabilities, yellow bars mean that information on $E0$ transition strengths is known, green bars mean measured cross sections to populate the coexisting configurations in direct reactions, light blue bars indicate that quadrupole moments of both configurations were measured, and dark blue bars correspond to quadrupole invariants. Stable nuclei are indicated with a darker shade.

in ^{72}Ge, the difference between the shapes of the two underlying configurations should be considerably larger in the former. This picture would be consistent with the multi-nucleon transfer results [2]. These observations are further supported by the systematics of quadrupole invariants obtained in Coulomb-excitation studies [196–200]. The $\langle Q^2 \rangle$ values of the ground states in $^{70-76}$Ge have similar values of about 0.2 e^2b^2, while those of the 0^+_2 states evolve considerably, from being consistent with zero in ^{74,76}Ge [199, 200], almost identical with that of the ground state in ^{72}Ge [196, 197]), to a value of 0.64(26) e^2b^2 in ^{70}Ge [198]). The recent detailed Coulomb-excitation studies of ^{72}Ge [196] and ^{76}Ge [201] have also confirmed a rotational character of the ground-state bands in these nuclei, with the $\langle Q^2 \rangle$ values being remarkably constant up to spin 8. The only significant deviation from this pattern is a slight reduction observed for the 0^+_1 state in ^{72}Ge, which may be attributed to the strong mixing with a less deformed configuration.

Triaxiality plays an important role in the structure of Ge nuclei. Gamma bands were identified in all Ge isotopes with $66 \leq A \leq 78$, and the level staggering observed in the γ band in ^{76}Ge [202], as well as the decay pattern with enhanced $\Delta I = 1$ transitions for that in ^{78}Ge [203], were discussed in the context of rigid triaxial deformation. Quadrupole invariants $\langle Q^3 \cos 3\delta \rangle$ were obtained for multiple states in both ground-state and γ bands in ^{72}Ge [196] and ^{76}Ge [201]. The corresponding $\langle \cos 3\delta \rangle$ values appear to be rather constant with spin and correspond to almost

maximum triaxiality. Similar observations were made for the ground-state band in ^{74}Ge, although the experimental information is limited only to its two lowest members [199]. The deduced fluctuations of $\langle Q^3 \cos 3\delta \rangle$ (see Sec. 2.4) for the 0_1^+, 2_1^+ and 2_2^+ states in ^{76}Ge are consistent with rigid triaxial deformation [201]. The $\langle \cos 3\delta \rangle$ values obtained for the 0_1^+ and 0_2^+ states in ^{72}Ge are very similar, in line with their strong mixing [196].

A Coulomb-excitation study of ^{66}Zn [204] yielded a $\langle Q^3 \cos 3\delta \rangle$ invariant for the ground state corresponding to an average δ of 44(8)°, demonstrating that triaxiality is also important for this nucleus. A similar conclusion was reached for ^{68}Zn [205] based on the strongly reduced $Q_s(2_1^+)$ value of +0.09(3) eb. Low-lying 0_2^+ states were observed in $^{62-72}$Zn, and the excitation energies of those in $^{66-72}$Zn display a characteristic parabolic pattern with a minimum for ^{70}Zn. The 2_3^+ state in ^{68}Zn was proposed to be a member of a deformed band built on the 0_2^+ state, based on a strong $B(E2; 2_3^+ \rightarrow 0_2^+)$ value of 17.4(14) W.u. [205], which is nonetheless comparable with the $B(E2; 2_1^+ \rightarrow 0_1^+)$ value (15.6(10) W.u.). While Ref. [204] reports that the $\langle Q^2 \rangle$ invariant for the 0_2^+ state in ^{66}Zn is considerably smaller than that for the ground state, the authors stress that the former may be strongly underestimated, as it includes contributions from only two lowest 2^+ states, and the 2^+ member of the band built on the 0_2^+ state has not been identified yet. Similarity between the deformations of the 0_2^+ states in $^{64-70}$Zn and those of the respective ground states would also be consistent with the measured $10^3 \times \rho^2(E0)$ strengths, which are in all cases below 10. Thus, while there are hints of shape coexistence in the Zn isotopes, perhaps unsurprisingly given their proximity to the Ge isotopes, the data are as yet insufficient to make a firm claim.

Low-lying 0_2^+ states were identified in ^{72,74,76}Se, while ^{68,70}Se present two rotational bands with $\Delta I = 2$, characterised by different moments of inertia: one built on the ground state and the other on a low-lying 2_2^+ state. The spectroscopic quadrupole moments measured for the 2_1^+ states in ^{76,78,80,82}Se [206, 207] suggest that these states are prolate deformed, and the level energies and $B(E2)$ values within the ground-state bands are consistent with their rotational character. The 2^+ and 4^+ members of the band built on the 0_2^+ state in ^{76}Se were recently identified in an inelastic neutron scattering study [208], and the $B(E2)$ values within this band were shown to be smaller than those in the ground-state band (e.g., $B(E2; 2_3^+ \rightarrow 0_2^+)$ = 31(5) W.u. versus $B(E2; 2_1^+ \rightarrow 0_1^+)$) = 44(1) W.u.). A β-decay study of ^{74}Se [209] has identified a 0_3^+ state at 1.675 MeV, and on the basis of the measured branching ratios suggested that together with the 2_3^+ state it may form a strongly deformed band, while the 0_2^+ state was interpreted as related to the vibration of the weakly-deformed ground state. While the spectroscopic quadrupole moment of the 2_1^+ state in ^{74}Se has not been unambiguously determined, the moment of inertia of the ground-state band is similar to those in the heavier Se isotopes, see Fig. 16, pointing to its prolate deformation. The similarity of these structures is further supported by the results of a ^{76}Se$(p, t)^{74}$Se study [210], which observed no substantial strength to the excited 0^+ states in ^{74}Se. The moments of inertia in the ground-state band in ^{72}Se resemble those for ^{74,76}Se, although the perturbation of excitation energies of its low-spin members is more significant than in the heavier Se nuclei, which may be due to the mixing of the coexisting configurations. The $B(E2; 2_2^+ \rightarrow 0_2^+)$ value of 36(3) W.u. significantly exceeds its counterpart in the ground-state band (23(2) W.u.), suggesting that the structure built on the 0_2^+ state is more deformed [211]. The intense $2_2^+ \rightarrow 2_1^+$ transition of 75(5) W.u. [211] suggests that the two configurations may strongly mix, in line with the observed evolution of the moments of inertia. On the other hand, the integrated cross section to populate the 0_2^+ state in ^{72}Se via the (t, p)

two-neutron pickup reaction was found to be 11% of that to the ground state [212], which limits the mixing amplitude of the 0^+ states, $\cos(\theta_0)$, to less than 0.3 assuming a two-state mixing model. A negative spectroscopic quadrupole moment was measured for the 2_1^+ state in ^{72}Se, supporting its prolate character [213].

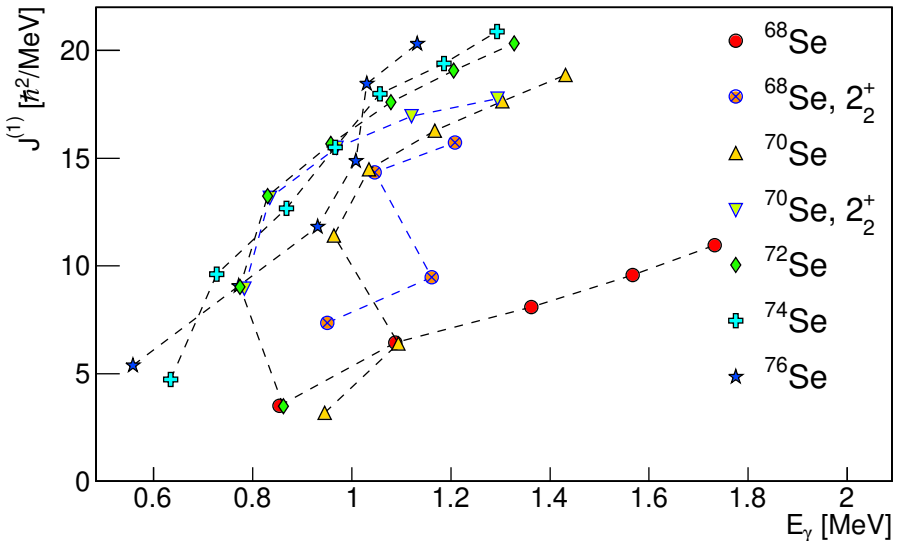

Figure 16: Kinematic moments of inertia for yrast states in ^{68,70,72,74}Se, and the bands built on the 2_2^+ state in ^{68,70}Se. Data are taken from the National Nuclear Data Center database [39].

Despite many experimental efforts, no excited 0^+ states are known at low excitation energy in ^{68,70}Se. The evolution of the moments of inertia in the band built on the 2_2^+ state in ^{70}Se is remarkably close to that observed for the ground-state band in ^{72}Se, as shown in Fig. 16. In contrast, the moments of inertia of the ground-state band in ^{70}Se evolve in a very irregular manner, which has been interpreted as due to a transition from an oblate shape at low spin to a prolate one at higher excitation energy, with a strong mixing of the two configurations [214]. An attempt has been made to measure the quadrupole moment of the 2_1^+ state in this nucleus by combining an integrated low-energy Coulomb-excitation cross section to populate this state [215] and its high-precision lifetime measurement [216]. Unfortunately, the precision of the former was not sufficient to firmly determine the sign of the quadrupole moment, although an oblate shape seems to be favoured. The moments of inertia in the ground-state band of ^{68}Se evolve smoothly with excitation energy, but remain much lower than those in the ground-state bands of heavier Se nuclei, which was attributed to the oblate shape of the former [217]. In contrast, the moments of inertia obtained for states of spin 8 and above in the second rotational structure in ^{68}Se closely follow those for the high-spin members of the ground-state band in ^{70}Se, while their irregular behaviour observed at lower spin may be linked to a strong mixing of the two configurations.

The existing data consistently point to shape coexistence in $^{68-76}$Se, with an important mixing of the coexisting configurations. In particular, a change of the ground-state configuration, with

respect to the heavier Se isotopes, seems to take place in ^{70}Se. A more precise measurement of the spectroscopic quadrupole moment of the 2^+_1 state in this nucleus would bring a definite proof of this scenario.

In the ^{72,74,76}Kr isotopes, the moments of inertia of the ground-state bands were observed to be perturbed at low spin, as readily seen in Fig. 17. Similarly, the reduced transition probabilities show a reduction of collectivity at low spin that has been attributed to shape mixing [218]. The mixing was first quantified, within the two-state mixing model, from the perturbation of the excitation energies of low-spin members of the ground-state rotational bands with respect to an extrapolation of energies of their high-spin members [219]. This analysis yielded an admixture of 27% of the 0^+_B configuration (see Eq. 36) to the ^{76}Kr ground state. From this analysis, the mixing of the 0^+ states reaches a maximum of 50% in ^{74}Kr, where also a maximum value of $10^3 \times \rho^2(E0; 0^+_2 \rightarrow 0^+_1) = 85(19)$ and minimum excitation energy of the 0^+_2 state are observed. In ^{72}Kr, the 0^+_2 excitation energy increases, and the mixing deduced from level energies is reduced to 10% [219]. The observed parabolic trend of the 0^+_2 excitation energy suggests that the two configurations cross at ^{74}Kr, where they are almost degenerate and maximally mixed [219]. The initial conclusions on the sign of the deformation, i.e., prolate or oblate, were derived from a comparison with theoretical models. For instance, by comparing the measured $B(E2; 2^+_1 \rightarrow 0^+_1)$ value with theoretical predictions, Iwasaki *et al.* [220] concluded that the first 2^+ state in ^{72}Kr has an oblate shape, which in turn suggested prolate shapes for the ground-state bands in heavier isotopes. Similarly, the enhancement of the $B(E2; 2^+_1 \rightarrow 0^+_1)$ in ^{70}Kr with respect to its mirror nucleus ^{70}Se was interpreted as resulting from a substantial difference between their shapes [221]. Direct evidence for different shapes of the two configurations came from low-energy Coulomb-excitation studies of ^{74}Kr and ^{76}Kr [222], which yielded spectroscopic quadrupole moments of the short-lived $2^+_{1,2,3}$ and 4^+_1 states in these nuclei, providing an experimental proof of prolate deformation in the ground-state bands and oblate deformation of the structures built on the 0^+_2 states. The mixing of the two configurations extracted from the measured $E2$ matrix elements via Eq. 38 was found to be consistent with the conclusions of the level-energy analysis for ^{74}Kr, while the discrepancies observed for ^{76}Kr were attributed to a significant mixing with the 2^+_2 bandhead of the γ band. Comparisons with beyond-mean-field calculations led to a conclusion that allowing for the triaxial degree of freedom is required for the theoretical description of these isotopes [222–224].

Experimental data on the neutron-deficient Sr isotopes are more scarce. In ^{80}Sr, the state at 1-MeV excitation energy was assigned 0^+ spin-parity from the angular distribution measured in the two-proton transfer reaction ^{78}Kr(^{3}He,n)^{80}Sr, and its strong population in this study was associated with shape coexistence [225]. No excited states built on this 0^+_2 level are known. Large deformations with $\beta_2 \simeq 0.4$ can be deduced for the ground states of ^{76,78,80}Sr from the measured $B(E2)$ values in the ground-state bands [226, 227] via Eq. 28. The level energies in these bands, contrary to those in ^{72,74}Kr, do not display strong perturbations at low spin, see Fig. 17.

The correlation between the $R_{42}=4^+_1/2^+_1$ excitation-energy ratio and the $B(E2; 2^+_1 \rightarrow 0^+_1)$ value expressed in W.u. and normalized to A [227], as shown in Fig. 18, suggests a similarity between ^{76,78,80}Sr and ^{72,74,76}Kr, with these $N \sim Z$ nuclei exhibiting a different behaviour than the heavier $Z \approx 40$ or $Z \approx 60$ isotopes. While the observed effect can be attributed to strong mixing in ^{72,74,76}Kr, there is currently no evidence for it in the Sr isotopes. Indeed, the excitation energies of the 2^+_1 and 4^+_1 states in ^{76,78,80}Sr are much lower than their counterparts in the Kr nuclei. Under the

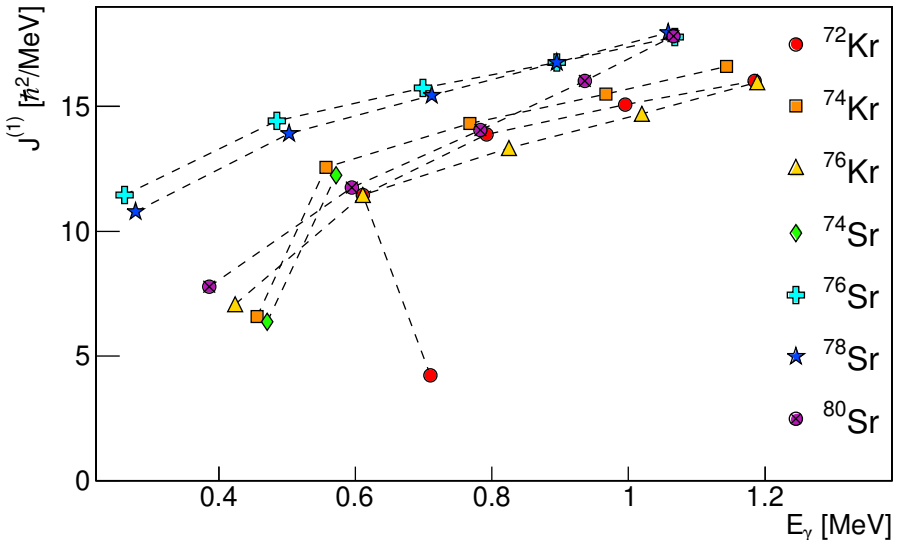

Figure 17: Kinematic moments of inertia, up to spin 10, for yrast states in ^{72,74,76}Kr and ^{74,76,78,80}Sr. Data are taken from the National Nuclear Data Center database [39].

assumption of a similar mixing strength as in the Kr isotopes [227], the increase of energy spacing between the ground state and the 2^+_1 state due to mixing is of the same order of magnitude as the 2^+_1 excitation energy in ^{76,78}Sr, making the R_{42} ratio much more sensitive to small mixing than, e.g., in the Kr isotopes. This calls for more spectroscopic data, such as the excitation energy of the 0^+_2 states in ^{76,78}Sr, currently unknown, and their decay properties. One should also note that the moments of inertia measured for ^{74}Sr [228] closely follow those for its mirror nucleus ^{74}Kr, which hints at a presence of a shape-coexisting state strongly mixed with the ground state, in analogy to ^{74}Kr.

Laser spectroscopy of Rb isotopes (Z=37) revealed large isomer shifts for ^{81}Rb [229] and ^{85}Rb [230]. There exists also an extensive set of ground-state spectroscopic quadrupole moments measured by laser spectroscopy for the odd-proton and odd-neutron isotopes between $Z = 32$ and $Z = 41$ [231], which complements those of the 2^+_1 states in even-even nuclei resulting from Coulomb-excitation studies. For even-even $N = 40$ isotones, one can observe an increase in the quadrupole moments, and hence deformation, when moving away from the closed shells and approaching the $N = Z$ nuclei (^{72}Ge: $Q_s(2^+_1) = -0.13(6)$ eb, ^{74}Se: $Q_s(2^+_1) = -0.36(7)$ eb, ^{74}Kr: $Q_s(2^+_1) = -0.7(2)$ eb). The spin-parities of the ground states in odd-mass $N \sim Z$ nuclei resulting from laser spectroscopy, together with their proposed Nilsson configurations, are presented in Fig. 19. For some of them, spectroscopic quadrupole moments are also known [231], and the corresponding shape (prolate or oblate) is indicated in the figure. From this overview, one can see that there is no convincing experimental evidence for oblate ground states, in particular in the vicinity of the $N = Z$ line. Except for the $N = 39$ ^{75}Kr and ^{77}Sr isotopes, all ground-state configurations involve orbitals arising from the pf shells. One should note here that although many spectroscopic

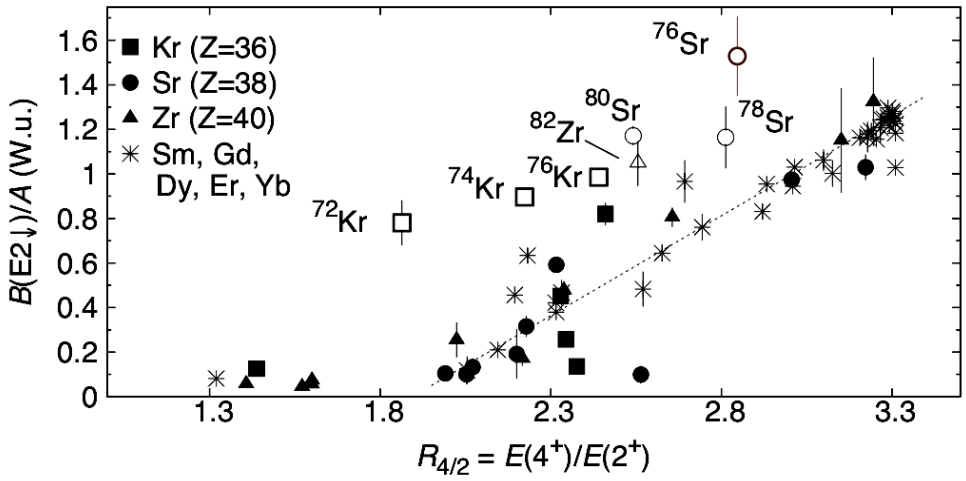

Figure 18: The correlation between the $R_{42}=4_1^+/2_1^+$ excitation-energy ratio and the $B(E2; 2_1^+ \rightarrow 0_1^+)$ values expressed in W.u. and normalized to A, for Kr, Sr, Zr ($Z = 36, 38, 40$) and Sm, Gd, Dy, Er, Yb isotopes ($Z = 62, 64, 66, 68, 70$). Figure from Ref. [227].

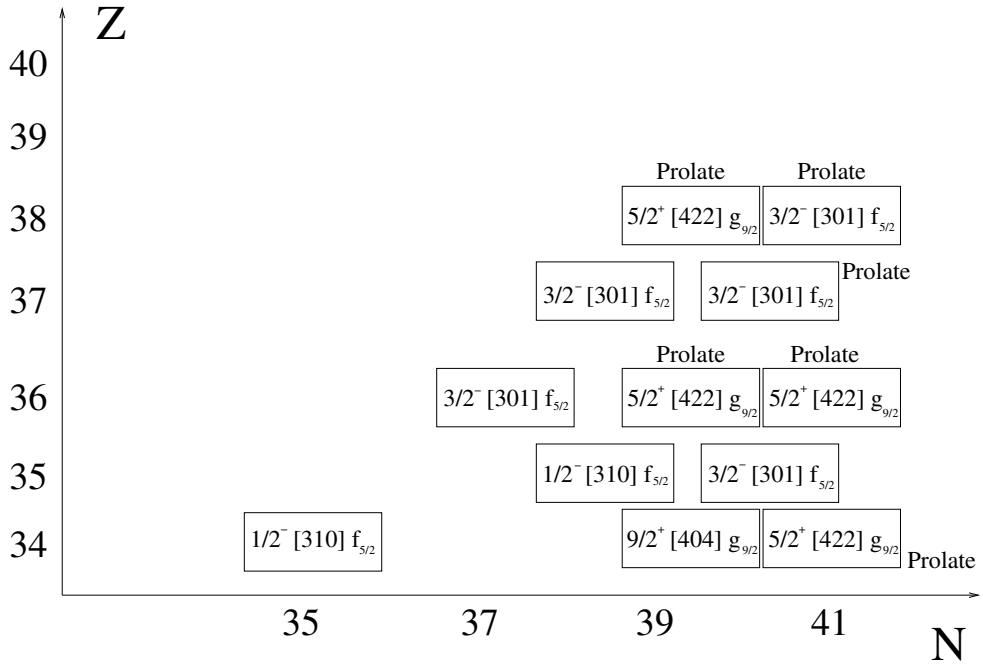

Figure 19: Ground-state spin-parity assignments resulting from laser spectroscopy in odd-mass N~Z nuclei, and proposed Nilsson configurations. The shape indicated next to the configuration is deduced from the measured ground-state Q_s value [231].

quadrupole moments have been measured, a proper determination of the deformation in the intrinsic frame of reference would require assumptions with regard to the axial symmetry. Strong

evidence exists, however, that the triaxial degree of freedom plays a major role in this mass region, and its importance evolves rapidly as a function of nucleon number, which would render such extractions of β_2 questionable.

3.4. Shape coexistence in A ≈ 100, Z ≈ 40 nuclei

The evolution of two-neutron separation energies shows that the binding energy of Rb, Sr, Y and Zr isotopes suddenly increases in the vicinity of $N = 60$ [232]. At the same neutron number, the systematics of the $\delta\langle r^2\rangle$, presented in Fig. 20, shows an abrupt increase of nuclear radii. These features have been interpreted as a consequence of dramatic increases of the ground-state deformations. The low-Z border of this phenomenon was established in the Kr isotopes by means of mass measurements, which do not show any deviation at N=60 from the prevailing trend toward the dripline [233]. The localized character of this effect suggests that it originates from the interaction between specific proton and neutron orbitals.

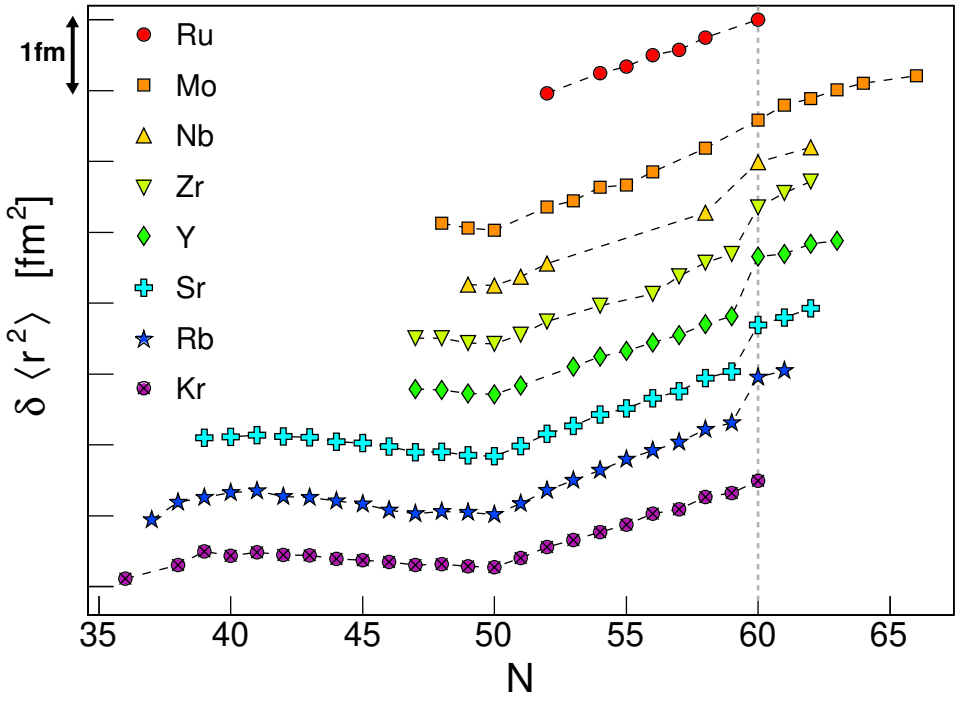

Figure 20: Changes in the mean-square-charge radii, $\delta\langle r^2\rangle$, as a function of the neutron number for the ground states of the Kr–Ru isotopes. An arbitrary displacement of 0.8 fm^2 at $N = 52$ has been introduced between the isotopic chains. Data are taken from Refs. [234–236].

The abrupt ground-state deformation change at $N = 60$ is now clearly established. It is unique in the nuclear chart: it occurs at exactly N=60 for several elements (Rb, Sr, Y and Zr); it is sudden (from spherical N=58 isotones to highly-deformed N=60 isotones); for elements lighter than Rb, or heavier than Zr, the change in deformation is more gradual. In contrast, while shape coexistence occurs throughout this mass region, the information on it is incomplete, and in particular direct

measurements of deformation of excited and ground states are scarce. New results have been obtained in the recent years, notably with the development of post-accelerated radioactive ion beams. The types of available data used to establish shape coexistence are shown in Fig. 21.

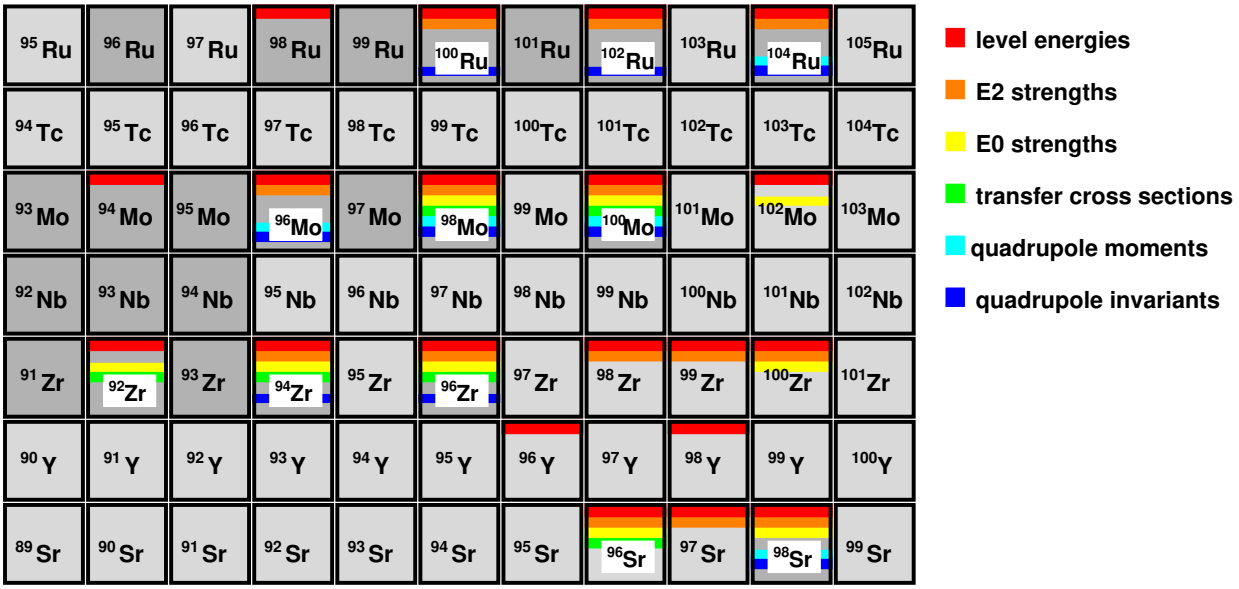

Figure 21: Summary of experimental data for nuclei exhibiting shape coexistence in the $A \approx 100$ region. Red bars indicate that shape-coexisting structures were proposed based on their level energies (e.g. observation of a low-lying 0^+ state, or rotational structures with very different moments of inertia), orange bars mean that additional information was obtained from $E2$ transition probabilities, yellow bars mean that information on $E0$ transition strengths is known, green bars mean measured cross sections to populate the coexisting configurations in direct reactions, light blue bars indicate that quadrupole moments of both configurations were measured, and dark blue bars correspond to quadrupole invariants. Stable nuclei are indicated with a darker shade.

3.4.1. Even-even nuclei with Z ≤40

The systematics of 2_1^+ excitation energies in the Sr and Zr isotopic chains show a sudden drop at $N = 60$, see Fig. 22 (left) and, by applying a simple geometrical model, one can relate it to a change of deformation from $\beta_2 = 0.1$ to $\beta_2 = 0.4$. In contrast, a more gradual evolution is observed for both lighter (i.e., Kr) and heavier nuclei (i.e., Mo, Ru). Similar conclusions can be reached from the $B(E2; 2_1^+ \rightarrow 0_1^+)$ values. Their systematics, recently extended by the measurements of Refs. [237, 239–242], are presented in Fig. 22 (right), where the $B(E2)$ values expressed in W.u. are normalized to the mass A for each isotope. This representation illustrates schematically the fraction of nucleons that contribute to the collectivity: if this ratio equals unity, all nucleons participate in the collective behaviour. The values for the Sr and Zr isotopes with $N \leq 60$ are very small, as expected for spherical nuclei. For ^{96,98}Zr, the local maximum of the 2_1^+ excitation energy (see left panel of Fig. 22), observed when the valence neutrons are filling the $s_{1/2}$ orbital, corresponds to a local minimum in the right panel of Fig. 22. At $N = 60$ and beyond, the ratio saturates at 1, consistent with an almost perfect rigid-rotor character. The evolution observed for Kr, Mo and Ru isotopes is again much more gradual.

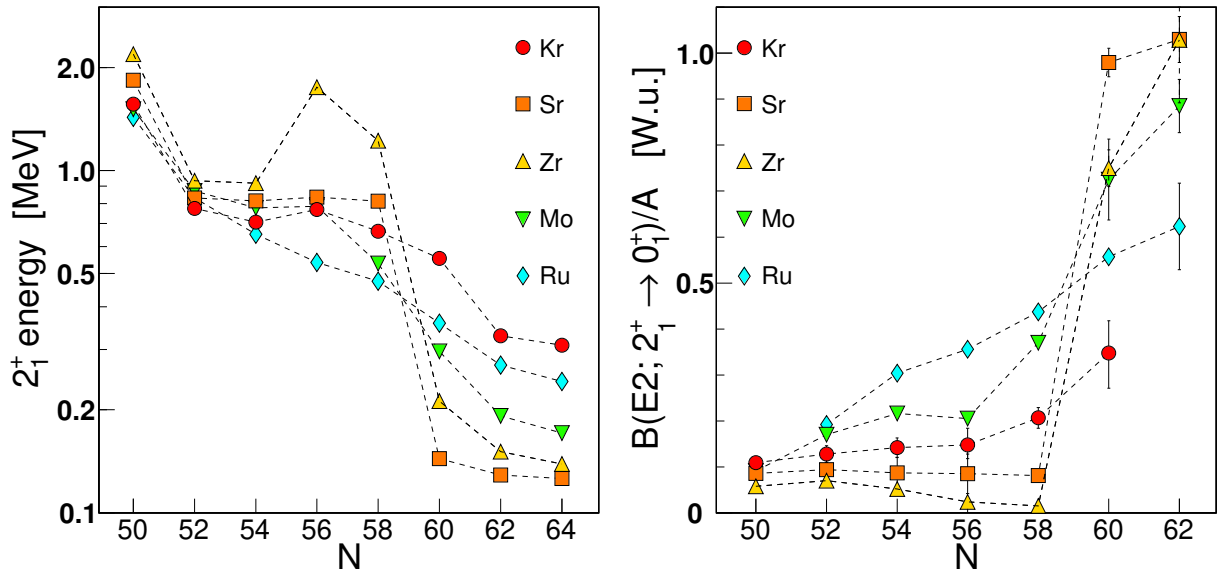

Figure 22: Left panel: Systematics of observed 2_1^+ excitation energies in Kr, Sr, Zr, Mo and Ru isotopes as a function of the neutron number. Right panel: Systematics of the $B(E2; 2_1^+ \rightarrow 0_1^+)$ values in Weisskopf units, normalized to the mass A, for Kr, Sr, Zr, Mo and Ru isotopes. Data are from the National Nuclear Data Center database [39] and Refs. [237–244]. For ^{98}Zr, the weighted average of the $B(E2; 2_1^+ \rightarrow 0_1^+)$ values from Refs. [237, 238] is plotted.

Low-lying 0^+ states, indicating possible shape coexistence, were identified in the Zr and Sr chains and, similar to the 2_1^+ state, a drop of the 0_2^+ energy is observed at $N = 60$, as can be seen in Fig. 23. A shape-coexistence scenario was therefore proposed where the 0_2^+ states for $N < 60$ correspond to a deformed configuration, which then becomes the ground state at $N = 60$, while the spherical configuration of the ground state for $N < 60$ becomes non-yrast.

There exist extensive experimental data on excited states in neutron-rich Sr isotopes. The spectroscopic quadrupole moment of the 2_1^+ state in ^{96}Sr, -22^{+33}_{-31} $e$fm^2, is compatible with zero, and combined with a moderate $B(E2; 2_1^+ \rightarrow 0_1^+)$ value of 7.8(4) W.u. is consistent with a vibrational character of the 2_1^+ state and a nearly spherical shape of the ground state [247–249]. Two low-lying 0^+ states at 1229 and 1465 keV were established by Jung *et al.* [250] and interpreted as candidates for a deformed band head, supporting the shape-coexistence scenario. A highly enhanced electric monopole transition of $10^3 \times \rho^2(E0) = 185(50)$ was observed between these two states [251, 252], indicating both the presence of a sizeable difference in deformation and mixing of the configurations; the proximity in energy of the states limits the mixing matrix element to < 120 keV. The $E0$ decays of the $0_{2,3}^+$ states to the ground state have not been observed. The 2_2^+ and 2_3^+ states are very close in energy to the 0_2^+ and 0_3^+ states, respectively, and can be considered as candidates for rotational band members. The 4_2^+, 6_2^+ and 8_2^+ states form a rotational band, but it is not clear to which band head they should be assigned. The lifetimes of the 6_2^+ and 8_2^+ states were measured [253] and indicate a rather weak deformation.

In ^{98}Sr, the ground-state band has a rotational character, and the large $B(E2)$ values between the excited states, deduced from lifetime measurements [267–273] and Coulomb excitation [247],

Table 4: Quadrupole invariant quantities $\langle Q^2 \rangle$ defined as in Eq. 26, which reduces to $\sum_j B(E2; 0_i^+ \rightarrow 2_j^+)$, for 0_i^+ states of nuclei in the $Z = 38-52$ region. The $\langle Q^2 \rangle$ quantities for excited 0^+ states should be considered as lower limits. The data used to obtain the $\langle Q^2 \rangle$ quantities are taken from Ref. [39] and/or from the references listed in the right column.

Isotope	$\langle Q^2(0_1^+) \rangle$ [e^2b^2]	$\langle Q^2(0_2^+) \rangle$ [e^2b^2]	$\langle Q^2(0_3^+) \rangle$ [e^2b^2]	Ref.
^{96}Sr	0.22(4)			[248]
^{98}Sr	1.30(4)	0.33(3)		[248]
^{94}Zr	0.116(5)	0.34(3)		[254]
^{96}Zr	0.033(4)	0.56(14)		[255]
^{96}Mo	0.286(7)	0.069(9)		[256]
^{98}Mo	0.292(19)	0.257(25)		[256]
^{100}Mo	0.47(3)	0.62(3)		[23]
^{100}Ru	0.527(7)	0.63(13)		
^{102}Ru	0.613(33)	0.35(6)		[257]
^{104}Ru	0.870(9)	0.52(12)		[258]
^{106}Pd	0.63(3)	0.87(4)		[259]
^{108}Pd	0.77(11)	1.22(13)		[259]
^{110}Pd	0.86(4)	1.58(16)		[259]
^{110}Cd	0.44(1)	0.51(8)		[260]
^{112}Cd	0.502(4)	1.24(21)	0.73(13)	[261]
^{114}Cd	0.524(14)	1.12(9)	1.26(16)	[262]
^{116}Cd	0.598(21)		1.04(37)	
^{114}Sn	0.183(11)	< 0.8		
^{116}Sn	0.211(6)	0.83(5)	1.68(14)	[263]
^{118}Sn	0.209(4)	1.03(33)		
^{118}Te	0.57(1)	1.2(4)		[264, 265]
^{124}Te	0.59(1)	0.44(6)		[266]

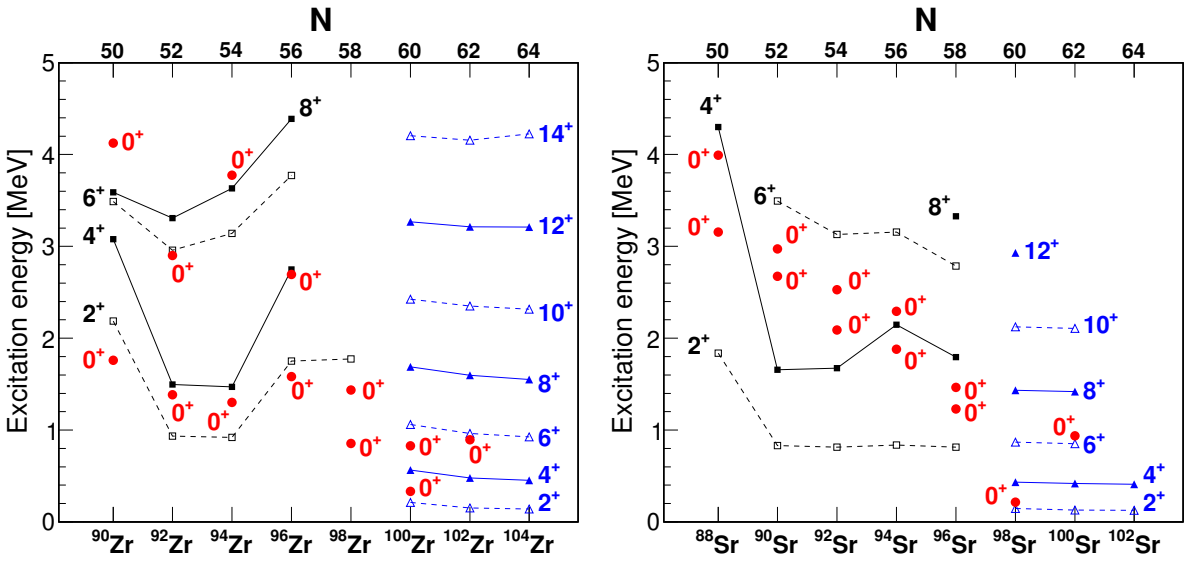

Figure 23: Systematics of selected excited states in $50 \leq N \leq 62$ Zr (left panel) and Sr isotopes (right panel). States belonging to the ground-state bands in isotopes with nearly spherical ground states are denoted with black squares, those built on the deformed ground states with blue triangles, and $0^+_{2,3}$ states with red circles. Data are taken from the National Nuclear Data Center database [39] and Refs. [245, 246].

are consistent with a deformed character of the ground state. A low-lying 0^+_2 state at 215.3 keV was established by Schussler *et al.* [274] and interpreted as the band head of a presumably spherical structure. A strong electric monopole transition of $10^3 \times \rho^2(E0) = 53(5)$ was measured between the 0^+_2 and 0^+_1 states, again supporting the shape-coexistence scenario [274, 275]. The spectroscopic quadrupole moments of states in the ground-state band, measured via low-energy Coulomb excitation, are large and negative [247–249], indicating a prolate deformation with β_2=0.5(1). While those for spin 4^+ and above are consistent with values deduced from the corresponding $B(E2)$ strengths assuming the rigid-rotor model, a reduction of the quadrupole moment is observed for the 2^+_1 state, which has tentatively been attributed to its significant triaxiality [248]. As there is no candidate for a low-lying γ band in ^{98}Sr, the role of triaxiality in this nucleus remains an open question. (A candidate γ band has been suggested [276] in the isotone ^{100}Zr with a bandhead at 1292 keV.) The spectroscopic quadrupole moment of the 2^+_2 state, $2^{+13}_{-12} e\text{fm}^2$, is compatible with zero, and the $B(E2; 2^+_2 \rightarrow 0^+_2)$ value of 7.4(3) W.u. is identical to the $B(E2; 2^+_1 \rightarrow 0^+_1)$ value in ^{96}Sr. The striking similarity of these two structures is further supported by the similarity of the quadrupole invariants $\langle Q^2 \rangle$ for the 0^+_1 state in ^{96}Sr and the 0^+_2 state in ^{98}Sr [248], as listed in Table 4. Together, these results provide firm experimental evidence for coexistence of a well-deformed ground-state band with a weakly deformed structure built on the 0^+_2 state in ^{98}Sr, and strongly support the analogy between the 0^+_1 state in ^{96}Sr and the 0^+_2 state in ^{98}Sr.

Very recently, information on the single-particle nature of excited states in ^{96}Sr was obtained from a study of the ^{95}Sr$(d, p)^{96}$Sr neutron-transfer reaction [277, 278]. The ^{95}Sr ground state is well described as a $\nu s_{1/2}$ spherical state, and thus the (d, p) reaction favours the population of spherical

states in ^{96}Sr of the form $\nu s_{1/2} \otimes \nu l_j$. The 0^+ states in ^{96}Sr were populated with spectroscopic factors of $C^2S = 0.19(3)$, 0.22(3), and 0.33(12) for the 0^+_1, 0^+_2, and 0^+_3 states, respectively. The small occupancy of the $s_{1/2}$ orbital in the ^{96}Sr ground-state wave function disagreed with shell model calculations, and was interpreted as possible evidence for a weakly oblate or triaxial shape [277]. While the uncertainty on the spectroscopic quadrupole moment of the 2^+_1 state measured via Coulomb excitation [247] does not exclude such a scenario, a weak prolate deformation seems to be favoured. The larger transfer strengths observed for the 0^+_2 and 0^+_3 states were interpreted within a two-state mixing model. Combined with the known $\rho^2(E0; 0^+_3 \rightarrow 0^+_2)$ value and under the assumption that the unperturbed 0^+_{def} deformed state is not directly populated, the wave function of the 0^+_2 level was determined to have a 40% admixture of the spherical component [277, 278]. It was suggested that ^{96}Sr may exhibit triple shape coexistence, with a weakly deformed ground state, and two excited 0^+ configurations – a deformed and a spherical one – which undergo strong mixing.

The existing experimental data for the Zr isotopes, summarized in Fig. 24, also point to configuration coexistence, with the types data used to support it shown in Fig. 21. In ^{94}Zr, the g-factor measurements indicate a neutron dominance in the wave function of the 2^+_1 state and proton dominance in that of the 2^+_2 state [279]. In addition, the 2^+_2 level at 1671 keV is populated an order of magnitude weaker than the 2^+_1 state in two-neutron pickup, ^{96}Zr$(p, t)^{94}$Zr [280], and two-neutron stripping, ^{92}Zr$(t, p)^{94}$Zr [281] reactions, consistent with a difference between the neutron configurations of these two states. Furthermore, from a comparison of deformation parameters obtained for the 2^+_2 state in inelastic proton scattering [282] and extracted from its electromagnetic decay, one can deduce $\beta_n/\beta_p \approx 0.83$, consistent with its proton character. The observation of the strongly enhanced $2^+_2 \rightarrow 0^+_2$ $E2$ transition of 19(2) W.u. [283] suggests that the 2^+_2 level belongs to a deformed band built on the 0^+_2 state. The $\langle Q^2 \rangle$ invariants, listed in Tab. 4, show that the 0^+_2 state in ^{94}Zr possesses greater deformation than the ground state. In ^{96}Zr, the $B(E2; 2^+_2 \rightarrow 0^+_1)$ value was recently measured using electron scattering [255]. The deduced $B(E2; 2^+_2 \rightarrow 0^+_2)$ value of 36(11) W.u., compared to the $B(E2; 2^+_1 \rightarrow 0^+_1)$ value of 2.3(3) W.u., demonstrates that an excited deformed configuration coexists with a nearly spherical ground state. From the $\langle Q^2 \rangle$ value for the former (Tab. 4) $\beta_2 \simeq 0.24$ can be estimated. In both ^{94}Zr and ^{96}Zr, there are strong $M1$ transitions observed between the 2^+_2 and 2^+_1 levels of $B(M1) \approx 0.15\ \mu^2_N$, which was suggested to be due to a mixed-symmetry component present in the 2^+_2 wave function [279, 284–286].

The lifetimes of excited states in ^{98}Zr ($N = 58$), measured following fission [237] and two-neutron transfer [238], suggest coexistence of two or three structures differing in deformation. The 2^+_3 level at 1745 keV is interpreted as built on the spherical ground state, consistent with its weak $E2$ decay to the ground state, as shown in Fig. 24. The 0^+_2 and 2^+_1 states seem to form a moderately deformed band, with $\beta_2 = 0.20(2)$ or $\beta_2 = 0.12^{+0.02}_{-0.01}$ deduced from the $B(E2; 2^+_1 \rightarrow 0^+_2)$ values of 28(6) W.u. [237] and 11^{+3}_{-2} W.u. [238], respectively. The important differences between the lifetimes of the 4^+_1 state reported in Refs. [237, 238] and the fact that the $B(E2; 4^+_1 \rightarrow 2^+_2)$ and $B(E2; 4^+_1 \rightarrow 2^+_1)$ values are comparable, make it difficult to conclude on the nature of remaining low-spin states in ^{98}Zr. Shown in Fig. 24 are two scenarios for the assignment of structures in ^{98}Zr. P. Singh *et al.* [237] postulate a second, more deformed structure to be built on the 0^+_3 level at 1436 keV, consisting of the 2^+_2 state at 1590 keV, the 4^+_1 level at 1843 keV, and the 6^+_1 level at 2491 keV. With their measured lifetimes [237], values of $\beta_2 \approx 0.25$ and $\beta_2 \approx 0.29$ are deduced for

the 4_1^+ and 6_1^+ states, respectively. In contrast, Ref. [238] reports much longer lifetimes generally, resulting in significantly smaller $B(E2)$ values, most notably of the $B(E2; 4_1^+ \rightarrow 2_2^+)$ value of 38^{+26}_{-13} W.u. In an alternative interpretation shown in Fig. 24, suggested by Karayonchev *et al.* [238], the 0_3^+, 2_2^+, 4_1^+ states form a two-quasiphonon triplet of weakly deformed states, and the 6_1^+ is a three-quasiphonon state, which is consistent with the $B(E2; 6_1^+ \rightarrow 4_1^+)/B(E2; 4_1^+ \rightarrow 2_2^+)$ ratio resulting from this study, and the enhanced $B(E2; 2_2^+ \rightarrow 2_1^+)$ value of 46^{+35}_{-14} W.u. On the other hand, in the shape-coexistence scenario the latter would suggest a strong mixing of the two deformed structures in ^{98}Zr, in line with the important mixing between the 0_2^+ and 0_3^+ states deduced for the $N = 58$ ^{96}Sr isotone from the ^{95}Sr$(d, p)^{96}$Sr neutron-transfer results [277, 278]. Moreover, the observation of a large $\rho^2(E0; 0_3^+ \rightarrow 0_2^+) = 0.076(6)$ value [102] demonstrates both a substantial change in deformation $\Delta\beta_2$ and mixing. A higher-lying 0^+ state, the 0_4^+ level at 1859 keV, decays with an enhanced $\rho^2(E0; 0_4^+ \rightarrow 0_3^+) = 0.061(8)$ [102], indicating a change in deformation β_2 also between the 0_3^+ and 0_4^+ states. The energy spectrum of ^{98}Zr and the measured $B(E2)$ values reasonably agree with the results of MCSM calculations [237] that suggest that the nearly spherical ground state coexists with two structures built on $0_{2,3}^+$ states, a moderately deformed and a strongly deformed one. The calculated proton and neutron occupancies for the 0_2^+ and 0_3^+ deformed states are very similar, and only minor differences between them lead to a change in deformation. A similarly good reproduction of the electromagnetic properties of ^{98}Zr has been achieved within a framework of the interacting boson model with configuration mixing (IBM-CM) [238], that interpreted the 0_1^+ and 2_3^+ levels as spherical single-particle states, and the remaining low-lying states were suggested to have an intruder character and be nearly spherical or weakly deformed and arranged in multiphonon structures. Consequently, the two models predict the $B(E2; 2_2^+ \rightarrow 0_3^+)$ values differing by one order of magnitude: in MCSM it is enhanced, being related to an in-band transition in a deformed structure, while in IBM-CM it is a hindered transition between two members of the two-quasiphonon triplet. Combining the lifetime of the 2_2^+ state [238] with the branching ratio for the $2_2^+ \rightarrow 0_3^+$ transition [287] yields an unphysical $B(E2; 2_2^+ \rightarrow 0_3^+)$ value of over 500 W.u., and consequently it is pertinent to remeasure these two values. A measurement of the quadrupole moments of the 2^+ states in ^{98}Zr would also likely be able to discriminate between the two theoretical interpretations.

Insight into the nature of the 0^+ states in the Zr isotopes can be ascertained from observations from transfer reactions. In a series of (t, p) reactions, the excited 0_2^+ states in ^{92}Zr and ^{94}Zr were weakly populated, with cross sections relative to the ground state of 5% and 4%, respectively, and no strength was observed to the 0_2^+ state in ^{98}Zr. In contrast, the 0_2^+ state in ^{96}Zr was populated with 39% of the ground-state cross section [288], suggestive of a neutron-pairing-vibration interpretation as might be expected due to the strong $d_{5/2}$ subshell closure. In the (p, t) reaction [280], significant strength was observed to high-lying states in ^{90}Zr, consistent with a neutron-pairing-vibration interpretation, but the 0_2^+ states in ^{92,94}Zr were weakly populated with relative strengths $< 5\%$. The enhanced population of the 0_2^+ state in ^{96}Zr was also observed in the $(d,^6\text{Li})$ reaction, where it was populated stronger by a factor 2.2 than the ground state, and much stronger than excited 0^+ states in other Zr isotopes [289]. From an analysis of the $(^3\text{He},d)$ and $(d,^3\text{He})$ reactions [290, 291], the fullness factors for the $\pi p_{1/2}$ orbital in the Zr ground states were deduced. The average of the two results yield ground-state wave functions with admixtures, a^2, for the $\pi(p_{1/2})^2$ component of 0.6, 0.5, 0.65, and 0.9 for ^{90,92,94,96}Zr, respectively. It was found that a qualita-

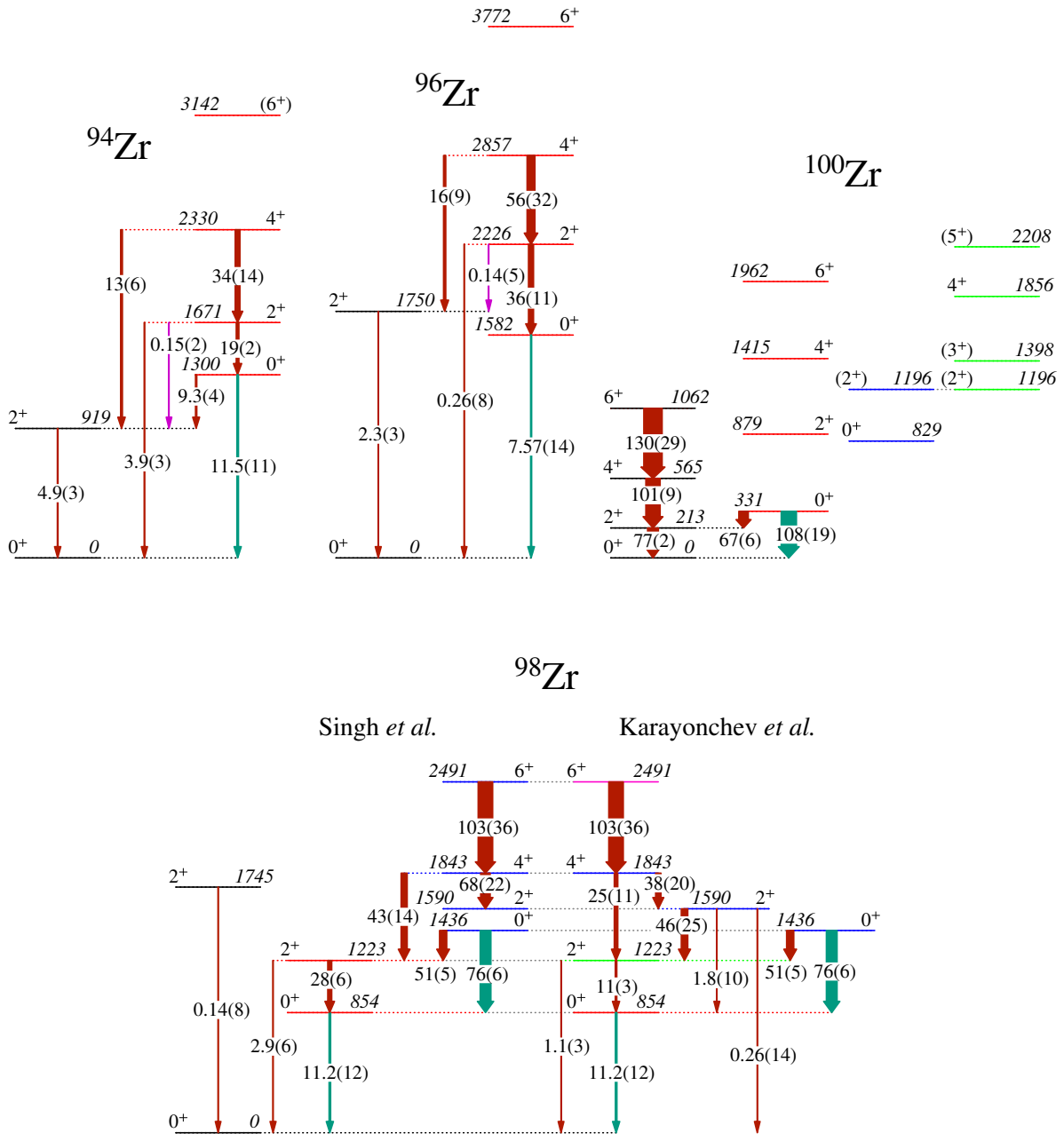

Figure 24: Properties of the low-lying states observed in the even-even Zr isotopes. The $E2$ transitions (rust coloured) are labelled with their $B(E2)$ values in W.u., the $E0$ transitions (green) with their $10^3 \times \rho^2(E0)$ values, and the $M1$ transitions (purple) with their $B(M1)$ values in μ_N^2. The levels are colour-coded according to assigned configurations. For ^{98}Zr, dashed gray lines are used to connect the same energy levels in the proposed band structures resulting from the two interpretation scenarios outlined in the text. For ^{100}Zr, the (2^+) state at 1196 keV has been alternatively suggested as a member of the 0_3^+ band (blue) [2], or as the head of the γ band (green) [276]. Data are taken from the National Nuclear Data Center database [39] and Refs. [102, 237, 238, 255, 276, 283].

tive explanation of the (d,^{6}Li) cross sections could be obtained with modelling of the 0^+_1 state as $a\pi(p_{1/2})^2 + b\pi(g_{9/2})^2$ with an orthogonal combination adopted for the 0^+_2 state, where the amplitude a is derived from the above admixture factors. These results demonstrated the role that the proton configuration was playing in the (d,^{6}Li) reaction – a result confirmed in the two-proton pickup (^{6}Li,^{8}B) reaction performed on targets of ^{92,94,96,98,100}Mo [292]. In the ^{98}Mo(^{6}Li,^{8}B)^{96}Zr reaction, an enhanced cross section to the 0^+_2 state in ^{96}Zr was observed, where it was populated with a cross section equal to that for the ground state, and in ^{98}Zr the cross section to populate the 0^+_2 state was found to exceed that for the ground state by a factor of 2.1. This was taken as evidence that the $\pi(p_{1/2})^2$ component in the ground-state wave function increased to 96%, and that of the $\pi(g_{9/2})^2$ component was 4% [292]. We note that this is in qualitative agreement with the MCSM results for ^{98}Zr [237, 293], although the calculated wave functions are far more complex than those of the simple analysis performed in Refs. [289, 292].

The similarity in the structures of ^{98}Sr and ^{100}Zr, with the 0^+_2 states decaying via enhanced $E0$ transitions to the ground state, and the structures built on them having much smaller moments of inertia compared to the ground-state band, was shown in Ref. [2]. Measurements on ^{100}Zr have been thus far mostly constrained to those using fission sources or β decay. Recent measurements [273] for ^{100}Zr, obtained from ^{248}Cm fission, have confirmed the lifetimes of states in the ground state band of the $8^+ - 12^+$ band members. Direct timing measurements [241], with ^{100}Zr obtained from ^{235}U and ^{241}Pu fission, were in agreement with the previously established lifetime of the 2^+_1 level, but gave a somewhat shorter lifetime for the 4^+_1 state. To date, no measurements of lifetimes have been performed for the rotational states in the 0^+_2 band.

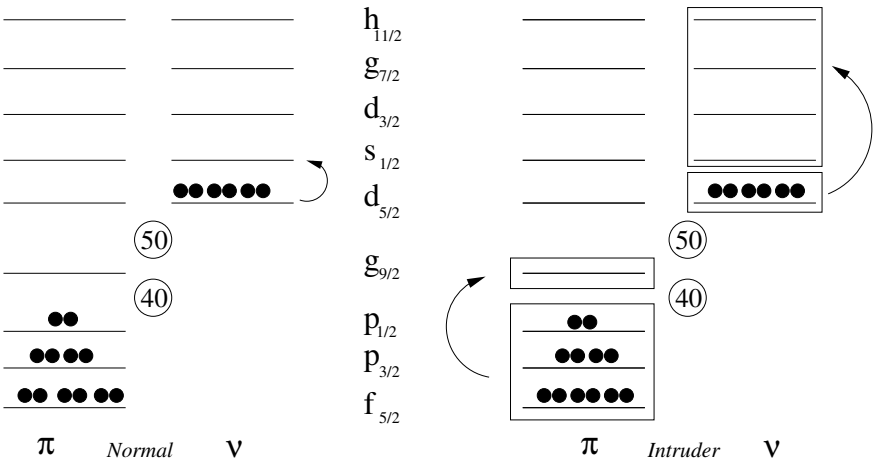

Figure 25: Orbitals relevant for the description of the $A = 100$ mass region in the spherical shell model. Their ordering follows the calculations of Refs. [237, 255, 293]. The energy spacing is arbitrary (see text for details).

Figure 25 shows the orbitals relevant for the present discussion and a schematic picture of the normal-ordered and intruder configurations as deduced from the studies of the even-even Zr and Sr isotopes presented in this section. In the calculations of Refs. [255, 293], the normal configuration corresponds to the 0^+_1 and 2^+_1 excitation in ^{96}Zr, with the 2^+_2 state as an intruder configuration, and these assignments are consistent with the experimental data. The $0^+_{2,3}$ and $2^+_{1,2}$ states in ^{98}Zr [237]

also are calculated to have intruder character, with proton $p-h$ excitations from the pf shell into the $g_{9/2}$ orbital and neutron excitations from the $d_{5/2}$ orbital into higher-lying shells, even including the $h_{11/2}$ orbital.

3.4.2. *Odd-mass and odd-odd nuclei with $Z \approx 40$*

In odd-mass isotopes, the spin and parity of the ground state and long-lived isomers give strong indication of the involved Nilsson orbitals. Figure 26 shows the systematics of ground and isomeric states in Zr, Y and Sr isotopes, highlighting those that have measured quadrupole moments. Isotones are presented in the same column and a colour code indicates the element.

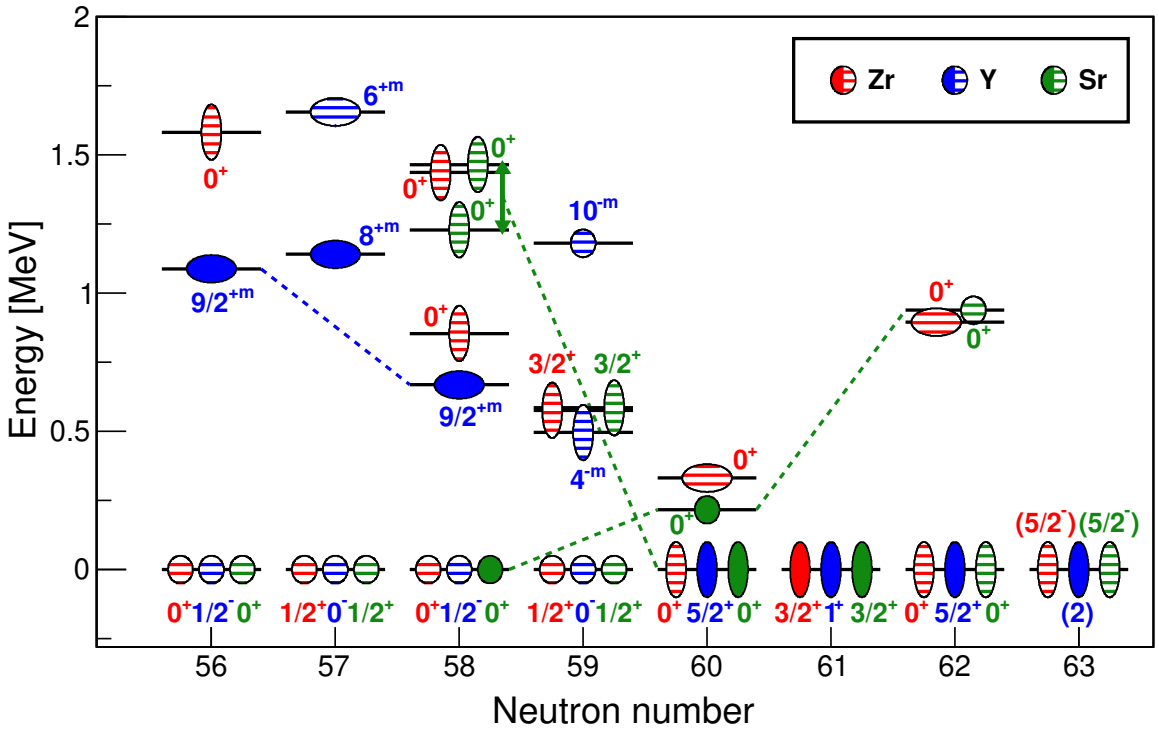

Figure 26: Systematics of shape-coexisting states in Zr (red), Y (blue) and Sr (green) isotopes with $56 \leq N \leq 63$. The horizontally stretched ellipses denote oblate deformation, vertically stretched ones prolate or triaxial, and circles nearly spherical shapes. Filled symbols are used if the deformation was extracted from spectroscopic quadrupole moments measured in laser spectroscopy or Coulomb excitation. Patterned symbols are used if the deformation was deduced from level energies or a comparison with model calculations. The dashed lines connect the levels if there are arguments for their configurations being similar. The arrow between the 1229-keV and 1465-keV states in ^{96}Sr denotes their strong mixing, with the deformed unperturbed configuration resembling that of the ground state in ^{98}Sr (see text for details). The interpretation used for ^{98}Zr is that from Ref. [237]; Fig. 24 displays an alternative interpretation from Ref. [238].

Even-neutron odd-proton nuclei. The spins and parities of the ground states of odd-mass yttrium isotopes with $48 \leq N \leq 58$ are $I^\pi = 1/2^-$, and the large single-proton pickup strengths from the

even-even Zr targets [290, 294] demonstrate that these ground states have a normal-order configuration with a single proton in the $2p_{1/2}$ orbital. The odd-A Y isotopes, $^{85-97}$Y, also possess $I^\pi = 9/2^+$ isomers that can be characterized as (predominately) $\pi g_{9/2}$ single-particle excitation. Spectroscopic quadrupole moments have been measured for many of these isomeric states [295], and they vary from $Q_s = -0.43(6)$ eb in ^{89}Y to $-0.76(8)$ eb for ^{97}Y. This latter value can be interpreted as favouring an oblate shape for the isomeric state that can be considered as $\pi g_{9/2} \otimes ^{96}$Sr(g.s.), and it has been suggested [296] that the weak-coupled states involving the $13/2^+$ $\pi g_{9/2} \otimes ^{96}$Sr($2^+_1$), and $17/2^+$ $\pi g_{9/2} \otimes ^{96}$Sr($4^+_1$) lie at 1657 keV and 2559 keV, respectively.

The low-lying states in the $N = 58$ isotones above $Z = 40$ appear as spherical, with the exception of ^{101}Tc. The most extensive assignments of the single-particle states are for ^{99}Nb populated with single-proton transfer reactions on ^{100}Mo [294], and favour a spherical shape, in agreement with the lack of rotational bands. In ^{101}Tc, on the other hand, rotational-like bands appear that have been described as arising from its asymmetric rotor character [297], and they display a strong similarity to the ground-state bands of ^{100}Mo and ^{102}Ru, both of which have a triaxial nature [23, 254].

At $N = 60$, the ^{99}Y ground state changes structure compared to the lighter Y isotopes and has $I^\pi = 5/2^+$ with a rotational band observed (see, e.g., Ref. [298]) that is assigned as the π5/2[422] configuration. As shown in Fig. 27, the 5/2[422] orbital also forms the ground-state configurations of ^{101}Nd and ^{103}Tc, and has been shown to persist in the heavier Y and Nb isotopes [301]. The deformed nature of ^{99}Y is supported by the value of $\beta_2 \simeq 0.4$ extracted from both laser spectroscopy [295] and in-beam γ-ray spectroscopy [299–301]. Lifetimes in the 5/2[422] ground-state rotational bands were also measured in ^{101}Y and ^{101,103,105}Nb [301], and they were shown to be consistent with deformations of $\beta_2 = 0.35 - 0.4$. It should be noted that the $B(E2; 2^+_1 \rightarrow 0^+_1) = 0.259(8)$ e^2b^2 in ^{98}Sr [247] is similar to the measured $B(E2; 9/2^+ \rightarrow 5/2^+) = 0.25(2)$ e^2b^2 for the 5/2[422] rotational band in ^{99}Y [301], strongly supporting comparable collectivity. There is no firm evidence for the appearance of spherical states in the $N = 60$ isotones shown in Fig. 27. In ^{97}Rb, an isomeric state at 77 keV was shown to have negative parity [302], and comparison to calculations favoured $I^\pi = 1/2$ or $3/2^-$ values for the level that could arise from either an oblate or a prolate shape. The ground-state band in ^{97}Rb, based on the 3/2[431] orbital, was determined to have a prolate shape with a large transitional quadrupole moment $Q_t = 2.95(5)$ eb [303].

Even-proton odd-neutron nuclei. The ground-state spins of the odd-mass Zr isotopes with $N > 50$ follow the expected pattern for neutrons above the $N = 50$ shell gap, with $I^\pi = 5/2^+$ for ^{91,93,95}Zr. The magnetic moments have been measured for the ground states with values of $\mu = -1.30362(2)$ μ_N for ^{91}Zr [304], and slightly less $|\mu| = 1.103(23)$ μ_N for ^{95}Zr [305]. The very strong populations of the ^{91,93,95}Zr ground states in single-neutron transfer reactions are consistent with a single-particle $\nu d_{5/2}$ configuration. In ^{97}Zr, the ground state has $I^\pi = 1/2^+$ with a measured magnetic moment of $\mu = -0.937(2)_{stat}(3)_{sys}$ μ_N, and was strongly populated in the ^{96}Zr(d, p) reaction with $L = 0$ and a spectroscopic factor of $S = 1$ [306], consistent with a single-particle $\nu s_{1/2}$ assignment.

Measurements of isotope shifts for the Zr isotopes, shown in Fig. 20, [307] demonstrate a sudden increase in the mean-square charge radii occurring at $N = 60$ (^{100}Zr). The ground state of ^{99}Zr, with $I^\pi = 1/2^+$, has a measured magnetic moment of $\mu = -0.930(1)_{stat}(3)_{sys}$ μ_N, nearly identical to that of ^{97}Zr. The apparent lack of a rotational band associated with the ground state,

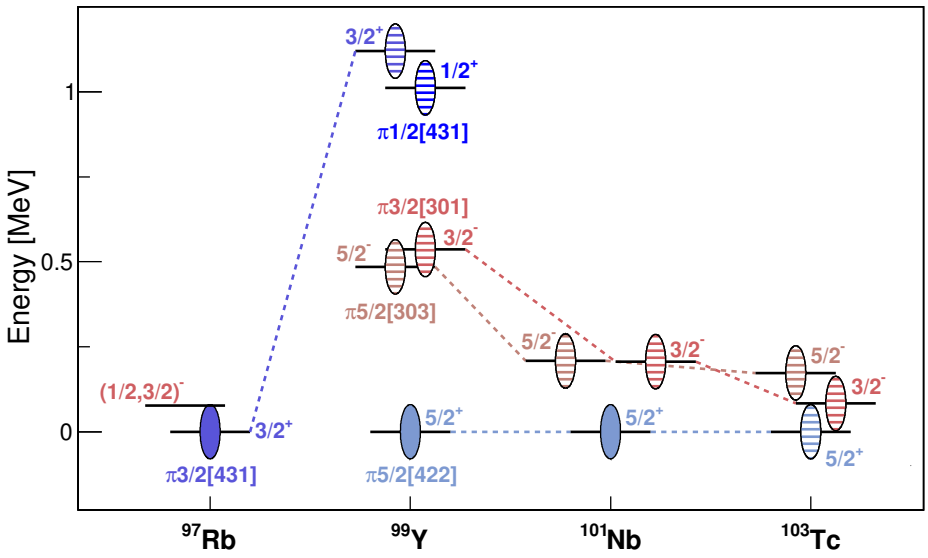

Figure 27: Low-lying non-rotational states in the $N = 60$ isotones ^{97}Rb, ^{99}Y, ^{101}Nb, and ^{103}Tc. The ellipses denote prolate deformation, filled symbols are used if the deformation was extracted from spectroscopic quadrupole moments measured in laser spectroscopy, and patterned symbols if it was deduced from level energies or a comparison with model calculations. The dashed lines connect the levels if there are arguments for their configurations being similar.

together with the trend observed in the isotope shifts and the magnetic moment, strongly favour a spherical or very weakly deformed shape for the ground state of ^{99}Zr. In contrast, the structure observed in ^{101}Zr, with a clear rotational band built on the $I^\pi = 3/2^+$ ground state, and the measured spectroscopic quadrupole moment of $Q_s = +0.812(56)$ eb [307], is consistent with a deformed nature of the ground state. The lack of observed rotational bands built on the $3/2^+$ and $7/2^+$ states in ^{99}Zr favours a spherical shape interpretation for those levels, and hence they are given the νl_j labels in Fig. 28. However, very recent measurements of the magnetic moments of the $3/2^+_1$ and $7/2^+_1$ states in ^{99}Zr [308] of $\mu = +0.42(6)$ and $|\mu| = 2.31(4)$, respectively, were interpreted within interacting boson-fermion model (IBFM) calculations. The wave functions were described as mixtures of the $d_{5/2}$, $g_{7/2}$, $s_{1/2}$, and $d_{3/2}$ spherical orbitals, as would be expected for deformed states. As pointed out in Ref. [308] the g-factor for the $7/2^+$ state exceeds the Schmidt limit (Eq. 24) for a single-particle $g_{7/2}$ state. The apparent disagreement over the interpretation of these low-lying levels has been pointed out in Refs. [309, 310], and emphasize the need for more experimental information on the excitations in ^{99}Zr.

There are rotational bands in ^{99}Zr, the lowest built on the state at 576 keV assigned as a mixture of the $\nu 3/2[411]$ and $\nu 3/2[422]$ orbitals, followed by the $\nu 3/2[541]$ configuration at 614 keV, and the $\nu 9/2[404]$ configuration at 1039 keV [311]. These states are also shown in Fig. 28. Very recent lifetime measurements [312] for the $\nu 3/2[411]$ and $\nu 3/2[541]$ band members result in transitional quadrupole moments consistent with deformations of $\beta_2 = 0.32(3)$ and $\beta_2 = 0.34(1)$. The band based on the $9/2[404]$ orbital has been identified in ^{101}Zr, as well as in the $N = 59$ isotone ^{97}Sr,

and the isomeric nature of the band head has been attributed to the hindrance of the γ-ray decays due to the $\Delta K = 3$ required (one degree of K forbiddenness for $E2$ transitions) to the lower-lying $K^\pi = 3/2^+$ orbital [313]. It should be noted that this demonstrates that K is already a good quantum number, and that the γ-ray transitions are hindered in spite of the allowed $g_{9/2} \rightarrow d_{5/2}$ single-particle transition that could occur between the spherical-basis orbitals that are dominant in the 9/2[404] and 3/2[411] configurations, respectively. The low-lying level structure of ^{97}Sr has a strong similarity to that of ^{99}Zr, possessing a $I^\pi = 1/2^+$ ground state, with a $3/2^+$ state at 167 keV and a $7/2^+$ state at 308 keV that are analogous to the spherical states in ^{99}Zr, as well as the $3/2^+$[411], $3/2^-$[541], and $9/2^+$[404] configurations with their associated rotational bands. Lifetime measurements [314, 315] for the spherical states and some rotational band members in ^{97}Sr and ^{99}Zr reinforced the previous determinations of the transitional quadrupole moments and are consistent with the assumed shapes. The $1/2^+$, $3/2^+$ and $7/2^+$ states in ^{97}Sr were populated in the (d, p) reaction [278] with strengths considerably lower than expected for spherical shell model states, but this was attributed to the complicated ^{96}Sr ground-state wave function as mentioned above. The most interesting result for ^{97}Sr was the observation of the $L = 2$ transfer to the 522-keV $(1/2^+)$ level, which lead to its re-assignment as $(3/2,5/2)^+$, with the $5/2^+$ spin-parity favoured due to the observation of such a state in ^{95}Sr [278]. It might be expected that the low-lying states in the $N = 59$ isotone ^{101}Mo would resemble those in ^{97}Sr and ^{99}Zr, but the data are inconclusive. The ^{101}Mo ground state has a $\nu s_{1/2}$ assignment, as revealed from the single-neutron transfer reaction [316]. The $L = 2$ transfer strength in the ^{100}Mo(d, p) reaction is highly fragmented, with the strongest transitions to the $5/2^+$ state at 57 keV and the $3/2^+$ state at 352 keV. This may favour their assignments as the $d_{5/2}$ and $d_{3/2}$ states, but the spectroscopic strengths are not sufficiently large to provide a convincing assignment. Further, the $3/2^+$ state at 13 keV, weakly populated in the single-neutron transfer reaction, may be a candidate for the $3/2^+$[411] state, but the associated rotational band has not been identified (we note that the 57-keV $5/2^+$ state decays with $B(E2; 5/2^+ \rightarrow 3/2^+) = 33(19)$ W.u. [39]). This difficulty to assign spherical and deformed states may be due to the triaxial deformation of the ^{100}Mo ground state [23], in contrast to the spherical ground states for ^{96}Sr and ^{98}Zr. Thus, shape coexistence has been established in ^{97}Sr and ^{99}Zr, but cannot yet be claimed in ^{101}Mo. It is to be noted that in the $N = 59$ isotone ^{95}Kr, the three lowest excited states also bear a strong resemblance to those in ^{97}Sr and ^{99}Zr, but higher-lying rotational bands are yet to be discovered.

On the other side of the shape transition at $N = 60$, the $N = 61$ isotones of Sr, Zr, and Mo might also be expected to exhibit shape coexistence. The low-lying states are shown in Fig. 28 (right) with their Nilsson classifications. Since the spherical structures beyond $N = 60$ are no longer expected to form the ground states, if they exist they would be located within a background of deformed and rotational states, making their identification extremely difficult. To date, the spectroscopic knowledge is insufficient to ascertain shape coexistence at $N = 61$ and beyond.

Odd-odd nuclei. In $N = 57$ ^{96}Y, the properties of the structures built on the 0^- ground state and the 8^+ isomer point to their nearly spherical shapes. The spectroscopic quadrupole moment of the 8^+, 9.6-s isomer, $-98(11)$ $e$fm^2, corresponds to a weak β_2 deformation of -0.16(2) [295]. A rotational band built on the (6^+), 181(9)-ns isomeric state at 1655 keV was recently identified, and its moment of inertia suggests an oblate deformation [317]. The non-observation of transitions between

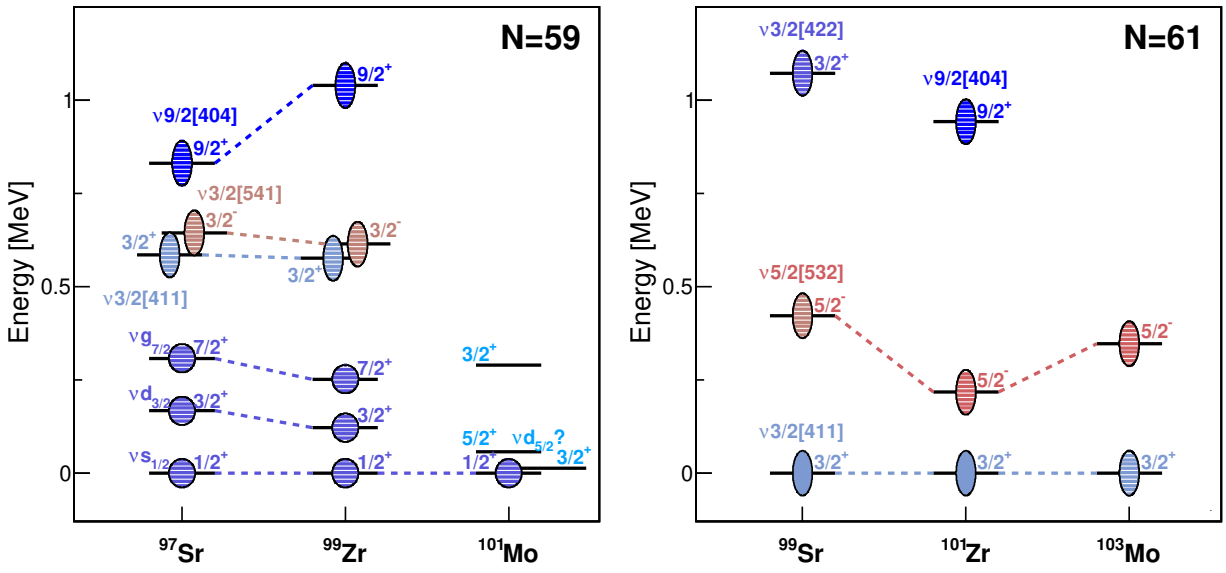

Figure 28: Low-lying non-rotational states in the (left) $N = 59$ isotones ^{97}Sr, ^{99}Zr, and ^{101}Mo and (right) $N = 61$ isotones ^{99}Sr, ^{101}Zr, and ^{103}Mo. The ellipses denote prolate deformation, and circles nearly spherical shapes. Filled symbols are used if the deformation was extracted from spectroscopic quadrupole moments measured in laser spectroscopy, and patterned symbols if the deformation was deduced from level energies or a comparison with model calculations. The dashed lines connect the levels if there are arguments for their configurations being similar. The states in ^{101}Mo are difficult to classify, as explained in the text.

this band and the structure identified above the 8^+, 9.6-s isomer, despite similar spins, is consistent with a large structural difference between the two configurations. In $N = 59$ ^{98}Y, detailed spectroscopy of the isomers [318] shows the coexistence of several deformed bands, including intruder configurations, as well as the presence at low excitation energy of the neutron $\nu 9/2[404]$ Nilsson orbital and a (8^+) spherical configuration similar to the 8^+ isomeric state in ^{96}Y.

3.4.3. Mo isotopes

The stable Mo isotopes have provided an excellent laboratory in which to study shape coexistence, as they span from the closed $N = 50$ shell ^{92}Mo to $N = 58$ ^{100}Mo. The systematics of the low-lying states in the even-even Mo isotopes are shown in Fig. 29, which include the recently discovered 0_2^+ states in ^{108,110}Mo [319]. The energy of the 0_2^+ state drops dramatically with increasing neutron number: at the closed neutron shell it is found at 2.5 MeV, then becomes the first excited state in $N = 56$ ^{98}Mo at 735 keV, and finally reaches a minimum in ^{100}Mo at 695 keV. It should be noted that the 2_1^+ state in ^{98}Mo does not have the high energy encountered in ^{96}Zr, but rather mirrors the trend observed in the Sr isotopes as shown in Fig. 22. Unlike Sr and Zr, however, the 2_1^+ energies do not undergo a sudden drop in energy when proceeding from $N = 58$ to $N = 60$, and the 0_2^+ energies are somewhat constant from ^{98}Mo to ^{102}Mo before rising slightly to approximately 1 MeV in ^{104}Mo. Detailed Coulomb-excitation studies of the stable ^{96,98,100}Mo

isotopes yielded quadrupole invariants for the ground and 0^+_2 states [23, 256, 320] as listed in Tab. 4. As shown in Fig. 30, the $\langle Q^2 \rangle$ values, calculated using Eq. 26, are vastly different for the 0^+_1 and 0^+_2 states in ^{96}Mo, with that for the 0^+_2 state possessing a very small value consistent with an approximately spherical shape. It is, in fact, difficult to identify the 2^+ state associated with the 0^+_2 state, as very similar $B(E2)$ values of < 1 W.u are measured for the transitions to the 0^+_2 level from each of the 2^+_2, 2^+_3, and 2^+_4 states [256]. The ground-state band, on the other hand, has definite collectivity with enhanced transitions and $B(E2; 2^+_1 \rightarrow 0^+_1) = 20.7(4)$ W.u. Unfortunately, the quadrupole moment for the 2^+_1 state has considerable uncertainty, with values ranging from $+0.04(8)$ or $-0.20(8)$ eb [304], or $-0.33(4)$ eb [256]. In the case of ^{98}Mo, both the 0^+_1 and 0^+_2 states have approximately the same values of $\langle Q^2 \rangle$; however, the values of $\langle \cos 3\delta \rangle$ (Eq. 29) indicate that the ground state is triaxial, whereas the 0^+_2 state is much closer to a prolate shape. The 2^+_3 state in ^{98}Mo appears to be associated with the 0^+_2 level with $B(E2; 2^+_3 \rightarrow 0^+_2) = 7.2(3)$ W.u. [320]. An $E0$ decay with $10^3 \times \rho^2(E0; 0^+_2 \rightarrow 0^+_1) = 27.3(11)$ [102] confirms the difference in shape between the two states. The invariant quantities $\langle Q^2 \rangle$ extracted for both the 0^+_1 and 0^+_2 states in ^{100}Mo are significantly greater than those for ^{98}Mo, with that for the 0^+_2 state being much larger, and the $\langle \cos 3\delta \rangle$ values repeat the pattern as in ^{98}Mo that the 0^+_2 state is prolate, and the 0^+_1 state is triaxial.

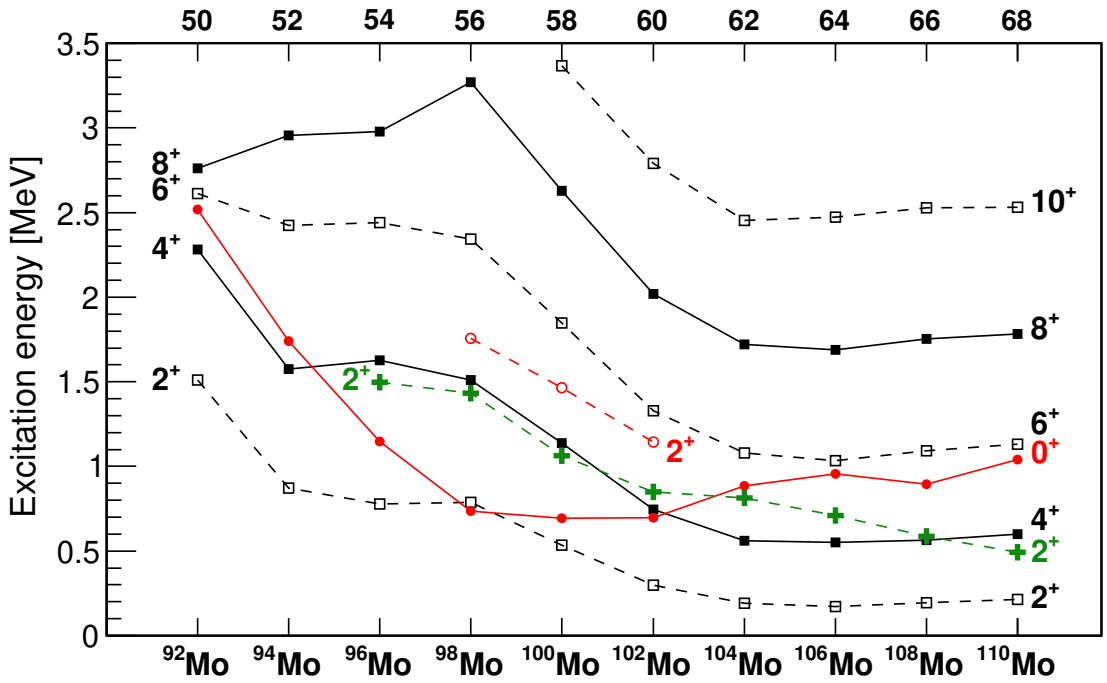

Figure 29: Energy systematics of positive-parity excited states in molybdenum isotopes with $50 \leq N \leq 68$, with ground-state structures denoted with black squares, 0^+_2 states and members of the bands built on them with red circles, and the 2^+_2 states (band heads of the $K = 2$ bands) with green crosses. Data are taken from the National Nuclear Data Center database [39] and Ref. [319].

The 2^+ member of the 0^+_2 band is well established as the 2^+_3 state with $B(E2; 2^+_3 \rightarrow 0^+_2) = 19.1(6)$ W.u. [23]. The $E0$ transition also becomes more enhanced, with $10^3 \times \rho^2(E0; 0^+_2 \rightarrow 0^+_1) = 36(6)$ [102]. For the $N = 60$ ^{102}Mo, the invariant quantities are not determined, but if we use the approximation that the 2^+_1 state exhausts most of the $E2$ strength to the ground state, $\langle Q^2 \rangle = 1.05(13)$ e^2b^2 can be estimated. The largest $E0$ transition in the Mo isotopes is observed in ^{102}Mo, with $10^3 \times \rho^2(E0; 0^+_2 \rightarrow 0^+_1) = 120(50)$ [102], definitely indicating that the 0^+_2 state possesses a significantly different deformation from that of the ground state.

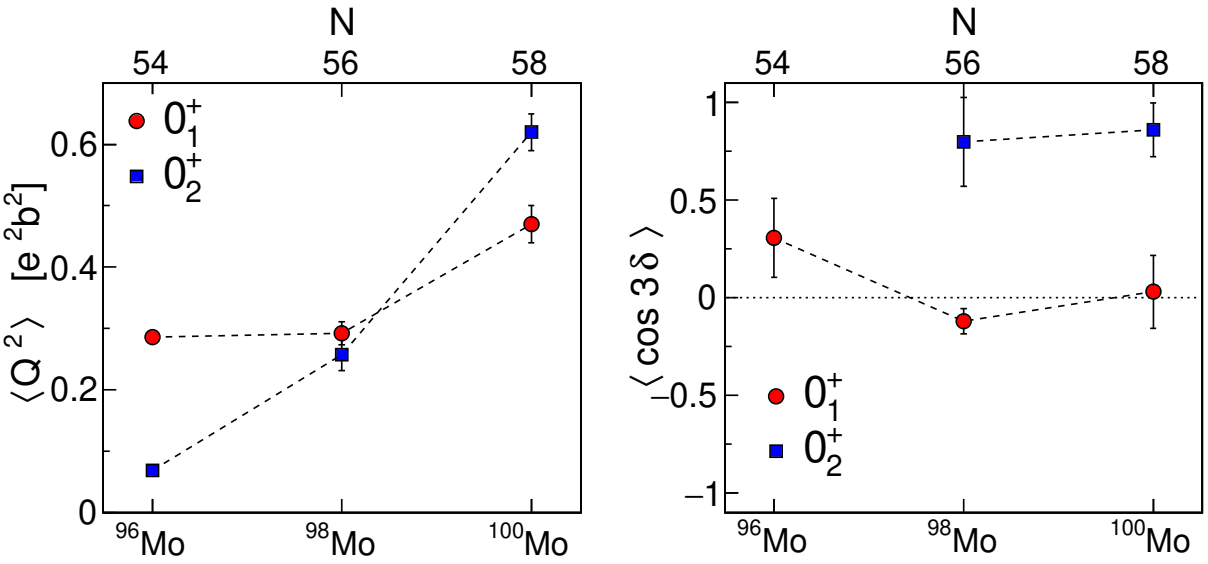

Figure 30: Quadrupole invariant quantities $\langle Q^2 \rangle$ and $\langle \cos 3\delta \rangle$ determined for the $^{96-100}$Mo isotopes. Data are from Refs. [23, 256, 320].

The proton vacancies and neutron occupancies (see Sect. 2.7) for ^{98}Mo and ^{100}Mo were extracted in an extensive series of single-proton and single-neutron transfer reactions on targets of ^{98,100}Mo and ^{100,102}Ru [321], and are shown in Fig. 31. The changes in the neutron occupancy between ^{98}Mo and ^{100}Mo reflect the additional two neutrons which are predominately in the $g_{7/2}$ and $h_{11/2}$ orbitals. Interestingly, one also sees a change in the proton occupancy, with a rearrangement from the $p_{1/2}$ and the $f_{5/2}$ orbital to the $g_{9/2}$ orbital. These changes in occupancy are reflected in the changes in deformation of the ground state, as outlined above. With these results, the Mo isotopes, specifically ^{98,100}Mo, offer the rare opportunity for understanding structure in medium-heavy nuclei in that detailed information on the shapes, through the sum-rule invariants, and the microscopic components of the wave functions are known to high precision.

3.4.4. Ru isotopes

The Ru isotopes, located adjacent to the Mo isotopes with their well-established examples of shape-coexisting structures, might be considered as candidates for shape coexistence as well, but the evidence in support of this has been sparse. The energy systematics of the 2^+_1 states,

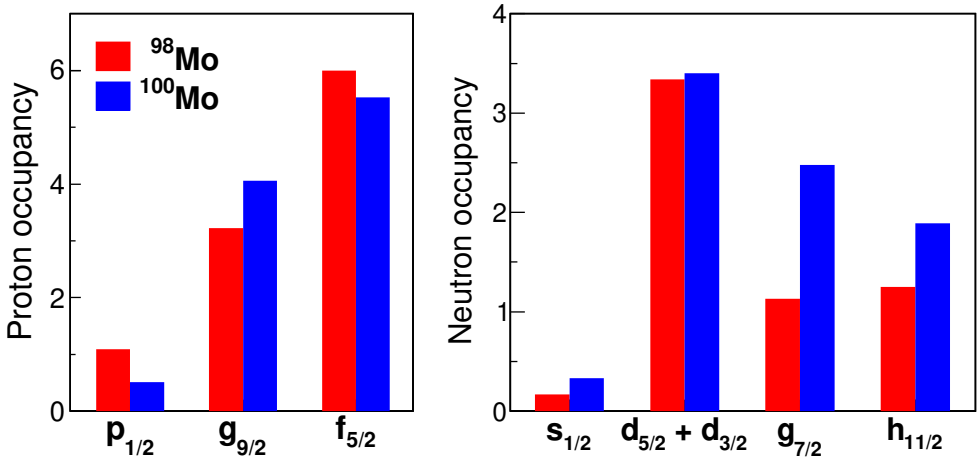

Figure 31: Occupancies extracted from results of transfer reactions on targets of ^{98,100}Mo [321] for the $\pi p_{1/2}$, $\pi g_{9/2}$, and $\pi f_{5/2}$ orbitals (left) and for the $\nu s_{1/2}$, $\nu d_{5/2} + d_{3/2}$, $\nu g_{7/2}$, and $\nu h_{11/2}$ orbitals (right). The proton occupancies have been deduced from the listed vacancies in Ref. [321]. The uncertainties on the total occupancies were estimated to be in the 0.2-0.3 range.

and the ratios $E(4_1^+)/E(2_1^+)$ have been used to suggest that the ground-state shape evolves from spherical for the lighter Ru isotopes, ^{96,98}Ru, to γ-soft and deformed for the heavier Ru isotopes ^{106,108}Ru, and this evolution has often been modeled using the IBM (see, e.g., Refs. [322–326]). Because of this evolution of the shape, it has been difficult to use the typical indicators of shape coexistence, such as the energy systematics of the 0_2^+ state for example. The best evidence for shape coexistence to date has been inferred from Coulomb excitation. The results from a Coulomb-excitation study of ^{104}Ru, performed by Stachel *et al.* [327], were used to suggest that the 0_2^+ state was not the first excited 0^+ state predicted by collective models, but rather was built on an "intruder" configuration with a smaller deformation and a higher degree of triaxiality than the ground state. The large number of matrix elements obtained in the Coulomb-excitation study of ^{104}Ru performed by Srebrny *et al.* [258] permitted several sum-rule invariant quantities to be determined, including both the $\langle Q^2 \rangle$ (Eq. 26) and $\langle \cos 3\delta \rangle$ (Eq. 29) for the ground state and 0_2^+ state, as listed in Tab. 4. The $\langle Q^2 \rangle$ values for the ground-state band were approximately constant at 0.9 e^2b^2 up to spin 8^+, which corresponds to $\beta_2 \approx 0.28$, and the dispersion in this value was $\sigma(Q^2) \approx 0.22(6)$ e^2b^2 (Eq. 35) [258], indicating some softness but far from vibrational. For the 0_2^+ state, the $\langle Q^2 \rangle \approx 0.52(12)$ e^2b^2 corresponds to $\beta_2 \approx 0.21$, significantly less than that of the ground state. The $\langle \cos 3\delta \rangle$ value for the ground state was approximately 0.38(12), which is equivalent to the shape parameter $\gamma \approx 25°$, and that for the 0_2^+ state 0.1(3), which indicates, within uncertainty, a maximally triaxial shape. The gradual change in the shape of the ground state of the Ru isotopes, in contrast to the rapid change observed in Sr and Zr isotopes, was suggested [328] as due to the occupation of protons in the $g_{9/2}$ orbital that block the promotion of protons from the lower pf orbitals.

A study of ^{102}Ru by Urban *et al.* [329], using the (n, γ) reaction, assigned the band built on the 0_2^+ state. Based on the energy systematics, beginning at $N = 52$ ^{96}Ru, it was suggested that the

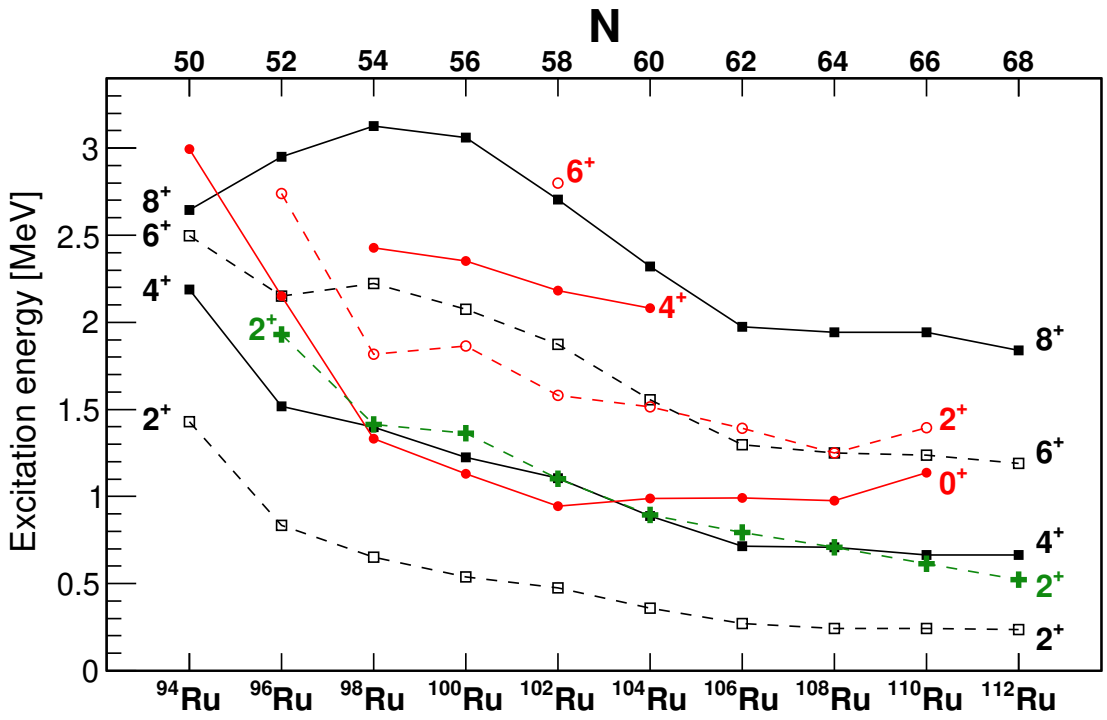

Figure 32: Observed excitation energies in the even-even Ru isotopes from $A = 94$ to $A = 112$ of states assigned to 0^+ bands, and the 2^+_2 state.Data taken from the National Nuclear Data Center database [39] and Ref. [254].

ground state in the lighter Ru isotopes was nearly spherical in shape, and it crossed with the 0^+_2 configuration in the region of ^{100,102}Ru to become the 0^+_2 state. The 0^+_2 state in ^{96}Ru was also suggested to possess a low deformation, but with increasing neutron number the deformation increased. The mixing in the crossing region resulted in both states taking on deformed characteristics.

A recent study of ^{98}Ru [254] has revealed the presence of bands built on the 0^+_2 and 2^+_2 states. Shown in Fig. 32 are the systematics of the ground-state band, the "γ" band, and the 0^+_2 band in the chain of Ru isotopes from ^{96}Ru to ^{106}Ru. It was noted that the $0^+ - 2^+ - 4^+$ level spacing of the ground-state band in ^{98}Ru matched that of the 0^+_2 band in ^{102}Ru, and the spacing in the 0^+_2 band in ^{98}Ru matched that of the ground-state band in ^{102}Ru. Focusing on the behaviour of the bands, rather than only the 0^+ band heads, it was suggested [254] that the crossing of the configurations occurs between ^{98}Ru and ^{100}Ru. The $\langle Q^2 \rangle$ quantities for ^{100,102,104}Ru for the 0^+_1 and 0^+_2 states, listed in Tab. 4, show a trend that the ground-state deformation is increasing with neutron number. The $\langle Q^2 \rangle$ invariant for the 0^+_2 state in ^{100}Ru is slightly greater than that of its ground state. In contract, in both ^{102,104}Ru the 0^+_2 $\langle Q^2 \rangle$ values are substantially lower than those of the ground states, consistent with the picture of crossing configurations.

3.4.5. *Configuration mixing in the $Z \approx 40$ region*

Experimental data, in particular $E2$ matrix elements, can be used to calculate the mixing amplitudes, $\cos^2\theta_I$, between the two pure (unperturbed) configurations. Following the method described in Ref. [222], using the complete set of $E2$ matrix elements in ^{98}Sr small mixing angles of $\cos^2\theta_0 = 0.82(2)$ and $\cos^2\theta_2 = 0.99(1)$ were extracted for the 0^+ and 2^+ wave functions, respectively [247–249]. An evaluation of the mixing angles for the 0^+ and 2^+ states requires a large set of $E2$ matrix elements, which is not available for many nuclei in this mass region. Assuming a negligible mixing between the 2^+ states, however, one can extract an approximate mixing angle for the 0^+ states from the $\langle 0_2^+||E2||2_1^+\rangle$ and $\langle 0_1^+||E2||2_1^+\rangle$ matrix elements using Eq. 39. The $\cos^2\theta_0$ values obtained in this way for $N = 58, 60$ Sr, Zr, Mo, Ru and Pd nuclei are presented in Tab. 5. In general, a rather weak mixing between the ground state and the excited configuration is observed for nuclei in this mass region, both inside and outside the region of enhanced ground-state deformation.

Table 5: Values of $\cos^2\theta_0$ for the mixing angles between the 0^+ states in $N = 58, 60$ nuclei extracted using Eq. 39. The second and fourth column show the $B(E2)$ values used for the calculations.

Element	$N = 58$		$N = 60$	
	$B(E2;2_1^+ \to 0_1^+)/B(E2;0_2^+ \to 2_1^+)$ $[e^2b^2]$	$\cos^2\theta_0$	$B(E2;2_1^+ \to 0_1^+)/B(E2;0_2^+ \to 2_1^+)$ $[e^2b^2]$	$\cos^2\theta_0$
Pd	0.10(5) / 0.038(3)[330]	0.93(8)	0.13(3) / 0.10(2)[334]	0.86(6)
Ru	0.127(1) / 0.010(1) [332]	0.984(2)	0.168(3) / 0.072(8) [258, 330]	0.92(1)
Mo	0.095(3) / 0.26(1) [23]	0.64(2)	0.209(25) / 0.19(8) [332]	0.84(7)
Zr	0.007(2) / 0.38(11)[237]	0.90(5)	0.206(11) / 0.037(3) [331]	0.965(5)
Sr	$0.045^{+0.011}_{-0.008}$ / 0.040(4) [247, 333]	0.85(5)	0.259(8) / 0.25(2)[247]	0.84(2)

3.5. *Shape coexistence around $Z = 50$*

The nuclei in the immediate vicinity of $Z = 50$, especially the Cd and Sn isotopes, have provided well-studied examples of shape coexistence (see, e.g., Ref. [6]). An advantage that this region offers is that the even-Z species have many stable isotopes, and thus a wide variety of probes have been used in their study. This is reflected in Fig. 33, which demonstrates the richness of experimental data supporting shape coexistence in specific nuclei from Pd through Te. Ironically, while long-recognized in the Cd and Sn isotopes, shape coexistence is less well established (or accepted) in the Te or Pd isotopes, and it is not widely observed in the odd-A isotopes.

3.5.1. *Cd isotopes*

The discovery of shape coexistence in the Cd isotopes is intimately linked with their suggestion as excellent examples of nearly harmonic vibrational motion. Very early studies [16, 17] identified additional 0^+ and 2^+ levels in the vicinity of the two-phonon triplet, which were suggested [335, 336] to belong to shape-coexisting structures. The shape-coexistence interpretation remained speculative until Meyer and Peker [337], using γ-ray spectroscopy following β-decay

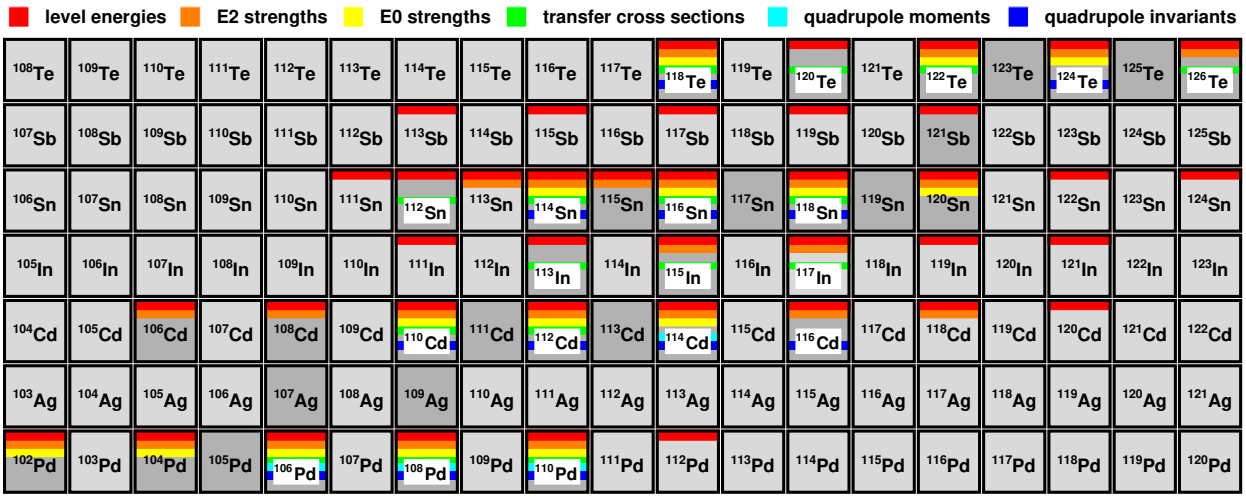

Figure 33: Summary of experimental data available for nuclei exhibiting shape coexistence in the Pd-Te region. Red bars indicate that shape-coexisting structures were proposed based on their level energies (e.g., observation of a low-lying 0^+ state, or rotational structures with very different moments of inertia), orange bars mean that additional information was obtained from $E2$ transition probabilities, yellow bars mean that information on $E0$ transition strengths is known, green bars mean measured cross sections to populate the coexisting configurations in direct reactions, light blue bars indicate that quadrupole moments of both configurations were measured, and dark blue bars correspond to quadrupole invariants. Stable nuclei are indicated with a darker shade.

of ^{110}In, observed a band-like structure built on the 0^+_2 state at 1473 keV in ^{110}Cd. Nearly simultaneously, Fielding *et al.* [338] reported very strong population of this state (amounting to 42% of the ground-state population) with the (^{3}He,n) two-proton-transfer reaction, as shown in Fig. 34. Also shown in Fig. 34 are the data for the ^{110}Pd(^{3}He,n)^{112}Cd reaction, where the 0^+_2 state is strongly populated with 55% of the ground-state cross section. These can be contrasted with the recent ^{114}Cd(p,t) two-neutron-transfer results [339] that populated the 0^+_2 state with only 1.7% of the ground-state cross section. It was suggested [337] that the configuration for the 0^+_2 state and the deformed band built on it was based on proton $2p-4h$ intruder configurations such as $\pi(g_{9/2})^{-4}(d_{5/2})^2$ or $\pi(g_{9/2})^{-4}(g_{7/2})^2$, an interpretation expanded upon by Heyde and co-workers [340, 341]. The two-proton stripping results, combined with the non-observation [342] of any excited states in ^{110}Cd in the (d,^{6}Li) transfer reaction, reveals that the intruder configuration possesses the characteristic signature of a proton pairing vibration.

The shape-coexisting intruder states in the ^{110,112,114}Cd isotopes were well studied in the 1980s and early 1990s, and these early data are summarized in the review by Wood *et al.* [6]. The systematics of the intruder bands in mid-neutron-shell Cd isotopes was expanded using in-beam γ-ray spectroscopy following light-ion fusion-evaporation reactions [343–348]. Candidates for the intruder band heads were also suggested in the heavier Cd isotopes, $^{116-120}$Cd, as well as in the lighter isotopes ^{106,108}Cd (see e.g. Refs.[343, 344]). The intruder band in ^{108}Cd was extended by Gade *et al.* [349] using a combination of β^+/EC decay and light-ion reactions, and those in ^{114,116}Cd by Juutinen *et al.* [350] using heavy-ion collisions. Thorslund *et al.* [351, 352] suggested that a sequence of states in ^{108}Cd involving the 4^+ at 2239 keV, the 6^+ at 2994 keV, and the 8^+ at 3861

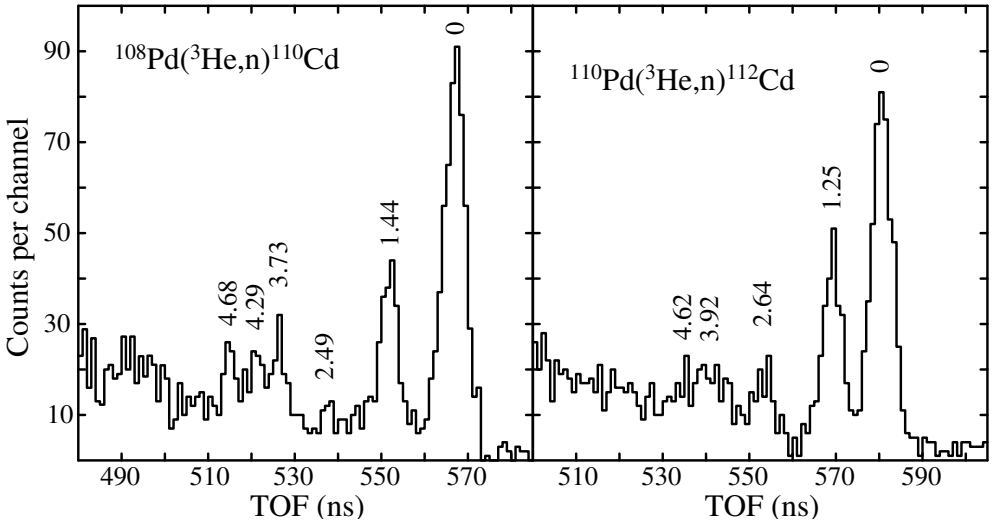

Figure 34: Time-of-flight spectra of neutrons emitted following the ^{108}Pd(^{3}He,n)^{110}Cd and ^{110}Pd(^{3}He,n)^{112}Cd reactions using 25-MeV ^{3}He beams. Figure reproduced from data in Fielding *et al.* [338].

keV, belonged to a deformed intruder band, but having a predominant $\nu(h_{11/2})^2$ structure rather than the proton $2p-4h$ configuration. Studies of ^{106}Cd [353], ^{110}Cd [354–356], ^{112}Cd [357–359], ^{114}Cd [360], and ^{116}Cd [361] using the $(n,n'\gamma)$ reaction elucidated the level schemes, and provided crucial level lifetimes determined via the Doppler-shift attenuation method (DSAM) [362].

Very recently, detailed spectroscopy following the β^+/EC decay of ^{110}In, and the β decay of ^{110,112}Ag, enabled the observation of very weak low-energy transitions between highly non-yrast states in ^{110}Cd and ^{112}Cd. From the known level lifetimes, the $B(E2)$ values for the in-band transitions were determined, and in many cases they corresponded to a highly collective nature [261, 363], leading to interpretation of these states as forming rotational-like bands. With the aid of beyond-mean-field calculations, it was suggested that multiple shape coexistence occurs in ^{110,112}Cd. Figure 35 shows the levels assigned to the 0_2^+ and 0_3^+ bands in ^{110,112}Cd [261, 363] based on the presence of enhanced $B(E2)$ values.

The 0^+ states in neighbouring Cd isotopes that have the same decay pattern as the 0^+ band heads assigned in ^{110,112}Cd [261, 363] may be considered candidates for analogous shape-coexisting structures. Shown in Fig. 36 are the properties of the 0_2^+ and 0_3^+ states in the Cd isotopes, showing the $B(E2;0^+ \rightarrow 2^+)$ and $\rho^2(E0)$ values, where known, as well as the (^{3}He,n) population relative to the ground state if measured. A feature of the decay of the original "intruder" band head is an enhanced transition rate for its decay to the 2_1^+ state; this is seen in ^{112,114}Cd [39, 261, 262]. For ^{110}Cd, only a lower limit for the lifetime of the 0_2^+ level is known that results in an upper limit of 40 W.u. for the $0_2^+ \rightarrow 0_1^+$ transition [356]. Recent results from Coulomb excitation [260] show that the $\langle Q^2 \rangle$ value for the 0_2^+ state is 0.51(8) e^2b^2, slightly larger than that of the ground state with 0.44(1) e^2b^2, as listed in Tab. 4. We contrast the decay of the 0_2^+ states in ^{110,112,114}Cd with those of the 0_3^+ states that clearly favour the decay to the 2_2^+ state. This pattern is also observed for ^{106,108}Cd, strongly suggesting that the natures of the 0_3^+ states in these nuclei are very similar.

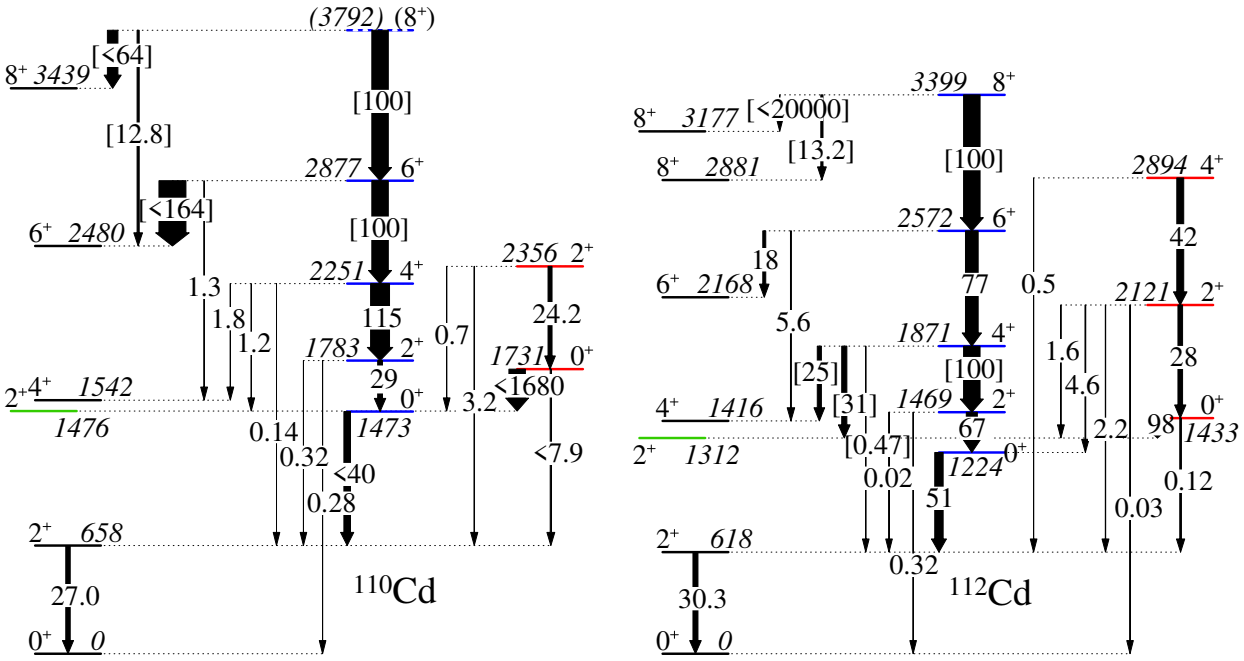

Figure 35: Portions of the low-lying level schemes of ^{110,112}Cd. The transitions are labelled with their $B(E2)$ values in W.u., with those in brackets displaying the relative $B(E2)$ values, normalized to 100 units for the in-band transition. Data are taken from the National Nuclear Data Center database [39], and Refs. [261, 356, 359, 363].

Moreover, for nuclei where the absolute value of the $0^+_3 \rightarrow 2^+_2$ transition rate has been measured, i.e., ^{112,114}Cd, it is highly enhanced. In the heavier Cd isotopes, the natures of the 0^+_2 and 0^+_3 states seem to interchange in ^{116}Cd, where the 0^+_2 state strongly favours the decay to the 2^+_2 state, and the 0^+_3 has an enhanced decay rate to the 2^+_1 state. The pattern becomes more confusing in ^{118}Cd. The intruder band head was assigned by Aprahamian *et al.* [364, 365] as the 0^+_3 state. An upper limit for the observation of the $0^+_3 \rightarrow 2^+_2$ decay was established, corresponding to the $B(E2;0^+_3 \rightarrow 2^+_2)/B(E2;0^+_3 \rightarrow 2^+_1)$ ratio lower than 19. The lifetime measurements by Mach *et al.* [366] provided an upper limit for the 0^+_3 level, leading to a lower limit of $B(E2;0^+_3 \rightarrow 2^+_1) > 1.2$ W.u., and determined the lifetime for the 0^+_2 state corresponding to $B(E2;0^+_2 \rightarrow 2^+_1) = 5.3(8)$ W.u. It thus appears that at ^{118}Cd and beyond, the nature of the $0^+_{2,3}$ bands changes, perhaps dramatically.

The energy systematics for the even-even Cd isotopes are shown in Fig. 37. The BMF calculations reported in Refs. [261, 363] suggested that the 0^+_2 states in ^{110,112}Cd possess triaxial shapes, with the wave-function distributions having mean values of $(\beta_2, \gamma) = (0.4, 20°)$. The 0^+_3 states in these nuclei were suggested to be oblate deformed. The oblate and the triaxial states may interchange their positions at ^{116}Cd. In reality, it is very likely that the degree of deformation of the states shifts dramatically as a function of the neutron number. Indicators of this are the kinematic moments of inertia, displayed in Fig. 38. We note some clear trends that can be observed from these plots. Firstly, the loci of points for the ground-state band begin with E_γ in the range of 0.5−0.65 MeV, and with $J^{(1)} \approx 5\,\hbar^2$/MeV. The intruder bands, by contrast, begin with loci of points

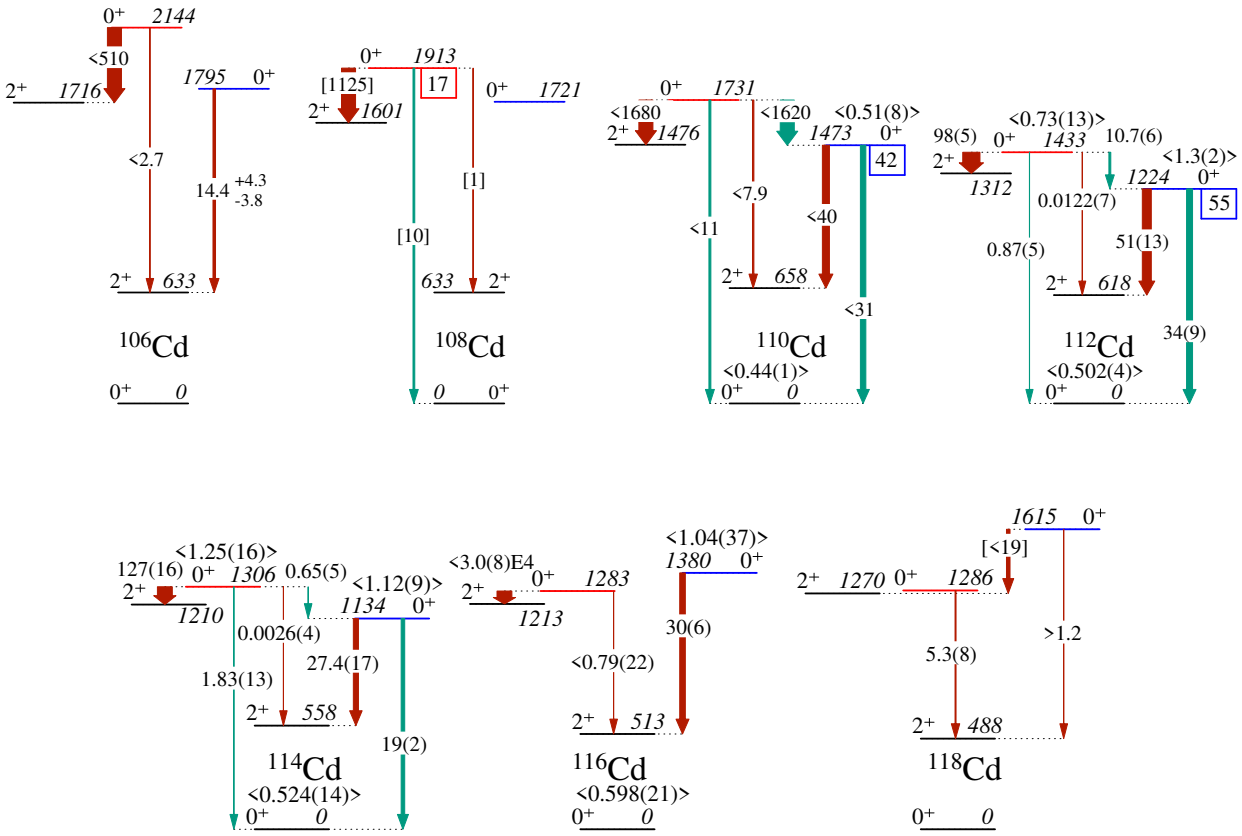

Figure 36: Properties of the low-lying 0^+ states observed in the mid-neutron-shell Cd isotopes. The widths of the arrows are proportional to the $B(E2)$ values (rust colour) and $10^3 \times \rho^2(E0)$ (green). The transitions are labelled with the absolute $B(E2)$ values in W.u. with uncertainties in parenthesis, or relative $B(E2)$ values in square brackets. The $E0$ transitions are labeled with their $10^3 \times \rho^2(E0)$ values, or the $X(E0/E2)$ value for the 0^+_3 state in ^{108}Cd relative to the $E2$ to the 2^+_1 level. The numbers inside boxes attached to the levels are the ratios (in %) of the (^{3}He,n) transfer cross sections to those of the ground state. Quantities contained within the brackets are the $\langle Q^2 \rangle$ e^2b^2 values; those for excited states, especially, should be considered as lower limits. Data are taken from the National Nuclear Data Center database [39] and Refs. [102, 260–262, 338, 353, 361, 363].

that span a wide range, with E_γ values from approximately 0.25 MeV to 0.575 MeV, and with $J^{(1)}$ ranging from 5 to 13 $\hbar^2$/MeV. In particular, we see that ^{114}Cd presents the smallest E_γ value, and then ^{112,116}Cd, ^{110,118}Cd, and ^{108,120}Cd form approximate pairs. Isotopes that have well-established intruder bands, namely ^{110,112,114}Cd, have $J^{(1)}$ moments that possess a concave shape and turn over at E_γ of approximately 0.4 MeV – in ^{110}Cd this is more gradual. The intruder band in ^{116}Cd is a notable exception. It is also be to noted that ^{118}Cd has a much steeper slope of $J^{(1)}$ *vs.* E_γ, perhaps indicating that its band assignment is in error. One should also mention that there is considerable uncertainty in the assignment of the 0^+_2 level in ^{120}Cd. The 883-keV transition feeding the 2^+_1 level, attributed [367, 368] to the decay of a 0^+ state at 1389 keV, was shown to be a doublet and these γ rays were placed elsewhere in the level scheme by Batchelder *et al.* [369]. This latest study, however, placed a previously unobserved transition of 630 keV feeding the 2^+_1 state, and suggested

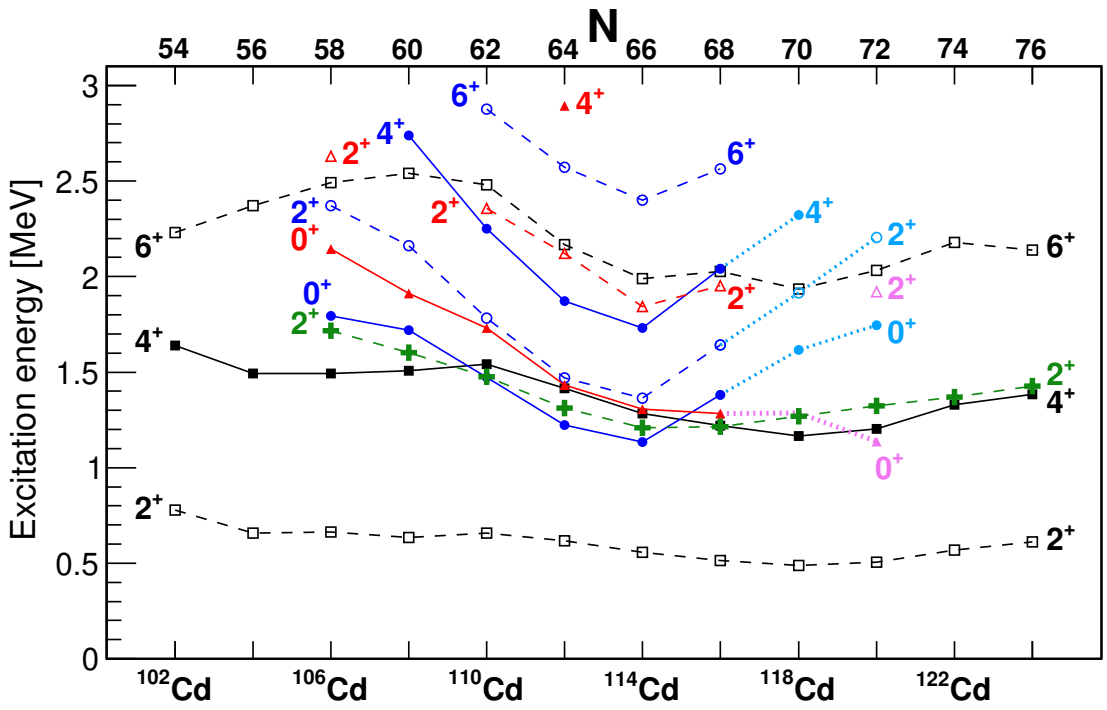

Figure 37: Observed excitation energies in the even-even Cd isotopes of states assigned to 0^+ bands, and the 2^+_2 state. The BMF calculations of Refs. [261, 363] predicted that the ground states in ^{110,112}Cd possessed prolate-deformed shapes with $\beta_2 \approx 0.2$, the "intruder" 0^+_2 states were suggested to have triaxially deformed shapes with $(\beta_2, \gamma) = (0.4, 20°)$, and the 0^+_3 states had oblate shapes with $\beta_2 \approx 0.3$. The states in neighbouring isotopes suggested to have similar shapes are shown in black (prolate), blue (triaxial), and oblate (red). For states that have tentative shape assignments, dotted lines and lighter colours are used. The 2^+_2 state, labelled as the "γ"-band head, is shown in green, and the calculations for ^{110,112}Cd suggest that it has a very similar β_2 to the ground state, and is maximally triaxial [261, 363]. Data taken from the National Nuclear Data Center database [39] and Ref. [369].

that a new level at 1136 keV was the 0^+_2 state. This latter assignment is adopted in Fig. 37.

Finally, the 0^+_4 states were postulated to be the heads of prolate bands in Refs. [261, 363]. Shown in Fig. 39 are data highlighting the $E2$ γ-ray decays of the $0^+_{2,3,4}$ states in ^{110,112,114}Cd, that clearly show the dominance of the 0^+_4 decays to the 2^+_3 levels, i.e. to members of the intruder bands built on the 0^+_2 states. The corresponding transition rate has been measured in ^{114}Cd, and found to be enhanced with $B(E2; 0^+_4 \rightarrow 2^+_3) = 18(6)$ W.u. [262]. Interestingly, the *higher* energy $E2$ transitions to the 2^+_2 levels are unobserved in these isotopes, with limits on the ratio of $B(E2; 0^+_4 \rightarrow 2^+_2)/B(E2; 0^+_4 \rightarrow 2^+_3)$ values of $< 0.65\%$ in ^{110}Cd, and $< 9.5\%$ in ^{112}Cd [356, 370]. In ^{112}Cd only there are band members suggested for a band built on the 0^+_4 state, namely the 2156-keV 2^+_5 state with $B(E2; 2^+_5 \rightarrow 0^+_4) = 34(15)$ W.u., and the 2711-keV 4^+_6 state with $B(E2; 4^+_6 \rightarrow 2^+_5) = 77(30)$ W.u. [261, 363].

The recent investigations of the odd-A Cd nuclei have been a series of high-spin studies of the neutron-deficient ^{105,107,109}Cd isotopes, mainly investigating the so-called "shears" bands, band

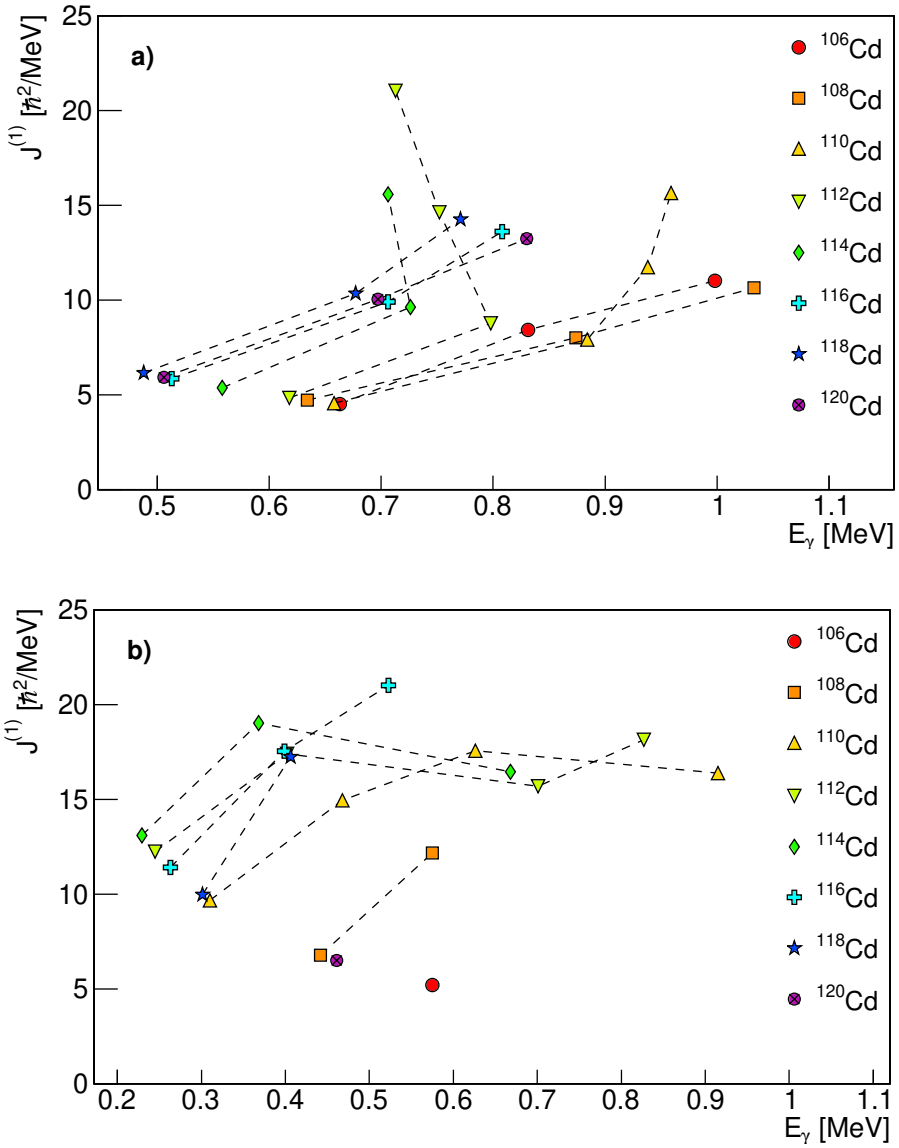

Figure 38: Kinematic moments of inertia of the low-lying states in the (a) ground-state bands and (b) intruder bands of the even-even Cd isotopes. Note the different horizontal scales used in the plots. The moments of inertia for the intruder bands are rather symmetric in their behaviour with respect to the neutron mid-shell, whereas those for the ground-state bands shift towards lower E_γ with increasing neutron number reaching a minimum at ^{118}Cd.

termination, anti-magnetic rotational bands, etc. (see, for example, Refs. [371–373]). Studies of ^{117,119}Cd following spontaneous fission of ^{252}Cf [374] and detailed g-factor measurements in ^{111,113}Cd [375, 376] should also be mentioned. The results of these studies were consistent with a deformed character of the cores. Shape coexistence at low spin has been difficult to establish in the odd-A Cd isotopes, primarily because of the high level density compared with the even-

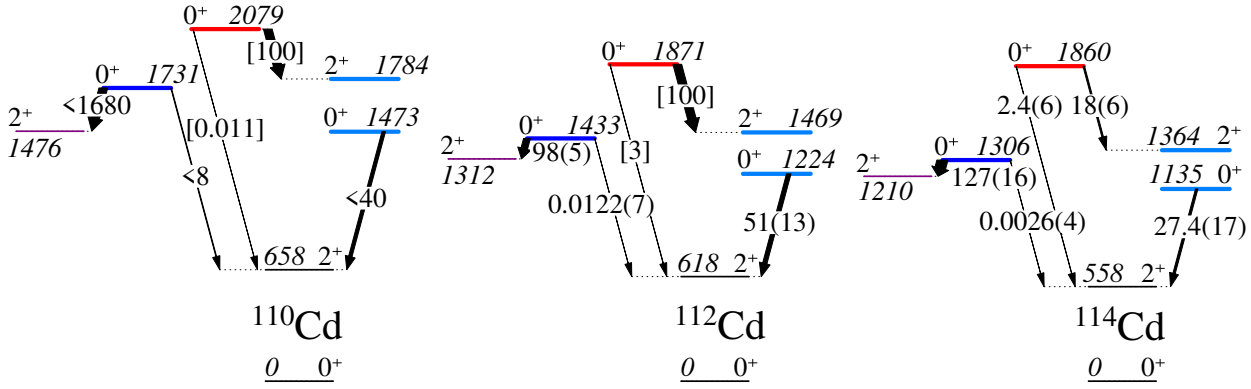

Figure 39: Summary of the observed decays of the 0^+_2, 0^+_3, and 0^+_4 levels in ^{110,112,114}Cd. The widths of the arrows are proportional to the $B(E2)$ values, and the transitions are labeled with the absolute $B(E2)$ values in W.u. with uncertainties in parenthesis, or relative $B(E2)$ values in square brackets. The data show the enhanced decay of the 0^+_2 intruder band heads to the 2^+_1 levels, the enhanced decay of the 0^+_3 states to the 2^+_2 γ-band heads, and the preferred decay of the 0^+_4 levels to the 2^+_3 intruder band members. Figure taken from Ref. [261].

even isotopes. Furthermore, the identification of single-particle states coupled to the intruder configuration of the even-even core can be complicated because of the suggested triaxial nature of the cores. To date, no firm examples of low-spin shape-coexisting states in the odd-A Cd isotopes have been identified.

3.5.2. Sn isotopes

The first evidence for proton $2p-2h$ intruder excitations in the Sn isotopes resulted from enhanced cross sections to excited 0^+ states measured in the Cd(^{3}He,n) reactions [338]. The very large populations observed for the 0^+_2 states in ^{114,116,118}Sn – comparable to, or greater than the ground-state cross sections – were strongly suggestive of a proton-pairing vibration and were not recognized immediately as evidence for shape coexistence. In ^{108,112}Sn, the ground-state and excited-state (^{3}He,n) populations are much larger than in the heavier isotopes, and they are also more fragmented, with larger cross sections to 0^+ states in the excitation energy range of 3.5–5 MeV [338]. These very large populations of the excited 0^+ states in the (^{3}He,n) reactions are in stark contrast to their weak populations (of typically a few percent) observed in the (p,t) two-neutron transfer reactions [380–385]. Those data for isotopes where both the (^{3}He,n) and the (p,t) cross sections have been measured, namely ^{112,114,116,118}Sn, are shown in Fig. 40. (In the (t,p) reaction, on the other hand, relatively stronger populations of 7% and 10% of the ground-state cross section were observed to the 0^+_2 and 0^+_3 states in ^{114}Sn [386], respectively, whereas in ^{118,120,126}Sn, their weak populations were observed [386, 387].) While the resolutions achieved in the (^{3}He,n) measurements were insufficient to resolve the 0^+_2 and 0^+_3 states, the data presented in Fig. 40 favour that it is the 0^+_2 state that is populated, and we make that assignment here. These data clearly show that the 0^+_2 states involve correlated proton-pair excitations.

A short time after the (^{3}He,n) study [338], Bron *et al.* [388] used the $(\alpha,2n\gamma)$ reactions to study states in ^{112,114,116,118}Sn. Rotational-like sequences built on the 0^+_2 states were observed up

to $I^{\pi} = 12^{+}$. The intrinsic configurations of the intruder bands were suggested to be mixtures of the $\pi(1/2[431])^2$ and $\pi(9/2[404])^2$ configurations, consistent with the observation of these Nilsson orbitals in the low excitation-energy regions in the neighbouring In and Sb isotopes (see, e.g., Ref. [2]). Shown in Fig. 41 are the excitation energy systematics of the intruder bands in the even-even Sn isotopes, showing a characteristic minimum near the neutron mid-shell (i.e., for ^{116}Sn). Also shown on the plot are the energies of the 0^+_3 states, which display a similar parabolic trend. The minimum at the neutron mid-shell is in contrast to the trends observed for the normal states. The trend of the 0^+_3 energy is suggestive of shape coexistence, but the evidence from the (^{3}He,n) reaction indicates that its structure may be different than that of the 0^+_2 state which seems to result from a coherent $\pi(2p-2h)$ configuration.

Further studies, employing heavy-ion fusion-evaporation reactions, have assigned the high-spin states based on proton $\pi(g_{9/2})^{-2}(g_{7/2})^2$ configurations in even-even $^{106-118}$Sn nuclei [389–393]. In a study of ^{108}Sn that measured lifetimes employing the DSAM, the transitional quadrupole moments were used to deduce the deformation of states up to spin $26\hbar$, and found that the intruder states above $12\hbar$, involving the alignment of a pair of $h_{11/2}$ neutrons coupled to the intruder $\pi(g_{9/2})^{-2}(g_{7/2})^2$ configuration, possess a moderate quadrupole deformation of $\beta_2 \simeq 0.20$ [394]. Above spin 26, the deformation appears to drop dramatically as the band-termination point is

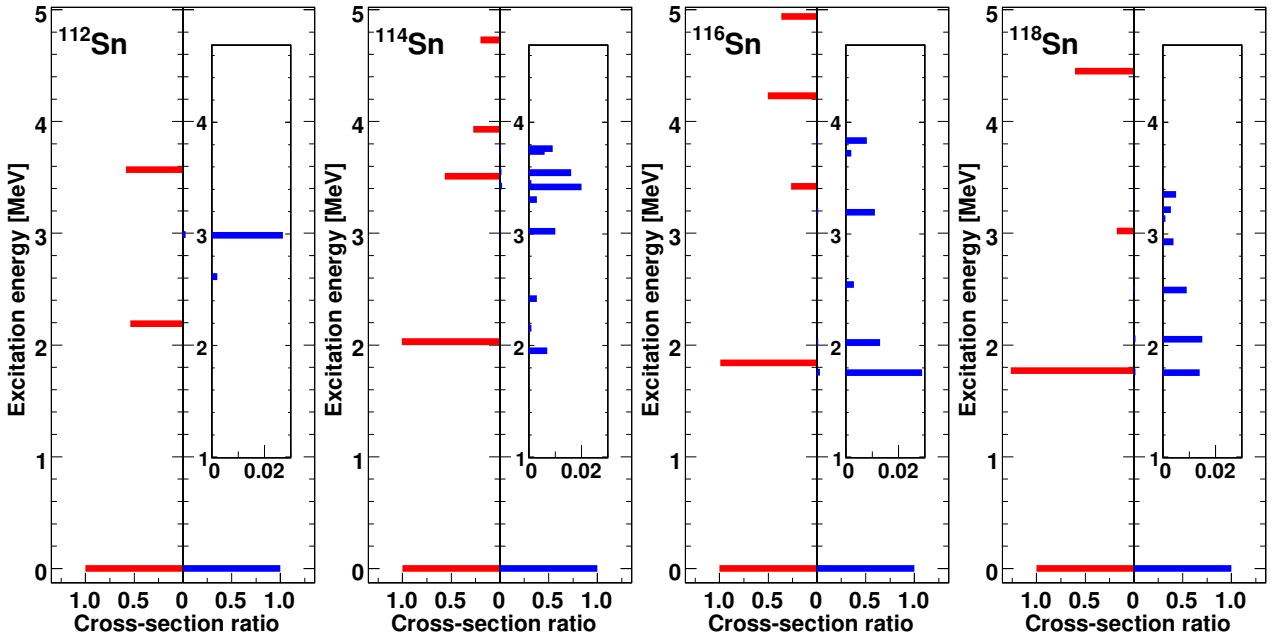

Figure 40: Cross sections for the population of excited 0^+ states normalised to those of the ground state. The bars on the left-hand side of the plots represent the ratios observed in the (^{3}He,n) reaction, and those on the right-hand side are for the (p,t) reactions. The insets on the right-hand sides of the plots display a ratio scale expanded to 0.03 (3%) to make the data more clearly observable. Large enhancements for population of excited 0^+ states are observed for the (^{3}He,n) reaction, whereas those for the (p,t) reaction rarely exceed a few percent. The data are taken from Refs. [338, 381–384].

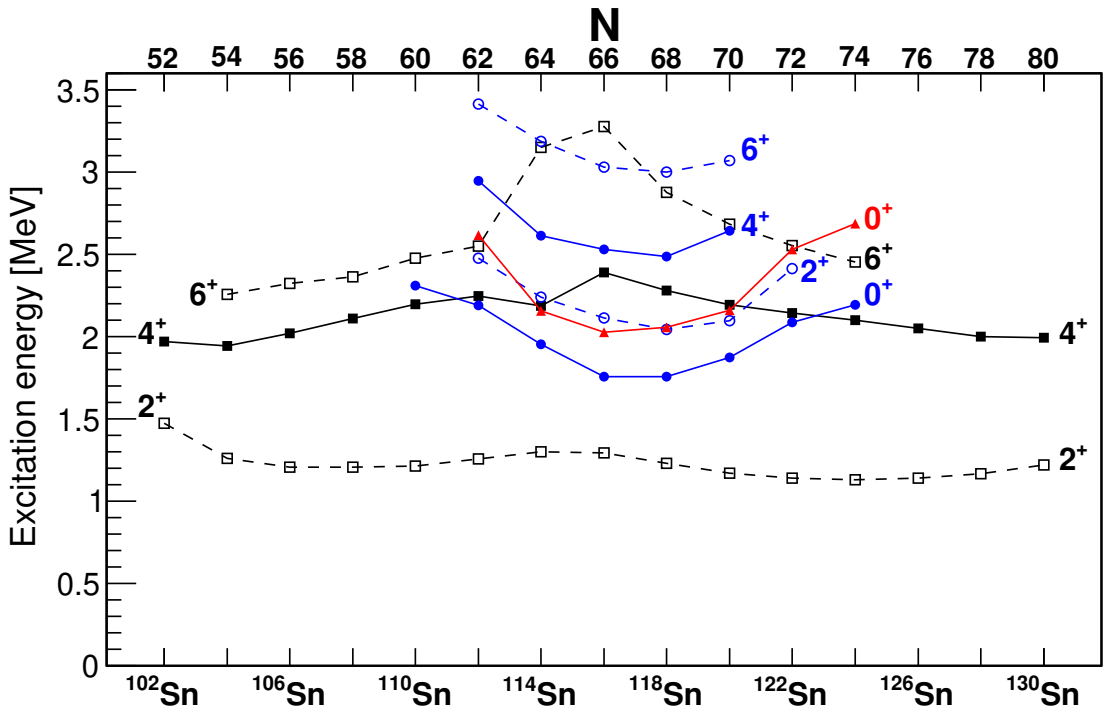

Figure 41: Observed excitation energies in the even-even Sn isotopes of states assigned to ground-state and 0^+_2 bands, and the 0^+_3 state. Data taken from the National Nuclear Data Center database [39].

reached [394]. A similar result was found for ^{112}Sn, where the intruder band was observed to spin-parity 26^+ by Ganguly *et al.* [398]. From lifetime measurements via DSAM, the transitional quadrupole moments were used to deduce the deformation of $\beta_2 \simeq 0.18$ for states with $I \geq 12\hbar$. Recoil-distance Doppler-shift (RDDS) measurements in ^{114}Sn [395], where the intruder band based on the 0^+_2 state was observed to spin $30\hbar$, determined the lifetimes for the deformed states up to spin (26^+), and a transitional quadrupole moment of $Q_t = 3.50(7)$ eb was deduced for states below the backbend at spin 12^+, referred to as the intruder-g band. Assuming an axially-symmetric rotor model, the deformation parameter $\beta_2 = 0.26$ was determined.

Lifetimes of low-spin states in ^{112,114}Sn were recently measured by Spieker *et al.* [397] using the $(p, p'\gamma)$ reaction. In ^{112}Sn, the new measurements result in $B(E2; 2^+_3 \rightarrow 0^+_2) = 28(7)$ W.u., and $B(E2; 4^+_3 \rightarrow 2^+_3) = 46(9)$ W.u. The lifetime of the 6^+ member, measured by Ganguly *et al.* [398], yields $B(E2; 6^+_3 \rightarrow 4^+_3) = 185(63)$ W.u. In ^{114}Sn, the corresponding values are < 44 W.u., 62(25) W.u., and 97(5) W.u., respectively [397]. The above $B(E2; 4^+_2 \rightarrow 2^+_2)$ values are in approximate agreement with results from a measurement [399] of the 4^+_2 lifetime in ^{116}Sn, performed with the fast-timing technique, that leads to $B(E2; 4^+_2 \rightarrow 2^+_2) = 40(13)$ W.u. The new results for ^{114}Sn raised a possibility that the 0^+_3 level should be considered as the intruder band head; however, IBM calculations of Ref. [397] suggested that the 0^+_2 and 0^+_3 states were highly mixed, which prevented a definitive assignment. The 0^+ intruder band head in ^{116}Sn was re-assigned by Pore *et al.* [263] as

the 0_3^+ state rather than the 0_2^+ level, based on the observation of the previously postulated [400], but unobserved, 85-keV $2_2^+ \rightarrow 0_3^+$ γ ray. The branching ratio of this transition was significantly revised with respect to the previous estimate [400], leading to $B(E2; 2_2^+ \rightarrow 0_3^+) = 99.7(84)$ W.u., much greater than $B(E2; 2_2^+ \rightarrow 0_2^+) = 44(5)$ W.u. in this nucleus. Using a two-state mixing model introduced in Sec. 2.5, these $B(E2)$ values can be reproduced assuming a $\sin^2\theta_0 = 0.31$ admixture of the normal-order wave function in the 0_3^+ state. Finally, it should also be noted that a recent high-statistics β-decay study [401] of ^{118}In found no evidence to support the reassignment of the natures of the 0_2^+ and 0_3^+ states in ^{118}Sn. These recent studies indicate that the structure of the shape-coexisting states in the Sn isotopes is more complicated than previously assumed.

Figure 42 displays the properties of the 0_2^+ and 0_3^+ states in the Sn isotopes. Strong similarities across many of the Sn isotopes can be observed with regard to the 0_2^+ states (^{124}Sn appears as a possible exception); strong two-proton transfer populations, weak two-neutron transfer populations, the appearance of rotational-like bands built upon them, and enhanced $E2$ transition rates to the 2_1^+ state. Where measured, the 0_3^+ states decay via a favoured $E0$ transition to the 0_2^+ state rather than to the ground state, which indicates clearly shape changes and mixing of the 0_2^+ and 0_3^+ states. In some cases, such as recently argued in ^{114,116}Sn [263, 397], the two excited 0^+ states may be so strongly mixed that assigning their character becomes difficult. The energy systematics presented in Fig. 41 uses the "traditional" assignments of the 0_2^+ states as the shape-coexisting band heads.

3.5.3. Te isotopes

Shape-coexisting states at low spin in the Te isotopes have been difficult to identify, primarily because the detailed spectroscopy has not been performed to the same extent as in the Cd or Sn isotopes. The experimental information on the even-even Te isotopes was summarized by Rikovska *et al.* [403], and through a comparison with IBM2 calculations it was argued, based on energies and the few known transition rates, that intruder states existed in their low-lying level schemes. Recent studies have begun to observe the key in-band γ-ray transitions. In ^{118}Te, a study using the ^{115}Sn$(\alpha, n\gamma)$ reaction [264] firmly established the spin-parity of 2^+ for the 1482-keV level, and measured its lifetime that permitted the determination of $B(E2; 2_2^+ \rightarrow 0_2^+) = 60^{+30}_{-17}$ W.u. Thus, evidence was provided supporting the 1482-keV 2^+ level as a member of a band built on the 957-keV 0_2^+ state. The 1976-keV 4^+ and 2517-keV 6^+ states were also tentatively assigned to the 0_2^+ band, but their in-band decays have yet to be observed The study of ^{120}Te, performed by Vanhoy *et al.* [404], employed the ^{118}Sn$(\alpha, 2n\gamma)$ reaction, as well as the β decay of ^{120}I, and postulated an intruder band with the 1103-keV 0_2^+, 1535-keV 2_3^+, 1924-keV 4_3^+, and the 2520-keV 6_3^+ levels, with the assignments for the two latter states rather speculative due to the lack of observed in-band transitions. ^{122}Te has been studied using both the $(n, n'\gamma)$ reaction, where lifetimes or limits for many low-spin states were established [405], and the ^{119}Sn$(\alpha, n\gamma)$ reaction [406]. The lifetime of the 2_3^+ level at 1752 keV was extracted [405], leading to $B(E2; 2_3^+ \rightarrow 0_2^+) = 194^{+26}_{-24}$ W.u. The degree of collectivity implied by the $B(E2; 2_3^+ \rightarrow 0_2^+)$ value is difficult to understand in view of the corresponding $B(E2)$ values in the region. Hicks *et al.* [405] suggested the 4^+ intruder-band member was the state at 2041 keV, but we note that its energy is somewhat lower than would be expected from the $2_3^+ \rightarrow 0_2^+$ energy spacing; the (4_4^+) level at 2448-keV may be a more suitable candidate, but the lack of observation of in-band transitions hampers firm conclusions.

For ^{124}Te, detailed spectroscopy was performed by von Egidy *et al.* [407] using the (n, γ)

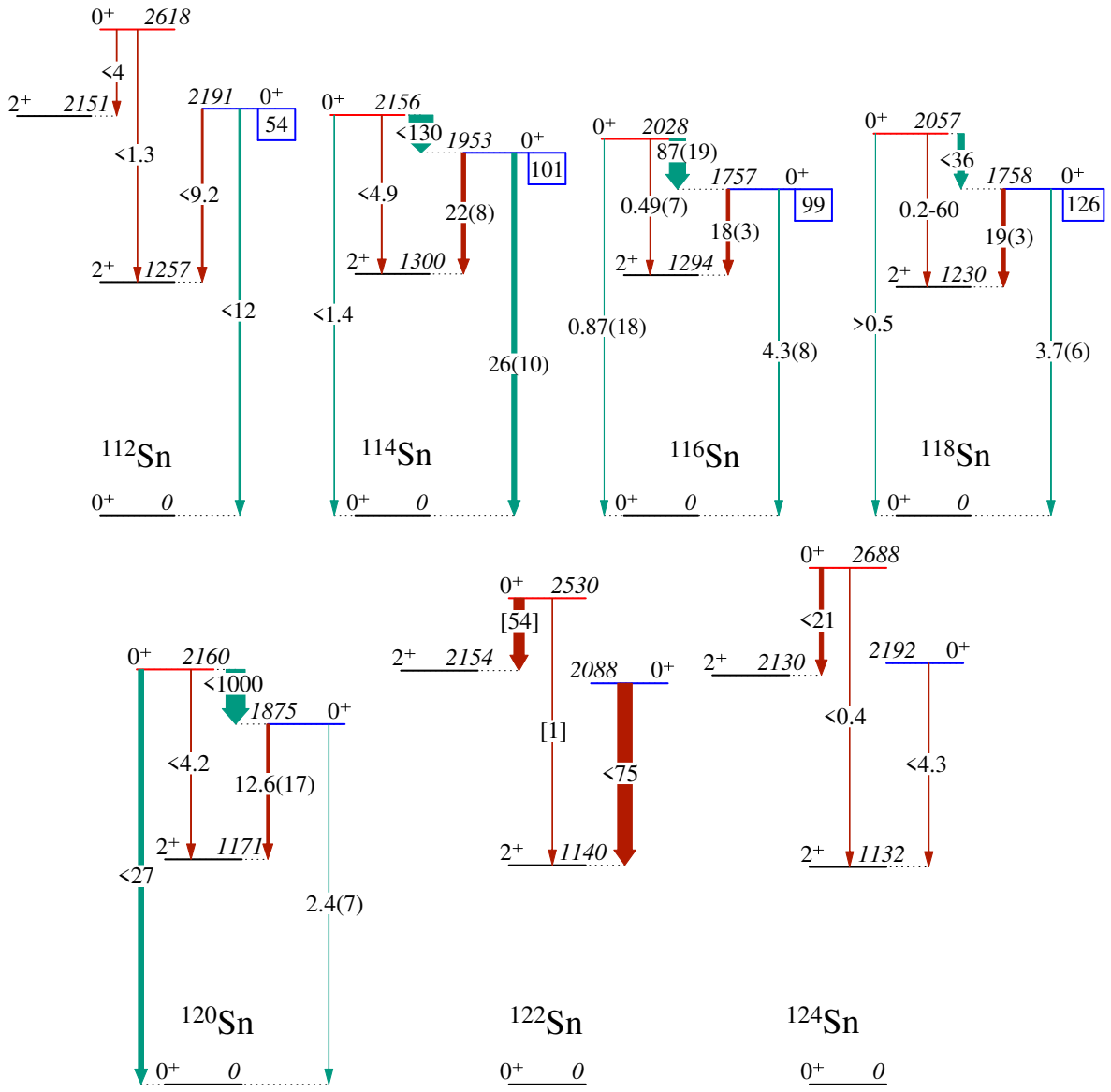

Figure 42: Properties of the low-lying 0^+ states observed in the mid-neutron-shell Sn isotopes. The widths of the arrows are proportional to the $B(E2)$ (rust colour) and $10^3 \times \rho^2(E0)$ values (green), and the transitions are labeled with the absolute $B(E2)$ values in W.u. with uncertainties in parenthesis, or relative $B(E2)$ values in square brackets, with a similar convention for the $\rho^2(E0)$ values. The data show an enhanced decay of the 0^+_2 intruder band heads to the 2^+_1 levels in $^{114-120}$Sn, in contrast to the much lower $B(E2; 0^+_3 \rightarrow 2^+_1)$ values. The numbers inside boxes attached to the levels are the ratios (in %) of the (^{3}He,n) transfer cross sections to those of the ground state. Data are taken from the National Nuclear Data Center database [39] and Refs. [102, 263, 338, 397, 401].

capture reaction that expanded upon the earlier work [408]. A transition feeding the 0^+_2 state at 1657 keV from the 2^+_3 state at 2039 keV was placed, and the lifetime of the 2^+_3 state was measured via the GRID method [409], and confirmed using the $(n, n'\gamma)$ reaction [266]. The resulting

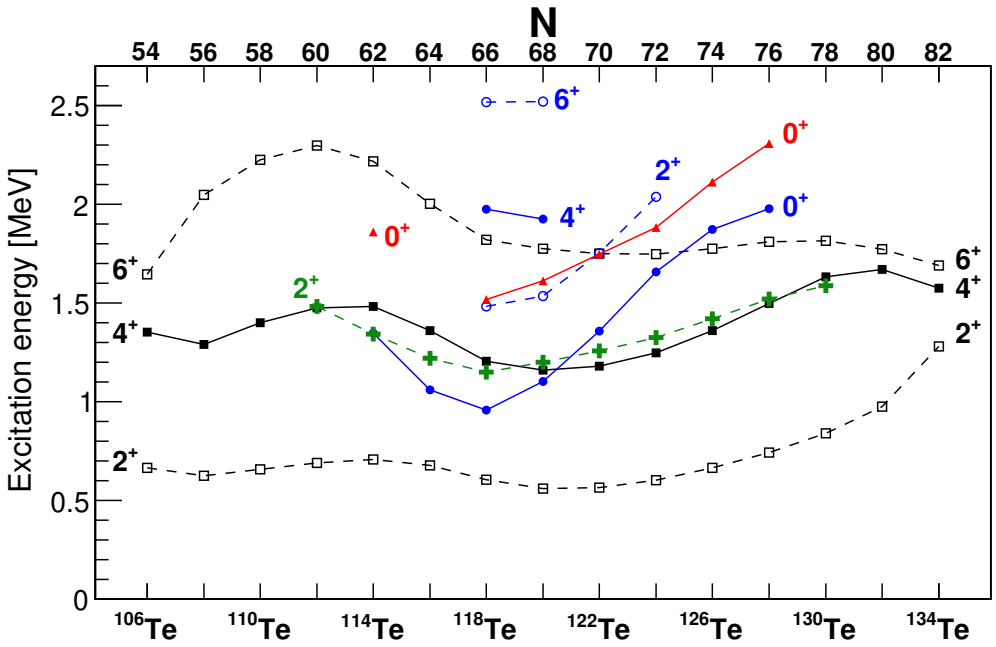

Figure 43: Observed excitation energies of states assigned to 0^+ bands, and the 2^+_2 state in the even-even Te isotopes. Data are taken from the National Nuclear Data Center database [39].

$B(E2; 2^+_3 \rightarrow 0^+_2) = 20(3)$ W.u. provided support for the identification of the 2^+_3 level as a member of a band built on the 0^+_2 state.

Figure 43 displays the energy systematics of the levels in the ground-state bands as well as those suggested to belong to the shape-coexisting intruder structures built on the 0^+_2 state in the even-even Te isotopes. The presumed intruder states follow the typical parabolic pattern observed for the intruder states in the Cd and Sn isotopes. Figure 44 displays the properties of the 0^+_2 and 0^+_3 states observed in $^{118-126}$Te, and as observed in the Cd isotopes (Fig. 36) and the Sn isotopes (Fig. 42), the 0^+_2 levels have enhanced $B(E2)$ values for the decays to the 2^+_1 levels. Further evidence in favour of a shape-coexisting character of these states comes from the presence of favoured $E0$ transitions between the 0^+_3 and 0^+_2 states, with $X(E0/E2)$ factors varying from 4.6(15) to 51(10) from ^{118}Te to ^{122}Te [102], and enhanced two-proton transfer cross sections observed in the Pd(^{3}He,n) reactions [338].

3.5.4. Pd isotopes

Guided by the observation of the $2p-2h$ and $2p-4h$ intruder states in the Sn and Cd isotopes, respectively, and the presence of deformed bands in the odd-A Ag and Rh isotopes (see, e.g., Refs. [411–415]), suggestions were made that such structures appear in the Pd isotopes as well [416–418]. Recent studies [419] of ^{106}Pd using the $(n, n'\gamma)$ reaction have measured a large number of level lifetimes and significantly expanded the level scheme. The levels were arranged into a series of rotational bands, as shown in Fig. 45. The measured lifetimes [420] were used to deduce the $\rho^2(E0)$ values from previously determined $X(E0/E2)$ values [421]. The $\rho^2(E0)$ values were

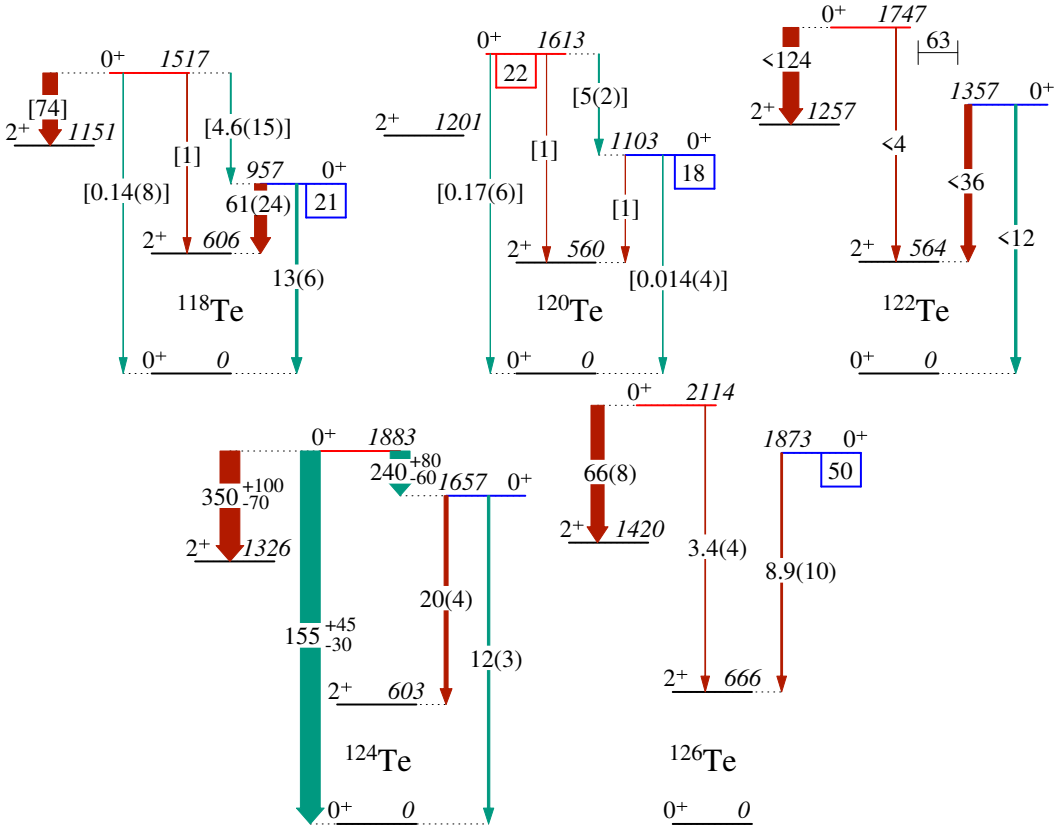

Figure 44: Properties of the low-lying 0^+ states observed in the mid-neutron-shell Te isotopes. The widths of the arrows are proportional to the $B(E2)$ (rust colour) and $10^3 \times \rho^2(E0)$ values (green). The transitions are labeled with the absolute $B(E2)$ values in W.u. with uncertainties in parenthesis, or relative $B(E2)$ values in square brackets. The $E0$ transitions are labeled with their $10^3 \times \rho^2(E0)$ values, or the $X(E0/E2)$ values. The numbers inside boxes attached to the levels are the ratios (in %) of the (^{3}He,n) transfer cross sections to those of the ground state; for ^{122}Te, the value is represented by a horizontal line at the centroid of the observed peak. Data are taken from the National Nuclear Data Center database [39] and Refs. [102, 338].

moderate in strength for the $E0$ decays of the $K^\pi = 0^+_2$ band members to the ground-state band. In contrast, a large $E0$ strength of $10^3 \times \rho^2(E0) = 96^{+43}_{-61}$ from the 2^+_5 state to the lowest $K^\pi = 2^+$ band head was determined, which lead to a suggestion that the 2^+_5 state is a $K = 2$ excitation built on the 0^+_2 state. It was also suggested that the 2^+_4 state at 1910 keV is a member of a band built on the 0^+_3 state at 1706 keV. This would yield a moment of inertia more than twice that of the ground-state band, implying that the 0^+_3 band is highly deformed. The 0^+_3 level decays to the 2^+_2 state with an enhanced $E2$ transition rate of $15.1^{+4.2}_{-3.0}$ W.u. [259, 419].

These findings in ^{106}Pd are consistent with the results of previous Coulomb-excitation work [13, 259, 422] on ^{106,108,110}Pd that provided a large number of matrix elements such that the invariant quantities $\langle Q^2 \rangle$ and $\langle Q^3 \cos 3\delta \rangle$ could be determined for a number of states in the three

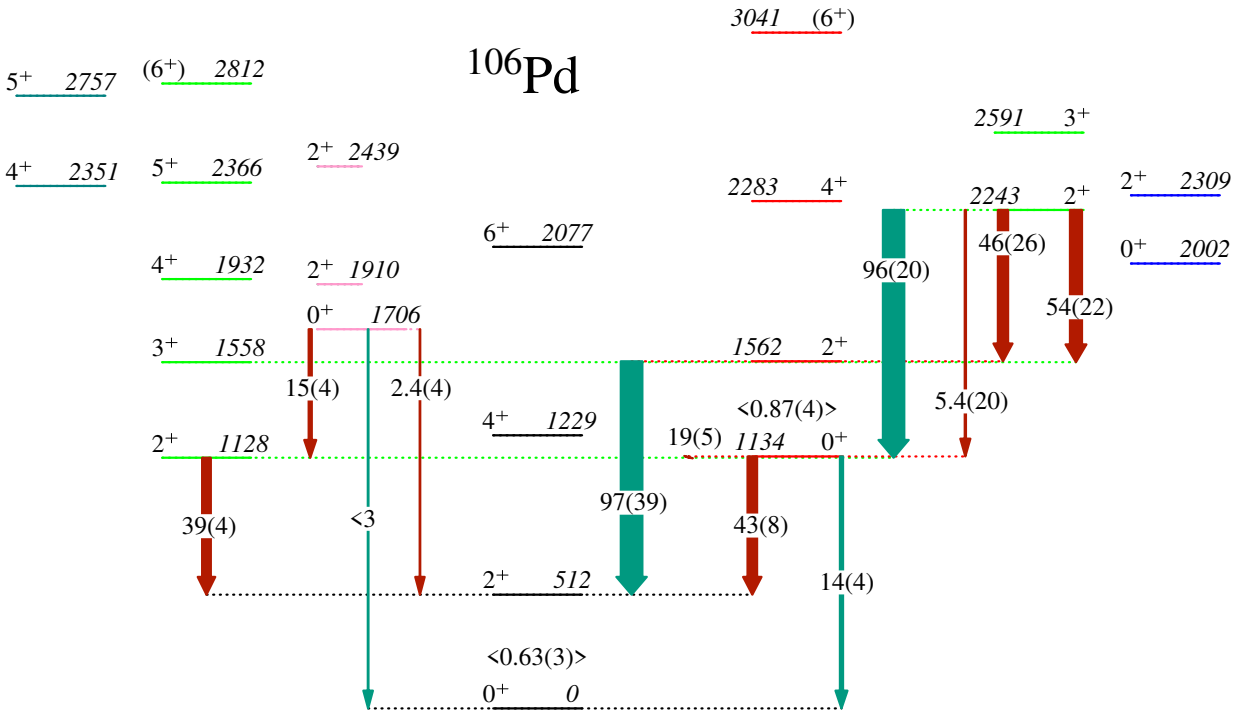

Figure 45: Partial level scheme of ^{106}Pd displaying levels arranged into rotational bands as assigned in Ref. [419]. The widths of the arrows are proportional to the $B(E2)$ values (rust colour) labeled with the absolute values in W.u. (only shown for the band heads, with weak transitions omitted for clarity) and $10^3 \times \rho^2(E0)$ (green), with uncertainties in parenthesis. Numbers in brackets written above the 0^+ levels are the $\langle Q^2 \rangle$ values (expressed in e^2b^2) from Ref. [259]. Members of the band built on the 0^+_3 level at 1706 keV have not been firmly assigned; shown above this level are two possible 2^+ candidates that have not yet been assigned to other structures. Asymmetric uncertainties have been averaged. Data are taken from the National Nuclear Data Center database [39] and Refs. [102, 419, 420].

nuclei. The $\langle Q^2 \rangle$ values increase nearly linearly with neutron number, 0.63(3) e^2b^2, $0.77^{+0.10}_{-0.11}$ e^2b^2, and $0.86^{+0.02}_{-0.06}$ e^2b^2 for the 0^+_1 state in ^{106,108,110}Pd, respectively, and 0.87(4) e^2b^2, $1.22^{+0.12}_{-0.14}$ e^2b^2, and $1.58^{+0.11}_{-0.22}$ e^2b^2 for the 0^+_2 state. In the axially-symmetric rotor model, $Q^2 \propto \beta_2^2$, and thus these could imply that, for example, in ^{110}Pd the deformation of the 0^+_2 state is approximately 40% larger ($\beta_2 \simeq 0.35$) than that of the ground state ($\beta_2 \simeq 0.25$). The $\langle \cos 3\delta \rangle$ quantities favour a prolate shape for the ground state and 0^+_2 state, but a triaxial one for the 0^+_3 state that has a similar $\langle Q^2 \rangle$ value to the ground state [13]. The combined information on the invariant quantities $\langle Q^2 \rangle$ and $\langle \cos 3\delta \rangle$, and the $\rho^2(E0)$ values, strongly supports shape coexistence in the mid-neutron-shell Pd isotopes.

Figure 46 displays the properties of the 0^+_2 and 0^+_3 states in $^{102-110}$Pd. As has been seen in the other nuclei in the vicinity of the $Z = 50$ closed shell, the 0^+_2 state has an enhanced decay to the 2^+_1 level, with weak-to-moderate $E0$ strengths for the decay to the ground state, and the 0^+_3 level favours the decay to the 2^+_2 state rather than the 2^+_1 state. A trend observed, using the data available from Coulomb excitation [259], is that the $B(E2; 0^+_2 \rightarrow 2^+_1)$ values become increasingly enhanced as the neutron number increases, indicating substantial structural changes in the levels correlated

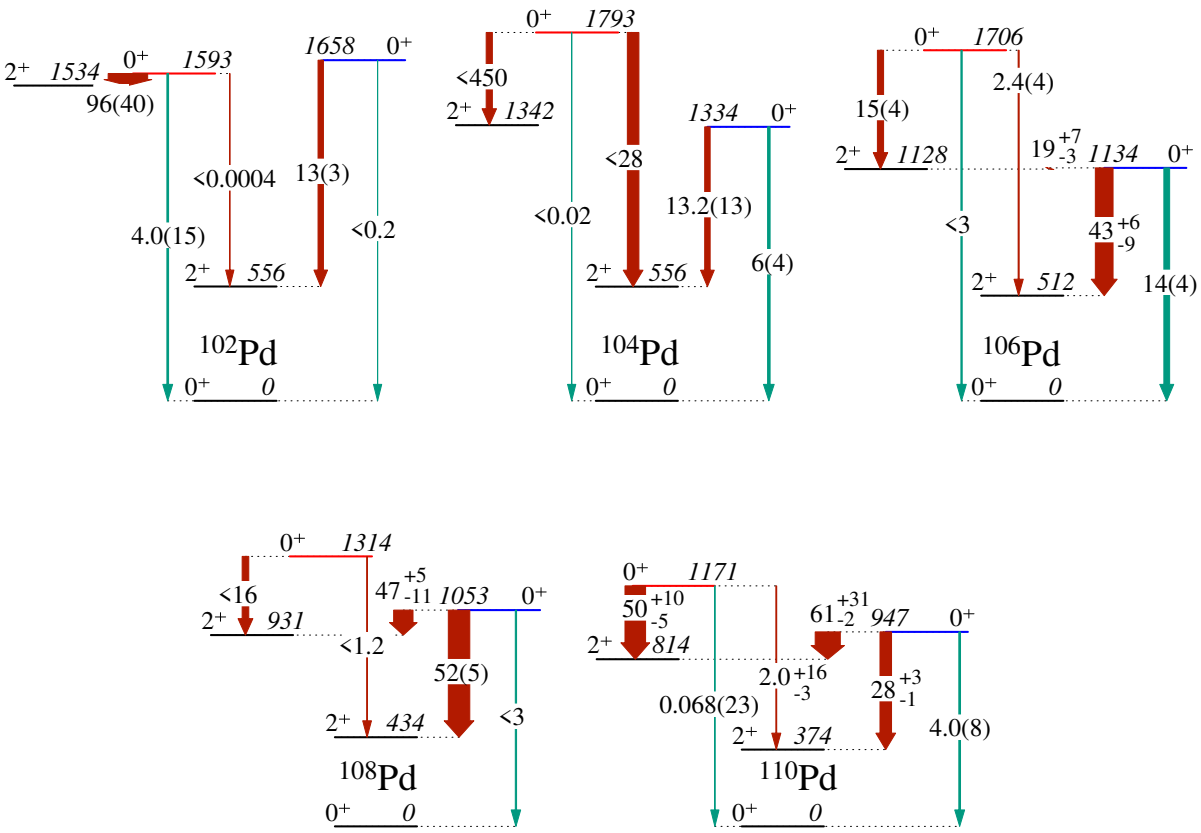

Figure 46: Properties of the low-lying 0^+ states observed in the mid-neutron-shell Pd isotopes. The widths of the arrows are proportional to the $B(E2)$ (rust colour) and $10^3 \times \rho^2(E0)$ values (green). The transitions are labeled with the absolute $B(E2)$ values in W.u. with uncertainties in parenthesis, or relative $B(E2)$ values in square brackets. The $E0$ transitions are labeled with their $10^3 \times \rho^2(E0)$ values. Data are taken from the National Nuclear Data Center database [39] and Refs. [102, 259, 423].

with the increasing degree of deformation.

3.6. Shape coexistence near N=90

For isotopic chains near $Z = 64$ and $N = 90$, rapid changes in the energies of the 2^+_1 state, and in the $B(E2; 2^+_1 \rightarrow 0^+_1)$ values, are observed that are very similar to those found in nuclei near $Z = 40$ and $N = 60$. Additionally, the discontinuities in the isotope shifts and two-neutron separation energies are strongly localized at $N = 90$, just as they are at $N = 60$. Very early studies [424–430] with two-neutron transfer reactions were interpreted in terms of shape coexistence, with the presence of "spherical" states in ^{152}Sm, populated strongly in the (t, p) reaction, and "deformed" states in ^{150}Sm, populated strongly in the (p, t) reaction. Using both (p, t) and (t, p) reactions, a consistent picture for the populations of the 0^+_2 and 0^+_3 states was established as well in the Nd, Gd, and Dy isotopes [431–439]. Figure 47 compares the ratios of the cross sections to excited 0^+_2 and 0^+_3 states, relative to the ground-state cross section. In all cases, very strong populations of the 0^+_2 states were observed in the two-neutron pickup reactions populating the $N = 88$ nuclei. Similarly,

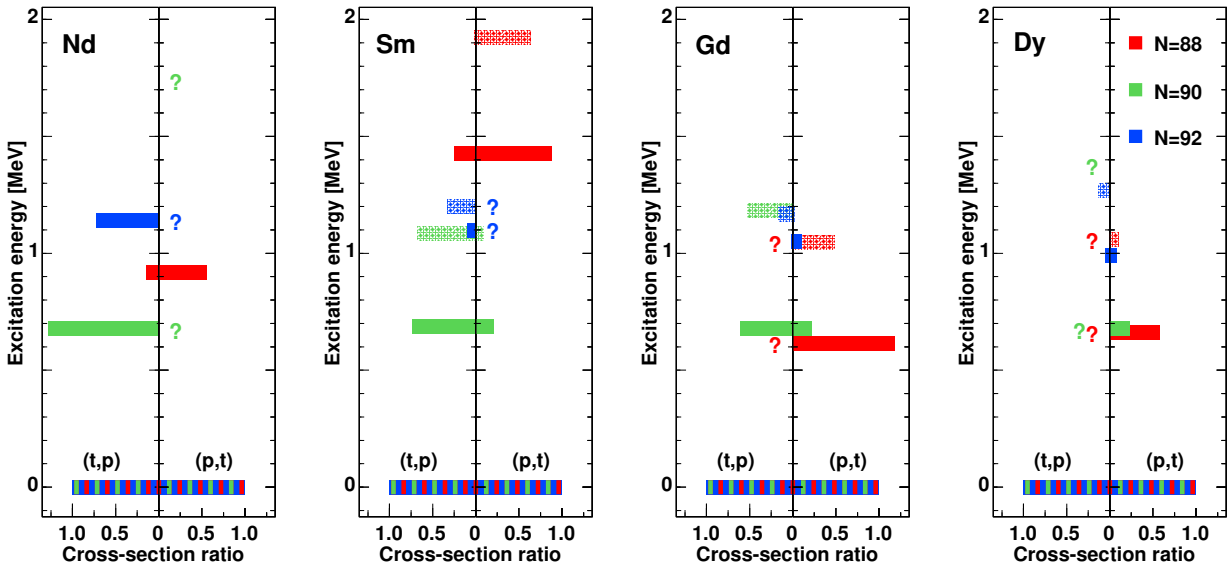

Figure 47: Cross sections for the population of excited 0^+_2 states (solid fill) and 0^+_3 states (patterned fill) in N=88,90,92 Nd, Sm, Gd and Dy isotopes, normalised to those of the ground state. The bars on the left-hand side of the plots represent the ratios observed in the (t, p) reactions, and those on the right-hand side are from the (p, t) reactions. The bar for the $N = 90$ Sm (p, t) cross section ratio for the 0^+_3 state represents an upper limit. Question marks imply that the experiment has not been performed. Data are taken from Refs. [425, 427, 431, 432, 434–439].

strong populations to the 0^+_3 states were also observed. Where known, the two-neutron stripping reactions populating $N = 88$ isotones observed much weaker strengths for populating the 0^+_2 states, and no observable strength to the 0^+_3 states. The two-neutron pickup reactions on $N = 92$ targets populate the 0^+_2 and 0^+_3 states in the $N = 90$ isotones with strengths, while significant, much smaller than those observed on the $N = 90$ targets. Conversely, the 0^+_2 and 0^+_3 states in the $N = 90$ isotones are very strongly populated in the stripping reactions. These population patterns are shown in Fig. 47. Support for the interpretation of shape coexistence came from the assignment of the 2^+ rotational band member at 1417 keV based on the 1256-keV 0^+_3 state in ^{150}Sm with a 2^+ to 0^+ separation of 161 keV, very close to the value of 122 keV in the ^{152}Sm ground-state band. The 4^+ band member was suggested [427] to be the 1819-keV state, which has a favoured relative $E2$ γ-ray decay to the 1417-keV 2^+ state, although further members of the band have not been assigned. The 0^+_3 states in the other $N = 88$ isotones, however, do not have candidates for band structures that would possess a significantly different moment of inertia from that of the ground-state or 0^+_2 bands in those nuclei. Recent in-beam γ-ray spectroscopy studies [440, 441] have failed to report a band based on the 0^+_3 state, which would be surprising if such a band had a large moment of inertia extending to moderate-to-high spin.

The rapid change in observables, such as the quadrupole moment and E^+_4/E^+_2 ratio, has lead to the suggestion [442–444] that a phase transition occurs in the shape degree of freedom across neutron number $N = 90$. Motivated by interacting boson model calculations, these ideas were

further developed, and it was suggested that ^{152}Sm lay at the critical point of a phase transition [445, 446], with several nearby $N = 90$ isotones close to the critical point. An unsettled question, however, is whether $N = 90$ nuclei represent a critical point of a phase transition or if they involve a complex shape coexistence. The distinction between the two descriptions was outlined by Heyde and co-workers [447]; in a phase-transition picture, the states of one limit of the Hamiltonian will spread out and eventually become the eigenstates of the other limit as determined by a suitable control parameter; for shape coexistence, one has a complete set of states, which arise from distinct Hilbert spaces, built on each shape.

The introduction of solutions to the Bohr model for the critical point of a phase transition motivated a large number of experimental studies. Quantum phase transitions of nuclear shapes, and the critical points in particular, are reviewed in Ref. [448]. Detailed spectroscopy, in particular through β decay [449–451], found that collective models failed to described the data well. Many of these studies focused on the properties of the 0_2^+ state and its associated rotational band, since one of the main successes of the critical-point solution is that it predicted, in a parameter-free manner, the energy ratio of $E(0_2^+)/E(2_1^+) = 5.67$, which is a nearly perfect match to the experimental energies (e.g. 5.57 in ^{152}Sm). As shown in Fig. 48, the moments of inertia for the 0_1^+ bands in ^{152}Sm and ^{154}Gd are nearly identical and significantly smaller than those of the 0_2^+ bands (it should be noted that the plots terminate at spin $10\hbar$ where the 0_2^+ band is crossed by another structure assigned as the S band (alignment of $(i_{13/2})^2$ neutrons). This suggests that the 0_1^+ band has a smaller underlying deformation than that of the 0_2^+ band. As outlined in Ref. [2], the $\rho^2(E0)$ values for the $E0$ transitions connecting the 0_1^+ and 0_2^+ bands in the $N = 90$ isotones ^{152}Sm, ^{154}Gd, and ^{156}Dy are highly enhanced, and in many cases are very precisely known. Using two-band-mixing calculations, Kulp *et al.* [452] were able to reproduce for ^{152}Sm the experimental level energies, $\rho^2(E0)$ values, $B(E2)$ values, and the isomer shift of the 2_1^+ state to within $\approx 10\%$ precision, using for the "unperturbed" 0_A^+ band energies those of ground-state band of ^{148}Ce, and for the deformed 0_B^+ band those of the ground-state band of ^{154}Sm. The mixing amplitudes determined were close to the strong-mixing limit, and are consistent with both the single-proton transfer [453] and single-neutron transfer reaction [454] results.

The detailed spectroscopic studies performed on ^{152}Sm and ^{154}Gd revealed the presence of weakly deformed bands based on the 0_3^+ states that were assigned as "pairing isomers"[3], a concept which had been introduced decades earlier [455]. As shown in Fig. 48, the 0_3^+ bands, while not known to high spin, have significantly lower moments of inertia. Elucidating these band structures is extremely challenging, and in spite of the high-statistics in-beam studies performed for ^{156}Dy (see, e.g. Refs. [456, 457]), the band associated with the 0_3^+ state has not been found.

The pairing isomer "second vacuum" has been advocated by Sharpey-Schafer and co-workers

[3]The pairing isomers are states constructed from a subset of Nilsson orbitals that are described as "oblate" (i.e. those with negative intrinsic quadrupole moments) which have pairing matrix elements G_{oo} amongst themselves that are approximately equal to the prolate-orbital pairing matrix elements G_{pp}, but for which the oblate-prolate pairing matrix elements G_{op} are very small. This results in an approximate decoupling of the subsets of single-particle states, and one can construct, in effect, two ground states. Depending on the relative distribution of oblate and prolate orbitals around the Fermi level, the usual BCS-like ground state coexists with an excited state with a distorted V^2 distribution of orbitals. In some extreme cases, the excited state can take the form of the ground state of the $A - 2$ system with the existence of two real particles (i.e., $V_i^2 \approx 1$).

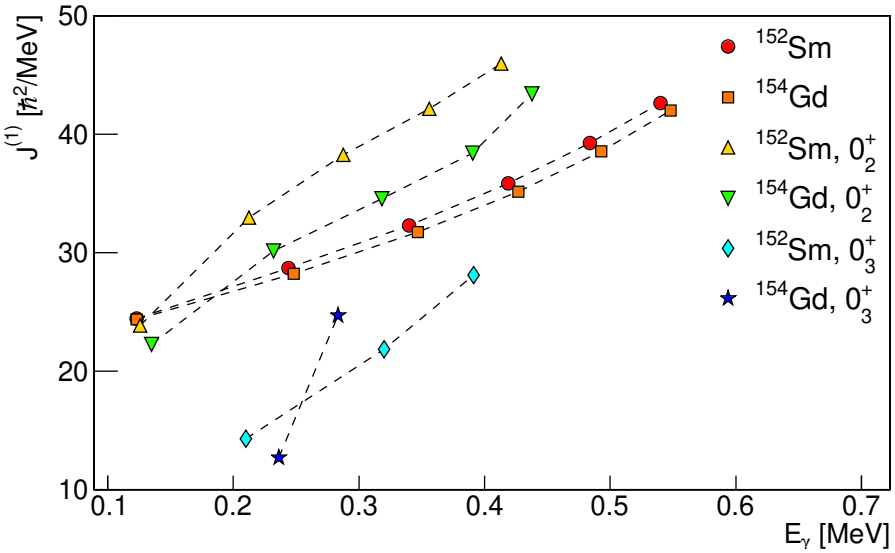

Figure 48: Kinematic moments of inertia of the low-lying states in the ground-state bands and bands built on the 0_2^+ and 0_3^+ states in the $N = 90$ ^{152}Sm, ^{154}Gd isotones.

[456, 458–461] as an explanation for the 0_2^+ states in the $N = 90$ isotones. In this interpretation, the second-vacuum state has a nearly full two-quasiparticle $\nu 11/2[505]$ oblate orbital. A consequence of this is that in the adjacent odd-A $N = 91$ isotones, states of the form $\nu 11/2[505] \otimes 0_2^+$ should not exist due to Pauli blocking. This appears to be the case; studies using in-beam fusion-evaporation reactions that should have observed such structures in ^{153}Sm [462], ^{155}Gd [460], and ^{157}Dy [463] proved negative. The study of ^{155}Gd, in particular, specifically searched for this structure and while it located the $\nu 11/2[505] \otimes 2_\gamma^+$ coupling, for example, and many other rotational bands, it concluded that the $\nu 11/2[505] \otimes 0_2^+$ configuration was nonexistent due to blocking [460].

In a recent review of evidence for vibrational states in deformed nuclei [461], it was pointed out that if the second-vacuum concept was valid, it might be expected that the excitations observed to be built on the ground state would also be present based on the 0_2^+ state, provided that they would not be dominated by contributions from the $\nu 11/2[505]$ orbital. Earlier studies have indeed suggested a pattern of repeated excitations in ^{152}Sm [464], and the data for ^{154}Gd also support the repetition of states [459, 461].

3.7. Shape coexistence around $Z = 82$

3.7.1. Even-even Hg nuclei

The first indication of shape coexistence in the $Z \approx 82$ region came from studies of the optical hyperfine structure in neutron-deficient mercury isotopes. A huge and unexpected isotope shift, corresponding to a $\Delta\beta_2^2$ deformation change exceeding 0.1, was observed between ^{185}Hg and ^{187}Hg [465], and initially interpreted as related to the possible existence of a new region of strong quadrupole deformation. Follow-up laser spectroscopy studies of ^{184,186,188}Hg [466] revealed a distinct odd-even staggering of mean-square charge radii of Hg isotopes, as shown in Fig. 49a.

This staggering, unique in the nuclear chart, has recently been shown [467, 468] to persist down to $A = 179$ ($N = 99$), where the nucleus returns to sphericity in its ground state. Additionally, while isotope shifts measured for the low-lying $13/2^-$ isomers in $^{187-191}$Hg closely follow those for the ground states, a large difference is observed between those for ^{185m}Hg and ^{185}Hg, again corresponding to a $\Delta\beta_2^2$ deformation change of more than 0.1 [469].

In-beam γ-ray spectroscopy studies of ^{186}Hg [470] and ^{184}Hg [471] have demonstrated that the weakly-deformed ground-state bands are crossed at low spin by a more deformed configuration, and the elongation of these two structures could be estimated from the moments of inertia as $\beta_2 \approx 0.1$ and $\beta_2 \approx 0.3$, respectively. The band heads of the more deformed structures were soon identified to have $I^\pi = 0^+$ and to decay to the ground state via enhanced $E0$ transitions [472–475]. Level systematics reveals a parabolic trend of their energies, centered at $N = 104$, as displayed in Fig. 49b. Currently such structures, crossing the weakly deformed ground-state band, are known down to ^{176}Hg [476], although in ^{176,178}Hg the low-spin non-yrast members of the deformed band have not been observed.

The microscopic configurations of the two coexisting structures in light Hg nuclei were inferred via systematic α-decay studies [477, 478]. In general, the α decays of the ^{186,188,190}Pb isotopes to the 0_2^+ states in ^{182,184,186}Hg are strongly hindered compared to the decays proceeding directly to the ground state, and the observed hindrance factors are of similar magnitude (≈10-20) for all three isotopes. This was interpreted as resulting from the normal-order configuration of the ground states of Pb and Hg nuclei and an intruder nature of the 0_2^+ states in ^{182,184,186}Hg: the population of an intruder state in the α decay of a normal-configuration state involves the removal of a proton pair from an orbital below the $Z = 82$ gap and the promotion of a proton pair across this gap. Consequently, the ground states of all even Pb and Hg nuclei in the vicinity of $N = 104$ were assumed to have similar configurations corresponding to normal-order shell occupation, while the 0_2^+ states in the Hg isotopic chain were interpreted as predominantly $\pi(2p-2h)$ intruders.

The measured hindrance factors for the Hg → Pt α decay, combined with the information on mixing in the Pt daughter nuclei obtained from the perturbation of energies in the rotational bands [479], were used to estimate the mixing of normal-order and intruder 0^+ states in ^{180,182,184}Hg. This analysis yielded a 3% admixture of the deformed configuration in the ground state of ^{180}Hg, while mixing of 16% and 18% was obtained for ^{182}Hg and ^{184}Hg, respectively [478]. Together with the admixtures deduced from the $\rho^2(E0; 0_2^+ \rightarrow 0_1^+)$ value for ^{188}Hg and its upper limit for ^{186}Hg [480], these values display a parabolic behavior as a function of neutron number with maximum mixing observed at the $N = 104$ mid-shell, where the intruding structure comes closest in energy to the ground state. The mixing of coexisting structures in Hg isotopes was also investigated by applying a two-band mixing model to level energies in the observed rotational bands [479, 481]. The most recent data on energies of yrast and non-yrast states were used as an input for the analysis performed in Ref. [481], which yielded a considerably lower mixing between the 0^+ states than the values deduced from the α-decay work of Ref. [478], but still with a maximum around $N = 102 - 104$ as shown in Fig. 50. In this context, measurements of $\rho^2(E0; 0_2^+ \rightarrow 0_1^+)$ in Hg isotopes with $A \leq 186$ are called for, as they would provide a direct measure of the degree of their mixing.

Different conclusions are reached if such analysis is applied to the 2^+ states [481]. The obtained mixing strengths suggest an inversion of configurations of the 2_1^+ state between ^{182}Hg and

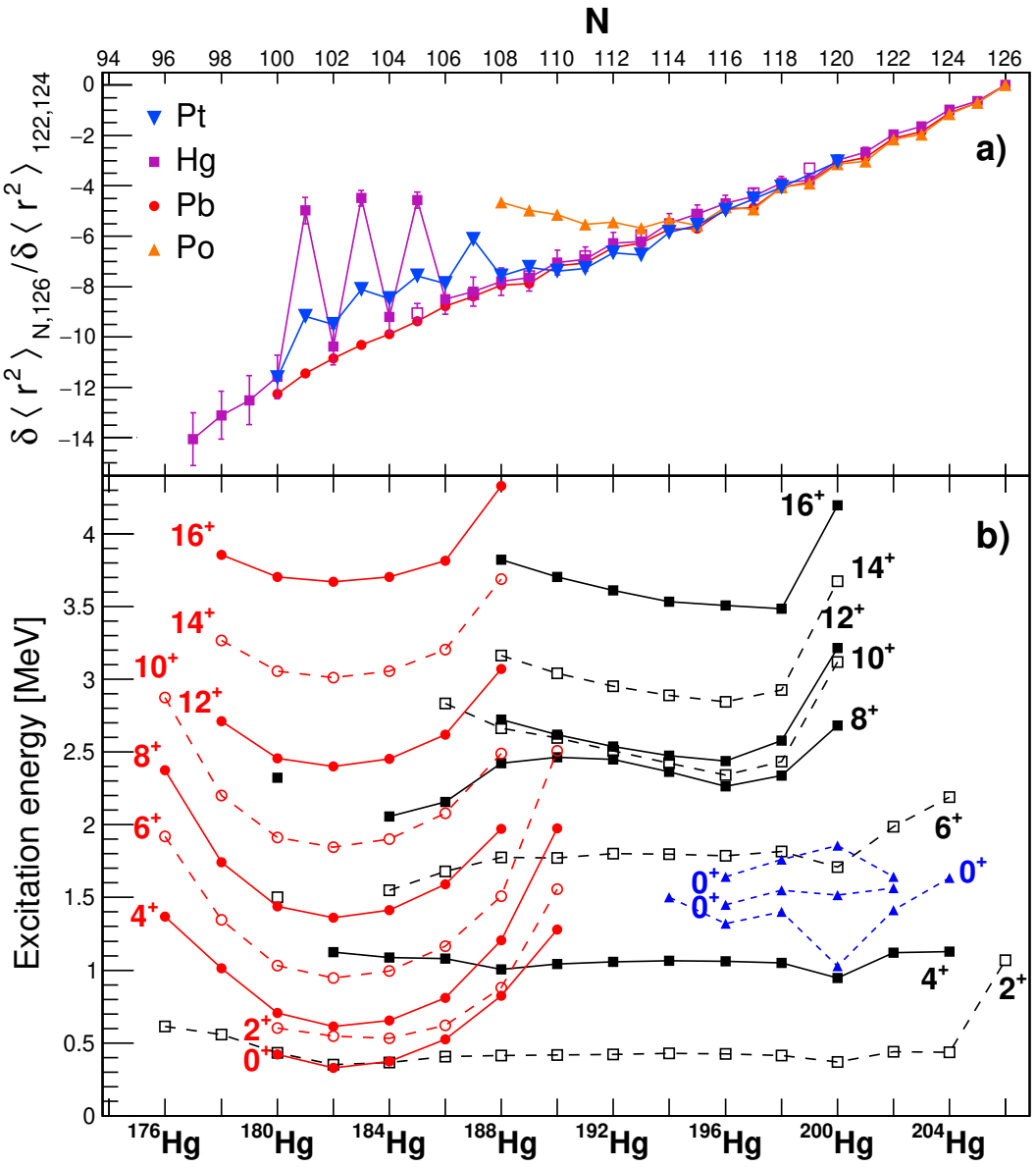

Figure 49: (Top) Changes in mean-square charge radii, relative to $N = 126$, as a function of the neutron number for Po (orange triangles), Pb (red circles) and Hg (magenta squares) isotopic chains, normalized to the difference in charge radius between $N = 122$ and $N = 124$. The data for Pt are also plotted (blue triangles) with the point for ^{196}Pt normalised to the value measured for ^{200}Pb to facilitate direct comparison. Filled symbols denote ground states and open symbols isomeric states. The values are taken from Refs. [234, 468]. (Bottom) Energy systematics of positive-parity excited states in the neutron-deficient even-even mercury isotopes, showing the assumed intruder (red circles) and ground-state bands (black squares). Other known low-lying 0^+ states are marked with blue triangles. Data are taken from the National Nuclear Data Center database [39].

^{184}Hg, with a nearly maximum mixing strength (51%) for the 2^+_1 state in the mid-shell ^{184}Hg nu-

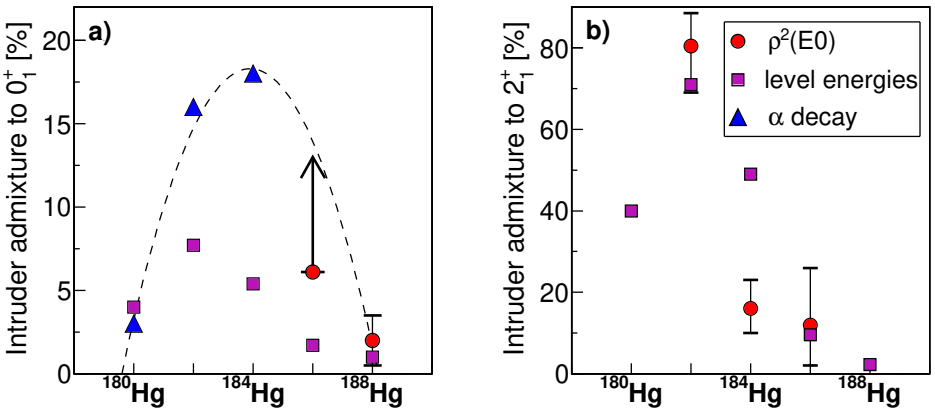

Figure 50: Admixtures of the intruder configuration to the wave functions of the (a) 0_1^+ and (b) 2_1^+ states in $^{180-188}$Hg deduced from level energies [481] (magenta squares), $\rho^2(E0)$ values (red circles) and α-decay hindrance factors [478] (blue triangles). The value corresponding to the lower limit for $\rho^2(E0; 0_2^+ \rightarrow 0_1^+)$ in ^{186}Hg is marked with an arrow. The differences of mean-square charge radii between the two configurations, necessary to extract the mixing coefficients from $E0$ transition strengths, were inferred from the odd-even staggering in the isotope shifts, see Fig. 49, following the procedure of Ref. [25]. As it not possible to determine from $E0$ data which configuration dominates the wave function of a specific state, in order to facilitate the comparison it was decided to adopt the scenario resulting from the level-energy analysis. The parabola is to guide the eye through $\rho^2(E0)$ and α-decay hindrance data in analogy to Fig. 28 in Ref. [25].

cleus. The configurations of the 2^+ states become more pure when moving away from $N = 104$, both towards lighter and heavier nuclei, as it was observed also for the 0^+ states. The enhanced $\rho^2(E0; 2_2^+ \rightarrow 2_1^+)$ transition strengths measured for ^{180}Hg [482], ^{182}Hg [483], ^{184}Hg [483] and ^{186}Hg [484, 485] support the importance of configuration mixing in the structure of 2^+ states in neutron-deficient Hg nuclei. These experimental data yield a consistent picture of two distinct configurations, weakly deformed oblate and strongly deformed prolate, that contribute in varying proportions to the observed low-lying states in $^{182-188}$Hg. The mixing of these two configurations gives rise to almost flat behaviour of the energy of the first excited 2^+ state, as shown in Fig. 49b, and of the $B(E2; 2_1^+ \rightarrow 0_1^+)$ values in $^{182-188}$Hg, even though the structures of 2_1^+ states are very different: while the intruder configuration dominates in ^{182}Hg, the contributions of both configurations are almost equal in ^{184}Hg, and finally the normal-order configuration prevails for ^{186,188}Hg.

The mixing coefficients reported in Ref. [481] can be combined with the information on electromagnetic transition probabilities in $^{180-188}$Hg in order to obtain information on the pure normal-order and intruder configurations. Lifetimes of excited states were measured applying Doppler-shift and fast-timing techniques to the ^{180,182}Hg [486, 487] and ^{184,186,188}Hg nuclei [471, 480, 481, 488–490] populated in fusion-evaporation reactions. While these studies were mostly limited to yrast states, they yielded lifetimes of states in both coexisting bands since the intruder band becomes yrast at low spin (see Fig. 49b). Finally, a low-energy Coulomb-excitation study with post-accelerated $^{182-188}$Hg beams provided magnitudes and signs of the reduced $E2$ matrix elements between the low-lying states of spin 0^+, 2^+ and 4^+ [491, 492]. As extensively discussed in Ref. [490], various assumptions were made when applying the two-band mixing approach to

the measured $B(E2)$ values or $E2$ matrix elements, even though multiple works relied on mixing coefficients of Ref. [481]. While in Ref. [481] the unperturbed transitional quadrupole moments depended both on spin and A, Ref. [490] assumed that the transitional quadrupole moments are constant within each band, and Ref. [492] postulated that the unperturbed configurations are the same in each of the $^{182-188}$Hg isotopes. As shown in Fig. 51, this leads to different conclusions concerning the overall deformation of the two unperturbed structures, which range from $\beta_2 \approx 0.22$ to $\beta_2 \approx 0.33$ for the intruder band and from $\beta_2 \approx 0.13$ to $\beta_2 \approx 0.22$ for the normal-order configuration. To complicate matters further, the $\rho^2(E0; 2_2^+ \rightarrow 2_1^+)$ value obtained for ^{184}Hg from a combination of Coulomb-excitation [492] and β-decay data [483] corresponds to considerably lower mixing than that deduced from the level energies, while a good agreement is observed for ^{182}Hg. The mixing of 2^+ states deduced from level energies in ^{186}Hg also agrees well with the result of an in-beam spectroscopic study [485] combined with the lifetime reported in Ref. [480], see Fig. 50.

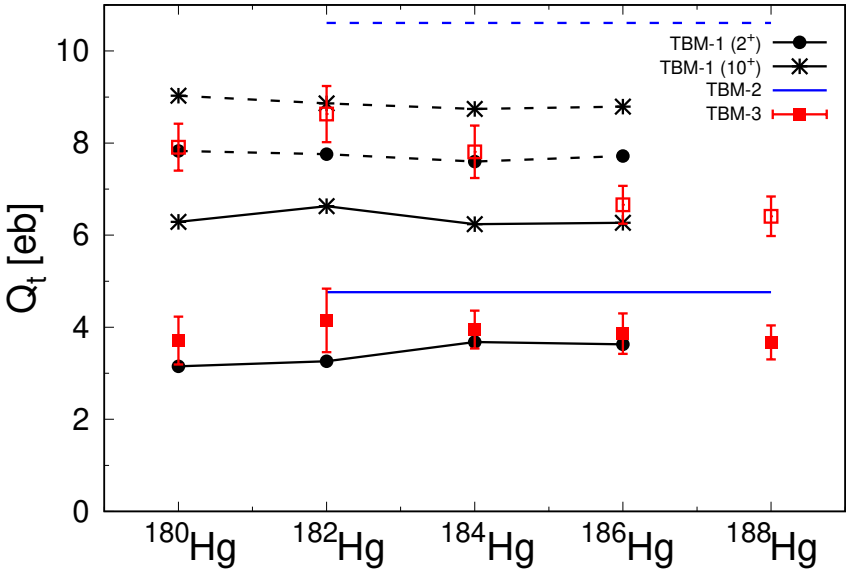

Figure 51: Transitional quadrupole moments for the normal-order (solid lines and filled squares) and intruder (dashed lines and open squares) configurations, obtained by applying the two-band mixing model to the measured $B(E2)$ values under different assumptions. TBM-1 [481] assumes that the unperturbed transitional quadrupole moments depend both on spin and A, TBM-3 [490] considers a dependence on A, and in TBM-2 [492] the unperturbed transitional quadrupole moments were both spin and mass independent. Figure adapted from Ref. [490].

The lack of consensus regarding the rotational character of unperturbed structures in $^{180-188}$Hg and their evolution with N, resulting in the differences between the deformation parameters extracted under various assumptions, seems to be due to the paucity of experimental information on the decay of non-yrast states, since in most cases only one transition probability is known in the ground-state band. While Ref. [490] yielded lifetimes of the 4^+ states in both coexisting structures, the precision is not sufficient to draw meaningful conclusions. The same is true for most matrix elements involving the 2_2^+ state, determined in Ref. [492]. Moreover, it is not clear to what extent the two-band mixing model is applicable to $^{180-188}$Hg. For example, for the higher-spin states in $^{180-188}$Hg, the analysis of Ref. [481] shows that their mixing decreases with spin and it no longer

follows a parabolic trend as a function of neutron number, but rather displays a monotonic increase with mass (e.g., the admixtures in the 4^+ states increase from 2% in ^{180}Hg to 20% in ^{188}Hg). This unexpected behaviour calls for experimental verification. An independent extraction of mixing coefficients from a large set of $E2$ matrix elements (see Eq. 38), as it was done for example in Ref. [222] for ^{74,76}Kr, or from $\rho^2(E0; I \rightarrow I)$ values measured for states with $I \geq 4$ would verify the validity of this approach. Similarly, measurements of spectroscopic quadrupole moments of low-lying states would also bring independent information on the deformation of the coexisting structures in $^{180-188}$Hg, their evolution with spin and their mixing. Currently, only the spectroscopic quadrupole moment of the 2^+_1 state in ^{188}Hg is known [492], but its precision is insufficient to draw conclusions.

Interestingly, a recent measurement of yrast-state lifetimes in ^{178}Hg [493] found that those of the states belonging to the deformed structure correspond to a β_2 deformation exceeding 0.4, considerably higher than those deduced for the excited structures in the heavier Hg isotopes. While the prevalent interpretation of the 0^+_2 states in $^{180-186}$Hg is that they result from two-proton excitations across the $Z = 82$ shell, the authors of Ref. [493] attribute the observed increase of the deformation for the corresponding structure in ^{178}Hg to the neutron contribution, in line with MCSM calculations [467], which successfully describe the even-odd shape staggering in $^{177-187}$Hg.

A recent study of ^{188}Hg [490], yielded, for the first time, lifetimes of the 14^+_1 and 16^+_1 excited states above the 12^+_1 154-ns isomer. They translate into transitional quadrupole moments significantly lower than those observed for lower-spin states (2.7(3) eb and 1.2(2) eb, respectively, compared to $\approx$ 3-5 eb and $\approx$ 6-10 eb for the two structures observed at low spin, see Figs. 51 and 60). This suggests that these states belong to a different, almost spherical structure, which is consistent with the conclusions of Ref. [494], attributing a $\nu(i_{13/2})^2$ character to this band. Moreover, the spectroscopic quadrupole moment of the 12^+_1 state was determined to be 0.91(11) eb [495], which, assuming $K = 12$, corresponds to Q_0 of 1.16(14)eb, consistent with the Q_t value determined from $B(E2; 16^+_1 \rightarrow 14^+_1)$. Together, these results form a strong body of evidence for multiple shape coexistence in ^{188}Hg.

Numerous low-lying 0^+ states were identified in stable Hg nuclei, in particular by means of two-neutron transfer reaction studies. The lowest three such states in each nucleus are plotted in blue in Fig. 49b (only those with firm spin assignments are taken into account). The natures of these states are unclear, although the 0^+_2 states were suggested as arising from neutron pairing vibrations [496]. The enhanced cross section to populate the 0^+_2 state in ^{200}Hg in the (p, t) transfer reaction (12% relative to that for the ground state [496, 497]) was explained [496] as arising from the gap in the neutron single-particle spectrum at $N = 120$ present for oblate shapes. Identification of bands constructed on these states, and measurements of transition probabilities within such structures, would be of great interest.

3.7.2. Even-even Pb and Po nuclei

The level of detail and precision concerning the coexisting structures in $Z = 82$ Pb and $Z = 84$ Po nuclei is lower compared to the Hg isotopes since in these isotopic chains the N=104 mid-shell lies considerably further from β stability. This is reflected in the types of available data supporting shape-coexisting structures as shown in Fig. 52. However, a consistent identification of normal-order and intruder states and an estimate of the mixing between them could be obtained from

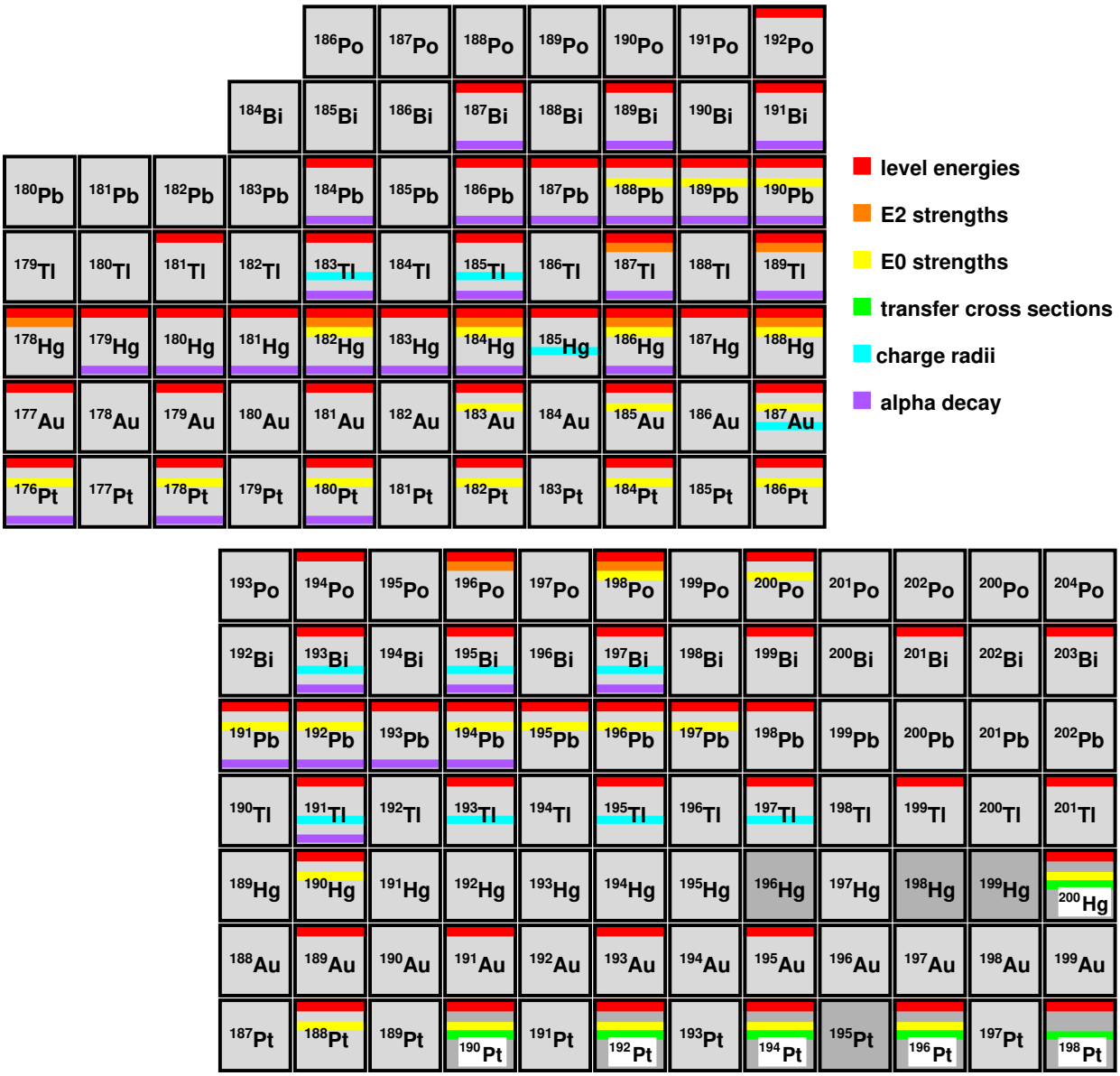

Figure 52: Summary of experimental data available for nuclei exhibiting shape coexistence in the light Pt-Po region. Red bars indicate that shape-coexisting structures were proposed based on their level energies (e.g. observation of a low-lying 0^+ state, or rotational structures with very different moments of inertia), orange bars mean that additional information was obtained from $E2$ transition probabilities, yellow bars mean that information on $E0$ transition strengths is known, green bars mean measured cross sections to populate the coexisting configurations in direct reactions, light blue bars indicate that charge radii of both configurations were measured, and magenta bars denote information from α-particle decay. Stable nuclei are indicated with a darker shade.

systematic studies of the α-decay hindrance [477, 498, 499]. The α decay of ^{194,196,198}Po proceeds preferentially to the ground states of the Pb daughter nuclei, but the competing decay to the intruder states in Pb becomes more probable when going toward $N = 104$. This trend persists for lighter

Po nuclei, with the ground-state-to-ground-state transitions becoming increasingly hindered [477, 500]. The α decay that involves the removal of two protons from orbitals above the $Z = 82$ closed shell was observed to be a factor of 3 to 4 times faster than that involving the removal of two protons from below the gap [501]. Thus, the observed gradual increase of probability of decays feeding the intruder states in Pb was explained by an admixture of the intruder configuration in the ground states of Po. This admixture would increase with decreasing N and eventually become dominant, which is consistent with the results of charge-radii measurements in the Po isotopic chain [502, 503], showing a monotonic increase of the ground-state deformation starting as early as at $A \leq 199$ ($N \leq 115$), see Fig. 49a.

The observation of the fine structure of the α decay of ^{190}Po allowed identification of two 0^+ states in ^{186}Pb [498]. On the basis of α-decay hindrance factors, the 532(21) keV 0^+_2 state was associated with a mainly $\pi(2p-2h)$ configuration. The decay to the 650(23) keV 0^+_3 state was observed to be more hindered than those to the $0^+_{1,2}$ states, which supports a $\pi(4p-4h)$ character of the former. Indeed, a transition from the normal-occupation component ($\pi 2p$) of the ground state in Po to a $\pi(4p-4h)$ state in Pb would involve a removal of two protons with the simultaneous promotion of a proton pair across the $Z = 82$ gap, leading to its significant hindrance. Similarly, a transition from the intruder admixture to the ground state in Po to a $\pi(4p-4h)$ state in Pb would imply a removal of two protons from below the $Z = 82$ gap, while the decay to a $\pi(2p-2h)$ configuration would be related to the removal of protons from above the closed proton shell and consequently it would proceed faster, as discussed above.

Two regular rotational bands were observed in ^{186}Pb [504, 505], see Fig. 53, which may be based on the two excited 0^+ states identified in the α-decay study [498]. However, the transitions between the observed 2^+ band heads of both bands and the $0^+_{2,3}$ states have not yet been identified. The intensity limits [505] correspond to $B(E2; 2^+_2 \rightarrow 0^+_2)$ and $B(E2; 2^+_2 \rightarrow 0^+_3)$ values exceeding that of $B(E2; 2^+_2 \rightarrow 0^+_1)$ by factors of 5 and 25, respectively. For comparison, the $B(E2; 2^+_2 \rightarrow 0^+_2)/B(E2; 2^+_2 \rightarrow 0^+_1)$ ratio in the neighbouring ^{184}Hg isotone is equal to 7(4) [492].

Low-lying 0^+ states in ^{188}Pb were observed in conversion-electron spectroscopy [506] and α decay [500, 507, 508] but the results are not fully consistent. Notably, a 0^+_3 state was postulated at 767(12) keV (Ref. [508]) and then at 725(2) keV (Ref. [506]). A later α-decay study [500] ruled out the former and put the latter in doubt, as a hindrance factor larger than 50 would be necessary to explain its non-observation in α decay. Again, no γ-ray transitions linking those states with the known 2^+ states were observed. On the other hand, the rotational structures on top of the $2^+_{1,2}$ states were identified and their moments of inertia were shown to be different [509], as shown in Fig. 54.

Experimental information for ^{190}Pb is more detailed, but the low-energy spectrum is dominated by the weakly deformed structures, including microsecond 11^- and 12^+ isomers assigned to different configurations, although a candidate prolate band was proposed [510]. An excited 0^+ state was identified in α-decay studies [511] at 658 keV, but no γ-ray transitions feeding this state are known. Similar low-lying 0^+ states, appearing below the first excited 2^+ state, were observed in ^{192}Pb and ^{194}Pb, and their $E0$ decay to the ground states corresponded to considerably lower monopole transition strengths ($10^3 \times \rho^2(E0; 0^+_2 \rightarrow 0^+_1) \approx 1$ [511]) than those measured for ^{186,188}Hg. While there are candidates for members of bands built on the 0^+_2 states in ^{192,194}Pb, as indicated on Fig. 53, no transition probabilities within these bands are known.

On the other side of the $N = 104$ mid shell, a single rotational band was identified in each of the

^{180}Pb [512], ^{182}Pb [513] and ^{184}Pb [514] nuclei. The moments of inertia of these band structures were found to be similar to those related to the deformed $\pi(4p-4h)$ configuration in the heavier Pb isotopes. Moreover, a low-lying 0^+_2 state in ^{184}Pb was observed to be preferentially fed in α decay of ^{188}Po [499]. Based on its excitation energy, this state was tentatively interpreted as the band-head of the observed rotational band. The parabolic pattern of the assumed $\pi(4p-4h)$ states is evident, as can be seen in Fig. 53, and strongly resembles that observed for the intruder states in Hg isotopes.

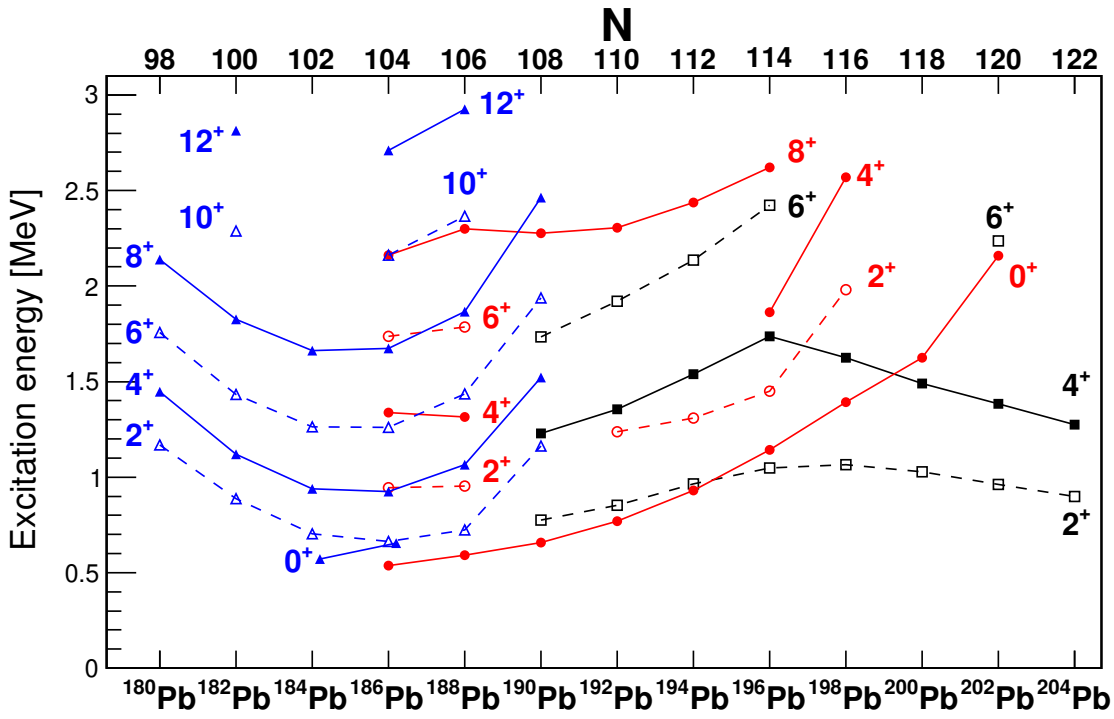

Figure 53: Energy systematics of positive-parity excited states in the neutron-deficient even-even lead isotopes, showing presumed spherical states (black squares), deformed $\pi(2p-2h)$ configuration (red circles), and deformed $\pi(4p-4h)$ configuration (blue triangles). Data are taken from the National Nuclear Data Center database [39]. For clarity, some points are slightly offset on the x axis.

Lifetimes in ^{186,188}Pb are known for the few lowest yrast states [515]. A strong reduction of transitional quadrupole moments, Q_t, deduced from the $B(E2; 2^+_1 \rightarrow 0^+_1)$ values, with respect to those extracted from $B(E2; I{+}2 \rightarrow I)$, $I \geq 2$ was attributed to different configurations of the ground state (spherical) and 4^+_1, 6^+_1, 8^+_1 (prolate deformed with β_2=0.29(5)). Moreover, a comparison of the $B(E2; 4^+_1 \rightarrow 2^+_1)$ value with those measured for the decay of higher-spin states reveals that the 2^+_1 state in ^{186}Pb has a pure deformed character, while for the 2^+_1 state in ^{188}Pb, assuming the two-state mixing model, one obtains a prolate contribution of 40% .

Three high-spin and high-K isomers have been identified in ^{188}Pb. Based on their decay properties, structures of bands observed on top of them, and g-factor measurements, they were assigned 9/2[624] $\otimes$ 7/2[514] two-quasineutron, 9/2[505] $\otimes$ 13/2[606] two-quasiproton and neutron $(i_{13/2})^2$

configurations, respectively [509, 516, 517]. In Ref. [516], the isomeric states were associated with three different potential wells corresponding to prolate, oblate and spherical shapes, respectively, suggesting that the coexistence of three distinct shapes extends to lower-spin states built in each well. This, for the moment, has not been experimentally confirmed. The 12^+ isomer in ^{188}Pb seems to be an analogue of the 12^+ isomer in ^{188}Hg. In the latter, however, lifetime measurements have demonstrated that the lower-spin states present higher deformation that those built on top of the spherical 12^+ isomer, which supports their assignment to different configurations.

The similarity of deformed structures in Hg and Pb nuclei is further evidenced by a comparison of the kinematic moments of inertia, $J^{(1)}$, plotted for yrast states in these nuclei as a function of γ-ray energy, as shown in Fig. 54. From spin 6^+ upwards, the yrast bands in ^{188}Pb and ^{186}Hg present a strikingly similar, regular behaviour. The irregular pattern of kinematic moments of inertia at lower spin can be related to the crossing and mixing of the two configurations characterised by different deformations. Interestingly, the moments of inertia obtained for ^{190}Po follow this pattern very closely, while those for ^{192,194}Po, which evolve smoothly, are considerably lower. In the absence of data on non-yrast states in these isotopes, it may still be concluded from this observation that a weakly deformed configuration forms the yrast states for $N \geq 108$ (i.e., in ^{192}Po and the heavier Po isotopes), and in ^{190}Po ($N = 106$) the prolate-deformed intruder states of spin 2^+ and above have descended in energy below their weakly deformed counterparts. This is consistent with the strong hindrance of the ground-state-to-ground-state α decay from ^{188}Po to ^{184}Pb [499], which suggests their different configurations, i.e., the intruding prolate-deformed 0^+ state becoming the ground state in ^{188}Po. In this context, a measurement of the charge radii in ^{188,190}Po would be of much interest.

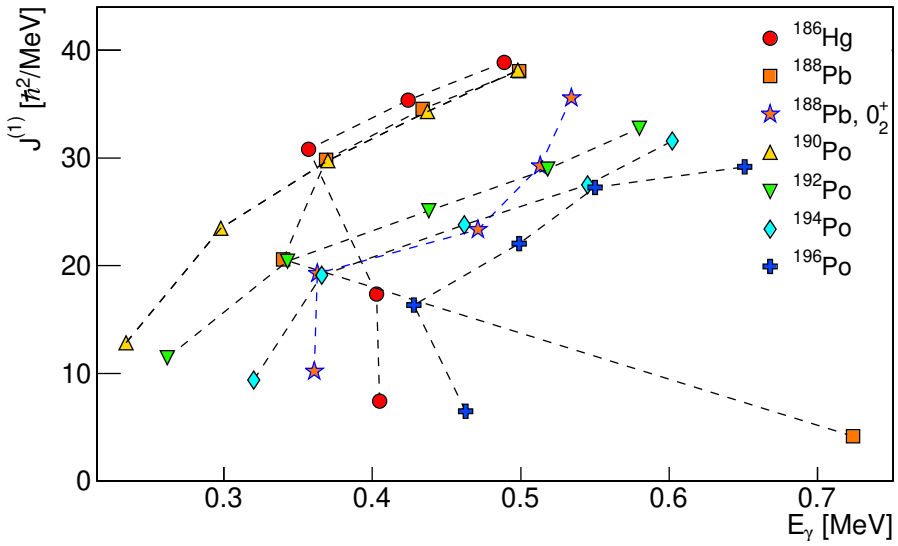

Figure 54: Kinematic moments of inertia for yrast states in ^{186}Hg, ^{188}Pb and ^{190,192,194,196}Po, and the band built on the 0_2^+ state in ^{188}Pb. For clarity, only states up to spin 10^+ are plotted. Data are taken from the National Nuclear Data Center database [39].

The level systematics in even-even $^{190-210}$Po isotopes reveals another intruding structure. The

low-lying yrast levels in $^{200-210}$Po can be attributed to a spherical $j = 9/2$ seniority structure, and their energies evolve smoothly until they drop sharply in ^{198}Po, as shown in Fig. 55. This drop in energy is accompanied by the appearance of low-lying 0^+ states, and candidates for low-spin members of bands built on them, which were identified in $^{196-202}$Po in α- and β-decay studies [518] as well as in γ-ray spectroscopy following fusion-evaporation reactions [519]. Their energies follow a similar parabolic behaviour as the yrast levels in $^{190-198}$Po. This was interpreted [518, 519] as an intrusion of an oblate $\pi(4p-2h)$ configuration, which mixes with the spherical states and pushes them down in energy. The levelling off of the level energies around ^{192}Po was suggested to be due to the intruder structure becoming the ground state [520]. The regularity of the kinematic moments of inertia for ^{192,194}Po and the fact that the $|Q_t|$ values for the $4^+ \rightarrow 2^+$ and $2^+ \rightarrow 0^+$ transitions in ^{194}Po are identical [515] support the picture of the ground states in ^{192,194}Po being dominated by the intruder configuration. On the other hand, lower moments of inertia are observed for low-spin states in ^{196}Po, as shown in Fig. 54, which can be attributed to the strong contribution of the spherical configuration to their structure. The observed [477, 500] gradual increase, with decreasing N, of hindrance factors for the ground-state-to-ground-state α decays of Po isotopes is also consistent with this scenario. Moreover, the spectroscopic quadrupole moments of the 2_1^+ states evolve from values compatible with zero for ^{200,202}Po to positive values for ^{196,198}Po [521], in line with the yrast states changing character from spherical seniority structures to weakly deformed intruder ones. One should note here that the $|Q_t|$ values in ^{194}Po correspond to a deformation parameter $|\beta_2| \approx 0.17(3)$ [515], similar to those of the normal-order configuration in the Hg isotopes, and that the moment of inertia of the structure built on the 0_2^+ state in ^{188}Pb is similar to those observed for the ground-state bands in ^{192,194}Po, as shown in Fig. 54.

Unfortunately, there is little information about the non-yrast states in the light Po isotopes apart from their energies. The 0_2^+ and 2_2^+ states in ^{196,198}Po were populated in a Coulomb-excitation study [521], and the $E2$ matrix elements related to their decay were determined, although with a rather low precision. An attempt to explain the measured $E2$ matrix elements within a two-state mixing model assuming the same unperturbed structures for $^{194-202}$Po [521] was less successful than the same procedure applied to the $^{182-188}$Hg nuclei in Ref. [492]; notably, deviations are observed for ^{198}Po. The spectroscopic quadrupole moments of the two unperturbed structures were 1.1 eb and -0.3 eb, supporting the scenario of a weakly deformed structure mixing with a nearly spherical one. However, given that the structure of light Po nuclei is likely to be influenced also by the more deformed prolate configuration descending to the ground state in ^{190}Po, it is not clear to what extent the two-state mixing model is applicable, which may explain the observed discrepancies.

The $E0$ transition strengths in light Po nuclei were estimated from missing γ-ray intensities in γ-γ coincidences [519, 523, 524] or X-ray intensities in Coulomb excitation [521]. Unfortunately, due to large uncertainties and conflicting values, no conclusions can be drawn from these data.

3.7.3. Even-even Pt nuclei

Moments of inertia of yrast bands in $^{178-186}$Pt display a similar, rather regular behaviour, consistent with their well-deformed character, see Fig. 56. The anomalies observed at low spin for ^{176,178}Pt were attributed [525, 526] to the change of configuration of the ground and lowest yrast states, which are less deformed than higher-spin states. A significantly lower moment of inertia is also determined for the yrast band in ^{188}Pt. A configuration change occurring between ^{176}Pt and

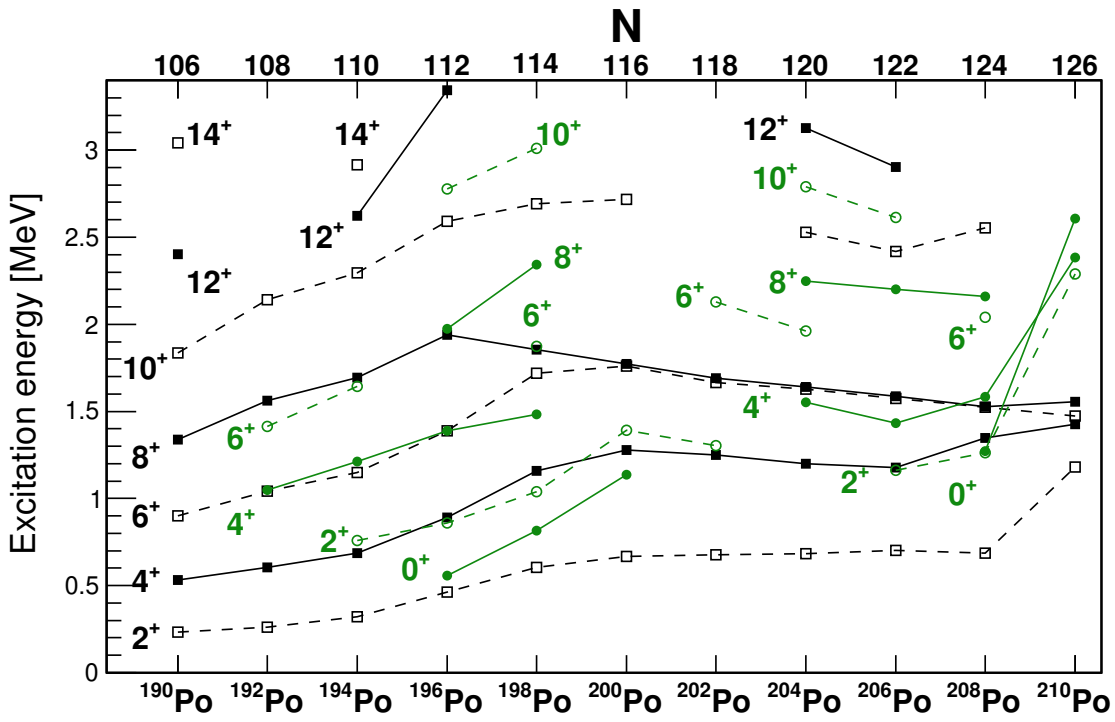

Figure 55: Energy systematics of positive-parity excited states in the neutron-deficient even-even polonium isotopes, showing ground-state bands (black squares) and non-yrast states (green circles). Data are taken from the National Nuclear Data Center database [39] and Ref. [522].

^{178}Pt is supported by the sudden increase of the hindrance factor for the α decay feeding the excited states that occurs for ^{176}Pt [477]. Since the ground states in Hg isotopes have a predominantly weakly deformed normal-order configuration, it implies that the same is true for the ground state in ^{176}Pt, while those in heavier Pt isotopes have a deformed intruder configuration. The resulting interpretation of energy spectra in Pt isotopes in terms of coexisting normal-order and intruder configuration is presented in Fig. 57.

Considerable progress has recently been achieved in the measurements of transition probabilities in neutron-deficient Pt isotopes [528–534]. Interestingly, many new lifetime measurements correspond to $E2$ transition strengths significantly larger compared to older data, which the authors tentatively attribute to a better treatment of side feeding. The transitional quadrupole moments deduced from lifetimes of the first four yrast states in $^{176-194}$Pt nuclei are presented in Fig. 58. They display a roughly trapezoid pattern, particularly evident for higher-spin states, with a plateau at about 7 eb stretching from $A = 178$ to $A = 186$, and a gradual decrease on its both sides. The values obtained for $^{190-194}$Pt are again nearly constant with Q_t about 4 eb, similar to the values observed for the weakly deformed states in Hg isotopes. In the region of the plateau, where the yrast bands are supposed to be dominated by the deformed intruder configuration, it is usually observed that the transitional quadrupole moments increase with spin up to spin 4^+ or 6^+, and then stabilise. It is tempting to attribute this behaviour to the mixing of the two configurations, which

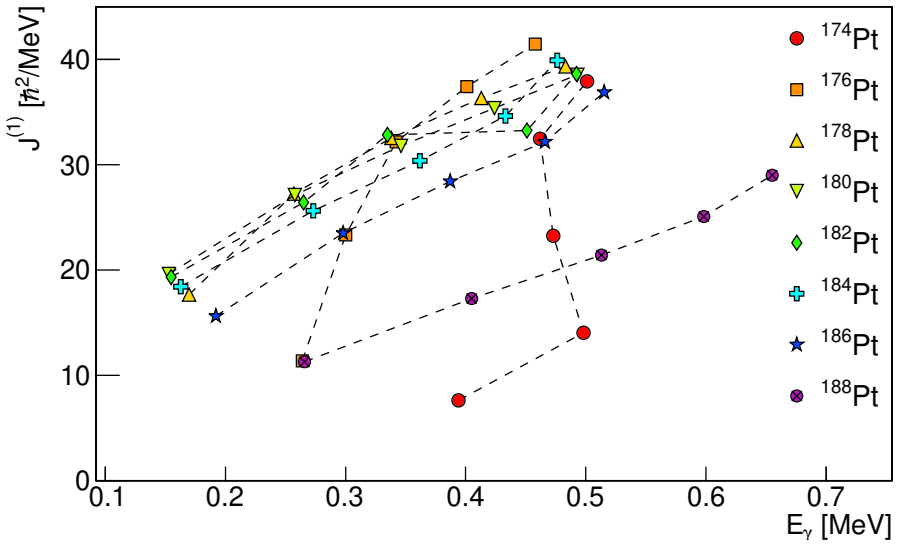

Figure 56: Kinematic moments of inertia for yrast states up to spin 10 in even-even $^{174-188}$Pt nuclei. Data are taken from the National Nuclear Data Center database [39].

decreases with spin, although, surprisingly, such an effect is not present for ^{180}Pt.

The importance of mixing in the structures of the light Pt isotopes is supported by an almost constant behaviour of the g factors of the 2^+_1 states in $^{180-198}$Pt [535–537]. In particular, the 70-80% mixing obtained for the 2^+ states in $^{184-188}$Pt from the two-band mixing model applied to level energies was in good agreement with the measured g factors [535].

3.7.4. Odd-mass Au, Tl and Bi nuclei

Due to the complexity of the excitation spectra, involving many multiplets, and low excitation energies of key states, the information on shape coexistence in odd-mass nuclei in this mass region is more limited compared to the even-even neighbours. Low-lying $9/2^-$ intruder states in the Tl isotopes (related to the proton $1h_{9/2}$ configuration) as well as the proton $3s_{1/2}$ hole states were identified via α-decay spectroscopy [538, 539]. Unhindered α-decay branches were observed between $^{187-195}$Bi $9/2^-$ ground states and $^{183-191}$Tl $9/2^-$ intruder states, and between the $^{187-195}$Bi $1/2^+$ intruder states and the $^{183-191}$Tl $1/2^+$ ground states [538]. The excitation energies of the $9/2^-$ intruder states in the Tl isotopes display a characteristic parabolic behaviour as a function of neutron number and follow a similar pattern as the $1/2^+$ intruder states in the odd-mass Bi isotopes for $N \geq 110$. For $N \leq 108$, the trend in the energies of the $1/2^+$ intruder states in the Bi isotopes deviates from those of the $9/2^-$ states. Interestingly, the decay of the $1/2^+$ state in ^{185}Bi ($N = 102$) to the ^{181}Tl ground state was found to be hindered (HF=14(3) [540]), which may indicate a change of configuration of the $1/2^+$ state between ^{185}Bi and the heavier Bi isotopes. The g factors of the $9/2^-$ intruder states in $^{183-197}$Tl and those of the $^{187-197}$Bi are very similar across a wide range of N, as shown in Fig. 59b, pointing to their similar microscopic configurations.

Measurements of the charge radii for both ground and isomeric states have been performed for a wide range of Bi and Tl isotopes. As displayed in Fig. 59a, dramatic differences are observed

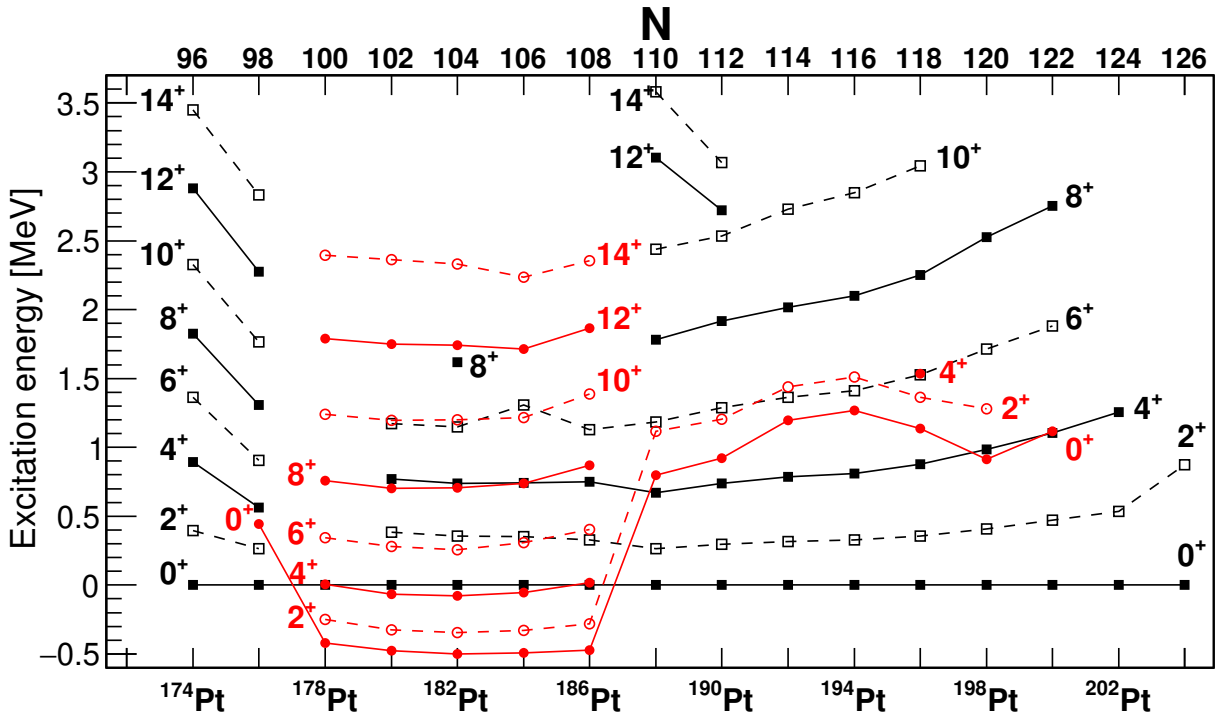

Figure 57: Energy systematics of positive-parity states in the neutron-deficient even-even platinum isotopes, plotted relative to the energy of the 0^+ state of normal-order configuration. Intruder states are marked with red circles and normal-order states with black squares. For clarity, γ bands are not plotted. Data are taken from the National Nuclear Data Center database [39] and Ref. [527].

[544] for the $\delta\langle r^2\rangle$ values for the $9/2^-$ isomer in the Tl nuclei *versus* the $1/2^+$ ground state, with the latter following closely those for the spherical Pb nuclei. Combined with the measured electric quadrupole moments, these results point to an oblate deformation of the $9/2^-$ states with $|\beta_2|$ of about 0.17. For the Bi isotopes, the β_2 deformation of the ground state starts to gradually deviate from sphericity below $N = 110$ ^{197}Bi, while that of the $1/2^+$ isomers in $^{193-197}$Bi is considerably larger and more constant [543]. The pattern of ground-state charge radii in light Bi isotopes resembles that observed for the Po chain (see Fig. 49), suggesting that a more deformed configuration may mix with that of the ground state when approaching the neutron mid-shell. Finally, the charge radii in the Au isotopic chain increase dramatically between $N = 108$ and $N = 107$. This is accompanied by a ground-state spin change from $1/2^+$ in ^{187}Au (normal-order configuration) to $5/2^-$ in ^{185}Au (intruder configuration).

There are multiple suggestions in Tl and Bi nuclei of rotational bands interpreted as resulting from coupling of the odd proton particle or hole to the normal-order or intruder configuration of the even-even core. For example, the bands built on $13/2^+$ isomers in ^{187,189}Bi were shown to share important similarities with those in ^{186,188}Hg associated to prolate shapes [546], while their analogues in ^{191,193}Bi have a strongly coupled character, indicating that they are associated instead with a weakly deformed core configuration [547, 548]. Based on the similarity of the moments

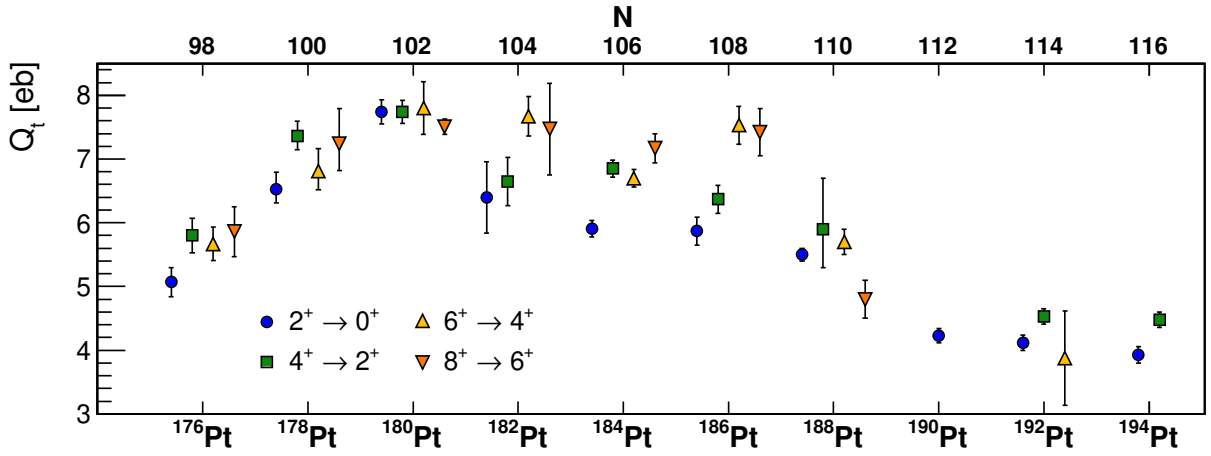

Figure 58: Transitional quadrupole moments Q_t calculated from lifetimes of 2^+_1, 4^+_1, 6^+_1 and 8^+_1 states in even-even $^{176-194}$Pt nuclei. For clarity, some points are slightly offset on the horizontal axis. Data are taken from the National Nuclear Data Center database [39] and Refs. [528–534].

of inertia between the rotational band built on the ground state of ^{193}Bi and the yrast band in ^{194}Po, the former was interpreted as resulting from coupling of a $1h_{9/2}$ proton to a deformed oblate configuration in ^{192}Pb [547]. The characteristics of the bands built on the $1/2^+$ intruder states are different for ^{191}Bi and ^{193}Bi, with the latter having a similar moment of inertia as the yrast bands in ^{188,190}Hg (indicating a weakly deformed oblate structure), and the former being significantly more deformed [548]. It would be interesting to investigate if this effect is visible in the isomer shift of the $1/2^+$ state in ^{191}Bi, and, as there is no significant difference in α-decay hindrance between the two Bi isotopes, in the charge radii of the ground state of the ^{187,189}Tl daughter nuclei.

Strongly-coupled bands constructed on the $9/2^-$ isomer were observed in even-neutron $^{183-189}$Tl isotopes [550–552] and their properties are consistent with the weak oblate deformation of the band head determined from the isomer shift. Similar bands associated with the $i_{13/2}$ intruder configuration were also seen in ^{187}Tl [550], ^{189}Tl [551] and the heavier Tl isotopes. Decoupled bands due to $i_{13/2}$, $h_{9/2}$ and $f_{7/2}$ intruders were identified in ^{183,185,187}Tl [550, 552] and from their spectroscopic properties they were associated to prolate deformation. Lifetime measurements in ^{187}Tl [553] and ^{189}Tl [554] confirmed that the transitional quadrupole moments in the structures identified as prolate and oblate strongly differ, as can be seen in Fig. 60. Interestingly, the transitional quadrupole moments for the prolate $i_{13/2}$ structures in odd-mass Tl and Au nuclei appear, on average, larger than those for the prolate $h_{9/2}$ bands, and closer to those obtained for ^{188}Pb than for the ^{186,188}Hg isotones. At the same time, the quadrupole moments for the oblate structures in odd-mass Tl nuclei are significantly lower than those measured for the oblate states in the Hg isotones.

In odd-mass Au nuclei both proton-particle and proton-hole configurations were observed, the former resulting from coupling to even-even Pt cores, while the latter involve coupling to even-even Hg cores. For example in ^{187}Au, structures resulting from coupling of the $1h_{11/2}$ proton hole to 0^+_1 and 0^+_2 states in ^{188}Hg were identified (i.e., $\pi(3h)$ and $\pi(2p-5h)$), as well as those where a $1h_{9/2}$ proton couples to 0^+_1 and 0^+_2 states in ^{186}Pt (i.e., $\pi(3p-6h)$ and $\pi(1p-4h)$) [556]. Similar structures

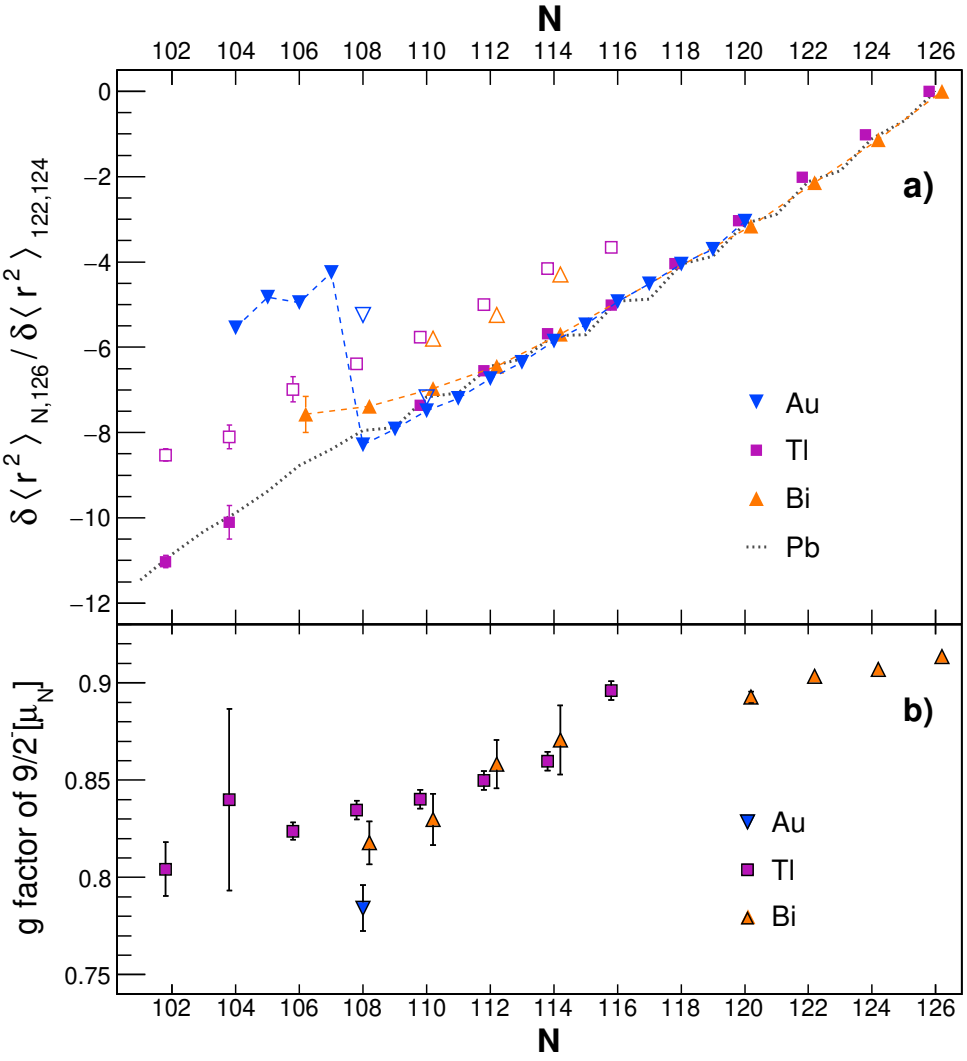

Figure 59: (Top) Changes in mean-square charge radii, relative to N=126, as a function of the neutron number for Tl (magenta squares) and Bi (orange triangles) isotopic chains, normalized to the difference in charge radius between N=122 and N=124, and compared to the data for Pb (gray dotted line). The data for Au isotopes are also plotted (blue triangles), with the point for ^{197}Au normalised to the value measured for ^{200}Pb to facilitate direct comparison. Filled symbols denote ground states and open symbols isomeric states. For clarity, only the values for odd-mass Tl and Bi isotopes are plotted, and they are slightly shifted on the horizontal axis. The values are taken from Refs. [234, 541, 542]. (Bottom) g factors for $9/2^-_1$ states in Bi (orange), Tl (magenta) and Au (blue). For clarity, values for Tl and Bi isotopes are slightly shifted on the horizontal axis. Data are from Refs. [542–545] and references therein.

were also observed in ^{185}Au, and transitions between them were shown to have $E0$ components, consistent with their different deformations [557]. A large isomer shift was measured for the $9/2^-$, $t_{1/2}$ = 2.3 s state in ^{187}Au, as shown in Fig. 59a. Interestingly, the g factor determined for this state is considerably lower [542] than those measured for the $9/2^-_1$ states in Tl and Bi nuclei, as seen in Fig. 59b.

Recently, a regular rotational band was observed built on the second $11/2^-$ state in ^{177}Au [558]. The head of this band, interpreted as formed by the coupling of a $1h_{11/2}$ proton hole to the 0^+_2 state in ^{178}Hg, presents a very different decay pattern than that observed for the analogous structure in ^{187}Au, as shown in Fig. 61. This suggests an important difference between the 0^+_2 structures in ^{178}Hg and ^{186}Hg, in line with the results of the lifetime measurements in ^{178}Hg [493] that yield a β_2 value of about 0.4 for the deformed configuration in ^{178}Hg, which is significantly larger than those estimated for the deformed structures in heavier Hg isotopes.

Almost constant excitation energies of the states associated with coupling of a $1h_{11/2}$ proton hole with the ground state of the Hg core are observed over the Au isotopic chain, which is similar to the behaviour of the 2^+_1 states in Hg isotopes. In contrast, the lowest states corresponding to the intruder configuration, $9/2^-$, display a parabolic trend with a minimum at $N = 104$ [559], as shown in Fig. 64. Recent measurements for ^{181,183}Au [560, 561] provided more data on the variety of normal-order and intruder states in these nuclei. In particular, in ^{183}Au an $E0$ transition feeding the first $3/2^-$ state of the $2d_{3/2} \otimes 3s_{1/2}$ proton-hole configuration was reported in Ref. [561]. Such an $E0$ decay has no counterparts in the neighbouring Au nuclei, suggesting that it may proceed from a deformed state of a configuration that has not been observed before. Identification of rotational states built on top of it would help to elucidate its character.

4. Conclusions

There has been tremendous progress in shape-coexistence studies in the past several decades that has been driven by a variety of factors. The data now available have resulted from the drive towards detailed spectroscopic studies. Especially noteworthy in this regard are the very high-

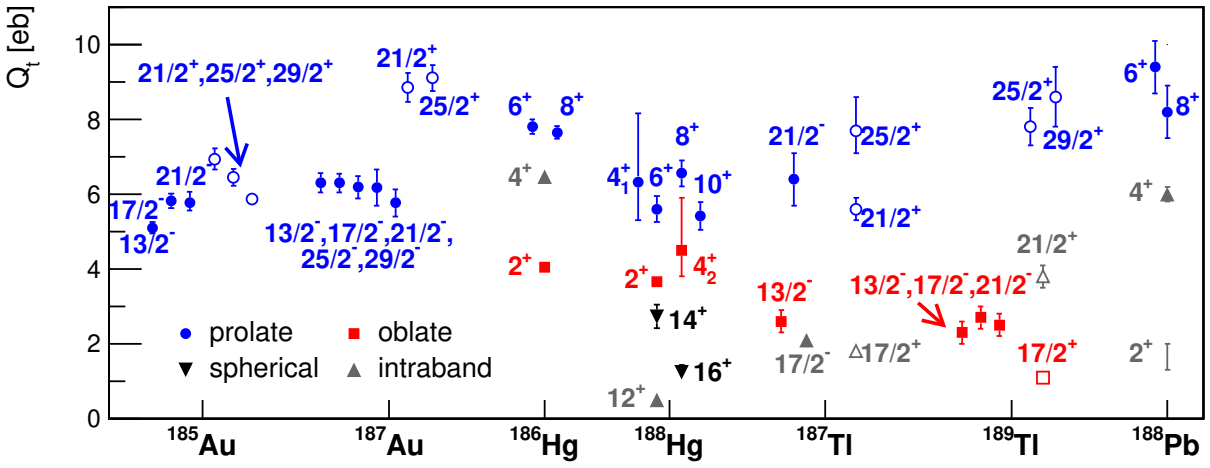

Figure 60: Transitional quadrupole moments Q_t calculated from lifetimes measured for ^{185,187}Au, ^{186,188}Hg, ^{187,189}Tl and ^{188}Pb ($N = 106, 108$), revealing a variety of structures differing in deformation. For odd-mass nuclei, full symbols denote $h_{9/2}$ states, while open symbols are used for $i_{13/2}$ structures. The points are labeled with the spin and parity of the de-exciting state. Data are from Refs. [481, 490, 515, 549, 553–555].

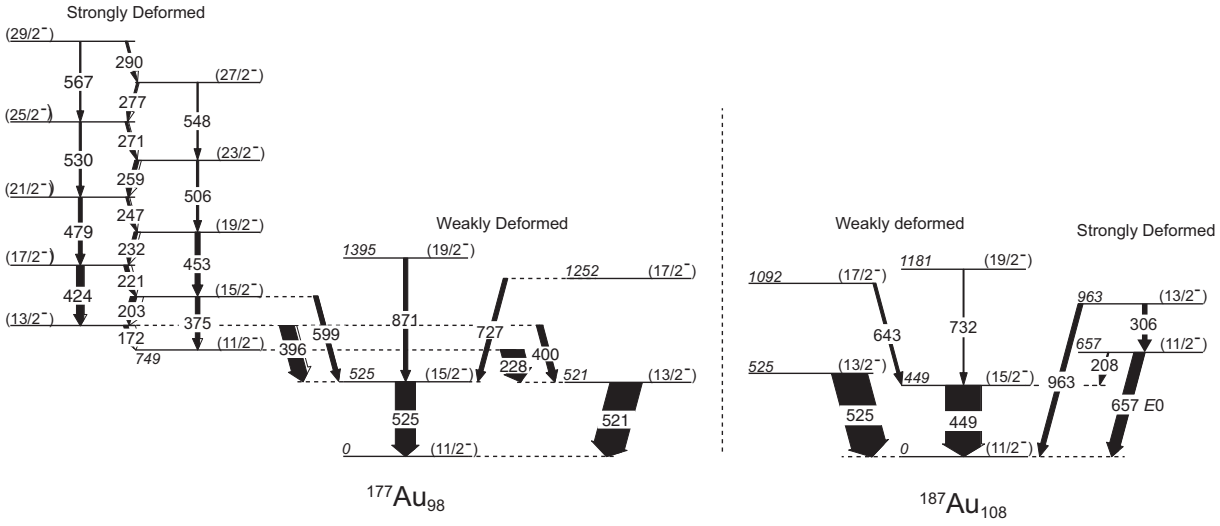

Figure 61: Partial level schemes of ^{177}Au and ^{187}Au displaying states associated with coupling of a $1h_{11/2}$ proton hole with 0^+_1 and 0^+_2 states in Hg cores, giving rise to nearly spherical and strongly deformed structures, respectively. Figure taken from Ref. [558].

statistics β-decay studies that enable the observation of low-energy transitions from non-yrast states, recoil-decay tagging that makes possible the separation and observation of nuclei with very low production cross sections, and also highly sensitive Coulomb-excitation experiments that provide large sets of electromagnetic matrix elements including quadrupole moments of short-lived excited states. The development of high-resolution and high-efficiency instrumentation for these studies, from particle detectors and recoil separators to HPGe γ-ray spectrometers, has enabled an unprecedented sensitivity. The wealth of data has also benefited tremendously from the availability of a variety of radioactive beam species, and the increasing intensity of such beams has opened new avenues of research, not only in regions of the nuclear chart previously inaccessible for detailed studies, but also enabling, for less exotic nuclei, the high-statistics measurements mentioned above. There have been theoretical advancements, including developments in beyond-mean-field calculations, large-scale and Monte-Carlo shell-model calculations, the widespread application of three-body forces and accounting for the tensor interactions, and the guidance for the calculations resulting from the underlying symmetries. The level of accuracy obtained in reproducing the experimental data using globally-derived interactions, rather than local fitting, has resulted in an increase in the level of confidence in interpreting the natures of the structures observed. The status of the field, from a unified experimental and theoretical viewpoint, was reviewed by Heyde and Wood [2] in 2011. Following in the footsteps of their earlier reviews, it emphasized the need for comprehensive spectroscopic studies of nuclei suggested to possess shape-coexisting structures, including measurements that provide absolute $B(E2)$ values, $\rho^2(E0)$ values, single- and multi-nucleon transfer cross sections, etc. It further suggested that the presence of shape-coexisting structures in nuclei may be the norm, and that we might expect them in nearly all nuclei except perhaps the very lightest. The role of multiparticle-multihole excitations was highlighted, and also

that of the "multishells", which made the large deformations observed near closed shells to be expected. Finally, the growth in the community directly involved in such studies, and the willingness to re-examine both open problems and previously understood structures for new insights, has created a vibrant atmosphere for collaboration and provided a diversity of perspectives. The confluence of these factors has made the present era of shape-coexistence studies perhaps the most exciting and rapidly developing in its history. In the following, we present a brief overview of the regions we have explored in the present work.

In the light-mass nuclei, many of the shape-coexisting structures display a multiparticle-multihole character. As has been shown in many calculations, states involving $2p-2h$, $4p-4h$, etc., configurations can be present at low excitation energies, and even become the ground states. The $N = 20$ "island-of-inversion" region is an excellent example of the latter. Measurements performed on ^{32}Mg are consistent with the ground state having a mixed $2p-2h$ and $4p-4h$ structure, and the normal-order $0p-0h$ 0^+ state has yet to be located. Such multiparticle-multihole structures can reach large deformations, as do those that have been known to exist at low energies in the Ca isotopes, with the superdeformed 0^+_3 state in ^{40}Ca involving a $8p-8h$ configuration, and the 0^+_2 state dominated by the $4p-4h$ excitations. The recent Coulomb-excitation study of ^{42}Ca measured the $\langle Q^2 \rangle$ and $\langle Q^3 \cos 3\delta \rangle$ quantities for both the ground state and the $6p-4h$ 0^+_2 state, the first such direct determination for a superdeformed structure. A candidate superdeformed band has also been suggested in ^{28}Si, coexisting with a normal-deformed oblate ground state, and the observed $E0$ decay of the 0^+_2 state in ^{24}Mg is consistent with its β_2 deformation of about 1.

At the double shell closure $Z, N = 28$, a highly-deformed $4p-4h$ structure is observed in ^{56}Ni, similar to those present in the $A \approx 40$ region. Low-lying proton pairing vibration states were postulated in $^{58-62}$Ni based on their enhanced population in proton-transfer reactions, with those in ^{58,60}Ni also possessing enhanced $E0$ transitions to the ground states. An explanation of these large $E0$ strengths, recently complemented by similarly large $\rho^2(E0)$ values for the $2^+_2 \rightarrow 2^+_1$ transitions in ^{58,60,62}Ni, remains elusive. An intense experimental effort in the last five years has clarified greatly the level schemes and spin-parity assignments for nuclei in the neighbourhood of ^{68}Ni. However, few relevant transition probabilities are currently known and no measurements of spectroscopic quadrupole moments have been performed. There are suggestions of triple shape coexistence in ^{64,66,68}Ni based on comparisons with theoretical calculations, with excited prolate and oblate states coexisting with spherical ground states. Two protons below Ni, the neutron-rich Fe isotopes have deformed ground states, and an observation of a low-lying 0^+_2 state in ^{66}Fe hints at shape coexistence. The properties of the ground-state bands in the Co isotopes with $N < 40$ point to their nearly spherical character, while those of the $(1/2^-)$ states identified at low excitation energy in ^{65,67}Co provide strong evidence for shape coexistence. In both the Ni and Co isotopes, the evolution of these configurations beyond $N = 40$, i.e., when the $\nu g_{9/2}$ is filled, remains an open question. Finally, in the vicinity of ^{78}Ni, first observations of low-lying deformed states involving neutron excitation across the $N = 50$ gap have been reported in, e.g., $N = 49$ ^{79}Zn and ^{81}Ge. At $N = 50$, low-lying deformed 0^+ states in ^{82}Ge and non-yrast deformed states in ^{78}Ni have been proposed, while an observation of a non-yrast state in ^{82}Zn, tentatively assigned as 0^+_2, represents the first hint of shape coexistence beyond $N = 50$. The persistence of deformed ground states towards $N = 50$, recently established in ^{66}Cr and ^{70,72}Fe nuclei [562] supports the hypothesis of a new "island of inversion" stretching from $N = 40$ to $N = 50$ and beyond. This would give

rise to coexistence of deformed and spherical configurations along its borders, analogous to those observed, e.g., at $N = 20$.

A consistent picture of shape coexistence in the $N \approx Z \approx 40$ nuclei has been obtained by combining high-resolution γ-ray and electron spectroscopy, with key results obtained in recent Coulomb-excitation and lifetime measurements. The results from those studies provided firm evidence for prolate and oblate shapes in ^{74,76}Kr, as well as indications for prolate-oblate shape coexistence in some of the Se and Ge isotopes. There is evidence for strong mixing of the configurations, and large $E0$ strengths were measured in this mass region, with $10^3 \times \rho^2(E0; 0_2^+ \rightarrow 0_1^+)$ values approaching 100 in the Kr isotopic chain. The $E0$ transition rates correlate with Z, with $10^3 \times \rho^2(E0; 0_2^+ \rightarrow 0_1^+)$ values of approximately 30 measured for the Se isotopes, while those for ^{70,72}Ge are close to 10. By combining the mixing angles deduced from level energies with the measured $E0$ strengths, the difference of deformation $\Delta\beta_2^2$ can be extracted, which is equal to 0.06–0.1 for ^{72,74,76}Kr, and 0.02–0.06 for ^{70,72}Ge. Another notable feature of this mass region is the importance of the triaxial degree of freedom. Structures interpreted as γ bands are observed at low excitation energy, and their band heads strongly mix with 2^+ states built on the shape-coexisting configurations. The systematics of the 2_1^+ excitation energies and $B(E2; 2_1^+ \rightarrow 0_1^+)$ values for $N = Z$ nuclei, presented in Fig. 62, show a rise in collectivity between ^{68}Se and ^{72}Kr followed by a more rapid increase between ^{72}Kr and ^{76}Sr. Beyond-mean-field calculations [563] predict a gradual transition along the $N = Z$ line from weakly deformed γ-soft ^{60}Zn and ^{64}Ge to well-deformed prolate ^{76}Sr, passing through moderately deformed triaxial shapes. The observed increase of deformation was thus suggested to be related to a gradual reduction of the importance of the triaxial degree of freedom, in connection with a decrease of the configuration mixing. Systematic measurements of spectroscopic quadrupole moments and quadrupole sum-rule invariants in these nuclei would provide a verification of such an interpretation.

In the $A \approx 100$ region, an impressive number of experimental results, contributing greatly towards understanding of shape coexistence, have been reported over the last decade. For these studies, state-of-the-art experimental devices and techniques were used, with the nuclei of interest produced via spontaneous fission or induced fission of actinides. The availability of intense radioactive beams for a variety of species has also increased dramatically, enabling measurements in this mass region that were not previously possible. Lifetime measurements of excited states and Coulomb-excitation experiments yielded rich sets of transitional and diagonal $E2$ matrix elements, enabling detailed comparisons with state-of-the-art theoretical models. In the Sr and Zr isotopes, where the spectroscopic data are most abundant, coexistence of nearly spherical normal-order states and deformed intruder states has been experimentally confirmed. Below $N = 60$, further studies are required to pin down the structure of low-lying 0^+ states. Multiple shape coexistence has been proposed in $N = 58$ ^{98}Zr and ^{96}Sr based on combined data on $E0$ and $E2$ transition strengths and neutron-transfer spectroscopic factors, but the recent conflicting measurements of lifetimes in ^{98}Zr highlight the difficulty of studies in this region. Interestingly, the mixing of wave functions between the ground state and the excited configurations in ^{96}Sr appears to be small, while the excited configurations seem to be strongly mixed. At $N = 60$, evidence of a nearly spherical excited configuration was reported in ^{98}Sr, while the data for ^{100}Zr are less detailed and therefore less conclusive. The sudden onset of deformation in the Zr isotopes has been reproduced for the first time, in terms of both level energies and transition probabilities, with the Monte-Carlo shell

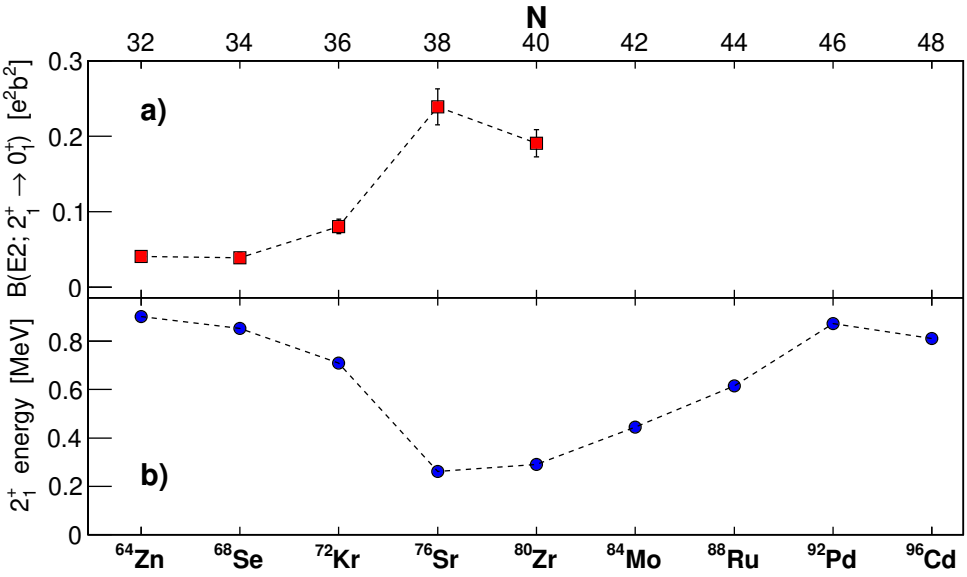

Figure 62: Systematics of the (a) $B(E2; 2_1^+ \rightarrow 0_1^+)$ values and (b) 2_1^+ excitation energies for $N = Z$ nuclei. Data are taken from the National Nuclear Data Center database [39] and Ref. [564].

model. These calculations suggested that multiple shape coexistence occurs in the Zr isotopes, with spherical, prolate, and oblate shapes present and their ordering evolving as a function of N. An experimental verification of this scenario is necessary. A multitude of low-lying deformed states with collective structures built on top of them were reported in odd-mass $A \approx 100$ nuclei from Kr to Ru, permitting the mapping of the different Nilsson orbitals before and after the shape transition at $N = 60$. While in odd-mass isotopes with $N < 60$ spherical ground states are observed to coexist with deformed bands, no evidence for low-lying spherical states beyond $N \geq 60$ has yet been obtained.

A compilation of quadrupole deformation parameters β_2 deduced from the measured spectroscopic quadrupole moments for odd-neutron Kr, Sr, Zr, Mo and Ru nuclei, and for odd-proton Rb, Y, Nb and Tc isotopes [231] is shown in Fig. 63. The β_2 systematics were extended by including the spectroscopic quadrupole moments of the 2_1^+ states in ^{94,96}Kr [243, 565], ^{96,98,100}Mo [23, 256, 320] and ^{102,104}Ru [39, 258], extracted from low-energy Coulomb-excitation experiments. They follow consistently the trend observed in laser spectroscopy.

Between $N = 50$ and 58, as the $d_{5/2}$ and $s_{1/2}$ orbitals are filled, the deformation is uniformly low ($\langle\beta_2\rangle \sim 0.1$) for all elements from Kr to Tc. The data resulting from both experimental approaches consistently point to an onset of deformation for nuclei from Rb to Nb when two neutrons are added to $N = 58$, i.e., the addition of neutrons to the $g_{7/2}$ orbital. Due to a large uncertainty, no conclusion can be drawn for ^{96}Kr, while the reduction of the quadrupole moment of the 2_1^+ state in ^{98}Sr has been tentatively attributed to its triaxial shape. Unfortunately, there is no experimental information for ^{102}Mo, but the β_2 deformation obtained for ^{104}Ru is considerably lower than the average $\langle\beta_2\rangle \sim 0.4$ for the $N \geq 60$ nuclei.

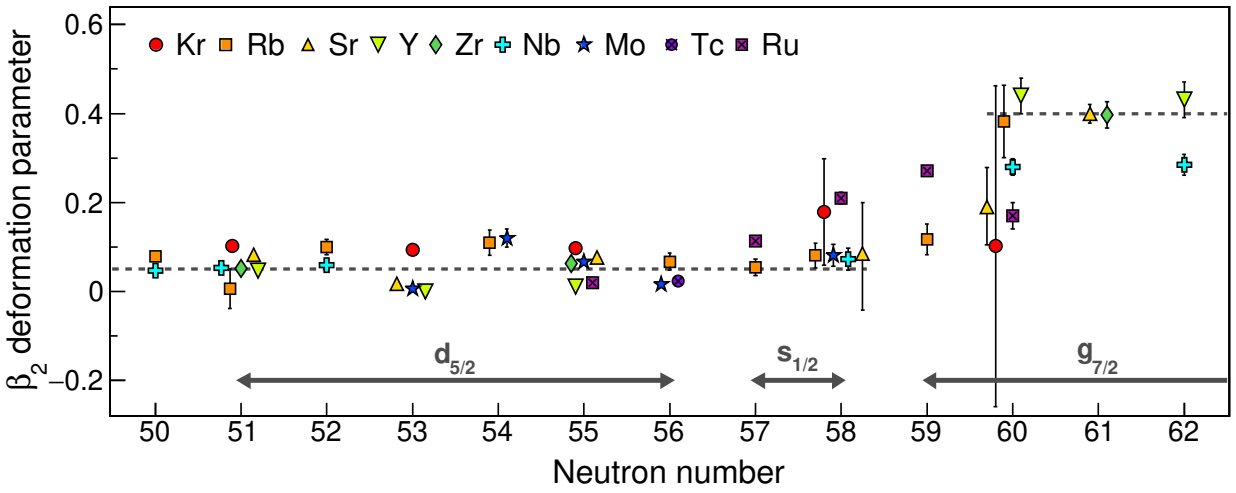

Figure 63: Quadrupole deformation parameter β_2 as a function of the neutron number in the Kr – Ru isotopic chains. The β_2 values are calculated, under assumption of axial symmetry, from the spectroscopic quadrupole moments of the ground states measured with laser spectroscopy, and from the diagonal $E2$ matrix elements of 2_1^+ states obtained via low-energy Coulomb excitation of even-even nuclei. Unfortunately, quadrupole moments for the ground states of ^{90,92}Rb ($I^\pi = 0^-$), $^{91,93,95-98}$Y ($I^\pi = 0^-$, $1/2^-$) and ^{99,101}Mo ($I^\pi = 1/2^+$) cannot be measured and those for $^{94-98,100}$Nb have not been measured yet. The spectroscopic quadrupole moments of the 2_1^+ states in ^{88,90,92}Kr, ^{90,92,94}Sr and $^{92,94,96-100}$Zr are currently unknown. In ^{94}Mo and ^{98,100}Ru the quadrupole moments of the 2_1^+ states were measured using the reorientation effect with light-ion beams and the analysis of Coulomb-excitation data yielded two alternative solutions, leading to different conclusions on the deformation. These data points are therefore not displayed. Shown schematically are the spherical orbitals at the Fermi level for neutrons. The dashed lines are to guide the eye. For clarity, some points are slightly offset on the horizontal axis.

The systematics presented in Fig. 63 highlights a particular behaviour at $N = 59$. While the onset of deformation is abrupt for all elements from $Z = 37$ to 41 when adding a pair of neutrons, at $N = 59$ a gradual evolution as function of the proton number emerges. The $^{96}_{37}$Rb$_{59}$ deformation is estimated as $\beta_2 \sim 0.12$, close to the mean value for $N \leq 58$ and well below that for $N \geq 60$. For $^{103}_{44}$Ru$_{59}$, the β_2 deformation approaches 0.3, which is slightly lower than the $N \geq 60$ systematics. Therefore, a more gradual shape change seems to take place when only one neutron is added to the $g_{7/2}$ orbital and when the number of protons in the pf shell increases. Unfortunately, measurements of the ground-state quadrupole moments in the $N = 59$ isotones between Sr and Tc are impossible due to their 1/2 spins.

Even if the ground-state shape transition at $N = 60$ seems to be well understood, there are open questions related to the structure of the non-yrast configurations. The rather smooth increase of deformation with the neutron number, observed for the neutron-rich Kr isotopes, requires further investigation, also in the context of possible shape coexistence, which has been predicted but never experimentally confirmed. Theoretical calculations indicate the importance of the triaxial degree of freedom in the Kr and Se isotopes, which also requires an experimental verification [566]. The experimental information on the neutron-rich Se isotopes around $N = 60$ is scarce due to their very exotic character, reflected in production rates at radioactive beam facilities, making

experiments using them currently prohibitive. With the first indications of shape coexistence in the very neutron-rich Ge isotopes at $N = 50$, the possible bridge between these two regions of deformation and shape coexistence should be addressed in the future.

A considerable number of new results in the $Z \approx 50$ region have been obtained over the past decade resulting in a substantial re-interpretation of the structure of many nuclei, foremost that of the Cd isotopes. While the shape-coexisting $\pi(2p-2h)$ intruder excitations have been known for some time, recent results [261, 363] have suggested the presence of multiple shape coexistence with the appearance of triaxial, oblate, and prolate structures. The key spectroscopic data for the 0_2^+ and 0_3^+ states were presented in Figs. 36 (Cd), 42 (Sn), 44 (Te), and 46 (Pd). Generally, the 0_2^+ levels have enhanced decays to the 2_1^+ states, and, where measured, are populated strongly in the (^{3}He,n) reaction. The 0_3^+ levels have enhanced decays to the 2_2^+ levels, and weak $E2$ transition strength to the 2_1^+ states. As outlined in Sect. 3.5.1, in the Cd isotopes it was suggested that the 0_2^+ and 0_3^+ states had different shapes. The high degree of similarity of the decay properties of the 0_2^+ states in Pd through Te is suggestive of a similar underlying configuration of enhanced deformation based on proton excitations. In Cd, Pd, and Te, the 0_3^+ states generally have enhanced decays to the 2_2^+ states, labelled as the head of a "γ" band, and a very weak decay to the 2_1^+ state, also suggesting a structural similarity. If multiple shape coexistence is firmly established in the Cd isotopes, these similarities of the decay patterns in other nuclei in the region provide strong motivation to explore their shapes as well through, for example, detailed Coulomb-excitation studies.

The $Z \approx 64$, $N \approx 90$ region continues to present a challenge to understand its structure, but also an opportunity to explore exotic pairing degrees of freedom. While it is clear that there is a rapid change in the shape progressing across $N = 90$, the question on the nature of the excited states remains open. The traditional interpretation involving shape-coexisting 0_3^+ states and low-lying 0_2^+ β-vibrational states has largely been refuted. Recent work has focused on pairing isomers and the important role of the $\nu 11/2[505]$ Nilsson orbital in both the 0_2^+, often referred to as the "second vacuum", and 0_3^+ states. The apparent absence of the $\nu 11/2[505] \otimes 0_2^+$ coupling in the adjacent odd-mass isotopes is consistent with this interpretation, and this observation emphasizes the importance of configuration-dependent pairing properties that are often overlooked.

The body of evidence concerning shape coexistence at and near $Z = 82$ seems the most extensive in the entire nuclear chart. Although this region is centered on the neutron mid-shell at $N = 104$, located far from the line of β stability, the neutron-deficient character of these nuclei allowed for efficient use of fusion-evaporation reactions to study their properties. Unique information on the microscopic character of low-lying 0^+ states could also be obtained from α-decay studies. In even- and odd-mass nuclei from Pt ($Z = 78$) to Po ($Z = 84$), normal-order structures were observed to be crossed at low excitation energies by a more deformed configuration dominated by $2p-2h$ excitations across the $Z = 82$ shell gap. As evidenced by the observed perturbation of energy levels, α-decay hindrance factors and the measured $E2$ and $E0$ transition strengths, the two coexisting structures undergo strong mixing. The systematics of the lowest intruder states in Pt, Au, Hg, Tl, Pb, Bi and Po isotopes, presented in Fig. 64, shows that while they display similar parabolic patterns, the exact minima shift from one isotopic chain to another, and the shape of the parabola also changes. This suggests that the microscopic configurations of these intruding structures, while similar, are not identical, involving different orbitals and/or a contribution from excitation of several pairs across the $Z = 82$ shell gap. This is supported, for example, by the

observation that the g factor of the $9/2^-$ state in ^{187}Au is different than those measured for its counterparts in $N = 108$ Tl and Bi isotones, as was shown in Fig. 59. While convincing *circumstantial* evidence is available for the existence of multiple shapes in this mass region, few examples of direct evidence have been provided to date, such as that obtained from measurements of quadrupole moments or invariant sum-rules from Coulomb excitation. The Hg isotopes provide some of the best data in this regard, but there still remains considerable uncertainty, as the discussion on the extraction of the mixing amplitudes in Sec. 3.7.1 indicates.

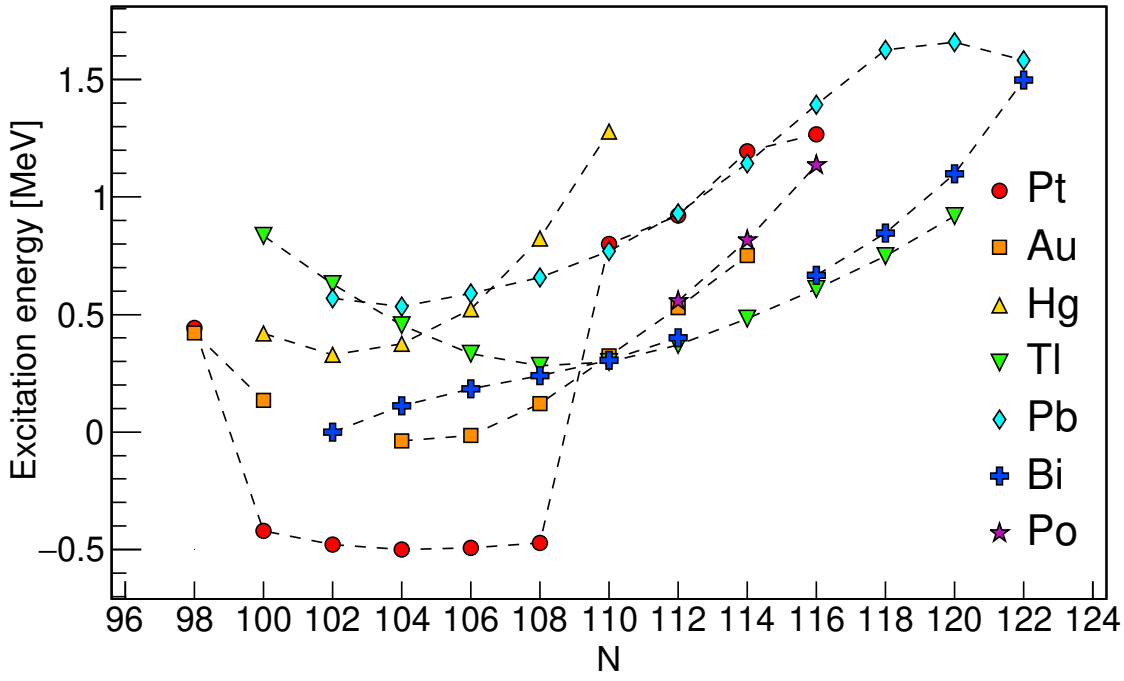

Figure 64: Systematics of excitation energies of lowest intruder structures in Pt (Z=78), Au (Z = 79), Hg (Z = 80), Tl (Z = 81), Pb (Z = 82), Bi (Z=83) and Po (Z= 84) isotopes with even neutron number. The energies of $\pi h_{9/2}$ structures in Au isotopes are given relative to the $\pi(s_{1/2})^{-1}$ states, and those of intruder 0^+ states in Pt isotopes relative to the normal-order 0^+ states.

A thread that is beginning to emerge in the field, as highlighted above, is that of multiple shape coexistence. While there were suggestions of this for decades, the famous example of ^{186}Pb was published only 21 years ago. Within the past several years there have been many additional candidates suggested for nuclei possessing multiple shapes. These candidates appear throughout the nuclear chart, to name as examples the Si, Ca, Ni, Zr, Cd, Hg, Pb and Au isotopes, and arise from a combination of experimental observations *and* theoretical calculations that have reached a high-degree of accuracy in their predictions. Some of the best candidates for multiple shapes are stable, and thus should be amenable for detailed studies. Future priority measurements should include detailed Coulomb-excitation studies to firmly establish the shapes through the use of sum-rule quantities, such as $\langle Q^2 \rangle$ and $\langle \cos 3\delta \rangle$. Experiments that probe the microscopic composition of the states,

single-nucleon and especially multi-nucleon transfer, should be pursued. A further key ingredient is the combined approach for structure studies, where coordinated measurements are undertaken that provide required data for precise and reliable level schemes. Highly-sensitive β-decay measurements, for example, can be used to observe very weak, but important in terms of transition probability, decay branches for non-yrast levels. Conversion-electron measurements to extract $E0$ branches for $I \rightarrow I$ transitions rely on accurate and precise intensities for the competing $M1$ and $E2$ transitions, and the determination of $\rho^2(E0)$ branches requires level lifetime measurements. These, in turn, provide crucial inputs and stringent constraints to analyses of Coulomb-excitation data.

The shape-coexistence phenomenon in atomic nuclei is one of the most impressive features of the field of nuclear structure, and, in a larger perspective, of a finite many-body quantum system. It is the manifestation of diverse quantum configurations having different spatial organisation competing for the ground-state energy. As stated in the introduction, the presence of shape coexistence permits the study of the contributions to the correlation energy within the same nucleus from different sources, in this case that associated with the quadrupole shape degree of freedom. The correlation energies arise from multiple sources, but chief among them are the pairing energies and the proton-neutron residual quadrupole interaction. Over the last decade, while we have gained much knowledge on shape-coexisting structures, many questions remain, and new regions and opportunities for exploration have opened.

Acknowlegdements

This work was supported in part by the Natural Sciences and Engineering Research Council (NSERC), Canada. MZ acknowledges discussions with K. Wrzosek-Lipska within the framework of the Polish (COPIN) – French (CNRS) International Research Project (IRP): The Collaboration COPIN-GANIL on physics of exotic nuclei – COPIGAL.

References

[1] H. Morinaga, Phys. Rev. **101**, 254 (1956).
[2] K. Heyde and J.L. Wood, Rev. Mod. Phys. **83**, 1467 (2011). doi.org/10.1103/RevModPhys.83.1467
[3] K. Heyde, P. Van Isacker, M. Waroquier, J.L. Wood, and R.A. Meyer, Phys. Rep. **102**, 291 (1983).
[4] T. Duguet, M. Bender, P. Bonche, and P.-H. Heenen, Phys. Lett. **B559**, 201 (2003).
[5] A. Poves, J. Phys. G: Nucl. Part. Phys. **43**, 020401 (2016).
[6] J.L. Wood, K. Heyde, W. Nazarewicz, M. Huyse, and P. Van Duppen, Phys. Rep. **215**, 101 (1992).
[7] N. Tsunoda, T. Otsuka, K. Takayanagi, N. Shimizu, T. Suzuki, Y. Utsuno, S. Yoshida, and H. Ueno, Nature 587, 66 (2020). doi:10.1038/s41586-020-2848-x
[8] J.L. Wood and K. Heyde, J. Phys. G: Nucl. Part. Phys. **43**, 020402 (2016).
[9] L.M. Robledo, T.R. Rodriguez, and R.R. Rodriguez-Guzmán, J. Phys. G: Nucl. Part. Phys. 46, 013001 (2018).
[10] T. Otsuka, Y. Tsunoda, T. Abe, N. Shimizu, and P. Van Duppen, Phys. Rev. Lett. 123, 222502 (2019).
[11] T. Otsuka, A. Gade, O. Sorlin, T. Suzuki, and Y. Utsuno, Rev. Mod. Phys. 92, 015002 (2020)
[12] K. Kumar, Phys. Rev. Lett. 28, 249 (1972).
[13] D. Cline, Ann. Rev. Nucl. Part. Sci. **36**, 683 (1986).
[14] A. Bohr and B.R. Mottelson, *Nuclear Structure*, Vols. I & II, World Scientific, Singapore (1998).
[15] J.M. Eisenberg and W. Greiner, *Nuclear Theory: Nuclear Models*, North-Holland Physics Publishing, Amsterdam, Netherlands, (1987).

[16] H.T. Motz, Phys. Rev. **104**, 1353 (1956).
[17] B.L. Cohen and R.E. Price, Phys. Rev. **118**, 1582 (1960).
[18] W. Urban, T. Rząca-Urban, J. Wiśniewski, I. Ahmad, A.G. Smith, and G.S. Simpson, Phys. Rev. C **99**, 064325 (2019).
[19] K. Heyde, J. Jolie, J. Moreau, J. Ryckebusch, M. Waroquier, P. Van Duppen, M. Huyse, J.L. Wood, Nucl. Phys. A 466, 189 (1987).
[20] G. Neyens, Rep. Prog. Phys. 66, 633 (2003).
[21] B. Castel and I.S. Towner, *Modern Theories of Nuclear Moments*, Oxford Studies in Nuclear Physics, Clarendon Press, 1990.
[22] W. Andrejtscheff and P. Petkov, Phys. Lett. B 329, 1 (1994).
[23] K. Wrzosek-Lipska, L. Próchniak, M. Zielińska, J. Srebrny, K. Hadyńska-Klęk, J. Iwanicki, M. Kisieliński, M. Kowalczyk, P.J. Napiorkowski, D. Piętak, and T. Czosnyka, Phys. Rev. C 86, 064305 (2012). doi:10.1103/PhysRevC.86.064305
[24] J. Srebrny and D. Cline, Int. J. Mod. Phys. E 20, 422 (2011).
[25] J.L. Wood, E.F. Zganjar, C. de Coster, and K. Heyde, Nucl. Phys. **A 651**, 323 (1999).
[26] J.P. Davidson, *Rev. Mod. Phys.* **37**, 105 (1965).
[27] B.A. Brown, A.B. Garnsworthy, T. Kibédi, and A.E. Stuchbery, Phys. Rev. C **95**, 011301(R) (2017).
[28] W. von Oertzen, M. Freer, and Y. Kanada-En'yo, Phys. Rep. **432**, 43 (2006).
[29] M. Freer, Rep. Prog. Phys. **70** 2149 (2007).
[30] M. Freer, H. Horiuchi, Y. Kanada-En'yo, D. Lee, and U.-G. Meißner, Rev. Mod. Phys. **90**, 035004 (2018).
[31] M. Itoh, H. Akimune, M. Fujiwara, U. Garg, H. Hashimoto, T. Kawabata, K. Kawase, S. Kishi, T. Murakami, K. Nakanishi, Y. Nakatsugawa, B.K. Nayak, S. Okumura, H. Sakaguchi, H. Takeda, S. Terashima, M. Uchida, Y. Yasuda, M. Yosoi, and J. Zenihiro, Nucl. Phys. **A738**, 268 (2004).
[32] M. Itoh, H. Akimune, M. Fujiwara, U. Garg, N. Hashimoto, T. Kawabata, K. Kawase, S. Kishi, T. Murakami, K. Nakanishi, Y. Nakatsugawa, B. K. Nayak, S. Okumura, H. Sakaguchi, H. Takeda, S. Terashima, M. Uchida, Y. Yasuda, M. Yosoi, and J. Zenihiro, Phys. Rev. C **84**, 054308 (2011).
[33] M. Freer, H. Fujita, Z. Buthelezi, J. Carter, R.W. Fearick, S.V. Förtsch, R. Neveling, S.M. Perez, P. Papka, F.D. Smit, J.A. Swartz, and I. Usman, Phys. Rev. C **80**, 041303(R) (2009).
[34] W.R. Zimmerman, N.E. Destefano, M. Freer, M. Gai, and F.D. Smit, Phys. Rev. C84, 027304(R) (2011).
[35] W.R. Zimmerman, M.W. Ahmed, B. Bromberger, S.C. Stave, A. Breskin, V. Dangendorf, Th. Delbar, M. Gai, S.S. Henshaw, J.M. Mueller, C. Sun, K. Tittelmeier, H.R. Weller, and Y.K. Wu, Phys. Rev. Lett. **110**, 152502 (2013).
[36] D.J. Marín-Lámbarri, R. Bijker, M. Freer, M. Gai, Tz. Kokalova, D.J. Parker, and C. Wheldon, Phys. Rev. Lett. **113**, 012502 (2014).
[37] Y. Kanada En'yo, Prog. Theor. Phys. **117**, 655 (2007).
[38] E.K. Warburton, C.J. Lister, D.E. Alburger, and J.W. Olness, Phys. Rev. C **23**, 1242 (1981).
[39] https://www.nndc.bnl.gov/ensdf/
[40] J.T.H. Dowie, T. Kibédi, D.G. Jenkins, A.E. Stuchbery, A. Akber, H.A. Alshammari, N. Aoi, A. Avaa, L.J. Bignell, M.V. Chisapi, B.J. Coombes, T.K. Eriksen, M.S.M. Gerathy, T.J. Gray, T.H. Hoang, E. Ideguchi, P. Jones, M. Kumar Raju, G.J. Lane, B.P. McCormick, L.J. McKie, A.J. Mitchell, N.J. Spinks, B.P.E. Tee, Phys. Lett. **B811**, 135855 (2020).
[41] D.G. Jenkins, C.J. Lister, M.P. Carpenter, P. Chowdury, N.J. Hammond, R.V.F. Janssens, T.L. Khoo, T. Lauritsen, D. Seweryniak, T. Davinson, P.J. Woods, A. Jokinen, H. Penttila, F. Haas, and S. Courtin, Phys. Rev. C **86**, 064308 (2012). doi.org/10.1103/PhysRevC.86.064308
[42] O. Häusser, T.K. Alexander, D. Pelte, B.W. Hooton, and H.C. Evans, Phys. Rev. Lett. **23**, 320 (1969).
[43] F. Glatz, P. Betz, J. Siefert, F. Heidinger, and H. Röpke, Phys. Rev. Lett. **46**, 1559 (1981).
[44] S. Kubono, K. Morita, M.H. Tanaka, A. Sakaguchi, M. Sugitani, and S. Kato, Phys. Rev. C **33**, 1524 (1986).
[45] C. Thibault, R. Klapisch, C. Rigaud, A.M. Poskanzer, R. Prieels, L. Lessard, and W. Reisdorf, Phys. Rev. C 12, 644 (1975).
[46] C. Détraz, M. Langevin, M.C. Goffri-Kouassi, D. Guillemaud, M. Epherre, G. Audi, C. Thibault, and F. Touchard, Nucl. Phys. A 394, 378 (1983).

[47] G. Huber, F. Touchard, S. Büttgenbach, C. Thibault, R. Klapisch, H.T. Duong, S. Liberman, J. Pinard, J.L. Vialle, P. Juncar, and P. Jacquinot, Phys. Rev. C 18, 2342 (1978).
[48] C. Détraz, D. Guillemaud, G. Huber, R. Klapisch, M. Langevin, F. Naulin, C. Thibault, L.C. Carraz, and F. Touchard, Phys. Rev. C 19, 164 (1979).
[49] T. Motobayashi, Y. Ikeda, Y. Ando, K. Ieki, M. Inoue, N. Iwasa, T. Kikuchi, M. Kurokawa, S. Moriya, S. Ogawa, H. Murakami, S. Shimoura, Y. Yanagisawa, T. Nakamura, Y. Watanabe, M. Ishihara, T. Teranishi, H. Okuno, and R.F. Casten, Phys. Lett. B 346, 9 (1995).
[50] B.V. Pritychenko, T. Glasmacher, P.D. Cottle, M. Fauerbach, R.W. Ibbotson, K.W. Kemper, V. Maddalena, A. Navin, R. Ronningen, A. Sakharuka, H. Scheit, and V.G. Zelevinsky, Phys. Lett. B 461, 322 (1999).
[51] H. Iwasaki, T. Motobayashi, H. Sakurai, K. Yoneda, T. Gomi, N. Aoi, N. Fukuda, Zs. Fülöp, U. Futakami, Z. Gacsi *et al.*, Phys. Lett. B 522, 227 (2001).
[52] V. Chisté, A. Gillibert, A. Lépine-Szily, N. Alamanos, F. Auger, J. Barrette, F. Braga, M.D. Cortina-Gil, Z. Dlouhy, V. Lapoux *et al.*, Phys. Lett. B 514, 233 (2001).
[53] J.A. Church, C.M. Campbell, D.-C. Dinca, J. Enders, A. Gade, T. Glasmacher, Z. Hu, R.V.F. Janssens, W.F. Mueller, H. Olliver, B.C. Perry, L.A. Riley, and K.L. Yurkewicz, Phys. Rev. C 72, 054320 (2005).
[54] K. Li, Y. Ye, T. Motobayashi, H. Scheit, P. Doornenbal, S. Takeuchi, N. Aoi, M. Matsushita, E. Takeshita, D. Pang, and H. Sakurai, Phys. Rev. C 92, 014608 (2015).
[55] H. Mach, L.M. Fraile, O. Tengblad, R. Boutami, C. Jollet, W.A. Plóciennik, D.T. Yordanov, M. Stanoiu, M.J.G. Borge, P.A. Butler *et al.*, Eur. Phys. J. A 25, 105 (2005).
[56] G. Neyens, J. Phys. G: Nucl. Part. Phys. 43, 024007 (2016).
[57] S. Takeuchi, N. Aoi, T. Motobayashi, S. Ota, E. Takeshita, H. Suzuki, H. Baba, T. Fukui, Y. Hashimoto, K. Ieki *et al.*, Phys. Rev. C 79, 054319 (2009).
[58] H.L. Crawford, P. Fallon, A.O. Macchiavelli, A. Poves, V.M. Bader, D. Bazin, M. Bowry, C.M. Campbell, M.P. Carpenter, R.M. Clark *et al.*, Phys. Rev. C 93, 031303(R) (2016).
[59] K. Wimmer, T. Kröll, R. Kruc̈ken, V. Bildstein, R. Gernhäuser, B. Bastin, N. Bree, J. Diriken, P. Van Duppen, M. Huyse *et al.*, Phys. Rev. Lett. 105, 252501 (2010).
[60] D. Bazin, B.A. Brown, C.M. Campbell, J.A. Church, D.C. Dinca, J. Enders, A. Gade, T. Glasmacher, P.G. Hansen, W.F. Mueller, H. Olliver, B.C. Perry, B.M. Sherrill, J.R. Terry, and J.A. Tostevin, Phys. Rev. Lett. 91, 012501 (2003).
[61] R. Elder, H. Iwasaki, J. Ash, D. Bazin, P.C. Bender, T. Braunroth, B.A. Brown, C.M. Campbell, H.L. Crawford, B. Elman *et al.*, Phys. Rev. C 100, 041301(R) (2019).
[62] O. Niedermeier, H. Scheit, V. Bildstein, H. Boie, J. Fitting, R. von Hahn, F. Köck, M. Lauer, U.K. Pal, H. Podlech *et al.*, Phys. Rev. Lett. 94 172501 (2005).
[63] M.Shamsuzzoha Basunia, Nucl. Data Sheets 111, 2332 (2010).
[64] C. Ouellet, B. Singh, Nucl. Data Sheets 112, 2199 (2012).
[65] A.N. Deacon, J.F. Smith, S.J. Freeman, R.V.F. Janssens, M.P. Carpenter, B. Hadinia, C.R. Hoffman, B.P. Kay, T. Lauritsen, C.J. Lister, D. O'Donnell, J. Ollier, T. Otsuka, D. Seweryniak, K.-M. Spohr, D. Steppenbeck, S.L. Tabor, V. Tripathi, Y. Utsuno, P.T. Wady, and S. Zhu, Phys. Rev. C 82, 034305 (2010).
[66] W. Schwerdtfeger, P.G. Thirolf, K. Wimmer, D. Habs, H. Mach, T.R. Rodriguez, V. Bildstein, J.L. Egido, L.M. Fraile, R. Gernhäuser *et al.*, Phys. Rev. Lett. 103, 012501 (2009).
[67] H. Nishibata, K. Tajiri, T. Shimoda, A. Odahara, S. Morimoto, S. Kanaya, A. Yagi, H. Kanaoka, M.R. Pearson, C.D.P. Levy, M. Kimura, N. Tsunoda, and T. Otsuka, Phys. Rev. C 102, 054327 (2020).
[68] A.O. Macchiavelli, H.L. Crawford, C.M. Campbell, R.M. Clark, M. Cromaz, P. Fallon, M.D. Jones, I.Y. Lee, M. Salathe, B.A. Brown, and A. Poves, Phys. Rev. C 94, 051303(R) (2016).
[69] A.O. Macchiavelli and H.L. Crawford, Phys. Scr. 92, 064001 (2017).
[70] J.R. Terry, B.A. Brown, C.M. Campbell, J.M. Cook, A.D. Davies, D.-C. Dinca, A. Gade, T. Glasmacher, P.G. Hansen, B.M. Sherrill, H. Zwahlen, D. Bazin, K. Yoneda, J.A. Tostevin, T. Otsuka, Y. Utsuno, and B. Pritychenko, Phys. Rev. C 77, 014316 (2008).
[71] B. Fernandez-Dominguez, B. Pietras, W.N. Catford, N.A. Orr, M. Petri, M. Chartier, S. Paschalis, N. Patterson, J.S. Thomas, M. Caamaño *et al.*, Phys. Lett. B 779, 124 (2018).
[72] G. Neyens, M. Kowalska, D. Yordanov, K. Blaum, P. Himpe, P. Lievens, S. Mallion, R. Neugart, N. Vermeulen,

Y. Utsuno, and T. Otsuka, Phys. Rev. Lett. 94, 022501 (2005).
[73] D. Miller, P. Adrich, B.A. Brown, V. Moeller, A. Ratkiewicz, W. Rother, K. Starosta, J.A. Tostevin, C. Vaman, and P. Voss, Phys. Rev. C 79, 054306 (2009).
[74] H. Nishibata, T. Shimoda, A. Odahara, S. Morimoto, S. Kanaya, A. Yagi, H. Kanaoka, M.R. Pearson, C.D.P. Levy, and M. Kimura, Phys. Lett. B 767, 81 (2017).
[75] H. Nishibata, S. Kanaya, T. Shimoda, A. Odahara, S. Morimoto, A. Yagi, H. Kanaoka, M.R. Pearson, C.D.P. Levy, M. Kimura, N. Tsunoda, and T. Otsuka, Phys. Rev. C 99, 024322 (2019).
[76] M. Seidlitz, D. Mücher, P. Reiter, V. Bildstein, A. Blazhev, N. Bree, B. Bruyneel, J. Cederkäll, E. Clément, T. Davinson *et al.*, Phys. Lett. B 700, 181 (2011)
[77] P. Himpe, G. Neyens, D. Balabanski, G. Bélier, J. Daugas, F. de Oliveira Santos, M.D. Rydt, K. Flanagan, I. Matea, P. Morel *et al.*, Phys. Lett. B 658, 2003 (2008).
[78] Z.Y. Xu, H. Heylen, K. Asahi, F. Boulay, J.M. Daugas, R.P. de Groote, W. Gins, O. Kamalou, A. Koszorús, M. Lykiardopoulou, T.J. Mertzimekis, G. Neyens, H. Nishibata, T. Otsuka, R. Orset, A. Poves, T. Sato, C. Stodel, J.C. Thomas, N. Tsunoda, Y. Utsuno, M. Vandebrouck, and X.F. Yang, Phys. Lett. B 782, 619 (2018).
[79] R. Lică, F. Rotaru, M.J.G. Borge, S. Grévy, F. Negoiţă, A. Poves, O. Sorlin, A.N. Andreyev, R. Borcea, C. Costache *et al.*, Phys. Rev. C 95, 021301(R) (2017).
[80] R.W. Ibbotson, T. Glasmacher, B.A. Brown, L. Chen, M.J. Chromik, P.D. Cottle, M. Fauerbach, K.W. Kemper, D.J. Morrissey, H. Scheit, and M. Thoennessen, Phys. Rev. Lett. 80, 2081 (1998).
[81] L.K. Fifield, C.L. Woods, R.A. Bark, P.V. Drumm, and M.A.C. Hotchkis, Nucl. Phys. A 440, 531 (1985).
[82] R.G.T. Zegers, R. Meharchand, Y. Shimbara, Sam M. Austin, D. Bazin, B.A. Brown, C.Aa. Diget, A. Gade, C.J. Guess, M. Hausmann *et al.*, Phys. Rev. Lett. 104, 212504 (2010).
[83] R. Lică, F. Rotaru, M.J.G. Borge, S. Grévy, F. Negoiţă, A. Poves, O. Sorlin, A.N. Andreyev, R. Borcea *et al.*, Phys. Rev. C 100, 034306 (2019).
[84] F. Rotaru, F. Negoita, S. Grévy, J. Mrazek, S. Lukyanov, F. Nowacki, A. Poves, O. Sorlin, C. Borcea, R. Borcea *et al.*, Phys. Rev. Lett. 109, 092503 (2012).
[85] R. Han, X.Q. Li, W.G. Jiang, Z.H. Li, H. Hua, S.Q. Zhang, C.X. Yuan, D.X. Jiang, Y.L. Ye, J. Li *et al.*, Phys. Lett. B 772, 529 (2017).
[86] M. Petri, P. Fallon, A.O. Macchiavelli, S. Heil, E. Rodriguez-Vieitez, D. Bazin, C.M. Campbell, R.M. Clark, M. Cromaz, A. Gade, T. Glasmacher, I.Y. Lee, S. Malbrunot-Ettenauer, S. Paschalis, A. Ratkiewicz, J.R. Terry, D. Weisshaar, and M. Wiedeking, Phys. Lett. B 748, 173 (2015).
[87] R. Middleton, J.D. Garrett and H.T. Fortune, Phys. Lett. **39B**, 339 (1972).
[88] C. Ellegaard, J.R. Lien, O. Nathan, G. Sletten, F. Ingebretsen, E. Osnes, P.O. Tjøm, O. Hansen and R. Stock, Phys. Lett. **40B**, 641 (1972).
[89] J.J. Simpson, W.R. Dixon, and R.S. Storey, Phys. Rev. Lett. **31**, 947 (1973).
[90] E.R. Flynn, O. Hansen, R.F. Casten, J.D. Garrett and F. Ajunberg-Selove, Nucl. Phys. A 246, 117 (1975).
[91] E. Ideguchi, D.G. Sarantites, W. Reviol, A.V. Afanasjev, M. Devlin, C. Baktash, R.V.F. Janssens, D. Rudolph, A. Axelsson, M.P. Carpenter *et al.*, Phys. Rev. Lett. 87, 222501 (2001).
[92] C.E. Svensson, A.O. Macchiavelli, A. Juodagalvis, A. Poves, I. Ragnarsson, S. Aberg, D.E. Appelbe, R.A.E. Austin, C. Baktash, G.C. Ball *et al.*, Phys. Rev. Lett. 85, 2693 (2000).
[93] R.A.E. Austin, *Lifetimes of Superdeformed States in* ^{38}Ar, Ph.D. thesis, McMaster University, Hamilton, Ontario, Canada (2004).
[94] E. Ideguchi, S. Ota, T. Morikawa, M. Oshima, M. Koizumi, Y. Toh, A. Kimura, H. Harada, K. Furutaka, S. Nakamura, *et al.*, Phys. Lett. B 686, 18 (2010).
[95] C.D. O'Leary, M.A. Bentley, B.A. Brown, D.E. Appelbe, R.A. Bark, D.M. Cullen, S. Ertürk, A. Maj, and A.C. Merchant, Phys. Rev. C 61, 064314 (2000).
[96] Abhijit Bisoi, M. Saha Sarkar, S. Sarkar, S. Ray, M. Roy Basu, Debasmita Kanjilal, Somnath Nag, K. Selvakumar, A. Goswami, N. Madhavan, *etal.*, Phys. Rev. C 88, 034303 (2013).
[97] K. Hadyńska-Kl̨ek, P.J. Napiorkowski, M. Zielińska, J. Srebrny, A. Maj, F. Azaiez, J.J. Valiente Dobon, M. Kicińska-Habior, F. Nowacki, H. Naidja, *et al.*, Phys. Rev. Lett. 117, 062501 (2016).
[98] C.J. Chiara, E. Ideguchi, M. Devlin, D.R. LaFosse, F. Lerma, W. Reviol, S.K. Ryu, D.G. Sarantites C. Baktash, A. Galindo-Uribarri *et al.*, Phys. Rev. C 67, 041303(R) (2003).

[99] S. Raman, C.W Nestor and P. Tikkanen, At. Data Nucl. Data Tables **78**, 1 (2001).
[100] S. Schielke, D. Hohn, K.-H. Speidel, O. Kenn, J. Leske, N. Gemein, M. Offer, J. Gerber, P. Maier-Komor, O. Zell *et al.*, Phys. Lett. B 571, 29 (2003).
[101] H.D. Gräf, H. Feldmeier, P. Manakos, A. Richter, E. Spamer, D. Strottman, Nucl. Phys. A 295, 319 (1978).
[102] T. Kibédi, R.H. Spear, At. Data Nucl. Data Tables 89, 77 (2005).
[103] K.-H. Speidel, S. Schielke, J. Leske, J. Gerber, P. Maier-Komor, S.J.Q. Robinson, Y.Y. Sharon and L. Zamick, Phys. Lett. B 632, 207 (2006).
[104] E.A. Stefanova, N. Benczer-Koller, G.J. Kumbartzki, Y.Y. Sharon, L. Zamick, S.J.Q. Robinson, L. Bernstein, J.R. Cooper, D. Judson, M.J. Taylor *et al.*, Phys. Rev. C 72 014309 (2005).
[105] S. Schielke, K.-H. Speidel, O. Kenn, J. Leske, N. Gemein, M. Offer, Y.Y. Sharon, L. Zamick, J. Gerber, and P. Maier-Komor, Phys. Lett. B 567, 153 (2003).
[106] K. Arnswald, T. Braunroth, M. Seidlitz, L. Coraggio, P. Reiter, B. Birkenbach, A. Blazhev, A. Dewald, C. Fransen, B. Fu *et al.*, Phys. Lett. B 772, 599 (2017).
[107] K. Hadyńska-Klęk, P.J. Napiorkowski, M. Zielińska, J. Srebrny, A. Maj, F. Azaiez, J.J. Valiente Dobon, M. Kicińska-Habior, F. Nowacki, H. Naidja, *et al.*, Phys. Rev. C 97, 024326 (2018).
[108] M. Avgoulea, Yu.P. Gangrsky, K.P. Marinova, S.G. Zemlyanoi, S. Fritzsche, D. Iablonskyi, C. Barbieri, E.C. Simpson, P.D. Stevenson, J. Billowes *et al.*, J. Phys. G 38, 025104 (2011).
[109] S. Grévy, F. Negoita, I. Stefan, N.L. Achouri, J.C. Angelique, B. Bastin, R. Borcea, A. Buta, J.M. Daugas, F. De Oliveira *et al.*, Eur. Phys. J. A 25, 111 (2005).
[110] C. Force, S. Grévy, L. Gaudefroy, O. Sorlin, L. Caceres, F. Rotaru, J. Mrazek, N.L. Achouri, J.C. Angelique, F. Azaiez *et al.*, Phys. Rev. Lett. 105, 102501 (2010).
[111] L. Caceres, D. Sohler, S. Grévy, O. Sorlin, Zs. Dombradi, B. Bastin, N.L. Achouri, J.C. Angelique, F. Azaiez, D. Baiborodin, *et al.*, Phys. Rev. C 85, 024311 (2012).
[112] D. Santiago-Gonzalez, I. Wiedenhöver, V. Abramkina, M.L. Avila, T. Baugher, D. Bazin, B.A. Brown, P.D. Cottle, A. Gade, T. Glasmacher *et al.*, Phys. Rev. C 83, 061305(R) (2011).
[113] J.J. Parker IV, I. Wiedenhöver, P.D. Cottle, J. Baker, D. McPherson, M.A. Riley, D. Santiago-Gonzalez, A. Volya, V.M. Bader *et al.*, Phys. Rev. Lett. 118, 052501 (2017)
[114] T. Glasmacher, B.A. Brown, M.J. Chromik, P.D. Cottle, M. Fauerbach, R.W. Ibbotson, K.W. Kemper, D.J. Morrissey, H. Scheit, D.W. Sklenicka, and M. Steiner, Phys. Lett. B 395, 163 (1997).
[115] L. Gaudefroy, J.M. Daugas, M. Hass, S. Grévy, Ch. Stodel, J.C. Thomas, L. Perrot, M. Girod, B. Rossé, J.C. Angelique *et al.*, Phys. Rev. Lett. 102, 092501 (2009).
[116] F. Sarazin, H. Savajols, W. Mittig, F. Nowacki, N.A. Orr, Z. Ren, P. Roussel-Chomaz, G. Auger, D. Baiborodin, A.V. Belozyorov *et al.*, Phys. Rev. Lett. 84, 5062 (2000).
[117] S. Momiyama, K. Wimmer, D. Bazin, J. Belarge, P. Bender, B. Elman, A. Gade, K.W. Kemper, N. Kitamura, B. Longfellow *et al.*, Phys. Rev. C 102, 034325 (2020).
[118] R. Chevrier, J.M. Daugas, L. Gaudefroy, Y. Ichikawa, H. Ueno, M. Hass, H. Haas, S. Cottenier, N. Aoi, K. Asahi *et al.*, Phys. Rev. Lett. 108, 162501 (2012).
[119] R.W. Ibbotson, T. Glasmacher, P.F. Mantica, and H. Scheit, Phys. Rev. C 59, 642 (1999).
[120] L.A. Riley, P. Adrich, T.R. Baugher, D. Bazin, B.A. Brown, J.M. Cook, P.D. Cottle, C.Aa. Diget, A. Gade, D.A. Garland *et al.*, Phys. Rev. C 80, 037305 (2009).
[121] T. Mijatović, N. Kobayashi, H. Iwasaki, D. Bazin, J. Belarge, P.C. Bender, B.A. Brown, A. Dewald, R. Elder, B. Elman *et al.*, Phys. Rev. Lett. 121, 012501 (2018).
[122] B. Longfellow, D. Weisshaar, A. Gade, B.A. Brown, D. Bazin, K.W. Brown, B. Elman, J. Pereira, D. Rhodes, and M. Spieker, Phys. Rev. Lett. 125, 232501 (2020).
[123] A. Gade, B.A. Brown, J.A. Tostevin, D. Bazin, P.C. Bender, C.M. Campbell, H.L. Crawford, B. Elman, K.W. Kemper, B. Longfellow, E. Lunderberg, D. Rhodes, and D. Weisshaar, Phys. Rev. Lett. 122, 222501 (2020).
[124] S. Takeuchi, M. Matsushita, N. Aoi, P. Doornenbal, K. Li, T. Motobayashi, H. Scheit, D. Steppenbeck, H. Wang, H. Baba, *et al.*, Phys. Rev. Lett. 109, 182501 (2012).
[125] K. Nowak, K. Wimmer, S. Hellgartner, D. Mücher, V. Bildstein, J. Diriken, J. Elseviers, L.P. Gaffney, R. Gernhäuser, J. Iwanicki *et al.*, Phys. Rev. C 93, 044335 (2016).

[126] D. Rudolph, C. Baktash, M.J. Brinkman, E. Caurier, D.J. Dean, M. Devlin, J. Dobaczewski, P.-H. Heenen, H.-Q. Jin, D.R. LaFosse, W. Nazarewicz, F. Nowacki, A. Poves, L.L. Riedinger, D.G. Sarantites, W. Satuła, and C.-H. Yu, Phys. Rev. Lett. **82**, 3763 (1999).

[127] W. Bohne, H. Fuchs, K. Grabisch, D. Hilscher, U. Jahnke, H. Kluge, T.G. Masterson, and H. Morgenstern, Nucl. Phys. **A245**, 107 (1975).

[128] D. Rudolph, C. Baktash, J. Dobaczewski, W. Nazarewicz, W. Satuła, M.J. Brinkman, M. Devlin, H.-Q. Jin, D.R. LaFosse, L.L. Riedinger, D.G. Sarantites, and C.-H. Yu, Phys. Rev. Lett. **80**, 3018 (1998).

[129] M. Albers, S. Zhu, A.D. Ayangeakaa, R.V.F. Janssens, J. Gellanki, I. Ragnarsson, M. Alcorta, T. Baugher, P.F. Bertone, M.P. Carpenter, C.J. Chiara, P. Chowdhury, H.M. David, A.N. Deacon, B. DiGiovine, A. Gade, C.R. Hoffman, F.G. Kondev, T. Lauritsen, C.J. Lister, E.A. McCutchan, C. Nair, A.M. Rogers, and D. Seweryniak, Phys. Rev. C 94, 034301 (2016).

[130] D. Rudolph, C. Baktash, M. Devlin, D.R. LaFosse, L.L. Riedinger, D.G. Sarantites, and C.-H. Yu, Phys. Rev. Lett. **86**, 1450 (2001).

[131] E.K. Johansson, D. Rudolph, I. Ragnarsson, L.-L. Andersson, D.A. Torres, C. Andreoiu, C. Baktash, M.P. Carpenter, R.J. Charity, C.J. Chiara, J. Ekman, C. Fahlander, O.L. Pechenaya, W. Reviol,R. du Rietz, D.G. Sarantites, D. Seweryniak, L.G. Sobotka, C.H. Yu, and S. Zhu, Phys. Rev. C **80**, 014321 (2009).

[132] W. Reviol, D. Sarantites, R. Charity, V. Tomov, D. Rudolph, R. Clark, M. Cromaz, P. Fallon, A. Macchiavelli, M. Carpenter, D. Seweryniak, and J. Dobaczewski, Nucl. Phys. **A682**, 28c (2001).

[133] D. Rudolph, I. Ragnarsson, W. Reviol, C. Andreoiu, M.A. Bentley, M.P. Carpenter, R.J. Charity, R.M. Clark, M. Cromaz, J. Ekman, C. Fahlander, P. Fallon, E. Ideguchi, A.O. Macchiavelli, M.N. Mineva, D.G. Sarantites, D. Seweryniak, and S.J. Williams, J. Phys. G: Nucl. Part. Phys. **37**, 075105 (2010).

[134] C.-H. Yu, C. Baktash, J.A. Cameron, M. Devlin, J. Eberth, A. Galindo-Uribarri, D.S. Haslip, D. R. LaFosse, T.J. Lampman, I.-Y. Lee, F. Lerma, A.O. Macchiavelli, S.D. Paul, D.C. Radford, I. Ragnarsson, D. Rudolph, D.G. Sarantites, C.E. Svensson, J.C. Waddington, J.C. Wells, and J.N. Wilson, Phys. Rev. C 65, 061302(R) (2002).

[135] M. Albers, S. Zhu, R.V.F. Janssens, J. Gellanki, I. Ragnarsson, M. Alcorta, T. Baugher, P.F. Bertone, M.P. Carpenter, C.J. Chiara, P. Chowdhury, A. Deacon, A. Gade, B. DiGiovine, C.R. Hoffman, F.G. Kondev, T. Lauritsen, C.J. Lister, E.A. McCutchan, D.S. Moerland, C. Nair, A.M. Rogers, and D. Seweryniak, Phys. Rev. C 88, 054314 (2013).

[136] D. Evers, W. Assmann, K. Rudolph, S.J. Skorka and P. Sperr, Nucl. Phys. **A198**, 268 (1972).

[137] D. Evers, W. Assmann, K. Rudolph, S.J. Skorka, and P. Speer, Nucl. Phys. **A230**, 109 (1974).

[138] W.P. Alford, R.A. Lindgren, D. Elmore and R.W. Boyd, Nucl. Phys. **A243**, 269 (1975).

[139] N. Stein, J.W. Sunier, and C.W. Woods, Phys. Rev. Lett. **38**, 587 (1977).

[140] L.J. Evitts, A.B. Garnsworthy, T. Kibédi, J. Smallcombe, M.W. Reed, A.E. Stuchbery, G.J. Lane, T.K. Eriksen, A. Akber, B. Alshahrani, M. de Vries, M.S.M. Gerathy, J.D. Holt, B.Q. Lee, B.P. McCormick, A.J. Mitchell, M. Moukaddam, S. Mukhopadhyay, N. Palalani, T. Palazzo, E.E. Peters, A.P.D. Ramirez, T. Tornyi, and S.W. Yates, Phys. Rev. C **99**, 024306 (2019).

[141] L.J. Evitts, A.B. Garnsworthy, T. Kibédi, J. Smallcombe, M.W. Reed, A.E. Stuchbery, G.J. Lane, T.K. Eriksen, A. Akber, B. Alshahrani, M. de Vries, M.S.M. Gerathy, J.D. Holt, B.Q. Lee, B.P. McCormick, A.J. Mitchell, M. Moukaddam, S. Mukhopadhyay, N. Palalani, T. Palazzo, E.E. Peters, A.P.D. Ramirez, T. Tornyi, and S.W. Yates, Phys. Lett. **B779**, 396 (2018).

[142] F. Recchia, C.J. Chiara, R.V.F. Janssens, D. Weisshaar, A. Gade, W.B. Walters, M. Albers, M. Alcorta, V.M. Bader, T. Baugher *et al.*, Phys. Rev. C 88, 041302 (2013). doi:10.1103/PhysRevC.88.041302

[143] R. Taniuchi, C. Santamaria, P. Doornenbal, A. Obertelli, K. Yoneda, G. Authelet, H. Baba, D. Calvet, F. Chateau, A. Corsi *et al.*, Nature 569, 53 (2019).

[144] N. Mărginean, D. Little, Y. Tsunoda, S. Leoni, R.V.F. Janssens, B. Fornal, T. Otsuka, C. Michelagnoli, L. Stan, F.C.L. Crespi *et al.*, Phys. Rev. Lett. 125, 102502 (2020). doi:10.1103/PhysRevLett.125.102502

[145] S. Leoni, B. Fornal, N. Mărginean, M. Sferrazza, Y. Tsunoda, T. Otsuka, G. Bocchi, F.C.L. Crespi, A. Bracco, S. Aydin *et al.*, Phys. Rev. Lett. 118, 162502 (2017). doi:10.1103/PhysRevLett.118.162502

[146] R. Grzywacz, R. Béraud, C. Borcea, A. Emsallem, M. Glogowski, H. Grawe, D. Guillemaud-Mueller, M. Hjorth-Jensen, M. Houry, M. Lewitowicz *et al.*, Phys. Rev. Lett. 81, 766 (1998). doi:10.1103/

PhysRevLett.81.766
[147] O. Perru, O. Sorlin, S. Franchoo, F. Azaiez, E. Bouchez, C. Bourgeois, A. Chatillon, J.M. Daugas, Z. Dlouhy, Zs. Dombrádi *et al.*, Phys. Rev. Lett. 96, 232501 (2006). doi:10.1103/PhysRevLett.96.232501
[148] A.F. Lisetskiy, B.A. Brown, M. Horoi, and H. Grawe, Phys. Rev. C 70, 044314 (2004). doi:10.1103/PhysRevC.70.044314
[149] M. Girod, Ph. Dessagne, M. Bernas, M. Langevin, F. Pougheon, and P. Roussel, Phys. Rev. C 37, 2600 (1988). doi:10.1103/PhysRevC.37.2600
[150] M. Bernas, Ph. Dessagne, M. Langevin, J. Payet, F. Pougheon, and P. Roussel, Phys. Lett. B 113, 279 (1982). doi:10.1016/0370-2693(82)90039-9
[151] S. Suchyta, S.N. Liddick, Y. Tsunoda, T. Otsuka, M.B. Bennett, A. Chemey, M. Honma, N. Larson, C.J. Prokop, S.J. Quinn, N. Shimizu, A. Simon, A. Spyrou, V. Tripathi, Y. Utsuno, and J.M. VonMoss, Phys. Rev. C **89**, 021301(R) (2014).
[152] D. Pauwels, J.L. Wood, K. Heyde, M. Huyse, R. Julin, and P. Van Duppen, Phys. Rev. C 82, 027304 (2010). doi:10.1103/PhysRevC.82.027304
[153] J. Elseviers, *Probing the semi-magicity of* ^{68}*Ni via the* ^{66}*Ni(t, p)*^{68}*Ni two-neutron transfer reaction in inverse kinematics*, Ph.D. thesis, KU Leuven, Belgium (2014).
[154] F. Flavigny, J. Elseviers, A.N. Andreyev, C. Bauer, V. Bildstein, A. Blazhev, B.A. Brown, H. De Witte, J. Diriken, V.N. Fedosseev *et al.*, Phys. Rev. C 99, 054332 (2019). doi:10.1103/PhysRevC.99.054332
[155] B. Crider, C.J. Prokop, S.N. Liddick, M. Al-Shudifat, A.D. Ayangeakaa, M.P. Carpenter, J.J. Carroll, J. Chen, C.J. Chiara, H.M. David *et al.*, Phys. Lett. B 763, 108 (2016). doi:10.1016/j.physletb.2016.10.020
[156] N. Bree, I. Stefanescu, P.A. Butler, J. Cederkäll, T. Davinson4, P. Delahaye, J. Eberth, D. Fedorov, V.N. Fedosseev, L.M. Fraile *et al.*, Phys. Rev. C 78, 047301 (2008).
[157] F. Flavigny, D. Pauwels, D. Radulov, I.J. Darby, H. De Witte, J. Diriken, D.V. Fedorov, V.N. Fedosseev, L.M. Fraile, M. Huyse *et al.*, Phys. Rev. C 91, 034310 (2015). doi:10.1103/PhysRevC.91.034310
[158] W.F. Mueller, B. Bruyneel, S. Franchoo, M. Huyse, J. Kurpeta, K. Kruglov, Y. Kudryavtsev, N.V.S.V. Prasad, R. Raabe, I. Reusen *et al.*, Phys. Rev. C 61, 054308 (2000). doi:10.1103/PhysRevC.61.054308
[159] C.J. Chiara, R. Broda, W.B. Walters, R.V.F. Janssens, M. Albers, M. Alcorta, P.F. Bertone, M.P. Carpenter, C.R. Hoffman, T. Lauritsen *et al.*, Phys. Rev. C 86, 041304 (2012). doi:10.1103/PhysRevC.86.041304
[160] B. Olaizola, L.M. Fraile, H. Mach, A. Poves, F. Nowacki, A. Aprahamian, J.A. Briz, J. Cal-González, D. Ghita, U. Köster, W. Kurcewicz, S.R. Lesher, D. Pauwels, E. Picado, D. Radulov, G.S. Simpson, and J.M. Udías, Phys. Rev. C 95, 061303 (2017). doi:10.1103/PhysRevC.95.061303
[161] M. Stryjczyk, Y. Tsunoda, I.G. Darby, H. De Witte, J. Diriken, D.V. Fedorov, V.N. Fedosseev, L.M. Fraile, M. Huyse, U. Köster *et al.*, Phys. Rev. C 98, 064326 (2018). doi:10.1103/PhysRevC.98.064326
[162] C.J. Chiara, D. Weisshaar, R.V.F. Janssens, Y. Tsunoda, T. Otsuka, J.L. Harker, W.B. Walters, F. Recchia, M. Albers, M. Alcorta *et al.*, Phys. Rev. C 91, 044309 (2015). doi:10.1103/PhysRevC.91.044309
[163] C.J. Prokop, B.P. Crider, S.N. Liddick, A.D. Ayangeakaa, M.P. Carpenter, J.J. Carroll, J. Chen, C.J. Chiara, H M. David, A.C. Dombos *et al.*, Phys. Rev. C 92, 061302 (2015). doi:10.1103/PhysRevC.92.061302
[164] A.I. Morales, G. Benzoni, H. Watanabe, Y. Tsunoda, T. Otsuka, S. Nishimura, F. Browne, R. Daido, P. Doornenbal, Y. Fang *et al.*, Phys. Lett. B 765, 328 (2017). doi:10.1016/j.physletb.2016.12.025
[165] A. Dijon, E. Clément, G. de France, G. de Angelis, G. Duchene, J. Dudouet, S. Franchoo, A. Gadea, A. Gottardo, T. Hüyük *et al.*, Phys. Rev. C 85, 031301 (2012). doi:10.1103/PhysRevC.85.031301
[166] W. Rother, A. Dewald, H. Iwasaki, S.M. Lenzi, K. Starosta, D. Bazin, T. Baugher, B.A. Brown, H.L. Crawford, C. Fransen, A. Gade, T.N. Ginter, T. Glasmacher, G.F. Grinyer, M. Hackstein, G. Ilie, J. Jolie, S. McDaniel, D. Miller, P. Petkov, Th. Pissulla, A. Ratkiewicz, C.A. Ur, P. Voss, K.A. Walsh, D. Weisshaar, and K.-O. Zell, Phys. Rev. Lett. 106, 022502 (2011).
[167] J. Ljungvall, A. Görgen, A. Obertelli, W. Korten, E. Clément, G. de France, A. Bürger, J.-P. Delaroche, A. Dewald, A. Gadea *et al.*, Phys. Rev. C 81, 061301(R) (2010). doi:10.1103/PhysRevC.81.061301
[168] M. Klintefjord, J. Ljungvall, A. Görgen, S.M. Lenzi, F.L. Bello Garrote, A. Blazhev, E. Clément, G. de France, J.-P. Delaroche, P. Désesquelles *et al.*, Phys. Rev. C 95, 024312 (2017). doi:10.1103/PhysRevC.95.024312
[169] B. Olaizola, L.M. Fraile, H. Mach, A. Poves, A. Aprahamian, J.A. Briz, J. Cal-González, D. Ghita, U. Köster, W. Kurcewicz, S.R. Lesher, D. Pauwels, E. Picado, D. Radulov, G.S. Simpson, and J.M. Udías, J. Phys. G: Nucl.

Part. Phys. 44, 125103 (2017). doi:10.1088/1361-6471/aa915e
[170] S.N. Liddick, B. Abromeit, A. Ayres, A. Bey, C.R. Bingham, B.A. Brown, L. Cartegni, H.L. Crawford, I.G. Darby, R. Grzywacz, *et al.*, Phys. Rev. C 87, 014325 (2013). doi:10.1103/PhysRevC.87.014325
[171] N. Vermeulen, S.K. Chamoli, J.M. Daugas, M. Hass, D.L. Balabanski, J.P. Delaroche, F. de Oliveira-Santos, G. Georgiev, M. Girod, G. Goldring *et al.*, Phys. Rev. C 75, 051302(R) (2007). doi:10.1103/PhysRevC.75.051302
[172] S. Lunardi, S.M. Lenzi, F. Della Vedova, E. Farnea, A. Gadea, N. Marginean, D. Bazzacco, S. Beghini, P.G. Bizzeti, A.M. Bizzeti-Sona *et al.*, Phys. Rev. C 76, 034303 (2007). doi:10.1103/PhysRevC.75.051302
[173] B. Olaizola, L.M. Fraile, H. Mach, A. Aprahamian, J.A. Briz, J. Cal-González, D. Ghita, U. Köster, W. Kurcewicz, S.R. Lesher, D. Pauwels, E. Picado, A. Poves, D. Radulov, G.S. Simpson, and J.M. Udias, Phys. Rev. C 88, 044306 (2013). doi:10.1103/PhysRevC.88.044306
[174] A. Shalit, I. Talmi, *Nuclear Shell Theory*, Courier Dover Publications (1967).
[175] D. Pauwels, O. Ivanov, N. Bree, J. Büscher, T.E. Cocolios, M. Huyse, Yu. Kudryavtsev, R. Raabe, M. Sawicka, J. Van de Walle, and P. Van Duppen, Phys. Rev. C 79, 044309 (2009). doi:10.1103/PhysRevC.79.044309
[176] D. Pauwels, O. Ivanov, N. Bree, J. Büscher, T.E. Cocolios, J. Gentens, M. Huyse, A. Korgul, Yu. Kudryavtsev, R. Raabe, M. Sawicka, I. Stefanescu, J. Van de Walle, P. Van den Bergh, P. Van Duppen, and W.B. Walters, Phys. Rev. C 78, 041307 (2008). doi:10.1103/PhysRevC.78.041307
[177] A. Dijon, E. Clément, G. de France, P. Van Isacker, J. Ljungvall, A. Görgen, A. Obertelli, W. Korten, A. Dewald, A. Gadea *et al.*, Phys. Rev. C 83, 064321 (2011). doi:10.1103/PhysRevC.83.064321
[178] B. Olaizola, L.M. Fraile, H. Mach, F. Nowacki, A. Poves, A. Aprahamian, J.A. Briz, J. Cal-González, D. Ghita, U. Köster, W. Kurcewicz, S.R. Lesher, D. Pauwels, E. Picado, D. Radulov, G.S. Simpson, and J.M. Udías, Phys. Rev. C 99, 024321 (2019). doi:10.1103/PhysRevC.99.024321
[179] V. Modamio, J.J. Valiente-Dobón, S. Lunardi, S.M. Lenzi, A. Gadea, D. Mengoni, D. Bazzacco, A. Algora, P. Bednarczyk, G. Benzoni *et al.*, Phys. Rev. C 88, 044326 (2013). doi:10.1103/PhysRevC.88.044326
[180] T. Lokotko, S. Leblond, J. Lee, P. Doornenbal, A. Obertelli, A. Poves, F. Nowacki, K. Ogata, K. Yoshida, G. Authelet *et al.*, Phys. Rev. C 101, 034314 (2020). doi:10.1103/PhysRevC.101.034314
[181] S.N. Liddick, W.B. Walters, C.J. Chiara, R.V.F. Janssens, B. Abromeit, A. Ayres, A. Bey, C.R. Bingham, M.P. Carpenter, L. Cartegni, J. Chen *et al.*, Phys. Rev. C 92, 024319 (2015). doi:10.1103/PhysRevC.92.024319
[182] A. Gade, R.V.F. Janssens, D. Bazin, P. Farris, A.M. Hill, S.M. Lenzi, J. Li, D. Little, B. Longfellow, F. Nowacki, A. Poves, D. Rhodes, J.A. Tostevin, and D. Weisshaar *et al.*, Phys. Rev. C 103, 014314 (2021). doi:10.1103/PhysRevC.103.014314
[183] S.N. Liddick, B. Abromeit, A. Ayres, A. Bey, C.R. Bingham, M. Bolla, L. Cartegni, H.L. Crawford, I.G. Darby, R. Grzywacz *et al.*, Phys. Rev. C 85, 014328 (2012). doi:10.1103/PhysRevC.85.014328
[184] X.F. Yang, C. Wraith, L. Xie, C. Babcock, J. Billowes, M.L. Bissell, K. Blaum, B. Cheal, K.T. Flanagan, R.F. Garcia Ruiz *et al.*, Phys. Rev. Lett. 116, 182502 (2016).
[185] R. Orlandi, D. Mücher, R. Raabe, A. Jungclaus, S.D. Pain, V. Bildstein, R. Chapman, G. de Angelis, J.G. Johansen, P. Van Duppen *et al.*, Phys. Lett. B 740, 298 (2015).
[186] J. Van de Walle, F. Aksouh, T. Behrens, V. Bildstein, A. Blazhev, J. Cederkäll, E. Clément, T.E. Cocolios, T. Davinson, P. Delahaye *et al.*, Phys. Rev. C 79, 014309 (2009).
[187] S. Ahn, D.W. Bardayan, K.L. Jones, A.S. Adekola, G. Arbanas, J.C. Blackmon, K.Y. Chae, K.A. Chipps, J.A. Cizewski, S. Hardy *et al.*, Phys. Rev. C 100, 044613 (2019).
[188] L.A. Montestruque, M.C. Cobian-Rozak, G. Szaloky, J.D. Zumbro, S.E. Darden, Nucl. Phys. A 305, 29 (1978)
[189] N.A. Detorie, P.L. Jolivette, C.P. Browne, and A.A. Rollefson, Phys. Rev. C 18, 991 (1978).
[190] B.L. Burks, R.E. Anderson, T.B. Clegg, E.J. Ludwig, B.C. Karp, and Y. Aoki, Nucl. Phys. A 457, 337 (1986).
[191] A. Gottardo, D. Verney, C. Delafosse, F. Ibrahim, B. Roussière, C. Sotty, S. Roccia, C. Andreoiu, C. Costache, M.-C. Delattre *et al.*, Phys. Rev. Lett. 116, 182501 (2016).
[192] F.H. Garcia, C. Andreoiu, G.C. Ball, A. Bell, A.B. Garnsworthy, F. Nowacki, C.M. Petrache, A. Poves, K. Whitmore, F.A. Ali *et al.*, Phys. Rev. Lett. 125, 172501 (2020).
[193] J.K. Hwang, J.H. Hamilton, A.V. Ramayya, N.T. Brewer, Y.X. Luo, J.O. Rasmussen, and S.J. Zhu, Phys. Rev. C 84, 024305 (2011).
[194] C. Shand, Zs. Podolyák, M. Górska, P. Doornenbal, A. Obertelli, F. Nowacki, T. Otsuka, K. Sieja, J.A. Tostevin,

Y. Tsunoda *et al.*, Phys. Lett. B 773, 492 (2017).
[195] P.-A. Söderström, S. Nishimura, Z.Y. Xu , K. Sieja, V. Werner, P. Doornenbal, G. Lorusso, F. Browne, G. Gey, H.S. Jung *et al.*, Phys. Rev. C 92, 051305(R) (2015).
[196] A.D. Ayangeakaa, R.V.F. Janssens, C.Y. Wu, J.M. Allmond, J.L. Wood, S. Zhu, M. Albers, S. Almaraz-Calderon, B. Bucher, M.P. Carpenter *et al.*, Phys. Lett. B 754, 254 (2016).
[197] B. Kotliński, T. Czosnyka, D. Cline, J. Srebrny, C.Y. Wu, A. Bäcklin, L. Hasselgren, L. Westerberg, C. Baktash, and S.G. Steadman, Nucl. Phys. A 519, 646 (1990).
[198] M. Sugawara, Y. Toh, T. Czosnyka, M. Oshima, T. Hayakawa, H. Kusakari, Y. Hatsukawa, J. Katakura, N. Shinohara, M. Matsuda, T. Morikawa, A. Seki, and F. Sakata, Eur. Phys. J. A 16, 409 (2003).
[199] Y. Toh, T. Czosnyka, M. Oshima, T. Hayakawa, H. Kusakari, M. Sugawara, Y. Hatsukawa, J. Katakura, N. Shinohara, and M. Matsuda, Eur. Phys. J. A 9, 353 (2000).
[200] Y. Toh, T. Czosnyka, M. Oshima, T. Hayakawa, H. Kusakari, A. Osa, M. Su- gawara, M. Koizumi, Y. Hatsukawa, J. Katakura, N. Shinohara, M. Matsuda, J. Phys. G: Nucl. Part. Phys. 27, 1475 (2001).
[201] A.D. Ayangeakaa, R.V.F. Janssens, S. Zhu, D. Little, J. Henderson, C.Y. Wu, D.J. Hartley, M. Albers, K. Auranen, B. Bucher *et al.*, Phys. Rev. Lett. 123, 102501 (2019).
[202] Y. Toh, C.J. Chiara, E.A. McCutchan, W.B. Walters, R.V.F. Janssens, M.P. Carpenter, S.Zhu, R. Broda, B. Fornal, B.P. Kay *et al.*, Phys. Rev. C 87, 041304(R) (2013).
[203] A.M. Forney, W.B. Walters, C.J. Chiara, R.V.F. Janssens, A.D. Ayangeakaa, J. Sethi, J. Harker, M. Alcorta, M.P. Carpenter, G. Gürdal *et al.*, Phys. Rev. Lett. 120, 212501 (2018).
[204] M. Rocchini, K. Hadyńska-Klęk, A. Nannini, A. Goasduff, M. Zielińska, D. Testov, T. R. Rodriguez, A. Gargano, F. Nowacki *et al.*, Phys. Rev. C 103, 014311 (2021).
[205] M. Koizumi, A. Seki, Y. Toh, A. Osa, Y. Utsuno, A. Kimura, M. Oshima, T. Hayakawa, Y. Hatsukawa, J. Katakura, M. Matsuda *et al.*, Nucl. Phys. A 730, 46 (2004).
[206] T. Hayakawa, Y. Toh, M. Oshima, A. Osa, M. Koizumi, Y. Hatsukawa, Y. Utsuno, J. Katakura, M. Matsuda, T. Morikawa, M. Sugawara, H. Kusakari, and T. Czosnyka, Phys. Rev. C 67, 064310 (2003). doi:10.1103/PhysRevC.67.064310
[207] A.E. Kavka, C. Fahlander, A. Bäcklin, D. Cline, T. Czosnyka, R.M. Diamond, D. Disdier, W.J. Kernan, L. Kraus, I. Linck *et al.*, Nucl. Phys. A 593, 177 (1995). doi:10.1016/0375-9474(95)00327-W
[208] S. Mukhopadhyay, B.P. Crider, B.A. Brown, S.F. Ashley, A. Chakraborty, A. Kumar, M.T.McEllistrem, E.E. Peters, F.M. Prados-Estévez, and S.W. Yates, Phys. Rev. C 99, 014313 (2019).
[209] E.A. McCutchan, C.J. Lister, T. Ahn, V. Anagnostatou, N. Cooper, M. Elvers, P. Goddard, A. Heinz, G. Ilie, D. Radeck, D. Savran, and V. Werner, Phys. Rev. C 87, 014307 (2013).
[210] S.J. Freeman, J.P. Schiffer, A.C.C. Villari, J.A. Clark, C. Deibel, S. Gros, A. Heinz, D. Hirata, C.L. Jiang, B.P. Kay *et al.*, Phys. Rev. C 75, 051301(R) (2007).
[211] E.A. McCutchan, C.J. Lister, T. Ahn, R.J. Casperson, A. Heinz, G. Ilie, J. Qian, E. Williams, R. Winkler, and V. Werner, Phys. Rev. C 83, 024310 (2011).
[212] H. Orihara, M. Takahashi, K. Murakami, Y. Ishizaki, T. Suehiro, K. Miura, Y. Hiratate, and H. Yamaguchi, University of Tokyo, Annual Report No. 3, 4 (1977).
[213] J. Henderson, C.Y. Wu, J. Ash, P.C. Bender, B. Elman, A. Gade, M. Grinder, H. Iwasaki, E. Kwan, B. Longfellow, T. Mijatovic, D. Rhodes, M. Spieker, and D. Weisshaar, Phys. Rev. Lett. 121, 082502 (2018). doi:10.1103/PhysRevLett.121.082502
[214] G. Rainovski, H. Schnare, R. Schwengner, C. Plettner, L. Käubler, F. Dönau, I. Ragnarsson, J. Eberth, T. Steinhardt, O. Thelen *et al.*, J. Phys. G: Nucl. Part. Phys. 28, 2617 (2002).
[215] A.M. Hurst, P.A. Butler, D.G. Jenkins, P. Delahaye, F. Wenander, F. Ames, C.J. Barton, T. Behrens, A. Bürger, J. Cederkäll *et al.*, Phys. Rev. Lett. 98, 072501 (2007). doi:10.1103/PhysRevLett.98.072501
[216] J. Ljungvall, A. Görgen, M. Girod, J.-P. Delaroche, A. Dewald, C. Dossat, W. Korten, B. Melon, R. Menegazzo, A. Obertelli, R. Orlandi, P. Petkov, T. Pissulla, S. Siem, R.P. Singh, J. Srebrny, Ch. Theisen, C.A. Ur, J.J. Valiente-Dobon, K.O. Zell, and M. Zielińska, Phys. Rev. Lett. 100, 102502 (2008).
[217] S.M. Fischer, D.P. Balamuth, P.A. Hausladen, C.J. Lister, M.P. Carpenter, D. Seweryniak, and J. Schwartz, Phys. Rev. Lett. 84, 4064 (2000).
[218] A. Görgen, E. Clément, A. Chatillon, A. Dewald, W. Korten, Y. Le Coz, N. Marginean, B. Melon,

R. Menegazzo, O. Möller, Ch. Theisen, D. Tonev, C.A. Ur, and K.O. Zell, Eur. Phys. J. A 26, 153 (2005).
[219] E. Bouchez, I. Matea, W. Korten, F. Becker, B. Blank, C. Borcea, A. Buta, A. Emsallem, G. de France, J. Genevey *et al.*, Phys. Rev. Lett. 90, 082502 (2003). doi:10.1103/PhysRevLett.90.082502
[220] H. Iwasaki, A. Lemasson, C. Morse, A. Dewald, T. Braunroth, V.M. Bader, T. Baugher, D. Bazin, J.S. Berryman, C.M. Campbell *et al.*, Phys. Rev. Lett. 112, 142502 (2014). doi:10.1103/PhysRevLett.112.142502
[221] K. Wimmer, W. Korten, T. Arici, P. Doornenbal, P. Aguilera, A. Algora, T. Ando, H. Baba, B. Blank, A. Boso *et al.*, Phys. Lett. B 785, 441 (2018). doi:10.1016/j.physletb.2018.07.067
[222] E. Clément, A. Görgen, W. Korten, E. Bouchez, A. Chatillon, J.-P. Delaroche, M. Girod, H. Goutte, A. Hürstel, Y. Le Coz *et al.*, Phys. Rev. C 75, 054313 (2007). doi:10.1103/PhysRevC.75.054313
[223] M. Girod, J.-P. Delaroche, A. Görgen, and A. Obertelli, Phys. Lett. B 676, 39 (2009). doi:10.1016/j.physletb.2009.04.077
[224] M. Bender, P. Bonche, and P.-H. Heenen, Phys. Rev. C 74, 024312 (2006). doi:10.1103/PhysRevC.74.024312
[225] W.P. Alford, R.E. Anderson, P.A. Batay-Csorba, R.A. Emigh, D.A. Lind, P.A. Smith, and C.D. Zafiratos, Nucl. Phys. A 330, 77 (1979). doi:10.1016/0375-9474(79)90538-4
[226] J. Heese, K.P. Lieb, S. Ulbig, B. Wörmann, J. Billowes, A.A. Chishti, W. Gelletly, C.J. Lister, and B.J. Varley, Phys. Rev. C 41, 603 (1990).
[227] A. Lemasson, H. Iwasaki, C. Morse, D. Bazin, T. Baugher, J.S. Berryman, A. Dewald, C. Fransen, A. Gade, S. McDaniel, A. Nichols, A. Ratkiewicz, S. Stroberg, P. Voss, R. Wadsworth, D. Weisshaar, K. Wimmer, and R. Winkler, Phys. Rev. C 85, 041303 (2012). doi:10.1103/PhysRevC.85.041303
[228] J. Henderson, D.G. Jenkins, K. Kaneko, P. Ruotsalainen, P. Sarriguren, K. Auranen, M.A. Bentley, P.J. Davies, A. Görgen, T. Grahn *et al.*, Phys. Rev. C 90, 051303(R) (2014).
[229] C. Thibault, F. Touchard, S. Büttgenbach, R. Klapisch, M. de Saint Simon, H.T. Duong, P. Jacquinot, P. Juncar, S. Liberman, P. Pillet, J. Pinard, J.L. Vialle, A. Pesnelle, and G. Huber, Phys. Rev. C 23, 2720 (1981). doi:10.1103/PhysRevC.23.2720
[230] J. Mackin, R.R. Dasari, C.H. Holbrow, J.T. Hutton, D.E. Murnick, M. Otteson, W.W. Quivers, Jr., G. Shimkaveg, and M.S. Feld, Phys. Rev. Lett. 66, 1681 (1991). doi:10.1103/PhysRevLett.66.1681
[231] N. Stone, At. Data Nucl. Data Tables 111-112, 1 (2016). doi:10.1016/j.adt.2015.12.002
[232] G. Audi, M. Wang, A.H. Wapstra, F.G. Kondev, M. MacCormick, X. Xu, and B. Pfeiffer, Chin. Phys. C 36, 1287 (2012).
[233] S. Naimi, G. Audi, D. Beck, K. Blaum, Ch. Böhm, Ch. Borgmann, M. Breitenfeldt, S. George, F. Herfurth, A. Herlert, M. Kowalska, S. Kreim, D. Lunney, D. Neidherr, M. Rosenbusch, S. Schwarz, L. Schweikhard, and K. Zuber, Phys. Rev. Lett. 105, 032502 (2010). doi:10.1103/PhysRevLett.105.032502
[234] I. Angeli and K.P. Marinova, At. Data Nucl. Data Tables 99, 69 (2013).
[235] E. Mané, A. Voss, J.A. Behr, J. Billowes, T. Brunner, F. Buchinger, J E. Crawford, J. Dilling, S. Ettenauer, C.D.P. Levy, O. Shelbaya, and M.R. Pearson, Phys. Rev. Lett. 107, 212502 (2011).
[236] D.H. Forest, R.A. Powis, E.C.A. Cochrane1, J.A.R. Griffith, and G. Tungate, J. Phys. G: Nucl. Part. Phys. 41, 025106 (2014).
[237] P. Singh, W. Korten, T.W. Hagen, A. Görgen, L. Grente, M.-D. Salsac, F. Farget, E. Clément, G. de France, T. Braunroth *et al.*, Phys. Rev. Lett. 121, 192501 (2018). doi:10.1103/PhysRevLett.121.192501
[238] V. Karayonchev, J. Jolie, A. Blazhev, A. Dewald, A. Esmaylzadeh, C. Fransen, G. Häfner, L. Knafla, J. Litzinger, C. Müller-Gatermann, J.-M. Régis, K. Schomacker, A. Vogt, N. Warr, A. Leviatan, and N. Gavrielov, Phys. Rev. C 102, 064314 (2020).
[239] J.-M. Régis, J. Jolie, N. Saed-Samii, N. Warr, M. Pfeiffer, A. Blanc, M. Jentschel, U. Köster, P. Mutti, T. Soldner *et al.*, Phys. Rev. C 90, 067301 (2014). doi:10.1103/PhysRevC.90.067301
[240] J.-M. Régis, J. Jolie, N. Saed-Samii, N. Warr, M. Pfeiffer, A. Blanc, M. Jentschel, U. Köster, P. Mutti, T. Soldner *et al.*, Phys. Rev. C 95, 054319 (2017). doi:10.1103/PhysRevC.95.054319
[241] S. Ansari, J.-M. Régis, J. Jolie, N. Saed-Samii, N. Warr, W. Korten, M. Zielińska, M.-D. Salsac, A. Blanc, M. Jentschel, U. Köster, P. Mutti, T. Soldner, G.S. Simpson, F. Drouet, A. Vancraeyenest, G. de France, E. Clément, O. Stezowski, C.A. Ur, W. Urban, P.H. Regan, Zs. Podolyák, C. Larijani, C. Townsley, R. Carroll, E. Wilson, H. Mach, L.M. Fraile, V. Paziy, B. Olaizola, V. Vedia, A.M. Bruce, O.J. Roberts, J.F. Smith, M. Scheck,

T. Kröll, A.-L. Hartig, A. Ignatov, S. Ilieva, S. Lalkovski, N. Marginean, T. Otsuka, N. Shimizu, T. Togashi, and Y. Tsunoda, Phys. Rev. C **96** 054323 (2017).

[242] B. Elman, A. Gade, D. Weisshaar, D. Barofsky, D. Bazin, P.C. Bender, M. Bowry, M. Hjorth-Jensen, K.W. Kemper, S. Lipschutz, E. Lunderberg, N. Sachmpazidi, N. Terpstra, W.B. Walters, A. Westerberg, S.J. Williams, and K. Wimmer, Phys. Rev. C 96, 044332 (2017).

[243] M. Albers, N. Warr, K. Nomura, A. Blazhev, J. Jolie, D. Mücher, B. Bastin, C. Bauer, C. Bernards, L. Bettermann *et al.*, Phys. Rev. Lett. 108, 062701 (2012). doi:10.1103/PhysRevLett.108.062701

[244] F. Flavigny, P. Doornenbal, A. Obertelli, J.-P. Delaroche, M. Girod, J. Libert, T.R. Rodriguez, G. Authelet, H. Baba, D. Calvet *et al.*, Phys. Rev. Lett. 118, 242501 (2017). doi:10.1103/PhysRevLett.118.242501

[245] Z.M. Wang, A.B. Garnsworthy, C. Andreoiu, G.C. Ball, P.C. Bender, V. Bildstein, D.S. Cross, G. Demand, R. Dunlop, L.J. Evitts *et al.*, Phys. Rev. C 93, 054301 (2016).

[246] S. Cruz, K. Wimmer, S.S. Bhattacharjee, P.C. Bender, G. Hackman, R. Krücken, F. Ames, C. Andreoiu, R.A.E. Austin, C.S. Bancroft *et al.*, Phys. Rev. C 102, 024335 (2020).

[247] E. Clément, M. Zielińska, A. Görgen, W. Korten, S. Péru, J. Libert, H. Goutte, S. Hilaire, B. Bastin, C. Bauer *et al.*, Phys. Rev. Lett. 116, 022701 (2016). doi:10.1103/PhysRevLett.116.022701

[248] E. Clément, M. Zielińska, S. Péru, H. Goutte, S. Hilaire, A. Görgen, W. Korten, D.T. Doherty, B. Bastin, C. Bauer *et al.*, Phys. Rev. C 94, 054326 (2016). doi:10.1103/PhysRevC.94.054326

[249] E. Clément, M. Zielińska, S. Péru, H. Goutte, S. Hilaire, A. Görgen, W. Korten, D.T. Doherty, B. Bastin, C. Bauer *et al.*, Phys. Rev. Lett. 117, 099902 (2016). doi:10.1103/PhysRevLett.117.099902

[250] G. Jung, B. Pfeiffer, L.J. Alquist, H. Wollnik, P. Hungerford, S.M. Scott, and W.D. Hamilton, Phys. Rev. C 22, 252 (1980). doi:10.1103/PhysRevC.22.252

[251] K. Kawade, G. Battistuzzi, H. Lawin, H.A. Selic, K. Sistemich, F. Schussler, E. Monnand, J.A. Pinston, B. Pfeiffer, and G. Jung, Z. Phys. A 304, 293 (1982). doi:10.1007/BF01421511

[252] G. Lhersonneau, B. Pfeiffer, K.-L. Kratz, T. Enqvist, P.P. Jauho, A. Jokinen, J. Kantele, M. Leino, J.M. Parmonen, H. Penttilä, and J. Äystö, Phys. Rev. C 49, 1379 (1994). doi:10.1103/PhysRevC.49.1379

[253] W. Urban, J.L. Durell, A.G. Smith, W.R. Phillips, M.A. Jones, B.J. Varley T. Rząca-Urban, I. Ahmad, L.R. Morss, M. Bentaleb, and N. Schulz, Nucl. Phys. A 689, 605 (2001). doi:10.1016/S0375-9474(00)00612-6

[254] P.E. Garrett, L. Makhathini, R.A. Bark, T.R. Rodríguez, S. Valbuena, V. Bildstein, T.D. Bucher, C. Burbadge, R. Dubey, T. Faestermann, R. Hertenberger, M. Kamil, E.A. Lawrie, K.G. Leach, A.D. MacLean, C. Mehl, S.H. Mthembu, N.J. Mukwevho, C. Ngwetsheni, S.S. Ntshangase, J.C. Nzobadila Ondze, J.N. Orce, B. Rebeiro, B. Singh, S. Triambak, E.C. Vyfers, H.-F. Wirth, Phys. Lett. **809**, 135762 (2020).

[255] C. Kremer, S. Aslanidou, S. Bassauer, M. Hilcker, A. Krugmann, P. von Neumann-Cosel, T. Otsuka, N. Pietralla, V.Yu. Ponomarev, N. Shimizu, M. Singer, G. Steinhilber, T. Togashi, Y. Tsunoda, V. Werner, and M. Zweidinger, Phys. Rev. Lett. 117, 172503 (2016), arXiv:1606.09057v1 [nucl-ex], doi:https://doi.org/10.1103/PhysRevLett.117.172503

[256] M. Zielińska, Ph.D thesis, University of Warsaw (2006), unpublished.

[257] P.E. Garrett, M. Zielińska, A. Bergmaier, T.R. Rodriguez, H. Bidaman, V. Bildstein, C. Burbadge, A. Diaz Varela, D. Doherty, T. Faestermann *et al.*, to be published.

[258] J. Srebrny, T. Czosnyka, Ch. Droste, S.G. Rohoziński, L. Próchniak, K. Zając, K. Pomorski, D. Cline, C.Y. Wu, A. Bäcklin, L. Hasselgren, R.M. Diamond, D. Habs, H.J. Körner, F.S. Stephens, C. Baktash, and R.P. Kostecki, Nucl. Phys. A 766, 25 (2006). doi:10.1016/j.nuclphysa.2005.11.013

[259] L.E. Svensson, C. Fahlander, L. Hasselgren, A. Bäcklin, L. Westerberg, D. Cline, T. Czosnyka, C.Y. Wu, R.M. Diamond, and H. Kluge, Nucl. Phys. **A584**, 547 (1995).

[260] K. Wrzosek-Lipska, L. Próchniak, P.E. Garrett, S.W. Yates, J.L. Wood, P.J. Napiorkowski, T. Abraham, J.M. Allmond, F.L. Bello Garrote, H. Bidaman, V. Bildstein, C. Burbadge, M. Chiari, A. Diaz Varela, D.T. Doherty, S. Dutt, K. Hadynska-Klek, M. Hlebowicz, J. Iwanicki, B. Jigmeddorj, M. Kisielinski, M. Komorowska, M. Kowalczyk, R. Kumar, T. Marchlewski, M. Matejska-Minda, B. Olaizola, F. Oleszczuk, M. Palacz, E. Pasquali, E.E. Peters, M. Rocchini, E. Shin, M. Saxena, J. Srebrny, A. Tucholski, Acta Phys. Pol. **B51**, 789 (2020).

[261] P.E. Garrett, T.R. Rodriguez, A. Diaz Varela, K.L. Green, J. Bangay, A. Finlay, R.A.E. Austin, G.C. Ball,

D.S. Bandyopadhyay, V. Bildstein, S. Colosimo, D.S. Cross, G.A. Demand, P. Finlay, A.B. Garnsworthy, G.F. Grinyer, G. Hackman, B. Jigmeddorj, J. Jolie, W.D. Kulp, K.G. Leach, A.C. Morton, J.N. Orce, C.J. Pearson, A.A. Phillips, A.J. Radich, E.T. Rand, M.A. Schumaker, C.E. Svensson, C. Sumithrarachchi, S. Triambak, N. Warr, J. Wong, J.L. Wood, and S.W. Yates, Phys. Rev. C 101, 044302 (2020). doi.org/10.1103/PhysRevC.101.044302

[262] C. Fahlander, A. Bäcklin, L. Hasselgren, A. Kavka, V. Mittal, L.E. Svensson, B. Varnestig, D. Cline, B. Kotlinski, H. Grein, E. Grosse, R. Kulessa, C. Michel, W. Spreng, H.J. Wollersheim, J. Stachel, Nucl. Phys. **A485**, 327 (1988).

[263] J.L. Pore, D.S. Cross, C. Andreoiu, R. Ashley, G.C. Ball, P.C. Bender, A.S. Chester, A. Diaz Varela, G.A. Demand, R. Dunlop, A.B. Garnsworthy, P.E. Garrett, G. Hackman, B. Hadinia, B. Jigmeddorj, A.T. Laffoley, A. Liblong, R. Kanungo, B. Noakes, C.M. Petrache, M.M. Rajabali, K. Starosta, C.E. Svensson, P.J. Voss, Z.M. Wang, J.L. Wood, and S.W. Yates, Eur. Phys. J. **A53**, 27 (2017).

[264] C. Mihai, A.A. Pasternak, S. Pascu, D. Filipescu, M. Ivaşcu, D. Bucurescu, G. Căta-Danil, I. Căta-Danil, D. Deleanu, D.G. Ghiţă, T. Glodariu, N. Mărginean, R. Mărginean, A. Negret, T. Sava, L. Stroe, G. Suliman, and N.V. Zamfir, Phys. Rev. C **83**, 054310 (2011).

[265] A.A. Pasternak, J. Srebrny, A.D. Efimov, V.M. Mikhajlov, E.O. Podsvirova, Ch. Droste, T. Morek, S. Juutinen, G.B. Hagemann, M. Piiparinen, S. Törmänen and A. Virtanen, E. Phys. J. **A13**, 435 (2002).

[266] S.F. Hicks, J.R. Vanhoy, P.G. Burkett, B.R. Champine, S.J. Etzkorn, P.E. Garrett, S.W. Yates, and Minfang Yeh, Phys. Rev. C **95**, 034322 (2017).

[267] H. Mach, F.K. Wohn, G. Molnár, K. Sistemich, J.C. Hill, M. Moszyński, R.L. Gill, W. Krips, and D.S. Brenner, Nucl. Phys. A 523, 197 (1991). doi:10.1016/0375-9474(91)90001-M

[268] H. Mach, M. Moszyński, R.L. Gill, F.K. Wohn, J.A. Winger, J.C. Hill, G. Molnár, K. Sistemich, Phys. Lett. B 230, 21 (1989). doi:10.1016/0370-2693(89)91646-8

[269] H. Ohm, G. Lhersonneau, K. Sistemich, B. Pfeiffer, and K.-L. Kratz , Z. Phys. A 327, 483 (1987).

[270] H. Mach, R.L. Gill, M. Moszyński, Nucl. Instrum. Methods A 280, 49 (1989). doi:10.1016/0168-9002(89)91272-2

[271] G. Lhersonneau, B. Pfeiffer, R. Capote, J.M. Quesada, H. Gabelmann, and K.-L. Kratz, Phys. Rev. C 65, 024318 (2002). doi:10.1103/PhysRevC.65.024318

[272] A.G. Smith, J.L. Durell, W.R. Phillips, M.A. Jones, M. Leddy, W. Urban, B.J. Varley, I. Ahmad, L.R. Morss, M. Bentaleb, A. Guessous, E. Lubkiewicz, N. Schulz, and R. Wyss, Phys. Rev. Lett. 77, 1711 (1996). doi:10.1103/PhysRevLett.77.1711

[273] A.G. Smith, J.L. Durell, W.R. Phillips, W. Urban, P. Sarriguren, and I. Ahmad, Phys. Rev. C 86, 014321 (2012). doi:10.1103/PhysRevC.86.014321

[274] F. Schussler, J.A. Pinston, E. Monnand, A. Moussa, G. Jung, E. Koglin, B. Pfeiffer, R.V.F. Janssens, and J. van Klinken, Nucl. Phys. A 339, 415 (1980). doi:10.1016/0375-9474(80)90024-X

[275] J. Park, A.B. Garnsworthy, R. Krücken, C. Andreoiu, G.C. Ball, P.C. Bender, A. Chester, A. Close, P. Finlay, P.E. Garrett, J. Glister, G. Hackman, B. Hadinia, K.G. Leach, E.T. Rand, S. Sjue, K. Starosta, C.E. Svensson, and E. Tardiff, Phys. Rev. C 93, 014315 (2016). doi:10.1103/PhysRevC.93.014315

[276] W. Urban, T. Rząca-Urban, J. Wiśniewski, A.G. Smith, G.S. Simpson, and I. Ahmad, Phys. Rev. C 100, 014319 (2019).

[277] S. Cruz, P.C. Bender, R. Krücken, K. Wimmer, F. Ames, C. Andreoiu, R.A.E. Austin, C.S. Bancroft, R. Braid, T. Bruhn *et al.*, Phys. Lett. B 786, 94 (2018). doi:10.1016/j.physletb.2018.09.031

[278] S. Cruz, K. Wimmer, P.C. Bender, R. Krücken, G. Hackman, F. Ames, C. Andreoiu, R.A E. Austin, C.S. Bancroft, R. Braid *et al.*, Phys. Rev. C 100, 054321 (2019). doi:10.1103/PhysRevC.100.054321

[279] V. Werner, N. Benczer-Koller, G. Kumbartzki, J.D. Holt, P. Boutachkov, E. Stefanova, M. Perry, N. Pietralla, H. Ai, K. Aleksandrova *et al.*, Phys. Rev. C 78, 031301(R) (2008).

[280] J.B. Ball, R.L. Auble, and P.G. Roos, Phys. Rev. C 4, 196 (1971).

[281] E.R. Flynn, J.G. Beery, A.G. Blair, Nucl. Phys. A 218, 285 (1974).

[282] J.K. Dickens, E. Eichler, and G.R. Satchler, Phys. Rev. 168, 1355 (1968).

[283] A. Chakraborty, E.E. Peters, B.P. Crider, C. Andreoiu, P.C. Bender, D.S. Cross, G.A. Demand, A.B. Garnsworthy, P.E. Garrett, G. Hackman *et al.*, Phys. Rev. Lett 110, 022504 (2013).

[284] E. Elhami, J.N. Orce, S. Mukhopadhyay, S.N. Choudry, M. Scheck, M.T. McEllistrem, and S.W. Yates, Phys. Rev. C 75, 011301(R) (2007).
[285] E. Elhami, J.N. Orce, M. Scheck, S. Mukhopadhyay, S.N. Choudry, M.T. McEllistrem, S.W. Yates, C. Angell, M. Boswell, B. Fallin, C.R. Howell, A. Hutcheson, H.J. Karwowski, J.H. Kelley, Y. Parpottas, A.P. Tonchev, and W. Tornow, Phys. Rev. C 78, 064303 (2008).
[286] E. Elhami, J.N. Orce, S. Mukhopadhyay, S.N. Choudry, M. Scheck, M.T. McEllistrem, and S.W. Yates, Phys. Rev. C 88, 029902 (2013).
[287] K. Becker, G. Jung, K.-H. Kobras, H. Wollnik, and B. Pfeiffer, Z. Phys. A 319, 193 (1984).
[288] E.R. Flynn, J.G. Beery, and A.G. Blair, Nucl. Phys. **A218**, 285 (1973).
[289] A. Saha, G.D. Jones, L.W. Put, and R.H. Siemssen, Phys. Lett. B82, 208 (1978).
[290] B.M. Preedom, E. Newman, and J.C. Hiebert, Phys. Rev. **166**, 1156 (1968).
[291] M.R. Cates, J.B. Ball, and E. Newman, Phys. Rev. **187**, 1682 (1969).
[292] R.S. Tickle, W.S. Gray, and R.D. Bent, Nucl. Phys. **A376**, 309 (1981).
[293] T. Togashi, Y. Tsunoda, T. Otsuka, and N. Shimizu, Phys. Rev. Lett. 117, 172502 (2016). doi:10.1103/PhysRevLett.117.172502
[294] E.R. Flynn, R.E. Brown, F. Ajzenberg-Selove, and J.A. Cizewski, Phys. Rev. C **28**, 575 (1983).
[295] B. Cheal, M.D. Gardner, M. Avgoulea, J. Billowes, M.L. Bissell, P. Campbell, T. Eronen, K.T. Flanagan, D.H. Forest, J. Huikari *et al.*, Phys. Lett. B 645, 133 (2007). doi:https://doi.org/10.1016/j.physletb.2006.12.053
[296] G. Lhersonneau, D. Weiler, P. Kohl, H. Ohm, K. Sistemich, and R.A. Meyer, Z. Phys. **A323**, 59 (1986).
[297] F. Hoellinger, N. Schulz, S. Courtin, B.J.P. Gall, M.-G. Porquet, I. Deloncle, A. Wilson, T. Kutsarova, A. Minkova, J. Duprat, H. Sergolle, C. Gautherin, and R. Lucas, Eur. Phys. J. **A4**, 319 (1999).
[298] Y.X. Luo, J.O. Rasmussen, I. Stefanescu, A. Gelberg, J.H. Hamilton, A.V. Ramayya, J.K. Hwang, S.J. Zhu, P.M. Gore, D. Fong, E.F. Jones, S.C. Wu, I.Y. Lee, T.N. Ginter, W.C. Ma, G.M. Ter-Akopian, A.V. Daniel, M.A. Stoyer, and R. Donangelo, J. Phys. G: Nucl. Part. Phys. **31**, 1303 (2005).
[299] E. Monnand, J.A. Pinston, F. Schussler, B. Pfeiffer, H. Lawin, G. Battistuzzi, K. Shizuma, and K. Sistemich, Z. Phys. A 306, 183 (1982). doi:10.1007/BF01415489
[300] F.K. Wohn, J.C. Hill, R.F. Petry, H. Dejbakhsh, Z. Berant, and R.L. Gill, Phys. Rev. Lett. 51, 873 (1983). doi:10.1103/PhysRevLett.51.873
[301] T.W. Hagen, A. Görgen, W. Korten, L. Grente, M.-D. Salsac, F. Farget, I. Ragnarsson, T. Braunroth, B. Bruyneel *et al.*, Phys. Rev. C 95, 034302 (2017). doi:10.1103/PhysRevC.95.034302
[302] M. Rudigier, G.S. Simpson, J.M. Daugas, A. Blazhev, C. Fransen, G. Gey, M. Hackstein, J. Jolie, U. Köster, T. Malkiewicz, T. Materna, M. Pfeiffer, M. Ramdhane, J.-M. Régis, W. Rother, T. Thomas, N. Warr, D. Wilmsen, J. Le Bloas, and N. Pillet, Phys. Rev. C **87**, 064317 (2013).
[303] C. Sotty, M. Zielińska, G. Georgiev, D.L. Balabanski, A.E. Stuchbery, A. Blazhev, N. Bree, R. Chevrier, S. Das Gupta, J.M. Daugas, T. Davinson, H. De Witte, J. Diriken, L.P. Gaffney, K. Geibel, K. Hadyńska-Klęk, F.G. Kondev, J. Konki, T. Kröll, P. Morel, P. Napiorkowski, J. Pakarinen, P. Reiter, M. Scheck, M. Seidlitz, B. Siebeck, G. Simpson, H. Törnqvist, N. Warr, and F. Wenander, Phys. Rev. Lett. **115**, 172501 (2015).
[304] N.J. Stone, Atom. Data Nucl. Data Tables **90**, 75 (2005).
[305] I. Berkes, M. De Jesus, B. Hlimi, M. Massaq, E.H. Sayouty, and K. Heyde, Phys. Rev. C **44**, 104 (1991).
[306] C.R. Bingham and G.T. Fabian, Phys. Rev. C **7**, 1509 (1973).
[307] H.L. Thayer, J. Billowes, P. Campbell, P. Dendooven, K.T. Flanagan, D.H. Forest, J.A.R. Griffith, J. Huikari, A. Jokinen, R. Moore, A. Nieminen, G. Tungate, S. Zemlyanoi, and J. Äystö, J. Phys. G: Nucl. Part. Phys. **29**, 2247 (2003).
[308] F. Boulay, G.S. Simpson, Y. Ichikawa, S. Kisyov, D. Bucurescu, A. Takamine, D.S. Ahn, K. Asahi, H. Baba, D.L. Balabanski, T. Egami, T. Fujita, N. Fukuda, C. Funayama, T. Furukawa, G. Georgiev, A. Gladkov, M. Hass, K. Imamura, N. Inabe, Y. Ishibashi, T. Kawaguchi, T. Kawamura, W. Kim, Y. Kobayashi, S. Kojima, A. Kusoglu, R. Lozeva, S. Momiyama, I. Mukul, M. Niikura, H. Nishibata, T. Nishizaka, A. Odahara, Y. Ohtomo, D. Ralet, T. Sato, Y. Shimizu, T. Sumikama, H. Suzuki, H. Takeda, L.C. Tao, Y. Togano, D. Tominaga, H. Ueno, H. Yamazaki, X.F. Yang, and J.M. Daugas, Phys. Rev. Lett. **124**, 112501 (2020).
[309] P.E. Garrett, Phys. Rev. Lett. **127**, 169201 (2021).

[310] F. Boulay, G.S. Simpson, Y. Ichikawa, S. Kisyov, D. Bucurescu, A. Takamine, D.S. Ahn, K. Asahi, H. Baba, D.L. Balabanski, T. Egami, T. Fujita, N. Fukuda, C. Funayama, T. Furukawa, G. Georgiev, A. Gladkov, M. Hass, K. Imamura, N. Inabe, Y. Ishibashi, T. Kawaguchi, T. Kawamura, W. Kim, Y. Kobayashi, S. Kojima, A. Kusoglu, R. Lozeva, S. Momiyama, I. Mukul, M. Niikura, H. Nishibata, T. Nishizaka, A. Odahara, Y. Ohtomo, D. Ralet, T. Sato, Y. Shimizu, T. Sumikama, H. Suzuki, H. Takeda, L.C. Tao, Y. Togano, D. Tominaga, H. Ueno, H. Yamazaki, X.F. Yang, and J.M. Daugas, Phys. Rev. Lett. **127**, 169202 (2021).

[311] C.Y. Wu, H. Hua, D. Cline, A.B. Hayes, R. Teng, R.M. Clark, P. Fallon, A. Goergen, A.O. Macchiavelli, and K. Vetter, Phys. Rev. C **70**, 064312 (2004).

[312] P. Spagnoletti, G. Simpson, S. Kisyov, D. Bucurescu, J.-M. Régis, N. Saed-Samii, A. Blanc, M. Jentschel, U. Köster, P. Mutti, T. Soldner, G. de France, C.A. Ur, W. Urban, A.M. Bruce, C. Bernards, F. Drouet, L.M. Fraile, L.P. Gaffney, D.G. Ghiţă , S. Ilieva, J. Jolie, W. Korten, T. Kröll, S. Lalkovski, C. Larijarni, R. Licą, H. Mach, N. Mărginean, V. Paziy, Zs. Podolyák, P.H. Regan, M. Scheck, J.F. Smith, G. Thiamova, C. Townsley, A. Vancraeyenest, V. Vedia, N. Warr, V. Werner, and M. Zielińska, Phys. Rev. C **100**, 014311 (2019).

[313] W. Urban, J.A. Pinston, J. Genevey, T. Rząca-Urban, A. Złomaniec, G. Simpson, J.L. Durell, W.R. Phillips, A.G. Smith, B.J. Varley, I. Ahmad, and N. Schulz, Eur. Phys. J. A 22, 241 (2004). doi:10.1140/epja/i2004-10037-5

[314] A.G. Smith, J.L. Durell, W.R. Phillips, W. Urban, P. Sarriguren, and I. Ahmad, Phys. Rec. C **86**, 014321 (2012).

[315] A. Esmaylzadeh, J.-M. Régis, Y.H. Kim, U. Köster, J. Jolie, V. Karayonchev, L. Knafla, K. Nomura, L.M. Robledo, and R. Rodríguez-Guzmán, Phys. Rev. C **100**, 064309 (2019).

[316] S.J. Freeman, D.K. Sharp, S.A. McAllister, B.P. Kay, C.M. Deibel, T. Faestermann, R. Hertenberger, A.J. Mitchell, J.P. Schiffer, S.V. Szwec, J.S. Thomas, and H.-F. Wirth, Phys. Rev. C **96**, 054325 (2017).

[317] Ł.W. Iskra, S. Leoni, B. Fornal, C. Michelagnoli, F. Kandzia, N. Marginean, M. Barani, S. Bottoni, N. Cieplicka-Oryńczak, G. Colombi *et al.*, Phys. Rev. C 102, 054324 (2020).

[318] W. Urban, M. Czerwiński, J. Kurpeta, T. Rząca-Urban, J. Wiśniewski, T. Materna, Ł.W. Iskra, A.G. Smith, I. Ahmad, A. Blanc*et al.*,Phys. Rev. C 96, 044333 (2017). doi:10.1103/PhysRevC.96.044333

[319] J. Ha, T. Sumikama, F. Browne, N. Hinohara, A.M. Bruce, S. Choi, I. Nishizuka, S. Nishimura, P. Doornenbal *et al.*, Phys. Rev. C 101, 044311 (2020). doi:10.1103/PhysRevC.101.044311

[320] M. Zielińska, T. Czosnyka, J. Choiński, J. Iwanicki, P.J. Napiorkowski, J. Srebrny, Y. Toh, M. Oshima, A. Osa, Y. Utsuno *et al.*, Nucl. Phys. A 712, 3 (2002). doi:10.1016/S0375-9474(02)01169-7

[321] S.J. Freeman, D.K. Sharp, S.A. McAllister, B.P. Kay, C.M. Deibel, T. Faestermann, R. Hertenberger, A.J. Mitchell, J.P. Schiffer, S.V. Szwec, J.S. Thomas, and H.-F. Wirth, Phys. Rev. C **96**, 054325 (2017).

[322] J. Stachel, P. Van Isacker and K. Heyde, Phys. Rev. C **25**, 650 (1982).

[323] I. Stefanescu, A. Gelberg, J. Jolie, P. Van Isacker, P. von Brentano, Y.X. Luo, S.J. Zhu, J.O. Rasmussen, J.H. Hamilton, A.V. Ramayya, X.L. Che, Nucl. Phys. A 789, 125 (2007).

[324] A. Giannatiempo, A. Nannini, P. Sona, D. Cutoiu, Phys. Rev. C 52, 2969 (1995).

[325] J.L.M. Duarte, T. Borello-Lewin, G. Maino, L. Zuffi, Phys. Rev. C 57, 1539 (1998).

[326] H. Duckwitz, M. Pfeiffer, M. Albers, C. Bernards, C. Fransen, J. Jolie, P. Petkov, D. Radeck, T. Thomas, and K.O. Zell, Nucl. Phys. **A903**, 18 (2013).

[327] J. Stachel, N. Kaffrell, E. Grosse, H. Emling, H. Folger, R. Kulessa, and D. Schwalm, Nucl. Phys. **A383**, 429 (1982).

[328] M. Sugita and A. Arima, Nucl. Phys. **A515**, 77 (1990).

[329] W. Urban, M. Jentschel, R.F. Casten, J. Jolie, Ch. Bernards, B. Maerkisch, Th. Materna, P. Mutti, L. Próchniak, T. Rząca-Urban, G.S. Simpson, V. Werner, and S. Ahmed, Phys. Rev. C **87**, 031304(R) (2013).

[330] J. Blachot, Nucl. Data Sheets 108, 2035 (2007).

[331] B. Singh, Nucl. Data Sheets 109, 297 (2008).

[332] D. De Frenne, Nucl. Data Sheets 110, 1745 (2009).

[333] H. Mach, F.K. Wohn, G. Molnár, K. Sistemich, John C. Hill, M. Moszyński, R.L. Gill, W. Krips, and D.S. Brenner, Nucl. Phys. A 523, 197 (1991). doi:10.1016/0375-9474(91)90001-M

[334] D. De Frenne, Nucl. Data Sheets 109, 943 (2008).

[335] L.K. Peker and M.E. Voichansky, Izv. Akad. Nauk SSSR Ser Fiz. **32**, 892 (1968).

[336] G. Gneuss and W. Greiner, Nucl. Phys. **A171**, 449 (1971).

[337] R. Meyer and L. Peker, Z. Phys. **A283**, 379 (1977).
[338] H.W. Fielding, R.E. Anderson, C.D. Zafiratos, D.A. Lind F.E. Cecil, H.H. Wieman, and W.P. Alford, Nucl. Phys. **A281**, 389 (1977).
[339] D.K. Sharp, S.J. Freeman, B.D. Cropper, P.J. Davies, T. Faestermann, T.M. Hatfield, R. Hertenberger, S.J.F. Hughes, P.T. MacGregor, and H.-F. Wirth, Phys. Rev. C **100**, 024329 (2019).
[340] K. Heyde, P. Van Isacker, M. Waroquier, G. Wenes, and M. Sambataro, Phys. Rev. **C25**, 3160 (1982).
[341] K. Heyde, P. Van Isacker, R.F. Casten, and J.L. Wood, Phys. Lett. **155B**, 303 (1985).
[342] P. Martin, J.B. Viano, J.M. Loiseaux, and Y. Le Chalony, Nucl. Phys. **A212**, 304 (1973).
[343] J. Kumpulainen, R. Julin, J. Kantele, A. Passoja, W.H. Trzaska, E. Verho, and J. Vaaramaki, Z. Phys. **A335**, 109 (1990).
[344] J. Kumpulainen, R. Julin, J. Kantele, A. Passoja, W.H. Trzaska, E. Verho, J. Vaaramaki, D. Cutoiu, and M. Ivascu, Phys. Rev. C **45**, 640 (1992).
[345] J. Kern, A. Bruder, S. Drissi, V.A. Ionescu, and D. Kusnezov, Nucl. Phys. **A512**, 1 (1990).
[346] M. Délèze, S. Drissi, J. Kern, P.A. Tercier, J.-P. Vorlet, J. Rikovska, T. Otsuka, S. Judge, and A. Williams, Nucl. Phys. **A551**, 269 (1993).
[347] M. Délèze, S. Drissi, J. Jolie, J. Kern, and J.-P. Vorlet, Nucl. Phys. **A554**, 1 (1993).
[348] S. Drissi, P.A. Tercier, H.G. Börner, M. Délèze, F. Hoyler, S. Judge, J. Kern, S.J. Mannanal, G. Mouze, K. Schreckenbach, J-.P. Vorlet, N. Warr, A. Williams, and C. Ythier, Nucl. Phys. **A614**, 137 (1997).
[349] A. Gade, A. Fitzler, C. Fransen, J. Jolie, S. Kasemann, H. Klein, A. Linnemann, V. Werner, P. von Brentano, Phys. Rev. C **66**, 034311 (2002).
[350] S. Juutinen, R. Julin, P. Jones, A. Lampinen, G. Lhersonneau, E. Mäkelä, M. Piiparinen, A. Savelius, and S. Törmänen, Phys. Lett. **B386**, 80 (1996).
[351] I. Thorslund, C. Fahlander, J. Nyberg, S. Juutinen, R. Julin, M. Piiparinen, R. Wyss, A. Lampinen, T. Lönnroth, D. Müller, S. Törmänen, A. Virtanen, Nucl. Phys. **A564**, 285 (1993).
[352] I. Thorslund, C. Fahlander, J. Nyberg, M. Piiparinen, R. Julin, S. Juutinen, A. Virtanen, D. Müller, H. Jensen, and M. Sugawara, Nucl. Phys. **A568**, 306 (1994).
[353] A. Linnemann, Ph.D. thesis, Universität zu Köln, 2005 (unpublished).
[354] F. Corminboeuf, T.B. Brown, L. Genilloud, C.D. Hannant, J. Jolie, J. Kern, N. Warr, and S.W. Yates, Phys. Rev. Lett. **84**, 4060 (2000).
[355] F. Corminboeuf, T.B. Brown, L. Genilloud, C.D. Hannant, J. Jolie, J. Kern, N. Warr, and S.W. Yates, Phys. Rev. C **63**, 014305 (2000).
[356] P.E. Garrett, J. Bangay, A. Diaz Varela, G.C. Ball, D.S. Cross, G.A. Demand, P. Finlay, A.B. Garnsworthy, K.L. Green, G. Hackman, C.D. Hannant, B. Jigmeddorj, J. Jolie, W.D. Kulp, K.G. Leach, J.N. Orce, A.A. Phillips, A.J. Radich, E.T. Rand, M.A. Schumaker, C.E. Svensson, C. Sumithrarachchi, S. Triambak, N. Warr, J. Wong, J.L. Wood, and S.W. Yates, Phys. Rev. C **86**, 044304 (2012).
[357] H. Lehmann, P.E. Garrett, J. Jolie, C.A. McGrath, Minfang Yeh, and S.W. Yates, Phys. Lett. B **387**, 259 (1996).
[358] P.E. Garrett, H. Lehmann, J. Jolie, C.A. McGrath, M. Yeh, W. Younes, and S.W. Yates, Phys. Rev. C **64**, 024316 (2001).
[359] P.E. Garrett, K.L. Green, H. Lehmann, J. Jolie, C.A. McGrath, M. Yeh, and S.W. Yates, Phys. Rev. **75**, 054310 (2007).
[360] D. Bandyopadhyay, S.R. Lesher, C. Fransen, N. Boukharouba, P.E. Garrett, K.L. Green, M.T. McEllistrem, and S.W. Yates, Phys. Rev. C **76**, 054308 (2007).
[361] M. Kadi, N. Warr, P.E. Garrett, J. Jolie, and S.W. Yates, Phys. Rev. C **68**, 031306(R) (2003).
[362] T.Belgya, G.Molnár, and S.W.Yates, Nucl. Phys. **A607**, 43 (1996).
[363] P.E. Garrett, T.R. Rodriguez, A. Diaz Varela, K.L. Green, J. Bangay, A. Finlay, R.A.E. Austin, G.C. Ball, D.S. Bandyopadhyay, V. Bildstein, S. Colosimo, D.S. Cross, G.A. Demand, P. Finlay, A.B. Garnsworthy, G.F. Grinyer, G. Hackman, B. Jigmeddorj, J. Jolie, W.D. Kulp, K.G. Leach, A.C. Morton, J.N. Orce, C.J. Pearson, A.A. Phillips, A.J. Radich, E.T. Rand, M.A. Schumaker, C.E. Svensson, C. Sumithrarachchi, S. Triambak, N. Warr, J. Wong, J.L. Wood, and S.W. Yates, Phys. Rev. Lett. **123**, 142502 (2019).
[364] A. Aprahamian, D.S. Brenner, R.F. Casten, R.L. Gill, A. Piotrowski, and K. Heyde, Phys. Lett. **B140**, 22 (1984).

[365] A. Aprahamian, D.S. Brenner, R.F. Casten, R.L. Gill, and A. Piotrowski, Phys. Rev. Lett. **59**, 535 (1987).
[366] H. Mach, M. Moszyński, R.F. Casten, R.L. Gill, D.S. Brenner, J.A. Winger, W. Krips, C. Wesselborg, M. Büscher, F.K. Wohn, A. Aprahamian, D. Alburger, A. Gelberg, and A. Piotrowski, Phys. Rev. Lett. **63**, 143 (1989).
[367] K. Kitao, Y. Tendow and A. Hashizume, Nucl. Data Sheets **96**, 241 (2002).
[368] Y. Wang, S. Rinta-Antila, P. Dendooven, J. Huikari, A. Jokinen, V.S. Kolhinen, G. Lhersonneau, A. Nieminen, S. Nummela, H. Penttilä, K. Peräjärvi, J. Szerypo, J.C. Wang, and J. Äystö, Phys. Rev. C **67**, 064303 (2003).
[369] J.C. Batchelder, N.T. Brewer, R.E. Goans, R. Grzywacz, B.O. Griffith, C. Jost, A. Korgul, S.H. Liu, S.V. Paulauskas, E.H. Spejewski, and D.W. Stracener, Phys. Rev. C **86**, 064311 (2012).
[370] K.L. Green, P.E. Garrett, R.A.E. Austin, G.C. Ball, D.S. Bandyopadhyay, S. Colosimo, D. Cross, G.A. Demand, G.F. Grinyer, G. Hackman, W.D. Kulp, K.G. Leach, A.C. Morton, C.J. Pearson, A.A. Phillips, M.A. Schumaker, C.E. Svensson, J. Wong, J.L. Wood, S.W. Yates, Phys. Rev. C **80**, 032502 (2009).
[371] Deepika Choudhury, A.K. Jain, M. Patial, N. Gupta, P. Arumugam, A. Dhal, R.K. Sinha, L. Chaturvedi, P.K. Joshi, T. Trivedi, R. Palit, S. Kumar, R. Garg, S. Mandal, D. Negi, G. Mohanto, S. Muralithar, R.P. Singh, N. Madhavan, R.K. Bhowmik, and S.C. Pancholi, Phys. Rev. C **82**, 061308(R) (2010).
[372] M. Kumar Raju, D. Negi, S. Muralithar, R.P. Singh, J.A. Sheikh, G.H. Bhat, R. Kumar, Indu Bala, T. Trivedi, A. Dhal, K. Rani, R. Gurjar, D. Singh, R. Palit, B.S. Naidu, S. Saha, J. Sethi, R. Donthi, and S. Jadhav, Phys. Rev. C **91**, 024319 (2015).
[373] Deepika Choudhury, A.K. Jain, G. Anil Kumar, Suresh Kumar, Sukhjeet Singh, P. Singh, M. Sainath, T. Trivedi, J. Sethi, S. Saha, S.K. Jadav, B.S. Naidu, R. Palit, H.C. Jain, L. Chaturvedi, and S.C. Pancholi, Phys. Rec. **87**, 034304 (2013).
[374] Y.X. Luo, J.O. Rasmussen, C.S. Nelson, J.H. Hamilton, A.V. Ramayya, J.K. Hwang, S.H. Liu, C. Goodin, N.J. Stone, S.J. Zhu, N.T. Brewer, Ke Li, I.Y. Lee, G.M. Ter-Akopian, A.V. Danielag, M.A. Stoyer, R. Donangelo, W.C. Ma, and J.D. Cole, Nucl. Phys. **A874**, 32 (2012).
[375] A.E. Stuchbery, S.K. Chamoli, and T. Kibédi, Phys. Rev. C **93**, 031302(R) (2016).
[376] B.J. Coombes, A.E. Stuchbery, A. Blazhev, H. Grawe, M.W. Reed, A. Akber, J.T.H. Dowie, M.S.M. Gerathy, T.J. Gray, T. Kibedi, A.J. Mitchell, T. Palazzo, Phys. Rev. C **100**, 024322 (2019).
[377] J. Meyer-ter-Vehn, Nucl. Phys. **A249**, 111 (1975).
[378] J. Meyer-ter-Vehn, Nucl. Phys. **A249**, 141 (1975).
[379] J. Gizon, A. Gizon, and J. Meyer-ter-Vehn, Nucl. Phys. **A277**, 464 (1977).
[380] P. Guazzoni, L. Zetta, A. Covello, A. Gargano, B.F. Bayman, G. Graw, R. Hertenberger, H.-F. Wirth, and M. Jaskóla, Phys. Rev. C **74**, 054605 (2006).
[381] P. Guazzoni, L. Zetta, A. Covello, A. Gargano, B.F. Bayman, G. Graw, R. Hertenberger, H.-F. Wirth, T. Faestermann, and M. Jaskóla Phys. Rev. C **85**, 054609 (2012).
[382] P. Guazzoni, L. Zetta, A. Covello, A. Gargano, G. Graw, R. Hertenberger, H.-F. Wirth, and M. Jaskóla Phys. Rev. C **69**, 024619 (2004).
[383] P. Guazzoni, L. Zetta, A. Covello, A. Gargano, B.F. Bayman, T. Faestermann, G. Graw, R. Hertenberger, H.-F. Wirth, and M. Jaskóla Phys. Rev. C **83**, 044614 (2011).
[384] P. Guazzoni, L. Zetta, A. Covello, A. Gargano, B.F. Bayman, T. Faestermann, G. Graw, R. Hertenberger, H.-F. Wirth, and M. Jaskóla Phys. Rev. C **78**, 064608 (2008).
[385] P. Guazzoni, M. Jaskóla, L. Zetta, A. Covello, A. Gargano, Y. Eisermann, G. Graw, R. Hertenberger, A. Metz, F. Nuoffer, and G. Staudt, Phys. Rev. C **60**, 054603 (1999).
[386] J.H. Bjerregaard, O. Hansen, O. Nathan, R. Chapman, and S. Hinds, Nucl. Phys. **A131**, 481 (1969).
[387] J.H. Bjerregaard, O. Hansen, O. Nathan, R. Chapman, and S. Hinds, Nucl. Phys. **A110**, 1 (1968).
[388] J. Bron, W.H.A. Hesselink, A. Vanpoelgest, J.J.A. Zalmstra, M.J. Uitzinger, H. Verheul, K. Heyde, M. Waroquier, H. Vincx, P. Van Isacker, Nucl. Phys. **A318**, 335 (1979).
[389] R. Wadsworth, H.R. Andrews, C.W. Beausang, R.M. Clark, J. DeGraaf, D.B. Fossan, A. Galindo-Uribarri, I.M. Hibbert, K. Hauschild, J.R. Hughes, V.P. Janzen, D.R. LaFosse, S.M. Mullins, E.S. Paul, L. Persson, S. Pilotte, D.C. Radford, H. Schnare, P. Vaska, D. Ward, J.N. Wilson, I. Ragnarsson, Phys. Rev. C **50** 483 (1994).
[390] R. Wadsworth, H.R. Andrews, R.M. Clark, D.B. Fossan, A. Galindo-Uribarri, J.R. Hughes, V.P. Janzen,

D.R. Lafosse, S.M. Mullins, E.S. Paul, D.C. Radford, H. Schnare, P. Vaska, D. Ward, J.N. Wilson, R. Wyss, Nucl. Phys. **A559**, 461 (1993).

[391] M. Wolińska-Cichocka, J. Kownacki, W. Urban, E. Ruchowska, W.A. Płóciennik, B. Bekman, Ch. Droste, W. Gast, R. Lieder, W. Męczyński, M. Kisieliński, A. Kordyasz, M. Kowalczyk, P. Kowina, J. Iwanicki, T. Morek, J. Perkowski, J. Srebrny, A. Stolarz, and J. Styczeń, Eur. Phys. J. **A24**, 259 (2005).

[392] H. Harada, T. Murakami, K. Yoshida, J. Kasagi, T. Inamura, T. Kubo, Phys. Lett. **B207**, 17 (1988).

[393] M. Schimmer, S. Albers, A. Dewald, A. Gelberg, R. Wirowski, P. von Brentano, Nucl. Phys. **A539**, 527 (1992).

[394] R. Wadsworth, R.M. Clark, J.A. Cameron, D.B. Fossan, I.M. Hibbert, V.P. Janzen, R. Krücken, G.J. Lane, I.Y. Lee, A.O. Macchiavelli, C.M. Parry, J.M. Sears, J.F. Smith, A.V. Afanasjev, I. Ragnarsson, Phys. Rev. Lett. **80**, 1174 (1998).

[395] J. Gableske, A. Dewald, H. Tiesler, M. Wilhelm, T. Klemme, O. Vogel, I. Schneider, R. Peusquens, S. Kasemann, K.O. Zell, P. von Brentano, P. Petkov, D. Bazzacco, C. Rossi Alvarez, S. Lunardi, G. de Angelis, M. de Poli, C. Fahlander, Nucl. Phys. **A691**, 551 (2001).

[396] A. Bäcklin, N.G. Jonsson, R. Julin, J. Kantele, M. Lountama, A. Passoja, and T. Poikolainen, Nucl. Phys. **A351**, 490, (1981).

[397] M. Spieker, P. Petkov, E. Litvinova, C. Müller-Gatermann, S.G. Pickstone, S. Prill, P. Scholz, and A. Zilges, Phys. Rev. C **97**, 054319 (2018).

[398] S. Ganguly, P. Banerjee, I. Ray, R. Kshetri, R. Raut, S. Bhattacharya, M. Saha-Sarkar, A. Goswami, S. Mukhopadhyay, A. Mukherjee, G. Mukherjee, S.K. Basu, Nucl. Phys. **A789**, 1 (2007).

[399] C.M. Petrache, J.-M. Régis, C. Andreoiu, M. Spieker, C. Michelagnoli, P.E. Garrett, A. Astier, E. Dupont, F. Garcia, S. Guo, G. Häfner, J. Jolie, F. Kandzia, V. Karayonchev, Y.-H. Kim, L. Knafla, U. Köster, B.F. Lv, N. Marginean, C. Mihai, P. Mutti, K. Ortner, C. Porzio, S. Prill, N. Saed-Samii, W. Urban, J.R. Vanhoy, K. Whitmore, J. Wisniewski, and S.W. Yates, Phys. Rev. C **99**, 024303 (2019).

[400] N.-G. Jonsson, A. Bäcklin, R. Julin, J. Kantele, M. Migahed, Institute of Physics, University of Uppsala, UUIP-1000 report (1979).

[401] K. Ortner, C. Andreoiu, M. Spieker, G.C. Ball, N. Bernier, H. Bidaman, V. Bildstein, M. Bowry, D.S. Cross, M.R. Dunlop, R. Dunlop, F.H. Garcia, A.B. Garnsworthy, P.E. Garrett, J. Henderson, J. Measures, B. Olaizola, J. Park, C.M. Petrache, J.L. Pore, K. Raymond, J.K. Smith, D. Southall, C.E. Svensson, M. Ticu, J. Turko, K. Whitmore, and T. Zidar, Phys. Rev. C **102**, 024323 (2020).

[402] T. Togashi, Y. Tsunoda, T. Otsuka, N. Shimizu, and M. Honma, Phys. Rev. Lett. **121**, 062501 (2018).

[403] J. Rikovska, N.J. Stone, P.M. Walker and W.B. Walters, Nucl. Phys. **A505**, 145 (1989).

[404] J.R. Vanhoy, R.T. Coleman, K.A. Crandell, S.F. Hicks, B.A. Sklaney, M.M. Walbran, N.V. Warr, J. Jolie, F. Corminboeuf, L. Genilloud, J. Kern, J.-L. Schenker, P.E. Garrett, Phys. Rev. C **68**, 034315 (2003).

[405] S.F. Hicks, G.K. Alexander, C.A. Aubin, M.C. Burns, C.J. Collard, M.M. Walbran, J.R. Vanhoy, E. Jensen, P.E. Garrett, M. Kadi, A. Martin, N. Warr, and S.W. Yates, Phys. Rev. C **71**, 034307 (2005).

[406] C. Mihai, A.A. Pasternak, D. Filipescu, M. Ivaşcu, D. Bucurescu, G. Căta-Danil, I. Căta-Danil, D. Deleanu, D.G. Ghiţă, T. Glodariu, Yu.N. Lobach, N. Mărginean, R. Mărginean, A. Negret, S. Pascu, T. Sava, L. Stroe, G. Suliman, and N.V. Zamfir, Phys. Rev. C **81**, 034314 (2010).

[407] T. von Egidy, H.-F. Wirth, I. Tomandl, and J. Honzátko, Phys. Rev. C **74**, 034319 (2006).

[408] R. Georgii, T. von Egidy, J. Klora, H. Lindner, U. Mayerhofer, J. Ott, W. Schauer, P. von Neumann-Cosel, A. Richter, C. Schlegel, R. Schulz, V.A. Khitrov, A.M. Sukhovoj, A.V. Vojnov, J. Berzins, V. Bondarenko, P. Prokofjevs, L.J. Simonova, M. Grinberg, Ch. Stoyanov, Nucl. Phys. **A592**, 307 (1995).

[409] C. Doll, H. Lehmann, H.G. Börner, and T. von Egidy, Nucl. Phys. **A672**, 3 (2000).

[410] M. Matoba, M. Hyakutake, K. Yagi, and Y. Aoki, Nucl. Phys. **A237**, 260 (1975).

[411] N. Kaffrell, P. Hill, J. Rogowski, H. Tetzlaff, N. Trautmann, E. Jacobs, P. De Gelder, D. De Frenne, K. Heyde, G. Skarnemark, J. Alstad, N. Blasi, M.N. Harakeh, W.A. Sterrenburg, K. Wolfsberg, Nucl. Phys. **A460**, 437 (1986).

[412] N. Kaffrell, P. Hill, J. Rogowski, H. Tetzlaff, N. Trautmann, E. Jacobs, P. de Gelder, D. de Frenne, K. Heyde, S. Börjesson, G. Skarnemark, J. Alstad, N. Blasi, M.N. Harakeh, W.A. Sterrenburg, K. Wolfsberg, Nucl. Phys. **A470**, 141 (1987).

[413] J. Rogowski, N. Kaffrell, D. De Frenne, K. Heyde, E. Jacobs, M.N. Harakeh, J.M. Schippers, S.Y. van der

Werf, Phys. Lett. **207B**, 125 (1988).
[414] J. Rogowski, J. Alstad, M.M. Fowler, D. De Frenne, K. Heyde, E. Jacobs, N. Kaffrell, G. Skarnemark, N. Trautmann, Z. Phys. **A337**, 233 (1990).
[415] G. Lhersonneau, B. Pfeiffer, J. Alstad, P. Dendooven, K. Eberhardt, S. Hankonen, I. Klöck, K.-L. Kratz, A. Nähler, R. Malmbeck, J.P. Omtvedt, H. Penttilä, S. Schoedder, G. Skarnemark, N. Trautmann, J. Äystö, Eur. Phys. J. **A1**, 285 (1998).
[416] J. Äystö, C.N. Davids, J. Hattula, J. Honkanen, K. Honkanen, P. Jauho, R. Julin, S. Juutinen, J. Kumpulainen, T. Lönnroth, A. Pakkanen, A. Passoja, H. Penttilä, P. Taskinen, E. Verho, A. Virtanen, M. Yoshii, Nucl. Phys. **A480**, 104 (1988).
[417] G. Lhersonneau, J.C. Wang, S. Hankonen, P. Dendooven, P. Jones, R. Julin, J. Äystö, Phys. Rev. C **60**, 014315 (1999).
[418] G. Lhersonneau, Y. Wang, R. Capote, J. Suhonen, P. Dendooven, J. Huikari, K. Peräjärvi, and J.C. Wang, Phys. Rev. C **67**, 024303 (2003).
[419] F.M. Prados-Estévez, E.E. Peters, A. Chakraborty, M.G. Mynk, D. Bandyopadhyay, N. Boukharouba, S.N. Choudry, B.P. Crider, P.E. Garrett, S.F. Hicks, A. Kumar, S.R. Lesher, C.J. McKay, M.T. McEllistrem, S. Mukhopadhyay, J.N. Orce, M. Scheck, J.R. Vanhoy, J.L. Wood, S.W. Yates, Phys. Rev. C **95**, 034328 (2017).
[420] E.E. Peters, F.M. Prados-Estévez, A. Chakraborty, M.G. Mynk, D. Bandyopadhyay, N. Boukharouba, S.N. Choudry, B.P. Crider, P.E. Garrett, S.F. Hicks, A. Kumar, S.R. Lesher, C.J. McKay, M.T. McEllistrem, S. Mukhopadhyay, J.N. Orce, M. Scheck, J.R. Vanhoy, J.L. Wood, and S.W. Yates, Eur. Phys. J. **A52**, 96 (2016).
[421] G.G. Colvin, F. Hoyler, S.J. Robinson, J. Phys. G **13**, 191 (1987).
[422] L.E. Svensson, Ph.D. thesis, *Coulomb excitation of vibrational nuclei*, Uppsala University, unpublished (1989).
[423] M. Luontama, R. Julin, J. Kantele, A. Passoja, W. Trzaska, A. Backlin, N.-G. Jonsson, L. Westerberg, Z. Phys. **A324**, 317 (1986).
[424] S. Hinds, J.H. Bjerregaard, O. Hansem, and O. Nathan, Phys. Lett. **14**, 48 (1965).
[425] J.H. Bjerregaard, O. Hansen, O. Nathan, and S. Hinds, Nucl. Phys. **86**, 145 (1966).
[426] P. Debenham and N.M. Hintz, Phys. Rev. Lett. **25**, 44 (1970).
[427] P.Debenham and N.M.Hintz, Nucl. Phys. **A195**, 385 (1972).
[428] W. McLatchie, J.E. Kitching and W. Darcey, Phys. Lett. **B30**, 529 (1969).
[429] W. McLatchie, J.E. Kitching and W. Darcey, Nucl. Phys. **A159**, 615 (1970).
[430] W. Oelert, G. Lindström and V. Reich, Nucl. Phys. **A233**, 237 (1974).
[431] J.R. Maxwell, G.M. Reynolds, and N.M. Hintz, Phys. Rev. **151**, 1000 (1966).
[432] R. Chapman, W. McLatchie and J.E. Kitching, Nucl. Phys. **A186**, 603 (1972).
[433] Th.W. Elze, J.S. Boyno and J.R. Huizenga, Nucl. Phys. **A187**, 473 (1972).
[434] D.G. Fleming, C. Günther, G. Hagemann, B. Herskind and P.O. Tjøm, Phys. Rev. C **8**, 806 (1973).
[435] M.A.M. Shahabuddin, D.G. Burke, I. Nowikow and J.C. Waddington, Nuci. Phys. **A340**, 109 (1980).
[436] G. Løvhøiden, T.F. Thorsteinsen, E. Andersen, M.F. Kiziltan and D.G. Burke, Nucl. Phys. **A494**, 157 (1989).
[437] J.J. Kolata and M. Oothoudt, Phys. Rev. C **15**, 1947 (1977).
[438] D.G. Burke, G. Løvhøiden, and T.F. Thorsteinsen, Nucl. Phys **A483**, 221 (1988).
[439] Tao Qu and D.G. Burke, Can. J. Phys. **70**, 1236 (1992).
[440] S.P. Bvumbi, J.F. Sharpey-Schafer, P.M. Jones, S.M. Mullins, B.M. Nyakó, K. Juhász, R.A. Bark, L. Bianco, D. M. Cullen, D. Curien, P.E. Garrett, P.T. Greenlees, J. Hirvonen, U. Jakobsson, J. Kau, F. Komati, R. Julin, S. Juutinen, S. Ketelhut, A. Korichi, E.A. Lawrie, J.J. Lawrie, M. Leino, T.E. Madiba, S.N.T. Majola, P. Maine, A. Minkova, N.J. Ncapayi, P. Nieminen, P. Peura, P. Rahkila, L.L. Riedinger, P. Ruotsalainen, J. Saren, C. Scholey, J. Sorri, S. Stolze, J. Timar, J. Uusitalo, and P.A. Vymers, Phys. Rev. C 87, 044333 (2013).
[441] S.N.T. Majola, Z. Shi, B.Y. Song, Z.P. Li, S.Q. Zhang, R.A. Bark, J.F. Sharpey-Schafer, D.G. Aschman, S.P. Bvumbi, T.D. Bucher, D.M. Cullen, T.S. Dinoko, J.E. Easton, N. Erasmus, P. T. Greenlees, D.J. Hartley, J. Hirvonen, A. Korichi, U. Jakobsson, P. Jones, S. Jongile, R. Julin, S. Juutinen, S. Ketelhut, B.V. Kheswa, N.A. Khumalo, E.A. Lawrie, J.J. Lawrie, R. Lindsay, T.E. Madiba, L. Makhathini, S.M. Maliage, B. Maqabuka, K.L. Malatji, P.L. Masiteng, P.I. Mashita, L. Mdletshe, A. Minkova, L. Msebi, S.M. Mullins, J. Ndayishimye, D. Negi, A. Netshiya, R. Newman, S.S. Ntshangase, R. Ntshodu, B.M. Nyakó, P. Papka, P. Peura, P. Rahkila, L.L. Riedinger, M.A. Riley, D.G. Roux, P. Ruotsalainen, J.J. Saren, C. Scholey, O. Shirinda, M.A. Sithole, J. Sorri,

M. Stankiewicz, S. Stolze, J. Timár, J. Uusitalo, P. A. Vymers, M. Wiedeking, and G.L. Zimba, Phys. Rev. C **100**, 044324 (2019).
[442] F. Iachello *et al.*, Phys. Rev. Lett. **81**, 1191 (1998).
[443] N.V. Zamfir *et al.*, Phys. Rev. C **60**, 054312 (1999).
[444] R.F. Casten *et al.*, Phys. Rev. Lett. **82**, 5000 (1999).
[445] F. Iachello, Phys. Rev. Lett. **87**, 052502 (2001).
[446] R.F. Casten *et al.*, Phys. Rev. Lett. **87**, 052503 (2001)
[447] K. Heyde *et al.*, Phys. Rev. C **69**, 054304 (2004).
[448] P. Cejnar, J. Jolie, and R.F. Casten, Rev. Mod. Phys. **82**, 2155 (2010).
[449] W.D. Kulp, J.L. Wood, K.S. Krane, J. Loats, P. Schmelzenbach, C.J. Stapels, R.-M. Larimer, and E.B. Norman, Phys. Rev. Lett. **91**, 102501 (2003).
[450] W.D. Kulp, J.L. Wood, K.S. Krane, J. Loats, P. Schmelzenbach, C.J. Stapels, R.-M. Larimer, and E.B. Norman, Phys. Rev. C **69**, 064309 (2004).
[451] W. D. Kulp, J.L. Wood, J.M. Allmond, J. Eimer, D. Furse, K.S. Krane, J. Loats, P. Schmelzenbach, C.J. Stapels, R.-M. Larimer, E.B. Norman, and A. Piechaczek, Phys. Rev. C **76**, 034319 (2007).
[452] W.D. Kulp *et al.*, arXiv:0706.4129 (2007).
[453] C.R. Hirning and D.G. Burke, Can. J. Phys. 55, 77 (1977).
[454] D.E. Nelson, D.G. Burke, J.C. Waddington, and W.B. Cook, Can. J. Phys. **51**, 2000 (1973).
[455] I. Ragnarsson and R.A. Broglia, Nucl. Phys. **A263**, 315 (1976).
[456] S.N.T. Majola, Z. Shi, B.Y. Song, Z.P. Li, S.Q. Zhang, R.A. Bark, J.F. Sharpey-Schafer, D.G. Aschman, S.P. Bvumbi, T.D. Bucher, D.M. Cullen, T.S. Dinoko, J.E. Easton, N. Erasmus, P.T. Greenlees, D.J. Hartley, J. Hirvonen, A. Korichi, U. Jakobsson, P. Jones, S. Jongile, R. Julin, S. Juutinen, S. Ketelhut, B.V. Kheswa, N.A. Khumalo, E.A. Lawrie, J.J. Lawrie, R. Lindsay, T.E. Madiba, L. Makhathini, S.M. Maliage, B. Maqabuka, K.L. Malatji, P.L. Masiteng, P.I. Mashita, L. Mdletshe, A. Minkova, L. Msebi, S.M. Mullins, J. Ndayishimye, D. Negi, A. Netshiya, R. Newman, S.S. Ntshangase, R. Ntshodu, B.M. Nyako, P. Papka, P. Peura, P. Rahkila, L.L. Riedinger, M.A. Riley, D.G. Roux, P. Ruotsalainen, J.J. Saren, C. Scholey, O. Shirinda, M.A. Sithole, J. Sorri, M. Stankiewicz, S. Stolze, J. Timar, J. Uusitalo, P.A. Vymers, M. Wiedeking, G.L. Zimba, Phys. Rev. C **100**, 044324 (2019).
[457] D.J. Hartley, L.L. Riedinger, R.V.F. Janssens, S.N.T. Majola, M.A. Riley, J.M. Allmond, C.W. Beausang, M.P. Carpenter, C.J. Chiara, N. Cooper, D. Curien, B.J.P. Gall, P.E. Garrett, F.G. Kondev, W.D. Kulp, T. Lauritsen, E.A. McCutchan, D. Miller, S. Miller, J. Piot, N. Redon, J.F. Sharpey-Schafer, J. Simpson, I. Stefanescu, X. Wang, V. Werner, J.L. Wood, C.-H. Yu, S. Zhu, J. Dudek, Physl Rev. C **95**, 014321 (2017).
[458] J.F.Sharpey-Schafer, R.A.Bark, S.P.Bvumbi, E.A.Lawrie, J.J.Lawrie, T.E.Madiba, S.N.T.Majola, A.Minkova, S.M.Mullins, P.Papka, D.G.Roux, J.Timar, Nucl. Phys. **A834**, 45c (2010).
[459] J.F. Sharpey-Schafer, S.M. Mullins, R.A. Bark, J. Kau, F. Komati, E.A. Lawrie, J.J. Lawrie, T.E. Madiba, P. Maine, A. Minkova, S.H.T. Murray, N.J.Ncapayi, P.A.Vymers, Eur. Phys. J. **A47**, 5 (2011).
[460] J.F. Sharpey-Schafer, T.E. Madiba, S.P. Bvembi, E.A. Lawrie, J.J. Lawrie, A. Minkova, S.M. Mullins, P. Papka, G.D. Roux, and J. timar, Eur. Phys. J. **A47**, 6 (2011).
[461] J.F. Sharpey-Schafer, R.A. Bark, S.P. Bvumbi, T.R.S. Dinoko, and S.N.T. Majola, Eur.Phys.J. A 55, 15 (2019).
[462] T. Hayakawa, M. Oshima, Y. Hatsukawa, J. Katakura, H. Iimura, M. Matsuda, N. Shinohara, Y. Toh, S. Mitarai, T. Shizuma, M. Sugawara, and H. Kusakari, Eur. Phys. J. **A9**, 153 (2000).
[463] S.N.T. Majola, R.A. Bark, L. Bianco, T.D. Bucher, S.P. Bvumbi, D.M. Cullen, P.E. Garrett, P.T. Greenlees, D. Hartley, J. Hirvonen, U. Jakobsson, P.M. Jones, R. Julin, S. Juutinen, S. Ketelhut, B.V. Kheswa, A. Korichi, E.A. Lawrie, P.L. Masiteng, B. Maqabuka, L. Mdletshe, A. Minkova, J. Ndayishimye, P. Nieminen, R. Newman, B.M. Nyakó, S.S. Ntshangase, P. Peura, P. Rahkila, L.L. Riedinger, M. Riley, D. Roux, P. Ruotsalainen, J. Saren, J.F. Sharpey-Schafer, C. Scholey, O. Shirinda, A. Sithole, J. Sorri, S. Stolze, J. Timár, J. Uusitalo, and G. Zimba, Phys. Rev. C **100**, 034322 (2019).
[464] P.E. Garrett, W.D. Kulp, J.L. Wood, D. Bandyopadhyay, S. Choudry, D. Dashdorj, S.R. Lesher, M.T. McEllistrem, M. Mynk, J.N. Orce, and S.W. Yates, Phys. Rev. Lett. **103**, 062501 (2009).
[465] J. Bonn, G. Huber, H. Kluge, L. Kluger, and E. Otten, Phys. Lett. B **38**, 308 (1972).
[466] T. Kühl, P. Dabkiewicz, C. Duke, H. Fischer, H.-J. Kluge, H. Kremmling, and E.-W. Otten, Phys. Rev. Lett. 39,

180 (1977).
[467] B. Marsh, T. Day Goodacre, S. Sels, Y. Tsunoda, B. Andel, A.N. Andreyev, N.A. Althubiti, D. Atanasov, A.E. Barzakh, J. Billowes *et al.*, Nature **14**, 1163 (2018).
[468] S. Sels, T. Day Goodacre, B.A. Marsh, A. Pastore, W. Ryssens, Y. Tsunoda, N. Althubiti, B. Andel, A.N. Andreyev, D. Atanasov *et al.*, Phys. Rev. C **99**, 044306 (2019).
[469] P. Dabkiewicz, F. Buchinger, H. Fischer, H.-J. Kluge, H. Kremmling, T. Kühl, A.C. Müller, and H.A. Schuessler, Phys. Lett. B 82, 199 (1979).
[470] D. Proetel, R.M. Diamond, P. Kienle, J.R. Leigh, K.H. Maier, and F.S. Stephens Phys. Rev. Lett. 31, 896 (1973).
[471] N. Rud, D. Ward, H.R. Andrews, R.L. Graham, J.S. Geiger, Phys. Rev. Lett. **31**, 1421 (1973).
[472] R. Béraud, C. Bourgeois, M. Desthuilliers, P. Kilcher, J. Letessier, J. Phys. Colloques 36, C5-101 (1975).
[473] C. Bourgeois, M. Bouet, A. Caruette, A. Ferro, R. Foucher, J. Fournet, A. Höglund, L. Kotfila, G. Landois, C. Liang *et al.*, J. Phys. France **37**, 49 (1976).
[474] J.D. Cole, J.H. Hamilton, A.V. Ramayya, W.G. Nettles, H. Kawakami, E.H. Spejewski, M.A. Ijaz, K.S. Toth, E.L. Robinson, K.S.R. Sastry *et al.*, Phys. Rev. Lett. **37**, 1185 (1976).
[475] J.H. Hamilton, A.V. Ramayya, E.L. Bosworth, W. Lourens, J.D. Cole, B. Van Nooijen, G. Garcia-Bermudez, B. Martin, B.N.S. Rao, H. Kawakami *et al.*, Phys. Rev. Lett. **35**, 562 (1975).
[476] M. Muikku, J.F.C. Cocks, K. Helariutta, P. Jones, R. Julin, S. Juutinen, H. Kankaanää, H. Kettunen, P. Kuusiniemi, M. Leino *et al.*, Phys. Rev. C 58, R3033(R) (1998).
[477] J. Wauters, N. Bijnens, P. Dendooven, M. Huyse, Han Yull Hwang, G. Reusen, J. von Schwarzenberg, P. Van Duppen, R. Kirchner *et al.*, Phys. Rev. Lett. 72, 1329 (1994).
[478] J. Wauters, N. Bijnens, H. Folger, M. Huyse, H.Y. Hwang, R. Kirchner, J. von Schwarzenberg, P. Van Duppen, Phys. Rev. C **50**, 2768 (1994).
[479] G.D. Dracoulis, Phys. Rev. C **49**, 3324 (1994).
[480] P. Joshi, E. Zganjar, D. Rupnik, S. Robinson, P. Mantica, H. Carter, J. Kormicki, R. Gill, W. Walters, C. Bingham *et al.*, Int. J. Mod. Phys. E **3**, 757 (1994).
[481] L.P. Gaffney, M. Hackstein, R.D. Page, T. Grahn, M. Scheck, P.A. Butler, P.F. Bertone, N. Bree, R.J. Carroll, M.P. Carpenter *et al.*, Phys. Rev. C **89**, 024307 (2014).
[482] R.D. Page, A.N. Andreyev, D.R. Wiseman, P.A. Butler, T. Grahn, P.T. Greenlees, R.D. Herzberg, M. Huyse, G.D. Jones, P.M. Jones *et al.*, Phys. Rev. C **84**, 034308 (2011).
[483] E. Rapisarda, A.N. Andreyev, S. Antalic, A. Barzakh, T.E. Cocolios, I.G. Darby, R.D. Groote, H.D. Witte, J. Diriken, J. Elseviers *et al.*, J. Phys. G: Nucl. Part. Phys. **44**, 074001 (2017).
[484] J.D. Cole, A.V. Ramayya, J.H. Hamilton, H. Kawakami, B. van Nooijen, W.G. Nettles, L.L. Riedinger, F.E. Turner, C.R. Bingham, H.K. Carter *et al.*, Phys. Rev. C **16**, 2010 (1977).
[485] M. Scheck, P.A. Butler, L.P. Gaffney, N. Bree, R.J. Carrol, D. Cox, T. Grahn, P.T. Greenlees, K. Hauschild, A. Herzan *et al.*, Phys. Rev. C **83**, 037303 (2011).
[486] T. Grahn, A. Petts, M. Scheck, P.A. Butler, A. Dewald, M.B. Gomez Hornillos, P.T. Greenlees, A. Görgen, K. Helariutta, J. Jolie *et al.*, Phys. Rev. C **80**, 014324 (2009).
[487] M. Scheck, T. Grahn, A. Petts, P.A. Butler, A. Dewald, L.P. Gaffney, M.B. Gomez Hornillos, A. Görgen, P.T. Greenlees, K. Helariutta *et al.*, Phys. Rev. C **81**, 014310 (2010).
[488] W. Ma, A. Ramayya, J. Hamilton, S. Robinson, J. Cole, E. Zganjar, E. Spejewski, R. Bengtsson, W. Nazarewicz, J.Y. Zhang, Phys. Lett. B **167**, 277 (1986).
[489] B. Olaizola, A.B. Garnsworthy, F.A. Ali, C. Andreoiu, G.C. Ball, N. Bernier, H. Bidaman, V. Bildstein, M. Bowry, R. Caballero-Folch *et al.*, Phys. Rev. C **100**, 024301 (2019).
[490] M. Siciliano, I. Zanon, A. Goasduff, P.R. John, T.R. Rodriguez, S. Péru, I. Deloncle, J. Libert, M. Zielińska, D. Ashad *et al.*, Phys. Rev. C 102, 014318 (2020).
[491] N. Bree, K. Wrzosek-Lipska, A. Petts, A. Andreyev, B. Bastin, M. Bender, A. Blazhev, B. Bruyneel, P.A. Butler, J. Butterworth *et al.*, Phys. Rev. Lett. **112**, 162701 (2014).
[492] K. Wrzosek-Lipska, K. Rezynkina, N. Bree, M. Zielińska, L.P. Gaffney, A. Petts, A. Andreyev, B. Bastin, M. Bender, A. Blazhev *et al.*, Eur. Phys. J. A **55**, 130 (2019).
[493] C. Müller-Gatermann, A. Dewald, C. Fransen, K. Auranen, H. Badran, M. Beckers, A. Blazhev, T. Braunroth,

D.M. Cullen, G. Fruet *et al.* Phys. Rev. C 99, 054325 (2019).
[494] K. Hardt, Y.K. Agarwal, C. Günther, M. Guttormsen, R. Kroth, J. Recht, F.A. Beck, T. Byrski, J.C. Merdinger, A. Nourredine, D.C. Radford, J.P. Vivien and C. Bourgeois, Z. Phys. A 312, 251 (1983).
[495] G.D. Dracoulis, T. Lonnroth, S. Vajda, O.C. Kistner, M.H. Rafailovich, E. Dafni, and G. Schatz, Phys. Lett. B 149, 311 (1984).
[496] M. Vergnes, G. Berrier-Ronsin, G. Rotbard, J. Skalski, and W. Nazarewicz, Nucl. Phys. **A 514**, 381 (1990).
[497] C. Bernards, R.F. Casten, V. Werner, P. von Brentano, D. Bucurescu, G. Graw, S. Heinze, R. Hertenberger, J. Jolie, S. Lalkovski *et al.*, Phys. Rev. C 87, 064321 (2013).
[498] A.N. Andreyev, M. Huyse, P. Van Duppen, L. Weissman, D. Ackermann, J. Gerl, F.P. Hessberger, S. Hofmann, A. Kleinböhl, G. Münzenberg *et al.*, Nature **405**, 430 (2000).
[499] A.N. Andreyev, D. Ackermann, P. Cagarda, J. Gerl, F. Hessberger, S. Hofmann, M. Huyse, A. Keenan, H. Kettunen, A. Kleinböhl *et al.*, Eur. Phys. J. A 6, 381 (1999).
[500] K. Van de Vel, A.N. Andreyev, D. Ackermann, H.J. Boardman, P. Cagarda, J. Gerl, F.P. Hessberger, S. Hofmann, M. Huyse, D. Karlgren *et al.*, Phys. Rev. C 68, 054311 (2003).
[501] J. Wauters, P. Dendooven, M. Huyse, G. Reusen, P. Van Duppen, P. Lievens, Phys. Rev. C 47, 1447 (1993).
[502] T.E. Cocolios, W. Dexters, M.D. Seliverstov, A.N. Andreyev, S. Antalic, A.E. Barzakh, B. Bastin, J. Büscher, I.G. Darby, D.V. Fedorov *et al.*, Phys. Rev. Lett. 106, 052503 (2011).
[503] M.D. Seliverstov, T.E. Cocolios, W. Dexters, A.N. Andreyev, S. Antalic, A.E. Barzakh, B. Bastin, J. Büscher, I.G. Darby, D.V. Fedorov *et al.*, Phys. Lett. B **719**, 362 (2013).
[504] W. Reviol, C.J. Chiara, O. Pechenaya, D.G. Sarantites, P. Fallon, and A.O. Macchiavelli, Phys. Rev. C 68, 054317 (2003).
[505] J. Pakarinen, I.G. Darby, S. Eeckhaudt, T. Enqvist, T. Grahn, P.T. Greenlees, V. Hellemans, K. Heyde, F. Johnston-Theasby, P. Jones, *et al.*, Phys. Rev. C 72, 011304(R) (2005).
[506] Y. Le Coz, F. Becker, H. Kankaanpää, W. Korten, E. Mergel, P.A. Butler, J.F.C. Cocks, O. Dorvaux, D. Hawcroft, K. Helariutta *et al.*, Eur. Phys. J. Direct A 3, 1 (1999).
[507] N. Bijnens, I. Ahmad, A.N. Andreyev, J.C. Batchelder, C.R. Bingham, D. Blumenthal, B.C. Busse, X.S. Chen, L.F. Conticchio, C.N. Davids *et al.*, Z. Phys. A 356, 3 (1996).
[508] R.G. Allatt, R.D. Page, M. Leino, T. Enqvist, K. Eskola, P.T. Greenlees, P. Jones, R. Julin, P. Kuusiniemi, W.H. Trzaska *et al.*, Phys. Lett. B 437, 29 (1998).
[509] G.D. Dracoulis, G.J. Lane, A.P. Byrne, T. Kibedi, A.M. Baxter, A.O. Macchiavelli, P. Fallon, and R.M. Clark, Phys. Rev. C 69, 054318 (2004).
[510] G.D. Dracoulis, A.P. Byrne, and A.M. Baxter, Phys. Lett. B 432, 37 (1998).
[511] P. Dendooven, P. Decrock, M. Huyse, G. Reusen, P. Van Duppen, and J. Wauters, Phys. Lett. B 226, 27 (1989).
[512] P. Rahkila, D.G. Jenkins, J. Pakarinen, C. Gray-Jones, P.T. Greenlees, U. Jakobsson, P. Jones, R. Julin, S. Juutinen, S. Ketelhut *et al.*, Phys. Rev. C 82, 011303(R) (2010).
[513] D.G. Jenkins, M. Muikku, P.T. Greenlees, K. Hauschild, K. Helariutta, P.M. Jones, R. Julin, S. Juutinen, H. Kankaanpää, N.S. Kelsall *et al.*, Phys. Rev. C 62, 021302(R) (2000).
[514] J.F. Cocks, M. Muikku, W. Korten, R. Wadsworth, S. Chmel, J. Domscheit, P.T. Greenlees, K. Helariutta, I. Hibbert *et al.*, Eur. Phys. J. A 3, 17 (1998).
[515] T. Grahn, A. Dewald, O. Möller, R. Julin, C.W. Beausang, S. Christen, I.G. Darby, S. Eeckhaudt, P.T. Greenlees, A. Görgen *et al.*, Phys. Rev. Lett. 97, 062501 (2006).
[516] G.D. Dracoulis, Phys. Scr. 2000, 54 (2000).
[517] G.D. Dracoulis, A.P. Byrne, A.M. Baxter, P.M. Davidson, T. Kibedi, T.R. McGoram, R.A. Bark, and S.M. Mullins, Phys. Rev. C 60, 014303 (1999).
[518] N. Bijnens, P. Decrock, S. Franchoo, M. Gaelens, M. Huyse, H.-Y. Hwang, I. Reusen, J. Szerypo, J. von Schwarzenberg, J. Wauters *et al.*, Phys. Rev. Lett. 75, 4571 (1995).
[519] D. Alber, R. Airier, C.E. Bach, D.B. Fossan, H. Grawe, H. Kluge, M. Lach, K.H. Maier, M. Schramm, R. Schubart *et al.*, Z. Phys. A 339, 225 (1991).
[520] R. Julin, K. Helariutta, and M. Muikku, J. Phys. G: Nucl. Part. Phys. 27, R109 (2001).
[521] N. Kesteloot, B. Bastin, L.P. Gaffney, K. Wrzosek-Lipska, K. Auranen, C. Bauer, M. Bender, V. Bildstein, A. Blazhev, S. Bönig *et al.*, Phys. Rev. C 92, 054301 (2015).

[522] B. Andel, A.N. Andreyev, S. Antalic, F.P. Hessberger, D. Ackermann, S. Hofmann, M. Huyse, Z. Kalaninova, B. Kindler, I. Kojouharov *et al.*, Phys. Rev. C 93, 064316 (2016).
[523] L.A. Bernstein, J.A. Cizewski, H.-Q. Jin, W. Younes, R.G. Henry, L.P. Farris, A. Charos, M.P. Carpenter, R.V.F. Janssens, T.L. Khoo *et al.*, Phys. Rev. C 52, 621 (1995).
[524] K. Helariutta, J.F.C. Cocks, T. Enqvist, P.T. Greenlees, P. Jones, R. Julin, S. Juutinen, P. Jämsen, H. Kankaanpää, H. Kettunen *et al.*, Eur. Phys. J. A 6, 289 (1999).
[525] B. Cederwall, R. Wyss, A. Johnson, J. Nyberg, B. Fant, R. Chapman, D. Clarke, F. Khazaie, J. C. Lisle, J.N. Mo *et al.*, Z. Phys. A 337, 283 (1990).
[526] G.D. Dracoulis, A.E. Stuchbery, A.P. Byrne, A.R. Poletti, S.J. Poletti, J. Gerl, and R.A. Bark, J. Phys. G: Nucl. Phys. 12, L97 (1986).
[527] P.R. John, J.J. Valiente-Dobon, D. Mengoni, V. Modamio, S. Lunardi, D. Bazzacco, A. Gadea, C. Wheldon, T.R. Rodriguez, T. Alexander *et al.*, Phys. Rev. C 95, 064321 (2017).
[528] C. Fransen, F. Mammes, R. Bark, T. Braunroth, Z. Buthelezi, A. Dewald, T. Dinoko, S. Förtsch, M. Hackstein, J. Jolie *et al.*, EPJ Web of Conferences 223, 01016 (2019).
[529] C. Müller-Gatermann, A. Dewald, C. Fransen, T. Braunroth, J. Jolie, J. Litzinger, J.M. Régis, F. von Spee, N. Warr, K.O. Zell, T. Grahn *et al.*, Phys. Rev. C 97, 024336 (2018).
[530] C. Müller-Gatermann, F. von Spee, A. Goasduff, D. Bazzacco, M. Beckers, T. Braunroth, A. Boso, P. Cocconi, G. de Angelis, A. Dewald *et al.*, Nucl. Inst. Meth. Phys. Res. A 920, 95 (2019).
[531] C.B. Li, F.Q. Chen, X.G. Wu, C.Y. He, Y. Zheng, G.S. Li, Q.M. Chen, Z.C. Gao, Q.L. Xia, W.P. Zhou *et al.*, Phys. Rev. C 90, 047302 (2014).
[532] K.A. Gladnishki, P. Petkov, A. Dewald, C. Fransen, M. Hackstein, J. Jolie, T. Pissulla, W. Rother, and K. Zell, Nucl. Phys. A 877, 19 (2012).
[533] J.C. Walpe, U. Garg, S. Naguleswaran, J. Wei, W. Reviol, I. Ahmad, M.P. Carpenter, and T.L. Khoo, Phys. Rev. C 85, 057302 (2012).
[534] Aman Rohilla, C.K. Gupta, R.P. Singh, S. Muralithar, S. Chakraborty, H.P. Sharma, A. Kumar, I.M. Govil, D.C. Biswas, and S.K. Chamoli, Eur. Phys. J. A 53, 64 (2017).
[535] A.E. Stuchbery, S.S. Anderssen, A.P. Byrne, P.M. Davidson, G.D. Dracoulis, and G.J. Lane, Phys. Rev. Lett. 76, 2246 (1996).
[536] S.S. Anderssen, A.E. Stuchbery, S. Kuyucak, Nucl. Phys. A 593, 212 (1995).
[537] F. Brandolini, N.H. Medina, A.E. Stuchbery, S.S. Anderssen, H.H. Bolotin, D. Bazzacco, D. De Acuña, M. De Poli, R. Menegazzo, P. Pavan *et al.*, Eur. Phys. J. A 3, 129 (1998).
[538] E. Coenen, K. Deneffe, M. Huyse, P. Van Duppen, and J.L. Wood, Phys. Rev. Lett. 54, 1783 (1985).
[539] H. Kettunen, T. Enqvist, T. Grahn, P.T. Greenlees, P. Jones, R. Julin, S. Juutinen, A. Keenan, P. Kuusiniemi, M. Leino *et al.*, Eur. Phys. J. A 17, 537 (2003).
[540] A.N. Andreyev, D. Ackermann, F.P. Hessberger, K. Heyde, S. Hofmann, M. Huyse, D. Karlgren, I. Kojouharov, B. Kindler, B. Lommel *et al.*, Phys. Rev. C 69, 054308 (2004).
[541] A.E. Barzakh, A.N. Andreyev, T.E. Cocolios, R.P. de Groote, D.V. Fedorov, V.N. Fedosseev, R. Ferrer, D.A. Fink, L. Ghys, M. Huyse *et al.*, Phys. Rev. C 95, 014324 (2017).
[542] A.E. Barzakh, D. Atanasov, A.N. Andreyev, M. Al Monthery, N.A. Althubiti, B. Andel, S. Antalic, K. Blaum, T.E. Cocolios, J.G. Cubiss *et al.*, Phys. Rev. C 101, 064321 (2020).
[543] A.E. Barzakh, D.V. Fedorov, V.S. Ivanov, P.L. Molkanov, F.V. Moroz, S.Yu. Orlov, V.N. Panteleev, M D. Seliverstov, and Yu.M. Volkov, Phys. Rev. C 95, 044324 (2017).
[544] A.E. Barzakh, L.Kh. Batist, D.V. Fedorov, V.S. Ivanov, K.A. Mezilev, P.L. Molkanov, F.V. Moroz, S.Yu. Orlov, V.N. Panteleev, and Yu.M. Volkov, Phys. Rev. C 88, 024315 (2013).
[545] A.E. Barzakh, D.V. Fedorov, V.S. Ivanov, P.L. Molkanov, F.V. Moroz, S.Yu. Orlov, V.N. Panteleev, M D. Seliverstov, and Yu.M. Volkov, Phys. Rev. C 94, 024334 (2016).
[546] A. Hürstel, Y. LeCoz, E. Bouchez, A. Chatillon, A. Görgen, P.T. Greenlees, K. Hauschild, S. Juutinen, H. Kettunen *et al.*, Eur. Phys. J. A 21, 365 (2004).
[547] P. Nieminen, S. Juutinen, A.N. Andreyev, J.F.C. Cocks, O. Dorvaux, K. Eskola, P.T. Greenlees, K. Hauschild, K. Helariutta, M. Huyse *et al.*, Phys. Rev. C 69, 064326 (2004).
[548] M. Nyman, S. Juutinen, D.M. Cullen, I. Darby, S. Eeckhaudt, T. Grahn, P.T. Greenlees, A. Herzan, U. Jakobs-

son, P. Jones *et al.*, Eur. Phys. J. A 51, 31 (2015).
[549] J.C. Walpe, U. Garg, S. Naguleswaran *et al.*, Acta Phys. Pol. B 26, 279 (1995).
[550] G.J. Lane, G.D. Dracoulis, A.P. Byrne, P.M. Walker, A.M. Baxter, J.A. Sheikh, and W. Nazarewicz, Nucl. Phys. A 586, 316 (1995).
[551] J. Sauvage, J. Genevey, B. Roussière, S. Franchoo, A.N. Andreyev, N. Barré, J.-F. Clavelin, H. De Witte, D.V. Fedorov, V.N. Fedoseyev *et al.*, Eur. Phys. J. A 39, 33 (2009).
[552] P.M. Raddon, D.G. Jenkins, C.D. O'Leary, A.J. Simons, R. Wadsworth, A.N. Andreyev, R.D. Page, M.P. Carpenter, F.G. Kondev, T. Enqvist *et al.*, Phys. Rev. C 70, 064308 (2004).
[553] S.K. Chamoli, P. Joshi, A. Kumar, Rajesh Kumar, R.P. Singh, S. Muralithar, R.K. Bhowmik, and I.M. Govil, Phys. Rev. C 71, 054324 (2005).
[554] S.K. Chamoli, Rajesh Kumar, I.M. Govil, P. Joshi, R.P. Singh, S. Muralithar, and R.K. Bhowmik, Phys. Rev. C 75, 054323 (2007).
[555] P. Joshi, A. Kumar, I.M. Govil, R.P. Singh, G. Mukherjee, S. Muralithar, R.K. Bhowmik, and U. Garg, Phys. Rev. C 69, 044304 (2004).
[556] D. Rupnik, E.F. Zganjar, J.L. Wood, P.B. Semmes, and P.F. Mantica, Phys. Rev. C 58, 771 (1998).
[557] C.D. Papanicolopulos, M.A. Grimm, J.L. Wood, E.F. Zganjar, M.O. Kortelahti, J.D. Cole, and H.K. Carter, Z. Phys. A 330, 371 (1988).
[558] M. Venhart, F.A. Ali, W. Ryssens, J.L. Wood, D.T. Joss, A.N. Andreyev, K. Auranen, B. Bally, M. Balogh, M. Bender *et al.*, Phys. Rev. C 95, 061302(R) (2017).
[559] M. Venhart, A.N. Andreyev, J.L. Wood, S. Antalic, L. Bianco, P.T. Greenlees, U. Jakobsson, P. Jones, R. Julin, S. Juutinen *et al.*, Phys. Lett. B 695, 82 (2011).
[560] M. Venhart, J.L. Wood, M. Sedlak, M. Balogh, M. Birova, A.J. Boston, T.E. Cocolios, L.J. Harkness-Brennan, R.-D. Herzberg, L. Holub *et al.*, J. Phys. G: Nucl. Part. Phys. 44, 074003 (2017).
[561] M. Sedlak, M. Venhart, J.L. Wood, V. Matousek, M. Balogh, A.J. Boston, T.E. Cocolios, L.J. Harkness-Brennan, R.-D. Herzberg, D.T. Joss *et al.*, Eur. Phys. J. A 56, 161 (2020).
[562] C. Santamaria, C. Louchart, A. Obertelli, V. Werner, P. Doornenbal, F. Nowacki, G. Authelet, H. Baba, D. Calvet, F. Château *et al.*, Phys. Rev. Lett. 115, 192501 (2015). doi:10.1103/PhysRevLett.115.192501
[563] A. Obertelli, T. Baugher, D. Bazin, J.-P. Delaroche, F. Flavigny, A. Gade, M. Girod, T. Glasmacher, A. Görgen, G.F. Grinyer, W. Korten, J. Ljungvall, S. McDaniel, A. Ratkiewicz, B. Sulignano, and D. Weisshaar, Phys. Rev. C 80, 031304 (2009). doi:10.1103/PhysRevC.80.031304
[564] R.D.O. Llewellyn, M.A. Bentley, R. Wadsworth, H. Iwasaki, J. Dobaczewski, G. de Angelis, J. Ash, D. Bazin, P.C. Bender, B. Cederwall *et al.*, Phys. Rev. Lett. 124, 152501 (2020).
[565] M. Albers, K. Nomura, N. Warr, A. Blazhev, J. Jolie, D. Mücher, B. Bastin, C. Bauer, C. Bernards, L. Bettermann *et al.*, Nucl. Phys. A 899, 1 (2013). doi:10.1016/j.nuclphysa.2013.01.013
[566] T.R. Rodríguez, Phys. Rev. C 90, 034306 (2014). doi:10.1103/PhysRevC.90.034306